



저작자표시-비영리-변경금지 2.0 대한민국

이용자는 아래의 조건을 따르는 경우에 한하여 자유롭게

- 이 저작물을 복제, 배포, 전송, 전시, 공연 및 방송할 수 있습니다.

다음과 같은 조건을 따라야 합니다:



저작자표시. 귀하는 원저작자를 표시하여야 합니다.



비영리. 귀하는 이 저작물을 영리 목적으로 이용할 수 없습니다.



변경금지. 귀하는 이 저작물을 개작, 변형 또는 가공할 수 없습니다.

- 귀하는, 이 저작물의 재이용이나 배포의 경우, 이 저작물에 적용된 이용허락조건을 명확하게 나타내어야 합니다.
- 저작권자로부터 별도의 허가를 받으면 이러한 조건들은 적용되지 않습니다.

저작권법에 따른 이용자의 권리는 위의 내용에 의하여 영향을 받지 않습니다.

이것은 [이용허락규약\(Legal Code\)](#)을 이해하기 쉽게 요약한 것입니다.

[Disclaimer](#)

공학박사학위논문

**Development of A New Methodology for  
Both Qualitative and Quantitative Surface  
Characterization of Carbon Nanomaterials**

탄소나노재료의 정성 및 정량 분석을 위한  
새로운 표면 분석 방법론에 관한 연구

2015년 2월

서울대학교 대학원

재료공학부

김 연 승

**Development of A New Methodology for  
Both Qualitative and Quantitative Surface  
Characterization of Carbon Nanomaterials**

지도교수 박종래

이 논문을 공학박사 학위논문으로 제출함

2014 년 10 월






서울대학교 대학원

재료공학부

김연승

김연승의 박사학위논문을 인준함

2014 년 12 월

위원장	조 천 호	
부위원장	박 종 래	
위원	장 지 영	
위원	박 진	
위원	이 영 석	

Abstract

**Development of A New Methodology for  
Both Qualitative and Quantitative Surface  
Characterization of Carbon Nanomaterials**

Yern Seung Kim

Department of Materials Science and Engineering

The Graduate School

Seoul National University

This thesis describes a titration methodology based on a universal titration equation for the surface characterization of carbon nanomaterials and their applications. Carbon nanomaterials are expected to become a next-generation functional material due to their extraordinary properties. Functionalization is one of the key procedures leading to viable applications of carbon nanomaterials as this process generates desired functional groups on their surfaces. These functional groups adjust the surface properties of carbon nanomaterials to enhance their dispersibility, adsorption properties, and reactivity levels, thereby potentially broadening the areas in which they may be used. With regard to these procedures, the precise elucidation of surface functional groups is significant for the proper utilization of functionalized carbon nanomaterials. Among the various characterization techniques which have been developed thus far, the titration method has

been widely adopted due to its simple operating principles and for the useful information it provides.

Titration methods of carbonaceous materials are largely categorized into indirect and direct methods. While direct titration provides information on the population of the acidic groups in specific  $pK_a$  ranges expressed in terms of the  $pK_a$  distribution function, indirect titration simply provides the concentrations of practical functional groups which are directly applicable regarding the use of carbon materials. Hence, indirect titration has been widely adopted for the surface characterization of various carbonaceous materials. However, for the easy adoption of indirect titration to carbon nanomaterials, complicated and inaccessible procedures compared to direct titration and sophisticated issues originating from the specific properties of carbon nanomaterials should be overcome. Therefore, the development of a titration method with a combination of the aforementioned advantages, i.e., the convenience of direct titration and the practical information of indirect titration, is crucial. The aim of the present study is to develop a titration methodology which utilizes the principles of the direct and indirect titration methods for the straightforward determination of the surface properties, and applications, of carbon nanomaterials.

Part I describes the general concept and definition of acidities of functionalized carbon nanomaterials. This is followed by an introduction to the basics of conventional titration methods. The contribution of the present study stems from theoretical considerations of the drawbacks of conventional titration methods and state-of-the-art works.

In Part II, a universal titration equation for the development of a titration methodology is theoretically derived and its validity is experimentally demonstrated. The derived equation is adapted to indirect titration conditions in which simple acidic molecules such as acidic carbon compounds (ACCs) are formed during the functionalization of carbon

nanotubes, or where atmospheric carbon dioxide (CO<sub>2</sub>) is involved in the standardization of readily adoptable indirect titration methods. The effects of ACCs and CO<sub>2</sub> are clearly elucidated on the basis of a universal titration equation. More importantly, this critical revisit of indirect titration shows that the conventional CO<sub>2</sub>-removal process is completely unnecessary. This makes indirect titration simpler and more accessible, with high precision in the results as well.

Part III develops a one-pot titration methodology by altering the conventional indirect and direct titration methods. In this method, the  $pK_a$  distribution functions of nitric acid-oxidized carbon nanotubes (CNTs) from direct titration are reconstructed into the concentrations of practical functional groups obtainable from indirect titration. The one-pot titration results were fairly comparable to the well-established indirect titration results, implying that the titration methodology developed in this study is universally applicable.

Part IV applies the titration methodology for an analysis of the dispersion behaviors of mixed acid-oxidized CNTs in neutral water. It is shown here that highly carboxylated ACCs on CNTs are easily ionized in neutral water and that they play a crucial role in the high-quality stable aqueous dispersion of CNTs. In addition, the mechanism of graphene oxide cross-linking aided by diamine ion bridges is proposed based on the titration methodology for the effective fabrication of GO fibers. These investigations and analyses of practical functional groups clearly show that the developed titration methodology is applicable for the actual utilization of carbon nanomaterials.

**Keywords: carbon nanomaterials, surface functionalization, surface characterization, surface functional groups, universal titration equation, titration methodology**

**Student Number: 2010-20584**

# Contents

## Part I General Introduction to Acidity of Carbon Nanomaterials and Titration Methods

### Chapter 1 Introduction ..... 2

1.1 General introduction to carbon nanomaterials and the surface characterization methods.....	2
1.1.1 Overview of carbon nanomaterials and their functionalization methods .....	2
1.1.1.1 Carbon nanomaterials.....	2
1.1.1.2 Surface functionalization of carbon nanomaterials .....	3
1.1.2 Overview of the surface characterization methods of carbon nanomaterials....	6
1.1.2.1 Fourier transformed infrared spectroscopy (FT-IR) .....	6
1.1.2.2 X-ray photoelectron spectroscopy (XPS).....	6
1.1.2.3 Thermogravimetric analysis (TGA) / Temperature programmed desorption (TPD) .....	7
1.1.2.4 Other characterization methods.....	7
1.2 Basics of titration methods for the surface characterization of carbon materials ...	10
1.2.1 Basic concept of the acidity on carbon materials.....	10
1.2.2 Indirect titration method .....	15

1.2.3 Direct titration method.....	18
1.3 State-of-the-art works on titration methods.....	20
1.3.1 Issues associated with indirect titration methods.....	20
1.3.1.1 Dissolution of acidic moieties.....	20
1.3.1.1.1 Carbon dioxide (CO <sub>2</sub> ).....	20
1.3.1.1.2 Acidic carbon compounds (ACCs).....	23
1.3.1.2 Procedure.....	26
1.3.1.3 Adoption of indirect titration methods.....	26
1.3.1.3.1 Adsorption property.....	26
1.3.1.3.2 Reaction chemistry.....	27
1.3.2 Issue on direct titration methods.....	29
1.3.2.1 Procedure.....	29
1.3.2.2 Adoption of direct titration methods.....	29
1.3.2.2.1 Practical functional groups calculation.....	29
1.3.2.2.2 Dispersion property.....	30
1.4 Aim and scope of this research.....	32
1.4.1 Development of universal titration equation.....	32
1.4.2 Standardization of indirect titration methods.....	32
1.4.3 Development of one-pot titration methodology.....	33
1.5 References.....	34



## **Part II Standardization of Indirect Titration Method for Surface Characterization of Carbon Nanomaterials**

### **Chapter 2 Effects of Carbon Dioxide and Acidic Carbon Compounds on The Analysis of Indirect Titration Curves..... 41**

2.1 Introduction.....	41
2.2 Experimental .....	43
2.2.1 Chemicals and materials .....	43
2.2.2 Potentiometric titration of model ACCs.....	43
2.2.3 Indirect titration of NCNTs with and without the removal of ACCs .....	44
2.3 Results and discussion .....	45
2.3.1 Theoretical derivation of universal titration equation .....	45
2.3.2 Adoption of model ACCs (BA, Ph) and CO <sub>2</sub> to the universal titration equation .....	52
2.3.3 Application of universal titration equation on the indirect titration of NCNTs .....	60
2.4 Conclusions.....	64
2.5 References.....	65

## **Chapter 3 A Simple Method for Analysis of Indirect Titration**

### **Results Regardless of The Carbon Dioxide Effect ..... 67**

3.1 Introduction.....	67
3.2 Experimental.....	69
3.2.1 Chemicals and materials .....	69
3.2.2 in-CO <sub>2</sub> -titration of pre-reaction bases .....	69
3.2.3 ex-CO <sub>2</sub> -titration of the pre-reaction bases .....	70
3.2.4 in- and ex-CO <sub>2</sub> -titration of MCNTs .....	70
3.2.5 Determination of the surface functionality of the MCNTs .....	72
3.3 Results and discussion .....	75
3.3.1 CO <sub>2</sub> effect on the in-CO <sub>2</sub> -titration behavior of each reaction base .....	75
3.3.2 Comparison of the in-CO <sub>2</sub> -titration behavior with the ex-CO <sub>2</sub> -titration behavior .....	85
3.3.3 Surface functionality of MCNTs as determined by in- and ex-CO <sub>2</sub> -titration..	88
3.4 Conclusions.....	92
3.5 References.....	93

## **Part III One-Pot Titration Methodology for Surface Characterization of Carbon Nanomaterials**

### **Chapter 4 One-pot Titration Methodology for The Surface Characterization of Oxidized Carbon Nanotubes..... 96**

4.1 Introduction.....	96
4.2 Experimental.....	96
4.2.1 Chemicals and materials.....	99
4.2.2 Indirect titration of oxidized CNTs.....	99
4.2.3 One-pot titration of oxidized CNTs.....	101
4.3 Results and discussion.....	102
4.3.1 Calculation of proton binding curve and $pK_a$ distribution function.....	102
4.3.2 Theoretical derivation of one-pot titration methodology.....	109
4.3.3 Practical application of one-pot titration methodology.....	116
4.3.4 Comparison between one-pot and indirect titration results of oxidized CNTs .....	129
4.4 Conclusions.....	138
4.5 References.....	139

## **Part IV One-Pot Titration Methodology for Applications of Carbon Nanomaterials**

### **Chapter 5 High-Quality Aqueous Dispersions of Carbon Nanotubes for Preparation of High-Performance Buckypapers..... 142**

5.1 Introduction.....	142
5.2 Experimental .....	145
5.2.1 Preparation of oxidized CNTs.....	145
5.2.2 Preparation of CNT dispersions and buckypapers .....	146
5.2.3 Characterization .....	147
5.3 Results and discussion .....	149
5.3.1 Preservation and removal of ACCs from CNTs after oxidization.....	149
5.3.2 Surface properties of ACC-removed and unremoved CNTs.....	151
5.3.3 Dispersion properties of CNTs in aqueous solution.....	164
5.3.4 Morphologies and properties of CNT buckypapers .....	168
5.4 Conclusions.....	175
5.5 References.....	176

**Chapter 6 Ionic Cross-Linking of Graphene Oxide and Diamines  
for Preparation of High-Performance Graphene Oxide  
Fibers ..... 179**

6.1 Introduction..... 179

6.2 Experimental ..... 183

    6.2.1 Preparation of GO solution spinning dope..... 183

    6.2.2 Preparation of diamine cross-linked GO fibers..... 184

    6.2.3 Characterization ..... 184

6.3 Results and discussion ..... 186

    6.3.1 Physical and chemical properties of GO..... 186

    6.3.2 Formation mechanism of GO fibers..... 191

    6.3.3 Properties and performances of GO fibers..... 199

6.4 Conclusions..... 207

6.5 References..... 208

**Chapter 7 Concluding Remarks..... 211**

# List of Tables

**Table 2.1.** Base components and their  $pK_b$  at 25°C.

**Table 2.2.** The compositions of three reaction bases titrated with 0.01 N HCl, and the various neutralized (or protonated) base species (see Figs. 2.2 – 2.6).

**Table 3.1.** Summary of in- and ex-CO<sub>2</sub>-titration systems

**Table 3.2.** The base equivalence of each pre-reaction base ( $eq_{B,pre}$ ) determined by the different measurement methods of NP from in- and ex-CO<sub>2</sub>- titration.

**Table 3.3.** The number of each functional group on the MCNTs determined by the different measurement methods of NP from the in- and ex-CO<sub>2</sub>-titrations.

**Table 4.1.** Comparison between one-pot and indirect titration results for the low ( $\theta_{max} \cdot c_C / Alk = 0.043$ ) and high ( $\theta_{max} \cdot c_C / Alk = 0.43$ ) normality ratio of N<sub>12</sub>CNT to the reaction bases

**Table 4.2.** Comparison between the uptake quantities of the reaction bases from one-pot and indirect titration.

**Table 4.3.** Comparison of the concentrations of functional groups from the one-pot and indirect titration methods (calculations based on Figs. 4.2f and 4.8d)

**Table 5.1.** Quantitative analysis of XPS C1s spectra of MCNT<sub>BW</sub>, MCNT<sub>NW</sub>, and MCNT<sub>AW</sub> in Fig. 5.2.

**Table 5.2.** Weight percent ( $W$ ) at 800 °C and the resultant estimation of weight fraction ( $wf$ ) of CNT and ACC of CNT samples and ACC.

**Table 5.3.** Comparison between the properties of freestanding CNT buckypapers in this work and those reported previously.

**Table 6.1.**  $pK_b$  values of  $DA_k$  and  $DA_k^+$  ( $k = 2, 6,$  and  $8$  in this work).

**Table 6.2.** Comparison of the mechanical properties of the GO fibers prepared in this work and those reported previously and coagulated using different coagulants, before and after a drawing process.

# List of Figures

**Fig. 1.1.** Schematic representation showing (a) covalent and (b) non-covalent surface modifications for the applications of carbon nanomaterials, including (c) dispersions for processing and composites, (d) adsorption for energy and environmental devices, and (e) linking between the carbon nanomaterials for assembled structures.

**Fig. 1.2.** Examples of the surface characterization techniques; (a) FT-IR spectra of composite GO membranes (GO/CA, GO-EDA/CA, GO-BDA/CA, GO-PPD/CA; CA, EDA, BDA, PPD specified cellulose acetate, ethylenediamine, buthlyenediamine, and *p*-phenylenediamine, respectively). (b) XPS C1s spectra of raw (r-SWNTs) and oxidized SWCNTs compared to a typical sample after an HNO<sub>3</sub> (o-SWNTs)/NaOH (b-SWNTs) treatment, (c) mass-spectra followed by TGA/TPD of CO<sub>2</sub> and CO with the decomposition of various types of oxygen functional groups.

**Fig. 1.3.** Schematic representation showing the general expression for the acid strength of the acids.

**Fig. 1.4.** Schematic representations showing the basic concept of acidity on (a) monoprotic, (b) diprotic, and (c) multiprotic acids.

**Fig. 1.5.** Schematic representation of (a) the process of the indirect titration method for carbon materials, including the reaction, filtration and titration steps, and (b) the selective neutralization of the major functional groups and the reaction bases as part of the indirect titration method.

**Fig. 1.6.** Schematic representation of (a) the process of direct titration method for carbon materials, and (b) the observable  $pK_a$  distribution function.



**Fig.1.7.** Titration curves (plotted as amount of carbon surface functionality) for different reaction bases after acidifications including (a)  $\text{NaHCO}_3$ , (b)  $\text{Na}_2\text{CO}_3$ , and (c)  $\text{NaOH}$ . (d) Titration curves of unacidified  $\text{NaOH}$ .

**Fig. 1.8.** Examples of the utilization of the indirect titration method for (a) an investigation of the water-adsorption sites of activated carbons, (b, c) the 2G functionalization of CNTs ((b) and (c) from two earlier works).

**Fig. 1.9.** Examples of utilization of indirect titration method for (a) investigation of water adsorption sites of activated carbons, (b, c) 2G functionalization of CNTs.

**Fig. 1.10.** Concentration of the ionized group or the proton binding isotherm as a function of the pH for (a) GO and (b) r-GO. The inset shows the  $\text{p}K_a$  distribution of the acid groups. The surface charge density [ $\text{C}/\text{m}^2$ ] for (c) GO and (d) r-GO calculated from the zeta potential (black lines) as a function of the pH, and the charge density [ $\text{C}/\text{g}$ ] as a function of the pH as calculated from the direct titration curve (blue lines).

**Fig. 2.1.** (a) Titration curves of 0.1 M solution containing an arbitrary phenolate ion with  $\text{p}K_b = 4$  (10 mL), calculated according to equation (2.4) (blue dotted line), (2.6) (green dashed line), and (2.8) (red solid line). (b) pH divergence for the curve plotted according to equation (2.6), and pH convergence to 2 (pH of 0.01 N HCl solution) for the curve calculated plotted according to equation (2.8).

**Fig. 2.2.** (a, b, c) Theoretical only and (d, e, f) both experimental and theoretical (I) titration curves, and (II) their first order derivatives, corresponding to the titrations of the reaction bases listed in Table 2.2.

**Fig. 2.3.** (I) Theoretical titration curves of (a) Bases 1, (b) Base 2 and (c) Base 3 and (II) the quantity variation of each base component during the titration of each reaction base without any dissolved  $\text{CO}_2$ .

**Fig. 2.4.** (I) Theoretical titration curves of (a) Bases 1, (b) Base 2 and (c) Base 3 and (II)

the quantity variation of each base component during the titration of each reaction base. Here, the quantity of dissolved CO<sub>2</sub> was assumed to be 0.01 mmol

**Fig. 2.5.** (I) Theoretical titration curves of (a) Bases 1, (b) Base 2 and (c) Base 3 and (II) the quantity variation of each base component during the titration of each reaction base. Here, the quantity of dissolved CO<sub>2</sub> was assumed to be 0.02 mmol.

**Fig. 2.6.** (a, b) Theoretical only and (c, d) both experimental and theoretical (I) titration curves and (II) their first-order derivatives, corresponding to the titration of the reaction base, 0.01 N NaOH (10 mL), with 0.01 N HCl. The acidic components dissolved in the reaction bases are (a, c) Ph and (b, d) BA.

**Fig. 2.7.** (I) Titration curves of (a) the prepared reaction base, 0.01 N NaOH itself (5 mL; reference) and the filtrate from (b) NCNT and (c) NCNT<sub>ACC</sub> containing reaction base, respectively, (II) and their first-order derivatives. The amount of dissolved CO<sub>2</sub> ( $Q_{CO_2}$ ) in each reaction base was determined from the  $Q_{H^+}$  difference between the two EPs on each titration curve.

**Fig. 2.8.** (a) CO<sub>2</sub>-effects-free titration curves of the prepared reaction base, 0.01 N NaOH itself (5 mL; reference) ( $I_{ref}$ ) and the filtrate from NCNT ( $I_{NCNT}$ ) and NCNT<sub>ACC</sub> ( $I_{NCNTACC}$ ) containing reaction base, respectively, together with the theoretical titration curves. (b) Magnified view of the titration curves around the EPs (red dashed box in (a)). The difference in  $Q_{H^+}$  value at pH 7 between  $I_{ref}$  and  $I_{NCNT}$ , and that of ACCs between  $I_{NCNT}$  and  $I_{NCNTACC}$  indicate the total acidity of NCNT ( $a_{NCNT}$ ) and that of ACCs ( $a_{ACC}$ ), respectively.

**Fig. 3.1.** (I) Experimental and theoretical in-CO<sub>2</sub>-titration curves and (II) their first order derivatives of different pre-reaction bases (a) NaOH, (b) Na<sub>2</sub>CO<sub>3</sub>, and (c) NaHCO<sub>3</sub> with different exposure times. The gray arrows indicate an increase in the exposure time.

**Fig. 3.2.** The calculated equivalence ratio of  $\text{HCO}_3^-$  and  $\text{CO}_3^{2-}$  ions in the reaction base at the equilibrium state with  $\text{CO}_2$ .

**Fig. 3.3.** (I) Theoretical titration curves and (II) their first order derivatives of 0.01 N NaOH (10 mL) reacted with different amounts of  $\text{CO}_2$ .

**Fig. 3.4.** (a) ex- $\text{CO}_2$ -titration curve and its first order derivative of the pre-reaction base  $\text{NaHCO}_3$ , and (b) the magnified view around the NPs (blue dotted box in (a)).

**Fig. 3.5.** (I) titration curves and (II) their first order derivatives of the reaction base NaOH from (a) the in- and (b) ex- $\text{CO}_2$ -titration systems before and after the reaction with the MCNTs. (b, d) The magnified view around the NP of the titrations (blue dotted box in (a) and (c) respectively).

**Fig. 4.1.** (a) Direct titration curve of HCl titrant solutions with (red circle) and without (Ref.; black square) the agitation of the  $\text{N}_{12}\text{CNT}$  and their theoretical counterparts (black solid lines), where  $Q_{\text{OH}^-}$  is the quantity of NaOH titrant solution, (b) proton binding isotherm ( $\theta$ ), and (c)  $\text{p}K_a$  distribution function ( $f(\text{p}K_a)$ ) of  $\text{N}_{12}\text{CNT}$ .

**Fig. 4.2.** Calculated titration curve of 10 mL of the 0.01 N reaction bases: (a) NaOH, (b)  $\text{Na}_2\text{CO}_3$ , and (c)  $\text{NaHCO}_3$  (black dashed lines refer to the reference reaction bases and red solid lines denote the mixture with 10 mg of  $\text{N}_{12}\text{CNT}$ ). (d)  $\text{pH}_e$  of the 0.01 N reaction base as a function of  $r_{\text{CO}_2}$ , (e) proton-dissociated  $f(\text{p}K_a)$  of  $\text{N}_{12}\text{CNT}$  ( $c_C = 1 \text{ mg/mL}$ ,  $\text{Alk} = 0.1 \text{ N}$ ), and (f) reaction base uptake quantity of  $\text{N}_{12}\text{CNT}$  as a function of  $r_{\text{CO}_2}$  from the one-pot titration (black solid line) method and the indirect titration (red dots) method.

**Fig 4.3.** Proton-dissociation  $f(\text{p}K_a)$  of (a) 10 and (b) 20 mg/mL  $\text{N}_{12}\text{CNT}$  in the 0.01 N reaction base. (c) Reaction base uptake quantity of  $\text{N}_{12}\text{CNT}$  as a function of  $r_{\text{CO}_2}$  with the variation of  $c_C$  of the reaction base.

**Fig. 4.4.** Proton dissociation  $f(pK_a)$  of 1 mg/mL  $N_{12}CNT$  in the reaction base with (a)  $Alk = 1$  mN and (b) 0.5 mN. (c) Reaction base uptake quantity of  $N_{12}CNT$  as a function of  $r_{CO_2}$  with the variation of  $Alk$  of the reaction base.

**Fig. 4.5.** Reaction base uptake quantity of  $N_{12}CNT$  as a function of (a)  $Alk$  and (b)  $c_C$  and (c, d) the corresponding resultant concentrations of the functional groups, respectively.

**Fig. 4.6.** One-pot titration diagram of  $N_{12}CNT$  exhibiting (a) the uptake quantity of the reaction bases and (b) the concentrations of functional groups as a function of  $Alk$  and  $c_C$ .

**Fig. 4.7.** (a) Experimental and theoretical titration curves of the mixture of 0.01 N HCl and (b) the proton-binding isotherms of  $N_6CNT$ ,  $N_{24}CNT$ , and  $N_{48}CNT$ .

**Fig 4.8.** Proton-dissociated  $f(pK_a)$  of 1 mg/mL (a)  $N_6CNT$ , (b)  $N_{24}CNT$ , and (c)  $N_{48}CNT$  in 0.01 N reaction bases. (d) Reaction base uptake quantities of  $N_6CNT$ ,  $N_{24}CNT$ , and  $N_{48}CNT$  as a function of  $r_{CO_2}$  from the one-pot titration and indirect titration methods.

**Fig. 4.9.** One-pot titration diagram of  $N_6CNT$  exhibiting (a) the uptake quantity of the reaction bases and (b) the concentrations of functional groups as a function of  $Alk$  and  $c_C$ .

**Fig. 4.10.** One-pot titration diagram of  $N_{24}CNT$  exhibiting (a) the uptake quantity of the reaction bases and (b) the concentrations of functional groups as a function of  $Alk$  and  $c_C$ .

**Fig. 4.11.** One-pot titration diagram of  $N_{48}CNT$  exhibiting (a) the uptake quantity of the reaction bases and (b) the concentrations of functional groups as a function of  $Alk$  and  $c_C$ .

**Fig. 5.1.** (a) The filtrates of  $MCNT_{AW}$  dissolved in the pH controlled water with HCl or

NaOH and (b) absorbance at  $\lambda = 550$  nm of the diluted filtrates. (c) Absorbance at  $\lambda = 550$  nm of the diluted filtrates of MCNT<sub>AW</sub> and neutral deionized water (pH 7) and NaOH aqueous solution (pH 12) as a function of number of wash.

**Fig. 5.2.** XPS C1s spectra of (a) MCNT<sub>BW</sub>, (b) MCNT<sub>NW</sub>, and (c) MCNT<sub>AW</sub>.

**Fig. 5.3.** (a) TGA and (b) differential thermogravimetry (DTG) profiles of MCNT<sub>BW</sub>, MCNT<sub>NW</sub>, MCNT<sub>AW</sub>, and ACC.

**Fig. 5.4.** (a) Proton binding isotherms ( $\theta$ ), (b) pK<sub>a</sub> distribution functions ( $f$ ) of MCNT<sub>BW</sub>, MCNT<sub>NW</sub>, and MCNT<sub>AW</sub>. (c) pK<sub>a</sub> distribution functions ( $f$ ) of ACCs on MCNT<sub>AW</sub> and MCNT<sub>NW</sub>.

**Fig. 5.5.** (a) Proton dissociated  $f(pK_a)$  of ACCs on MCNT<sub>AW</sub> (1 mg/mL) in the pH-controlled aqueous solutions, and (b) the number and the percent degree of ionized functional groups on the ACCs as a function of the initial pH (pH<sub>i</sub>) of the aqueous solutions.

**Fig. 5.6.** Proton dissociated  $f(pK_a)$  of CNT and ACC normalized by weight of CNT showing the ionization behavior of (a) MCNT<sub>BW</sub>, (b) MCNT<sub>NW</sub> and (c) MCNT<sub>AW</sub> dispersed in neutral water (1 mg/mL).

**Fig. 5.7.** Concentration-normalized absorbance of visible light ( $\lambda = 550$  nm) after the centrifugation (red dashed line) and zeta potential (black solid line) of CNT aqueous dispersions as a function of the number of active ACCs on CNTs.

**Fig. 5.8.** (a, b, c) Digital photos and (d, e, f) SEM images of the buckypapers fabricated from (a, d) MCNT<sub>BW</sub>, (b, e) MCNT<sub>NW</sub>, and (c, f) MCNT<sub>AW</sub>.

**Fig. 5.9.** The active number and degree of ionization of ACCs of MCNT<sub>AW</sub> as a function of concentration of CNT in water.

**Fig. 5.10.** Representative stress–strain curves collected from the buckypapers of MCNT<sub>BW</sub>, MCNT<sub>NW</sub>, and MCNT<sub>AW</sub>.

**Fig. 6.1.** (a) SEM, (b) AFM images of single layer GO sheets, and (c) photograph of the collected as-spun GO gel fibers.

**Fig. 6.2.** POM images of (a) 0.25, (b) 0.5, (c) 1, (d) 2.5, (e) 5, and (f) 10 mg/mL aqueous GO solutions.

**Fig. 6.3.** (a) Proton binding isotherm ( $\theta(\text{pH})$ ) and (b)  $\text{p}K_a$  distribution function ( $f(\text{p}K_a)$ ) of GO sample.

**Fig. 6.4.** Schematic illustrations of formation of ion bridges between GO layers and (a)  $\text{DA}_2$ , (b)  $\text{DA}_6$ , (c)  $\text{DA}_8$ , and (d, e) break of ion bridge by HCl washing ( $\text{DA}_6$  in this case).

**Fig. 6.5.** Concentrations of fully ionized diamines ( $c_{\text{DA}_k^{2+}}$ ) with respect to that of diamine molecules ( $c_{\text{DA}_k}$ ) in 10 mg/mL GO solutions.

**Fig. 6.6.** SEM images showing the surfaces and cross-sectional morphologies of (a, d)  $\text{GO\_DA}_2$ , (b, e)  $\text{GO\_DA}_6$ , (c, f)  $\text{GO\_DA}_8$ , and (g, h, i) magnified view of cross-section of each GO fiber ((d, e, f), respectively).

**Fig. 6.7.** FT-IR spectra of the unreacted GO film and the diamine cross-linked GO fibers.

**Fig. 6.8.** XPS C1s spectra of the (a) unreacted GO film, and of the diamine cross-linked GO fibers ((b)  $\text{GOF\_DA}_2$ , (c)  $\text{GOF\_DA}_6$ , and (d)  $\text{FOG\_DA}_8$ ).

**Fig. 6.9.** XRD patterns collected from the unreacted GO film and from the diamine cross-linked GO fibers.

**Fig. 6.10.** Representative stress–strain curves collected from the  $\text{GOF\_DA}_2$ ,  $\text{GOF\_DA}_6$ , and  $\text{GOF\_DA}_8$  samples.

**Part I**

**General Introduction to Acidity of**

**Carbon Nanomaterials**

**and Titration Methods**

# Chapter 1 Introduction

## 1.1 General introduction to carbon nanomaterials and the surface characterization methods

### 1.1.1 Overview of carbon nanomaterials and their functionalization methods

#### 1.1.1.1 Carbon nanomaterials

Carbon (C) is tremendous element which abundantly exists in numerous matters on the earth. The chemical bonds between carbon atoms can be tuned by changing the hybridizations of the orbitals in the carbon atom to the  $sp$ ,  $sp^2$ , and  $sp^3$  types. This unique property of carbon atoms makes carbon materials, which are mainly composed of carbon atoms, among the most useful and attractive materials ever discovered [1]. Carbon materials can be transformed into various allotropes by changing their atomic configurations, instilling very different properties in them. The resulting materials range from the soft graphite used in lubricants or pencil lead to diamond, the hardest material in the world.

Carbon nanomaterials, represented as carbon nanotube (CNT), and graphene, are now being one of the most fascinating materials which are potentially applicable to next-generation energy and environmental devices due to their outstanding properties [2, 3]. The major building blocks of carbon nanomaterials are hexagonally arranged  $sp^2$ -bonded carbons with planar aromatic structures defined as a “graphene layer.” The nano-sized shapes and related specific properties of carbon nanomaterials can be tuned and tailored through different arrangements of this graphene layer [4]. Carbon material simply



composed of a single graphene layer itself is referred to as “graphene.” Since the first experimental isolation of graphene from the surface of graphite using the “Scotch tape” method [5], various unique electrical, optical and mechanical properties depending on the size (graphene quantum dots) [6], dimension (graphene nanoribbons) [7], and the structural stacking characteristics (from bilayer to multi-layer graphene) [8] have been reported. Rolling a graphene layer into a nano-sized cylinder results in a “carbon nanotube” (CNT) [9]. Similar to graphene, the electrical/mechanical properties of CNTs are highly dependent on the rolling direction (metallic/semiconducting) [10], the number of walls (single-walled (SWCNT) to multi-walled (MWCNT) CNT) [11], and the defects generated in the graphene layers if the CNTs [12].

#### **1.1.1.2 Surface functionalization of carbon nanomaterials**

Unfortunately, the outstanding intrinsic properties which originate from the graphene layers of carbon nanomaterials have not been sufficiently realized in useful applications thus far. As part of the effort to realize these applications, carbon nanomaterials have been hybridized into other types of materials as composite fillers or as components in devices [13]. They have also been assembled into bulk structures in the form of fibers [14, 15], films [16, 17], or even foams [18, 19]. These processes usually include a surface functionalization step during which the surfaces of the carbon nanomaterials are chemically or physically decorated with various functional groups or molecules [20]. These functionalities give carbon nanomaterials affinity with matrixes or solvents to function as bridges for high-performance carbon nanomaterial assemblies. Specifically, wettability or solubility to aqueous or organic solvents can be adjusted for processing or for the preparation of composite materials [21]. In addition, the adsorption properties of novel metals or pollutants can be controlled for energy and environmental applications

[22-24]. The functional groups can be modified further by other functional groups (defined as second-generation (2G) functionalization) or can be utilized with crosslinking agents between the carbon nanomaterials of self-assembled structures [20, 25, 26].

Functionalization techniques for carbon nanomaterials are mainly categorized into covalent or non-covalent approaches [20]. The covalent functionalization of CNTs involves the direct attachment of heterogeneous-atom-containing functional groups onto the periphery of the surfaces of CNTs through various treatments involving acids, organic chemicals, oxidizing gases, or plasma [20, 25]. Covalent modifications of graphene are generally achieved by the synthesis of graphene oxides (GOs) from the chemical exfoliation of graphite by the modified Hummer's method to generate oxygen-containing functional groups dominated by hydroxyl, epoxy, and carboxylic groups [27]. Meanwhile, non-covalent functionalization methods utilize amphiphilic surfactants or polymers. Both of which are friendly to graphene layers on carbon nanomaterials and desired solvents or matrixes [16, 20, 28].

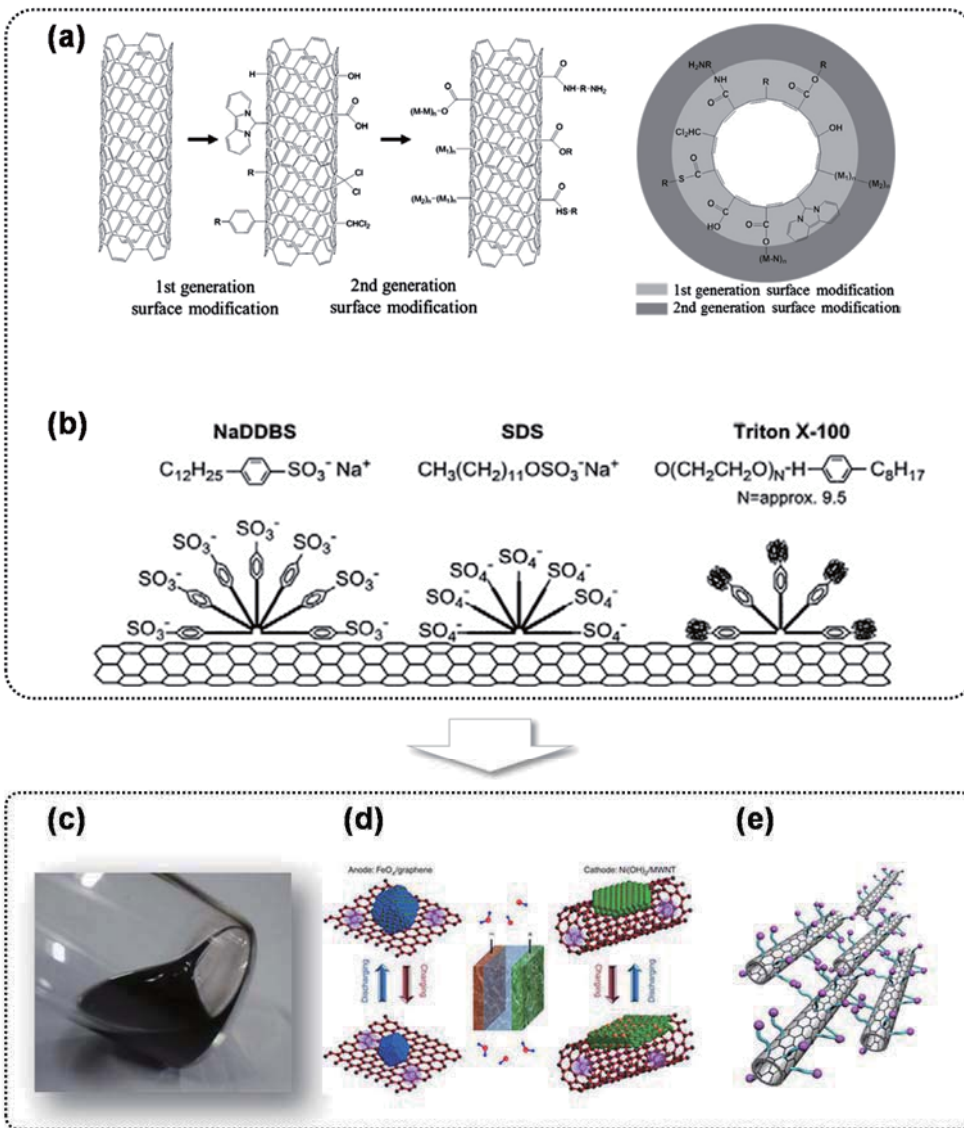


**Fig. 1.1.** Schematic representation showing (a) covalent [20] and (b) non-covalent [28] surface modifications for the applications of carbon nanomaterials, including (c) dispersions for processing and composites, (d) adsorption for energy and environmental devices [24], and (e) linking between the carbon nanomaterials for assembled structures.

### **1.1.2 Overview of the surface characterization methods of carbon nanomaterials**

For the proper utilization of these function groups for various applications of carbon nanomaterials, it is important to correlate the population of the functional groups and the resultant properties. Therefore, the qualification and quantitation of these surface functional groups have been thoroughly studied using various experimental techniques [17, 29-34].

#### **1.1.2.1 Fourier transformed infrared spectroscopy (FT-IR)**

FT-IR detects the vibration energies which originate from the stretching, bending, scissoring, wagging, twisting, or rocking of chemical bonds which absorb infrared light. This technique qualifies numerous types of functional groups with different vibration modes and is thereby particularly useful for the detection of 2G functionalization processes, including amidation or esterification (Fig. 1.2a) [17, 30]. However, the sensitivity of the infrared absorbance is lower than that of other techniques, as the carbon usually absorbs the entire infrared range, making the exact quantification of these groups unlikely.

#### **1.1.2.2 X-ray photoelectron spectroscopy (XPS)**

XPS is one of the most widely utilized and well-established techniques for the surface characterization of various materials, including metals, ceramics, and polymers. In an XPS analysis, the binding energies (BE) of photoelectrons emitted as a result of X-ray irradiation to the core electrons of the samples, which differ depending on the elements and their chemical states, are measured. This technique is useful for the quantitative elucidation of atomic compositions (apart from that of hydrogen) of functionalized carbon nanomaterials and of the chemical compositions of these atoms [31]. For example,

the bonding states (including carbon single/double bonds) of carbon atoms with heteroatoms can be estimated by deconvoluting the C1s spectra, which are generally located around a BE value of 285 eV (Fig. 1.2b) [32]. Deconvolution of the other XPS peaks of heteroatoms from functional groups (e.g., oxygen with BE ~ 530 eV or nitrogen with BE ~ 400 eV) may provide additional information about surface functionalities of carbon nanomaterials.

### **1.1.2.3 Thermogravimetric analysis (TGA) / Temperature programmed desorption (TPD)**

TGA and TPD utilize the different thermal stability levels of surface functional groups or physically attached moieties on the graphene layers of carbon nanomaterials [33]. For oxygen-containing groups, less thermally stable functional groups than graphene layers generally evolve into volatile gases such as carbon dioxide (CO<sub>2</sub>) or carbon monoxide (CO) with a thermal treatments at an elevated temperature, as shown in Fig. 1.2c [33, 34]. In terms of the measurement principles, TGA detects the weight loss of samples, while TPD senses the evolved gases from their thermal conductivity differences with a reference gas (H<sub>2</sub> or Ar) during a heat treatment. Both methods can use a mass-spectrometer to differentiate the evolved gas for the further qualification of functional groups such as carboxylic acids/anhydrous, lactones, phenols, and/or quinones (Fig. 1.2c) [33].

### **1.1.2.4 Other characterization methods**

While the three major characterization techniques described above directly qualify functional groups on carbon nanomaterials, other techniques provide evidence of the surface functionalization from the deviations in the surface properties (zeta potential,

inverse gas chromatography (IGC)) or of the physical states of the graphene layers (Raman spectroscopy or ultraviolet – visible – near-infrared spectroscopy (UV-Vis-NIR)) of the carbon nanomaterials [20].

The zeta potential effectively shows charges which originate from ionized functional groups on colloidal particles in dispersions of these materials under certain applied voltages [35]. The zeta potential additionally provides information about the dispersion state or stability of carbon nanomaterials in solvents from the amplitude of the potential ( $|\zeta|$ ; good and poor dispersion for  $|\zeta|$  and a voltage level higher and lower than 15 mV, respectively) [36].

IGC measures the Hansen solubility parameters of carbon nanomaterials possibly converted by certain surface modifications [37]. These parameters consists of the three major components which are dispersion ( $\delta_d$ ), polar ( $\delta_p$ ), and hydrogen-bonding ( $\delta_h$ ) interaction parameter. Surface modification methods usually increase  $\delta_p$  and  $\delta_h$ , which also implies that modification methods increase the dispersibility of carbon nanomaterials in aqueous or organic solvents.

The Raman spectra are generally recognized to provide a radial breathing mode (RBM; only valid for SWCNTs) and the degree of ordered graphitic structures (intensity ratio between the G and D peaks;  $I_G/I_D$ ), both of which most likely decrease with covalent surface functionalization with the generation of the defects on the graphene layers [38]. Similarly, UV-vis-NIR is useful for showing evidence of covalent functionalization by diminishing van-Hove singularities, a characteristic of  $\pi$ -conjugated CNT structures, after the modification process [39].

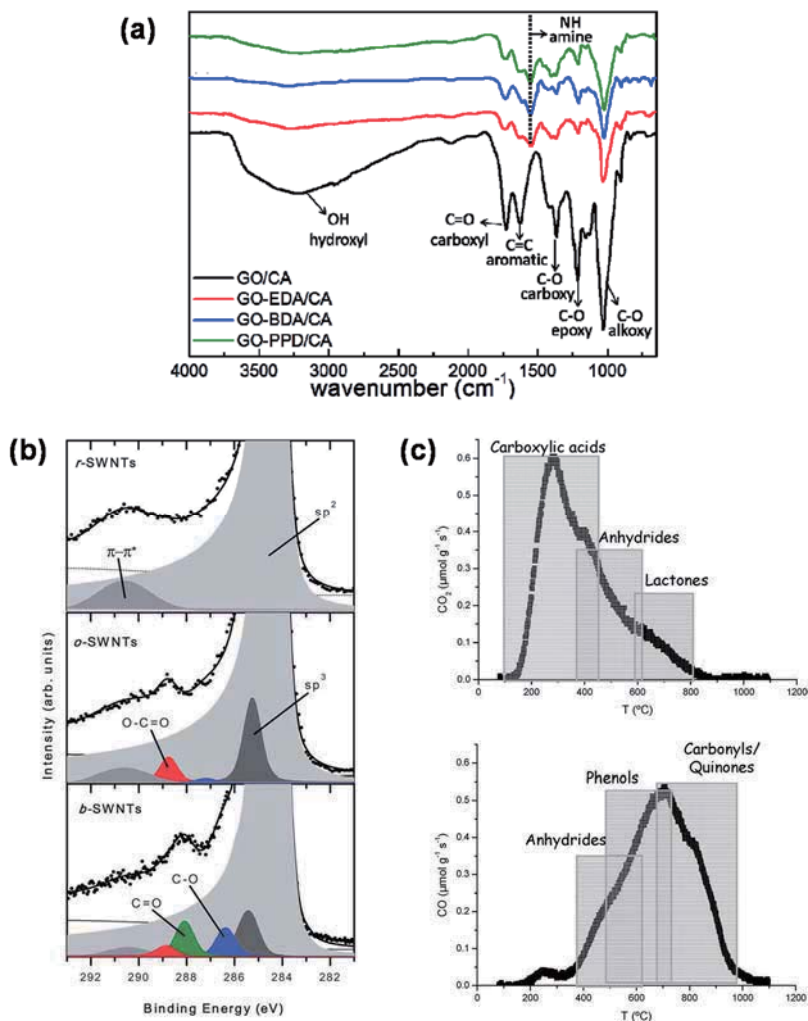


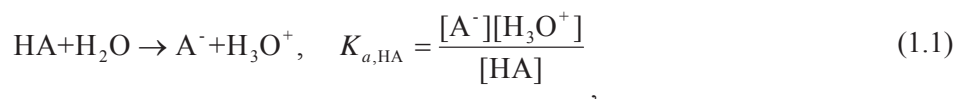
**Fig. 1.2.** Examples of the surface characterization techniques; (a) FT-IR spectra of composite GO membranes (GO/CA, GO-EDA/CA, GO-BDA/CA, GO-PPD/CA; CA, EDA, BDA, PPD specified cellulose acetate, ethylenediamine, buthlyenediamine, and *p*-phenylenediamine, respectively) [17]. (b) XPS C1s spectra of raw (r-SWNTs) and oxidized SWCNTs compared to a typical sample after an  $\text{HNO}_3$  (o-SWNTs)/NaOH (b-SWNTs) treatment [32], (c) mass-spectra followed by TGA/TPD of  $\text{CO}_2$  and CO with the decomposition of various types of oxygen functional groups [33].

## 1.2 Basics of titration methods for the surface characterization of carbon materials

Among the numerous characterization methods assessed thus far, the titration method is a powerful tool for elucidating populations of functional groups with acid or base characteristics on carbon surfaces. Titration methods can be generally categorized into two major types: the indirect and direct titration methods.

### 1.2.1 Basic concept of the acidity on carbon materials

To promote an accurate understanding of the basic principles of titration, I consider initially the concept of the acidity of carbon materials. As widely accepted, an acid and a base donate or accept a hydrogen ion (or a proton,  $H^+$ ), respectively, according to the definition by Johannes Brønsted and Thomas Lowry in 1923 (the Brønsted-Lowry definition) [40]. This definition states that the strength of an acid or a base can be readily defined in terms of the acid or base ionization constant  $K_a$  or  $K_b$ , respectively. The definition of the acid ionization constant for simple monoprotic acid (HA) molecules (single proton source) can be expressed as follows:



or simply as





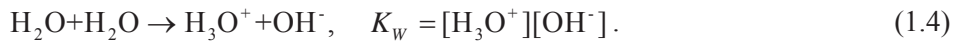
which is based on the Arrhenius definition. The ionized specie,  $A^-$ , is defined as the conjugated base of HA, as  $A^-$  can act as base via the equation



with the base ionization constant  $K_{b,A^-}$ . The relationship between  $K_{a,HA}$  and  $K_{b,A^-}$  is determined by combining equations (1.1) and (1.2), as

$$K_{a,HA} \cdot K_{b,A^-} = [H_3O^+][OH^-] = K_w, \quad (1.3)$$

where  $K_w$  is the self-ionization constant of water ( $\sim 10^{-14}$  at 25 °C) in the following reaction



The general standards for the determination of the strength of an acid or a base are recognized as  $pK_a$  or  $pK_b$ , respectively. These are defined as

$$\begin{aligned} pK_a &= -\log K_a \\ pK_b &= -\log K_b \end{aligned} \quad (1.5)$$

In this definition, an acid with a lower  $pK_a$  value implies a stronger one, and vice versa (Fig. 1.3) [40].

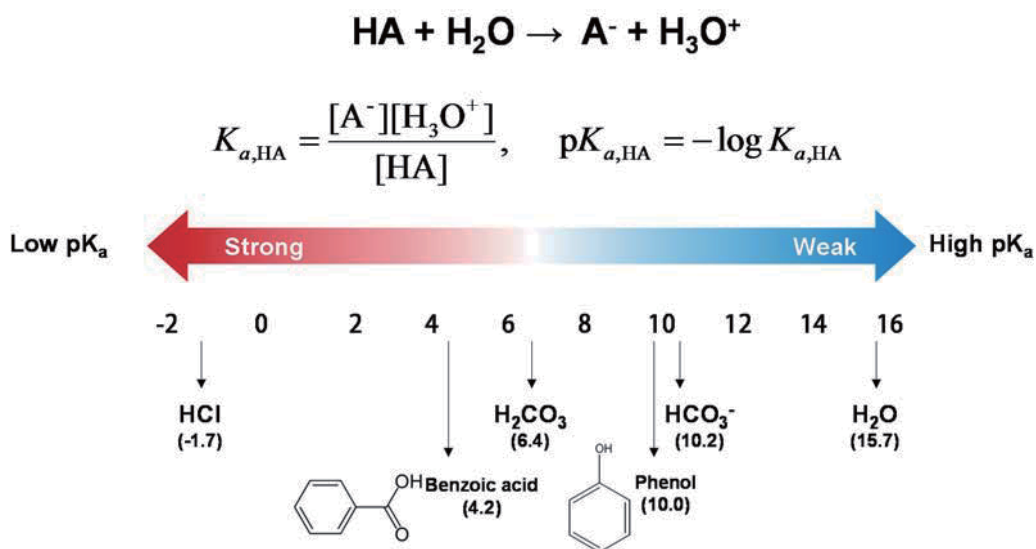


**Fig. 1.3.** Schematic representation showing the general expression for the acid strength of the acids.

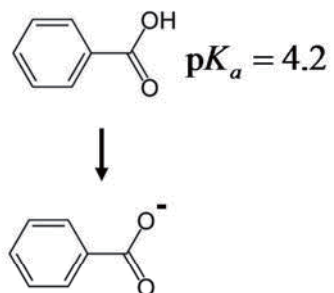
Diprotic acids such as terephthalic acid ( $pK_{a,1} = 3.5$ ,  $pK_{a,2} = 4.3$ ) or carbonic acid ( $H_2CO_3$ ;  $pK_{a,1} = 6.4$ ,  $pK_{a,2} = 10.3$ ) contain two proton sources with different  $pK_a$  values (Fig. 1.4b). The second proton in the diprotic acid does not undergo proton dissociation as readily as the first one due to the electric fields generated by the first deprotonation process. This results in a higher value of  $pK_{a,2}$  as compared to the value of  $pK_{a,1}$ . The addition of a proton source generally increases the number of  $pK_a$  acids with higher values than the former ones.

Moreover, defining the discrete  $pK_a$  values of each proton source in these multiprotic polymeric acids or carbons is impossible because the molecular weights or structures differ from molecule to molecule, thereby continuously distributing the population of the acidic groups. In this case, the acidity levels of these polymeric molecules or carbons are defined on the basis of  $pK_a$  distribution functions,  $f(pK_a)$  [41]. In this definition,  $f(pK_a)$  determines the quantity of the acidic groups lying within a specific  $pK_a$  range as

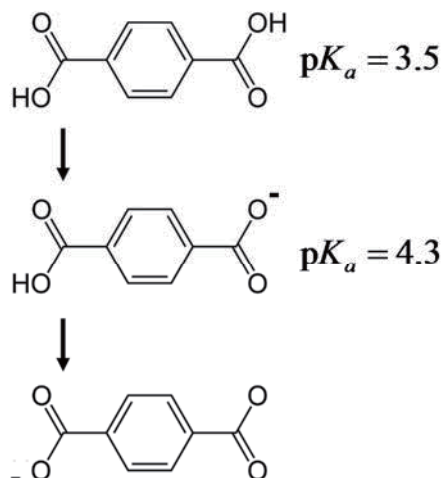
$$q_a = \int_{pK_{a,i}}^{pK_{a,f}} f(pK_a) dpK_a. \quad (1.6)$$

where  $q_a$  is the concentration [meq/g] of the acidic groups between  $pK_{a,i}$  and  $pK_{a,f}$ . In other words, the population of the acidities is obtained from the integrated area of  $f(pK_a)$  between  $pK_{a,i}$  and  $pK_{a,f}$  as shown in Fig. 1.4c. A detailed meaning of  $f(pK_a)$  for the description of the multiprotic acid from equation (1.6) will be given in **Chapter 4**.

**(a) Monoprotic acid  
(Benzoic acid)**



**(b) Diprotic acid  
(Terephthalic acid)**



**(c) Multiprotic acid (functionalized carbon materials)**

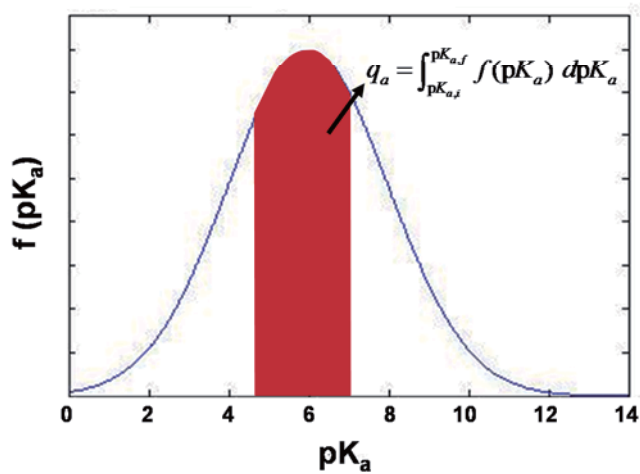


**Fig. 1.4.** Schematic representations showing the basic concept of acidity on (a) monoprotic, (b) diprotic, and (c) multiprotic acids.

### 1.2.2 Indirect titration method

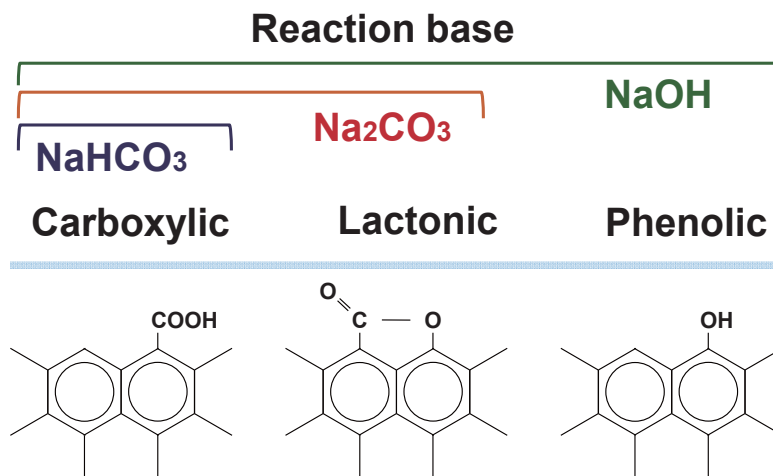
The titration method is a traditional quantification tool in chemistry for the determination of the unclear equivalence levels of specific components (defined as titrands) by a standard acid or base solution (defined as a titrant) with a clearly established concentration. The elemental principle for the determination of the number of functionalities on the surfaces of carbons by the indirect titration method involves the selective neutralization of acidic groups with different acid strengths. This technique is also called the Boehm titration method, named after Hanns-Peter Boehm, who first developed the method [42, 43]. Since the development of this useful technique, it has been utilized by numerous researchers for the surface characterization of various carbon materials, including activated carbons [42-48], carbon blacks [49, 50], carbon nanotubes (CNTs) [22, 25, 51-60], graphite oxides (GOs) [23, 61-65], and other allotropes of carbon [66-69].

As described in the previous section, a variety of functional groups can be generated on the surfaces of carbon materials during the functionalization process. Among these groups, Boehm suggested three which mainly affect the nature of the surfaces of carbon materials: the carboxylic, lactonic, and phenolic groups (Fig. 1.5a) [8]. These oxygen-containing functional groups have acidic characteristics with different strengths, which can be expressed in terms of  $pK_a$ . The  $pK_a$  values of these acidic groups are generally reported as ranging from 3 to 6 for the carboxylic group (the strongest group), 7 to 9 for the lactonic group, and 8 to 11 for the phenolic group (the weakest group) [70]. Therefore, each functional group interacts differently when neutralized by bases with different strengths in acid-base reactions in a process defined as 'selective neutralization'. Boehm suggested that sodium hydroxide ( $\text{NaOH}$ ;  $pK_b = -1.7$ ) neutralizes all acidic functional groups, sodium carbonate ( $\text{Na}_2\text{CO}_3$ ;  $pK_b = 3.8$ ) neutralizes the carboxylic and lactonic

groups, while sodium bicarbonate ( $\text{NaHCO}_3$ ;  $\text{p}K_b = 7.6$ ) neutralizes only the phenolic group [8]. These general bases ( $\text{NaOH}$ ,  $\text{Na}_2\text{CO}_3$ , and  $\text{NaHCO}_3$ ), typically used for selective neutralization as part of the titration process, are defined as reaction bases. The quantification of acidic groups (the equivalence of the acidic group as a percentage of the weight (simply defined as the concentration) [meq/g]) on carbon materials can be readily determined from the equivalence uptake of each reaction base by the target functional groups obtained from the general Boehm titration procedures.

The indirect titration procedure consists of three steps: 1) reaction, 2) filtration, and 3) titration (Fig. 1.5b) [42, 43]. Generally during these processes, carbon materials are neutralized with a reaction base (reaction step), with a subsequent filtration step. The filtered reaction base, of which the equivalence is reduced by the uptake, is then titrated by an acid titrant. Hereafter in the thesis, the reaction bases before and after the reaction with carbon materials are denoted as pre- and post-reaction bases, respectively. The post-reaction base is titrated by an acid titrant (typically  $\text{HCl}$ ) solution to determine the uptake of each pre-reaction base (the titration step). Therefore, the differences between the uptake equivalences of these post-reaction bases suggest the number or concentration of each functional group on carbon materials [49, 50]. In some cases, the post-reaction base is acidified by an excess of an acidic (typically  $\text{HCl}$ ) solution for the removal of any carbon dioxide ( $\text{CO}_2$ ) which may be dissolved in the reaction base and which may affect the titration results (acidification step) between the filtration and titration steps [50].

(a)



(b)

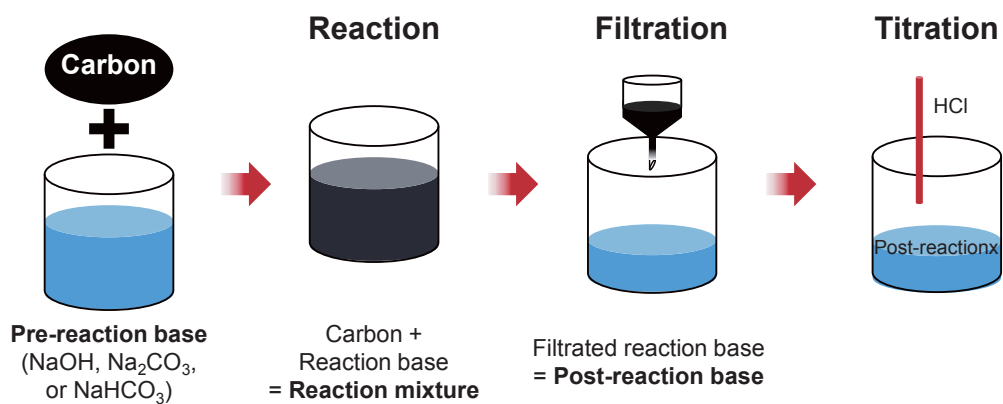


**Fig. 1.5.** Schematic representation of (a) the process of the indirect titration method for carbon materials, including the reaction, filtration and titration steps, and (b) the selective neutralization of the major functional groups and the reaction bases as part of the indirect titration method.

### 1.2.3 Direct titration method

The indirect titration method assume that the acidity levels of carbon materials are divided into three major groups, the carboxylic, lactonic, and phenolic groups, with definite  $pK_a$  values. On the other hand, the direct titration method assumes that these acidic groups are distributed within a specific  $pK_a$  boundary and that they can be defined using the  $pK_a$  distribution function described in the previous section [71, 72].

In contrast to the indirect titration method, carbon samples are simply mixed and agitated with a reference titrand, which is either an acid or a base, and then titrated with the titrant. The direct titration curves provide the proton binding isotherms,  $\theta(\text{pH})$ , which show the concentrations of the proton-dissociated acidic sites with respect to the pH during the titration experiments. This can be expressed as

$$\theta(\text{pH}) = \theta_0 + \int_{pK_{a,0}}^{pK_{a,f}} \frac{K_a}{[H^+] + K_a} f(pK_a) dpK_a, \quad (1.7)$$

where  $pK_{a,0}$  and  $pK_{a,f}$  denote the initial and final  $pK_a$  values of the desired  $pK_a$  window, respectively,  $\theta_0$  represents the concentrations of the proton-dissociated acidic groups with  $pK_a$  values outside of the  $pK_a$  range [71, 72]. Some studies have roughly estimated  $\theta(\text{pH})$  in the titration curve from the difference in the equivalence values between the reference titrant with and without the agitation of the carbon samples [35]. However,  $\theta(\text{pH})$  is accurately calculated from the proton balance equation [72] or by the modified Henderson-Hasselbalch equation, which will be described in **Chapter 4** in detail.

$f(pK_a)$  can then be calculated by solving the integral equation (1.7) of which the analytic solution [73] was established and can be expressed by



$$\begin{aligned}
f(pK_a) &= \left[ \sum_{i=0}^n (-1)^i \frac{\pi^{2i}}{(2i+1)!(\ln 10)^{2i}} \frac{\partial^{2i+1} \theta(\text{pH})}{\partial (\text{pH})^{2i+1}} \right]_{\text{pH}=\text{p}K_a} \\
&= \left[ \frac{\partial \theta(\text{pH})}{\partial \text{pH}} - \frac{\pi^2}{3!(\ln 10)^2} \frac{\partial^3 \theta(\text{pH})}{\partial (\text{pH})^3} + \frac{\pi^4}{5!(\ln 10)^4} \frac{\partial^5 \theta(\text{pH})}{\partial (\text{pH})^5} - \dots \right]_{\text{pH}=\text{p}K_a}
\end{aligned}
\tag{1.8}$$

The direct titration method has been widely utilized for the measurement for  $f(pK_a)$  of various carbon materials ranging from conventional carbons (e.g., carbon blacks, activated carbons) [71-75] to carbon nanomaterials (e.g., CNTs, GOs) [35, 76-83] and for other types of carbonaceous materials [84] with different functionalization methods to show the populations of the acidities of these carbons.

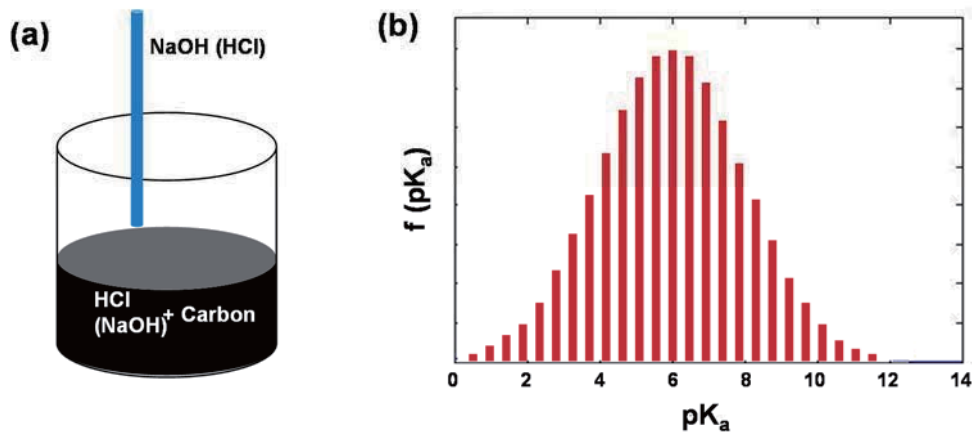


**Fig. 1.6.** Schematic representation of (a) the process of direct titration method for carbon materials, and (b) the observable  $pK_a$  distribution function.

## **1.3 State-of-the-art works on titration methods for carbon nanomaterials**

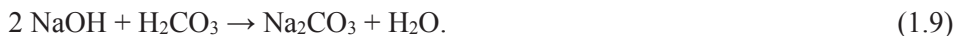
### **1.3.1 Issues associated with indirect titration methods**

#### **1.3.1.1 Dissolution of acidic moieties**

Though the basic concept of the indirect titration method for the surface quantification of carbon materials is simple, the reliability and reproducibility of the results cannot be guaranteed unless all of the experimental steps are conducted with great care. For this purpose, several researchers have tried to generalize the specific procedures of indirect titration, in which small experimental errors can induce enormous discrepancies. The most troublesome factor pertaining to the indirect titration method is the dissolution of acidic elements such as carbon dioxide in air [50], or acidic carbon compounds generated during the functionalization of carbon nanomaterials [55]. These moieties are easily dissolved in the reaction bases throughout the indirect titration process (Fig. 1.5b), thus affecting the titration results [50, 55].

##### **1.3.1.1.1 Carbon dioxide (CO<sub>2</sub>)**

Carbon dioxide exists at a rate of only 0.03 % in atmospheric air, but it significantly affects the titration of both pre- and post-reaction bases by providing H<sub>2</sub>CO<sub>3</sub> and distorting the titration curves when it is dissolved into a reaction base during indirect titration procedures. CO<sub>2</sub>-induced H<sub>2</sub>CO<sub>3</sub> easily reacts, especially with the reaction base NaOH to generate Na<sub>2</sub>CO<sub>3</sub> by the following reaction [85, 86]:



The dissolved CO<sub>2</sub> can only be extracted out to the atmosphere with the addition of a strong acid, HCl, by



with vigorous stirring and a heat treatment or N<sub>2</sub> degasification to facilitate the reaction,



for the complete and rapid removal of CO<sub>2</sub> in an acidic condition [43, 50, 87-89]. Therefore, for the acidification step, an excess amount of HCl solution has typically been inserted between the filtration and titration steps in the indirect titration method.

Recently, Goertzen et al. tried to standardize this acidification step to find an optimized means of removing CO<sub>2</sub> and determining the end point of the titration process for the proper utilization of the indirect titration method [50]. Various post-treatments of acidified reaction bases, including degasification with an inert gas (N<sub>2</sub>, Ar), putting them into an N<sub>2</sub>-filled glove box, heating them, and refluxing them have been attempted. Among these methods, degasification with an inert gas is considered to be the most efficient method for the rapid exclusion of CO<sub>2</sub> from a reaction base (Fig. 1.7) [50]. The titration curves of reaction bases, NaOH, show the two inflection points, implying the dissolution of H<sub>2</sub>CO<sub>3</sub> in the reaction bases (Fig. 1.7d). After the continuous purging of N<sub>2</sub> into the acidified reaction bases (Fig. 1.7b), the titration curves became straight, with a pH range of 4 to 10, implying the gradual removal of H<sub>2</sub>CO<sub>3</sub> from the reaction bases. The standardized acidification process is also used for the surface characterization of carbon blacks given its high precision and good reproducibility. Though the suggested

standardization process may provide a well-organized optimized procedure for indirect titration, it is still too complicated and inaccessible to be easily adopted. Moreover, there still remained two distinct inflection points even after the sufficient degasification of the acidified reaction bases (Figs. 1.7a – 1.7c) indicating the preservation of irremovable  $\text{H}_2\text{CO}_3$ .

The research on the removal of  $\text{CO}_2$  through an acidification process may lack fundamental consideration of the effects of  $\text{CO}_2$  on the titration of the reaction bases. Therefore, a critical revisit to move beyond the conventional acidification process is necessary.

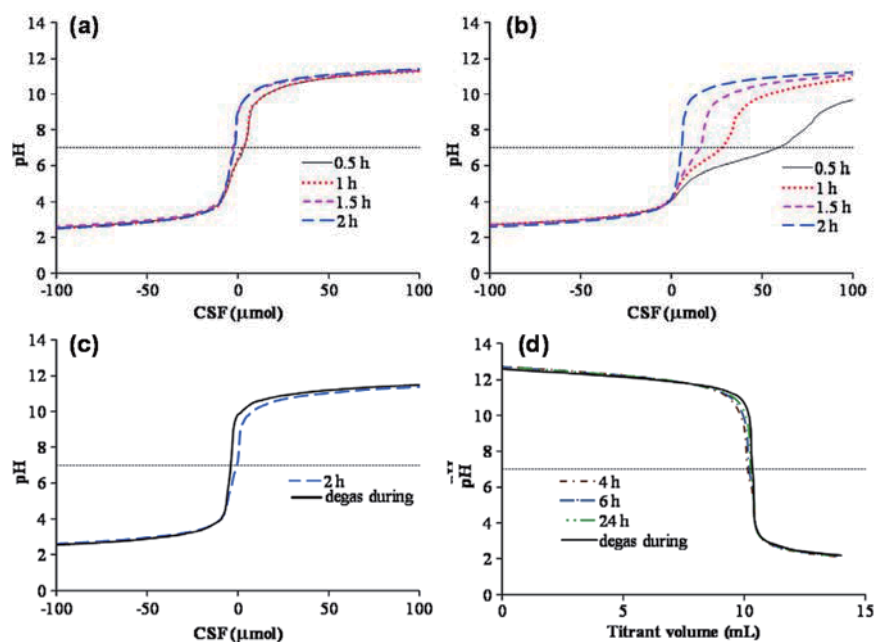


**Fig.1.7.** Titration curves (plotted as amount of carbon surface functionality) for different reaction bases after acidifications including (a)  $\text{NaHCO}_3$ , (b)  $\text{Na}_2\text{CO}_3$ , and (c)  $\text{NaOH}$ . (d) Titration curves of unacidified  $\text{NaOH}$  [50].

### 1.3.1.1.2 Acidic carbon compounds (ACCs)

When CNTs are acid-oxidized, the side walls of CNTs concurrently disintegrate to a certain extent to yield acidic carbon compounds (ACCs) [25, 32, 55, 90-93] (Fig. 1.8a). These groups are easily adsorbed back onto the surfaces of CNTs by  $\pi$ - $\pi$  interactions and are reported to affect the chemical and physical properties of CNTs. In applications of CNTs, ACCs may play a key role in the dispersions of CNTs, like surfactants. For example, Sung *et al.* reported that ACCs on oxidized SWCNTs make the CNTs more dispersible in solvents and enhance the electrical performances of the resultant transparent thin films by achieving compact packing of the individual CNTs [93]. On the other hand, ACCs are necessarily removed by thorough washing with a basic aqueous solution to increase the reactivity of CNTs with organic molecules [25, 57, 91, 94]. In addition, the functional groups of the ACCs can influence the interfacial interaction between CNTs and matrices [25] when fabricated to composites, and hence the mechanical performance of the given composite, although it is not clear at this stage whether it would be a positive or negative enhancement. Similar acidic fragmented moieties were also observed in carbon nanomaterials such as biochars or GOs [69]. Under such circumstances, it becomes very important to confirm the number of acidic groups on both the carbon nanomaterials themselves and on the ACCs separately.

Recently, Wang *et al.* attempted to measure the functionality of ACCs (termed fulvic acids in this work) present in a CNT sample using the indirect titration method [55]. In their attempt, the post-reaction base, NaOH, of nitric acid-oxidized MWCNTs, was titrated with an aqueous HCl solution both before and after the elimination of ACCs. They obtained typical titration curves before (Fig. 1.8b) and after (Fig. 1.8c) the removal of ACCs from the oxidized CNTs for more than 3 h. The most conspicuous difference between the two titration curves was the positions of the end points (EPs). Distinct EPs

at pH levels of 8 and 5 were obtained before ACC removal (Fig. 1.8b), but one EP at pH 7 (Fig. 1.8c) was obtained after ACC removal. The authors attributed the two EPs in this curve to the presence of sodium phenolate and sodium carboxylate, formed by the neutralization of the phenolic and carboxylic groups of the ACCs in the reaction base. The total acidity of the ACCs and acid-oxidized MWCNTs appeared to be determined by the difference between the theoretical equivalence of the reaction base and the equivalence at the first EP at a pH of 8 in the indirect titration curve of MWCNTs with ACCs not removed. Similarly, the acidity of pure MWCNTs appeared to be determined by the difference between the theoretical equivalence of the reaction base and the equivalence at the EP at pH 7 in the corresponding titration curve. The difference between the acidity of MWCNTs with and without the removal of ACC should be, consequently, attributed to the acidic functionalities of the ACCs present [55].

However, as shown in Fig. 1.8e, the oxidation time is not correlated with the quantity of ACC functionalities, which is contrary to what one may expect. Moreover, it was shown that CO<sub>2</sub> affects the titration curves similarly [50] to the manner in which they are affected in the previous section (Fig. 1.7d). Hence, the interpretation of the titration curve may be misleading if the CO<sub>2</sub> effects are not carefully considered.

Along with the CO<sub>2</sub> effects, phenolic or carboxylic groups on the ACCs will indeed affect the titration behaviors of the post-reaction bases, as they are easily dissolved in a basic solution [50, 55]. However, methods to elucidate ACC effects have scarcely been reported thus far. More importantly, a determination of the acidic properties of ACCs may promote a better understanding of the roles of ACCs on various applications of carbon nanomaterials, including those involving CNT dispersions or reaction chemistry.

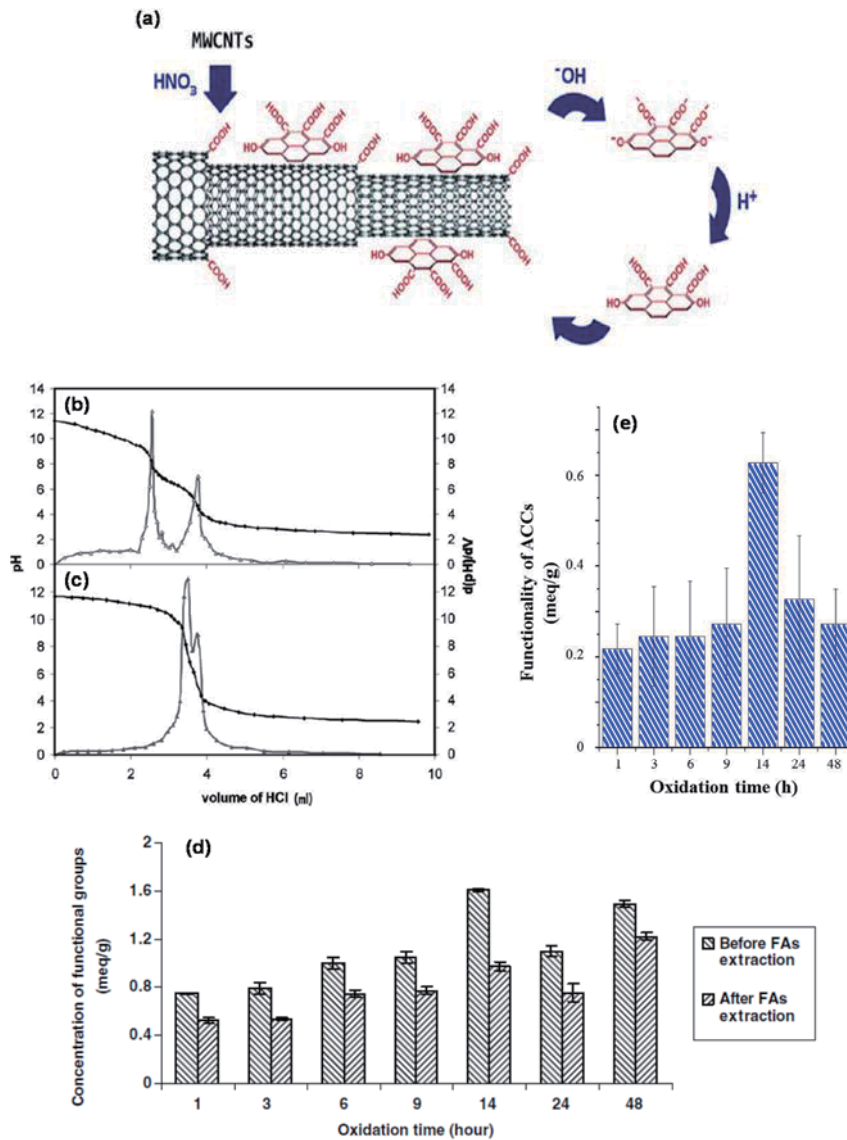


**Fig. 1.8.** (a) Schematic representation of the formation of ACCs [55]. Indirect titration curves and the first-order derivatives for the NaOH post-reaction bases of MWCNTs oxidized with nitric acid for more than 3 hours, (b) before, and (c) after the removal of ACCs. (d) The resultant concentrations of acidic groups on MWCNTs before and after ACC removal [55]. (e) The ACC functionalities derived from (d).

### **1.3.1.2 Procedure**

As discussed in section 1.2.2, the procedure of indirect titration includes many steps, which may be quite complicated compared to those of the direct titration method and the other surface characterization techniques [42, 43, 72]. These procedures should be repeated for three types of reaction bases (NaOH, Na<sub>2</sub>CO<sub>3</sub>, and NaHCO<sub>3</sub>) with sufficient reproducibility testing to guarantee the precision and reliance of the titration results. These complicated procedures themselves are the major drawbacks of the indirect titration method.

Moreover, filtration steps for highly oxidized CNTs individually dispersed in a reaction base [25, 95] or GO with a two-dimensional nanostructure [96] are difficult or even impossible. These carbon nanomaterials may serve as the secondary filters with nanopores and inhibit the filtration of the reaction mixture, which is an essential step in the indirect titration process. In these cases, the surface characterization of carbon nanomaterials using indirect titration becomes unavailable.

### **1.3.1.3 Adoption of indirect titration methods**

#### **1.3.1.3.1 Adsorption property**

Surface functional groups promote the adsorption of various molecules or ions by increasing the ion-exchange capability of the carbon surface, thereby making the carbon materials efficient candidates for the energy and environmental devices, including secondary batteries, supercapacitors [24, 59], pollutants filters or adsorbers [23, 48, 63], or catalyst supports [97]. The indirect titration technique has been applied in an effort to understand the roles of various functional groups on the adsorption properties of carbon materials [23, 48, 59, 63].

For example, Carrasco-Marin *et al.* demonstrated the effects of acidic or basic groups on



activated carbons on the adsorption properties of water [45]. In this work, the numbers of water-absorbable sites ( $N_{ao}$ ) and oxygen functional groups ( $m(\text{carb})$ ,  $m(\text{lac})$ ,  $m(\text{phe})$ , and  $m(\text{base})$ ) were correlated to investigate the number of water molecules ( $w_i$ ;  $i$  ranges from 1 to 4) interacting with each functional group (Fig. 1.9a). The results showed that *ca.* 3 molecules interacted with the carboxylic and lactonic groups, while *ca.* 1.5 molecules interacted with the phenolic and basic groups.

### 1.3.1.3.2 Reaction chemistry

Functionalized carbon nanomaterials have also been linked to various molecules or chemicals (2G functionalization) to enhance the dispersion ability and stability of carbons in proper solvents or matrixes to simplify their processing steps and to prepare composites [25, 98-104]. 2G functionalization was also applied as a type of linkage between carbon structures to improve the mechanical or electrical performances of carbon nanomaterial assemblies or composites [25, 57, 105].

Indirect titration methods were also used to determine the efficiency of the 2G functionalization of carbon nanomaterials. Worsley *et al.* attached octadecylamine (ODA) covalently to carboxylic groups on SWCNTs to make them dispersible in tetrahydrofuran [25]. The degree of ODA loading was determined from the difference between the numbers of carboxylic groups before and after the DCC (1,3-dicyclohexylcarbodiimide) coupling amidation reaction (Fig. 1.9b). A similar investigation was reported for the covalent bonding of *n*-butylamine to carboxylic groups on MWCNTs by means of EDAC (1-ethyl-3-(3-dimethylaminopropyl) carbodiimide hydrochloride) coupling amidation (Fig. 1.9c) [57]. The covalent reactivity of carboxylated MWCNTs was determined to range from 58 to 78 % depending on the oxidation degree of the MWCNTs.

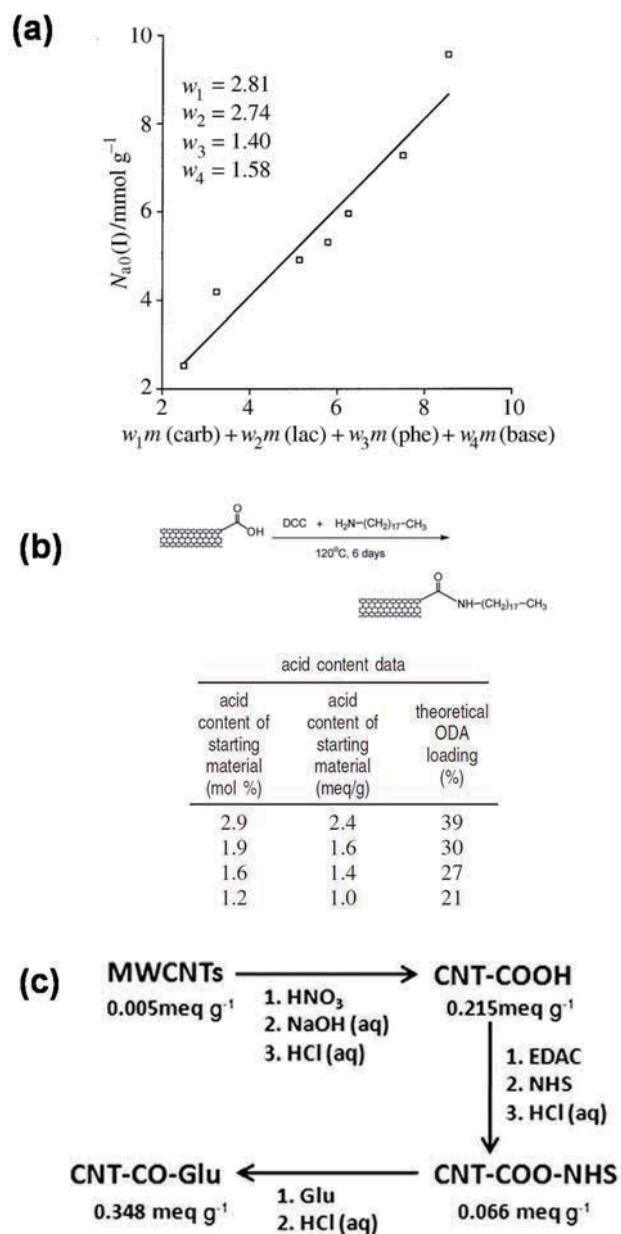


**Fig. 1.9.** Examples of the utilization of the indirect titration method for (a) an investigation of the water-adsorption sites of activated carbons [45], (b, c) the 2G functionalization of CNTs ((b) and (c) from two earlier works ([25] [57], respectively)).

### **1.3.2 Issue on direct titration methods**

#### **1.3.2.1 Procedure**

Compared to the indirect titration method, direct titration is simpler in that the carbon samples are mixed with the titrant and simply titrated with the proper titrants. While indirect titration provides practical information about the acidic groups on carbon materials, as discussed in the previous section, direct titration only determines the population of the acidities on the acidic groups in the given  $pK_a$  windows [42, 72]. It is useful to discern the fraction of strong or weak acids ( $pK_a$  lower or higher than 7, respectively) to improve the understanding of the function of carbon nanomaterials [77, 80, 83, 84, 106-108]. However, the practical roles of these functional groups in applications of carbon materials are rarely proposed in the literature.

#### **1.3.2.2 Adoption of direct titration methods**

##### **1.3.2.2.1 Practical functional groups calculation**

Only few works have evaluated practical functional groups such as carboxylic, lactonic, and phenolic groups with direct titration methods. For example, trials were conducted for a comparison of the direct titration results of activated carbons to the indirect titration results and to investigate the concentrations of the resulting major functional groups [72]. For this purpose, the pH values of the reaction mixtures of carbon samples and reaction bases were measured before the filtration steps in the indirect titration. These pH values then replaced the proton binding isotherms of the activated carbons obtained from direct titration measurements to determine the concentrations of proton-dissociated sites of the carbon samples in the reaction mixtures. The equivalence of the ionized functional groups were assumed to be identical to the uptake of each reaction base upon indirect titration [72].

#### 1.3.2.2.2 Dispersion property

Oxygen-containing functional groups tune the surfaces of the carbon materials to exhibit hydrophilic properties and make them more dispersible in aqueous or numerous organic solvents. Recently, a detailed investigation of the roles of functional groups on the dispersion properties of carbon nanomaterials was reported [35]. In this work, the surface charges on GO sheets as a function of the pH of the dispersion were calculated based on proton binding isotherms from direct titration methods and then compared to the corresponding zeta potentials to understand the dispersion properties of GO and reduced GO (r-GO) in water with respect to the pH (Fig. 1.10). The pH range at which GO (above pH 4) and r-GO (above pH 8) become dispersible was investigated on the basis of their  $pK_a$  distribution functions. The wider range of the dispersible pH range of GO relative to that of r-GO was attributed to more acidic groups ( $pK_a$  4.3, 6.6 and 9.0) by a large amount, though this amount was diminished after the chemical reduction of GO [35].

Though the works introduced in the previous and present sections concentrated on investigations of the actual functions of acidic groups on carbons as defined by the  $pK_a$  distribution from direct titrations, additional pH measuring procedures for the dispersions of carbon samples were necessary, and these were accomplished by putting the pH value into the proton binding isotherms. These proposed methods may be only adopted under limited experimental conditions in carbon material applications; however, the universal adoption of a method applicable to a wider range of environments was unavailable.

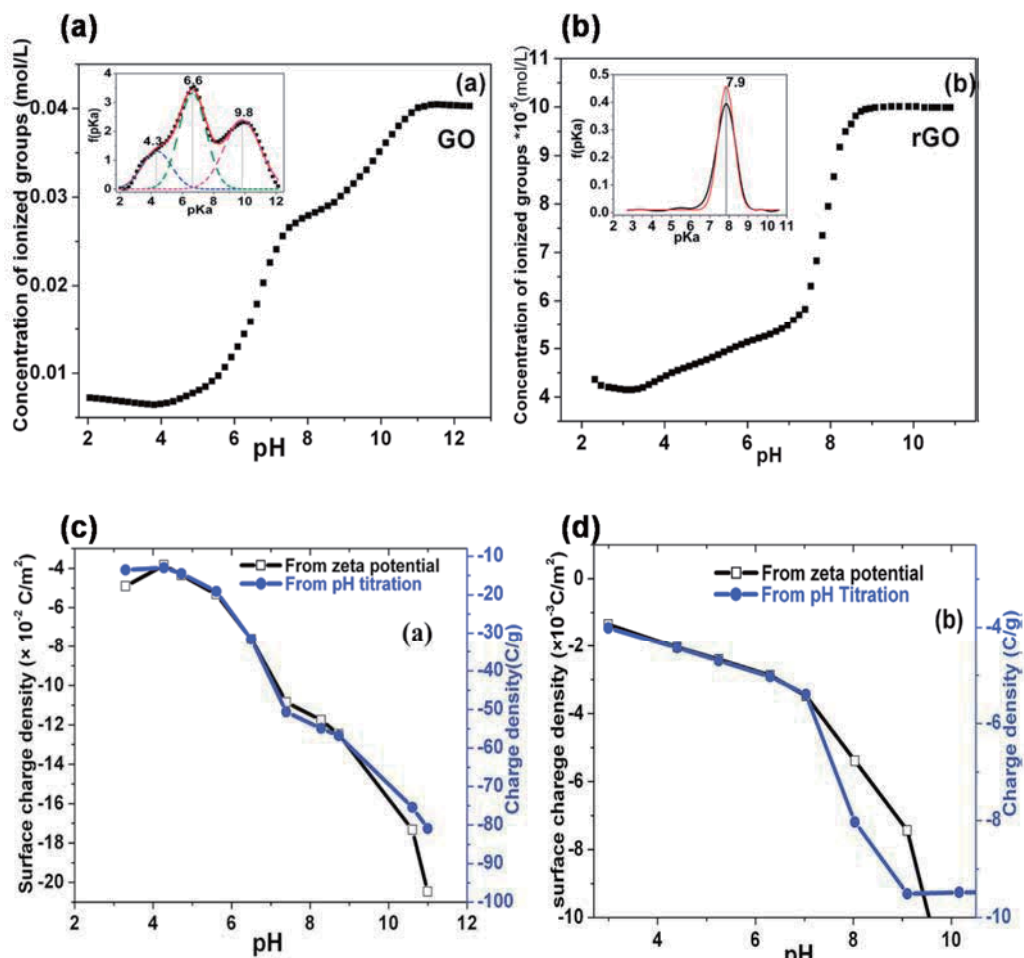


**Fig. 1.10.** Concentration of the ionized group or the proton binding isotherm as a function of the pH for (a) GO and (b) r-GO. The inset shows the  $pK_a$  distribution of the acid groups. The surface charge density [ $\text{C/m}^2$ ] for (c) GO and (d) r-GO calculated from the zeta potential (black lines) as a function of the pH, and the charge density [ $\text{C/g}$ ] as a function of the pH as calculated from the direct titration curve (blue lines) [35].

## 1.4 Aim and scope of this research

Considering the state-of-the-art works described above, the aim of this study is to develop a titration methodology for the surface characterization of carbon nanomaterials penetrating the concepts of indirect and direct titrations. This titration methodology provides practical information about the functional groups and their essential roles in applications of carbon nanomaterials

### 1.4.1 Development of universal titration equation

A universal titration equation based on the modification of general Henderson-Hasselbalch equation was developed. This will be discussed in **Chapter 2**. This equation display titration behaviors of every acid or base regardless of the number of the proton donating or accepting sites or the type of titrant or titrand in the aqueous titration system, thereby being universally applicable to both indirect and direct titration results.

### 1.4.2 Standardization of indirect titration methods

The universal titration equation was first applied in an indirect titration system in which only mono- or diprotic acids and bases are present to prove the validity of the developed methodology. In **Chapter 2**, the effects of phenolic and carboxylic groups of ACCs on the indirect titration curves will be discussed using simple model ACCs. Subsequently, the CO<sub>2</sub> effects on the titration behaviors of the reaction bases (NaOH, Na<sub>2</sub>CO<sub>3</sub>, and NaHCO<sub>3</sub>) in the indirect titration method will be fundamentally described in **Chapter 3**. The proposed standardization process makes the procedures of indirect titration much simpler, with precise and accurate results.

### **1.4.3 Development of one-pot titration methodology**

A one-pot titration methodology, which presents the practical information on the acidic functional groups from  $pK_a$  distribution function of carbon nanomaterials will be developed in **Chapter 4**. For this purpose, the universal titration equation will be applied to nitric acid-oxidized MWCNTs, which are multiprotic acids. The one-pot titration methodology will be extensively utilized with mixed acid-oxidized MWCNTs and GOs to investigate the functions of the acidic groups in applications of carbon nanomaterials, including the dispersion and reaction chemistry. These areas will be presented in **Chapter 5** and **Chapter 6**, respectively.

## 1.5 References

- [1] Inagaki M, Kang F, *Fundamental Science of Carbon Materials in Materials Science and Engineering of Carbon: Fundamentals* (2<sup>nd</sup> Ed.), Tsinghua University Press, Beijing (2014) 17-217.
- [2] De Volder MFL, Tawfick SH, Baughman RH, Hart AJ, *Science*, 339 (2013) 535-9.
- [3] Geim AK, Novoselov KS, *Nat Mater*, 6 (2007) 183-91.
- [4] Bianco A, Cheng HM, Enoki T, Gogotsi Y, Hurt RH, Koratkar N, et al., *Carbon*, 65 (2013) 1-6.
- [5] Novoselov KS, Geim AK, Morozov SV, Jiang D, Zhang Y, Dubonos SV, et al., *Science*, 306 (2004) 666-9.
- [6] Ponomarenko LA, Schedin F, Katsnelson MI, Yang R, Hill EW, Novoselov KS, et al., *Science*, 320 (2008) 356-8.
- [7] Li XL, Wang XR, Zhang L, Lee SW, Dai HJ, *Science*, 319 (2008) 1229-32.
- [8] Reina A, Jia XT, Ho J, Nezich D, Son HB, Bulovic V, et al., *Nano Lett*, 9 (2009) 30-5.
- [9] Endo M, Takeuchi K, Igarashi S, Kobori K, Shiraishi M, Kroto HW, *J Phys Chem Solids*, 54 (1993) 1841-8.
- [10] Liu HP, Nishide D, Tanaka T, Kataura H, *Nat Commun*, 2 (2011) 309-1-8.
- [11] Li HJ, Lu WG, Li JJ, Bai XD, Gu CZ, *Phys Rev Lett*, 95 (2005) 086601-1-4.
- [12] Tasis D, Tagmatarchis N, Bianco A, Prato M, *Chem Rev*, 106 (2006) 1105-36.
- [13] Guadagno L, De Vivo B, Di Bartolomeo A, Lamberti P, Sorrentino A, Tucci V, et al., *Carbon*, 49 (2011) 1919-30.
- [14] Boncel S, Sundaram RM, Windle AH, Koziol KKK, *Acs Nano*, 5 (2011) 9339-44.
- [15] Cong HP, Ren XC, Wang P, Yu SH, *Sci Rep*, 2 (2012) 613-1-6.
- [16] Berhan L, Yi YB, Sastry AM, Munoz E, Selvidge M, Baughman R, *J Appl Phys*, 95 (2004) 4335-45.
- [17] Hung WS, Tsou CH, De Guzman M, An QF, Liu YL, Zhang YM, et al., *Chem Mater*, 26 (2014) 2983-90.



- [18] Khanderi J, Hoffmann RC, Schneider JJ, *Nanoscale*, 2 (2010) 613-22.
- [19] Li N, Zhang Q, Gao S, Song Q, Huang R, Wang L, et al., *Sci Rep*, 3 (2013) 1604-1-6.
- [20] Kim SW, Kim T, Kim YS, Choi HS, Lim HJ, Yang SJ, et al., *Carbon*, 50 (2012) 3-33.
- [21] O'Connor I, Hayden H, Coleman JN, Gun'ko YK, *Small*, 5 (2009) 466-9.
- [22] Azadi P, Farnood R, Meier E, *J Phys Chem A*, 114 (2010) 3962-8.
- [23] Garcia-Gallastegui A, Iruretagoyena D, Gouvea V, Mokhtar M, Asiri AM, Basahel SN, et al., *Chem Mater*, 24 (2012) 4531-9.
- [24] Wang HL, Liang YY, Gong M, Li YG, Chang W, Mefford T, et al., *Nat Commun*, 3 (2012) 917-1-8
- [25] Worsley KA, Kalinina I, Bekyarova E, Haddon RC, *Journal of the American Chemical Society*, 131 (2009) 18153-8.
- [26] Frehill F, Vos JG, Benrezzak S, Koos AA, Konya Z, Ruther MG, et al., *J Am Chem Soc*, 124 (2002) 13694-5.
- [27] Dreyer DR, Park S, Bielawski CW, Ruoff RS, *Chem Soc Rev*, 39 (2010) 228-40.
- [28] Islam MF, Rojas E, Bergey DM, Johnson AT, Yodh AG, *Nano Lett*, 3 (2003) 269-73.
- [29] Wepasnick KA, Smith BA, Bitter JL, Fairbrother DH, *Anal Bioanal Chem*, 396 (2010) 1003-14.
- [30] Hu H, Zhao B, Hamon MA, Kamaras K, Itkis ME, Haddon RC, *J Am Chem Soc*, 125 (2003) 14893-900.
- [31] Estrade-Szwarckopf H, *Carbon*, 42 (2004) 1713-21.
- [32] Flavin K, Kopf I, Del Canto E, Navio C, Bittencourt C, Giordani S, *J Mater Chem*, 21 (2011) 17881-7.
- [33] Figueiredo JL, Pereira MFR, *Catal Today*, 150 (2010) 2-7.
- [34] Yang SJ, Kim T, Jung H, Park CR, *Carbon*, 53 (2013) 73-80.
- [35] Konkana B, Vasudevan S, *J Phys Chem Lett*, 3 (2012) 867-72.
- [36] Sun Z, Nicolosi V, Rickard D, Bergin SD, Aherne D, Coleman JN, *J Phys Chem C*, 112 (2008) 10692-9.

- [37] Lim HJ, Lee K, Cho YS, Kim YS, Kim T, Park CR, *Phys Chem Chem Phys*, 16 (2014) 17466-72.
- [38] Marcoux PR, Schreiber J, Batail P, Lefrant S, Renouard J, Jacob G, et al., *Phys Chem Chem Phys*, 4 (2002) 2278-85.
- [39] O'Connell MJ, Bachilo SM, Huffman CB, Moore VC, Strano MS, Haroz EH, et al., *Science*, 297 (2002) 593-6.
- [40] Oxtoby DW, Gillis HP, Nachtrieb NH, *Acid-base Equilibria in Principles of Modern Chemistry (5<sup>th</sup> Ed.)*, Thomson Learning, Inc, Washington, D.C. (2002) 317-60.
- [41] Strelko V, Malik DJ, Streat M, *Carbon*, 40 (2002) 95-104.
- [42] Boehm HP, Heck W, Sappok R, Diehl E, *Angew Chem Int Edit*, 3 (1964) 669-77.
- [43] Boehm HP, *Carbon*, 32 (1994) 759-69.
- [44] Moreno-Castilla C, Carrasco-Marin F, Mueden A, *Carbon*, 35 (1997) 1619-26.
- [45] Carrasco-Marin F, Mueden A, Centeno TA, Stoeckli F, Moreno-Castilla C, *J Chem Soc Faraday T*, 93 (1997) 2211-5.
- [46] Demiral H, Demiral I, Karabacakoglu B, Tumsek F, *Chem Eng Res Des*, 89 (2011) 206-13.
- [47] Xiao B, Thomas KM, *Langmuir*, 21 (2005) 3892-902.
- [48] Fletcher AJ, Uygur Y, Thomas KM, *J Phys Chem C*, 111 (2007) 8349-59.
- [49] Oickle AM, Goertzen SL, Hopper KR, Abdalla YO, Andreas HA, *Carbon*, 48 (2010) 3313-22.
- [50] Goertzen SL, Theriault KD, Oickle AM, Tarasuk AC, Andreas HA, *Carbon*, 48 (2010) 1252-61.
- [51] Le Leuch LM, Bandosz TJ, *Carbon*, 45 (2007) 568-78.
- [52] Menzel R, Lee A, Bismarck A, Shaffer MSP, *Langmuir*, 25 (2009) 8340-8.
- [53] Horikawa T, Kitakaze Y, Sekida T, Hayashi J, Katoh M, *Bioresource Technol*, 101 (2010) 3964-9.
- [54] Hulicova-Jurcakova D, Seredych M, Jin YG, Lu GQ, Bandosz TJ, *Carbon*, 48 (2010) 1767-78.

- [55] Wang ZW, Shirley MD, Meikle ST, Whitby RLD, Mikhalovsky SV, Carbon, 47 (2009) 73-9.
- [56] Moaseri E, Baniadam M, Maghrebi M, Karimi M, Chem Phys Lett, 555 (2013) 164-7.
- [57] Wang Z, Korobeinyk A, Whitby RLD, Meikle ST, Mikhalovsky SV, Acquah SFA, et al., Carbon, 48 (2010) 916-8.
- [58] Hanelt S, Orts-Gil G, Friedrich JF, Meyer-Plath A, Carbon, 49 (2011) 2978-88.
- [59] Canete-Rosales P, Ortega V, Alvarez-Lueje A, Bollo S, Gonzalez M, Anson A, et al., Electrochim Acta, 62 (2012) 163-71.
- [60] Doroodmand MM, Shafie Z, Sensor Actuat a-Phys, 207 (2014) 32-8.
- [61] Pan N, Guan DB, Yang YT, Huang ZL, Wang RB, Jin YD, et al., Chem Eng J, 236 (2014) 471-9.
- [62] Li M, Liu C, Xie Y, Cao H, Zhao H, Zhang Yi, Carbon, 66 (2014) 302-11.
- [63] Machida M, Mochimaru T, Tatsumoto H, Carbon, 44 (2006) 2681-8.
- [64] Whitby RLD, Korobeinyk A, Glevatska KV, Carbon, 49 (2011) 722-5.
- [65] Moghaddam MB, Goharshadi EK, Entezari MH, Nancarrow P, Chem Eng J, 231 (2013) 365-72.
- [66] Wu ZH, Pittman CU, Gardner SD, Carbon, 33 (1995) 597-605.
- [67] Grzyb B, Hildenbrand C, Berthon-Fabry S, Begin D, Job N, Rigacci A, et al., Carbon, 48 (2010) 2297-307.
- [68] Fidel RB, Laird DA, Thompson ML, J Environ Qual, 42 (2013) 1771-8.
- [69] Tsechansky L, Graber ER, Carbon, 66 (2014) 730-3.
- [70] Leon y Leon CA, Radovic LR, Interfacial Chemistry and Electrochemistry of Carbon Surfaces in Chemistry and Physics of Carbon, Marcel Dekker, New York (1994) 213-310.
- [71] Jagiello J, Bandosz TJ, Schwarz JA, Carbon, 32 (1994) 1026-8.
- [72] Contescu A, Contescu C, Putyera K, Schwarz JA, Carbon, 35 (1997) 83-94.
- [73] Bandosz TJ, Jagiello J, Contescu C, Schwarz JA, Carbon, 31 (1993) 1193-202.
- [74] Matsumura Y, Hagiwara S, Takahashi H, Carbon, 14 (1976) 163-7.

- [75] Barkauskas J, Dervinyte M, *J Serb Chem Soc*, 69 (2004) 363-75.
- [76] Ren XM, Li JX, Tan XL, Wang XK, *Dalton T*, 42 (2013) 5266-74.
- [77] Cheng HX, Zeng KF, Yu JT, *J Radioanal Nucl Ch*, 298 (2013) 599-603.
- [78] Mabayoje O, Seredych M, Bandosz TJ, *J Colloid Interf Sci*, 378 (2012) 1-9.
- [79] Whitby RLD, Gun'ko VM, Korobeinyk A, Busquets R, Cundy AB, Laszlo K, et al., *Acs Nano*, 6 (2012) 3967-73.
- [80] Lemos BRS, Teixeira IF, Machado BF, Alves MRA, de Mesquita JP, Ribeiro RR, et al., *J Mater Chem A*, 1 (2013) 9491-7.
- [81] Seredych M, Mabayoje O, Bandosz TJ, *J Phys Chem C*, 116 (2012) 2527-35.
- [82] Zhao GX, Wen T, Yang X, Yang SB, Liao JL, Hu J, et al., *Dalton T*, 41 (2012) 6182-8.
- [83] Seredych M, Bandosz TJ, *J Mater Chem A*, 1 (2013) 11717-27.
- [84] Seredych M, Kosciński M, Sliwinska-Bartkowiak M, Bandosz TJ, *Acs Sustain Chem Eng*, 1 (2013) 1024-32.
- [85] Plummer LN, Busenberg E, *Geochim Cosmochim Acta*, 46 (1982) 1011-40.
- [86] Pohorecki R, Moniuk W, *Chem Eng Sci*, 43 (1988) 1677-84.
- [87] Hu H, Bhowmik P, Zhao B, Hamon MA, Itkis ME, Haddon RC, *Chem Phys Lett*, 345 (2001) 25-8.
- [88] Shaffer MSP, Menzel R, Lee A, Bismarck A, *Langmuir*, 25 (2009) 8340-8.
- [89] Rockstraw DA, Guo YP, *Micropor Mesopor Mat*, 100 (2007) 12-9.
- [90] Salzmann CG, Llewellyn SA, Tobias G, Ward MAH, Huh Y, Green MLH, *Adv Mater*, 19 (2007) 883-7.
- [91] Del Canto E, Flavin K, Movia D, Navio C, Bittencourt C, Giordani S, *Chem Mater*, 23 (2011) 67-74.
- [92] Worsley KA, Kondrat RW, Pal SK, Kalinina I, Haddon RC, *Carbon*, 49 (2011) 4982-6.
- [93] Sung SJ, Kim T, Yang SJ, Oh JY, Park CR, *Carbon*, 81 (2014) 524-34.
- [94] Nasibulina LI, Anoshkin IV, Nasibulin AG, Cwirzen A, Penttala V, Kauppinen EI, *J Nanomater*, (2012), 169262-1-6.

- [95] Haddon RC, Sippel J, Rinzler AG, Papadimitrakopoulos F, *Mrs Bull*, 29 (2004) 252-9.
- [96] Bunch JS, Verbridge SS, Alden JS, van der Zande AM, Parpia JM, Craighead HG, et al., *Nano Lett*, 8 (2008) 2458-62.
- [97] Hafez IH, Berber MR, Fujigaya T, Nakashima N, *Sci Rep*, 4 (2014), 6295-1-8.
- [98] Zhang XF, Sreekumar TV, Liu T, Kumar S, *J Phys Chem B*, 108 (2004) 16435-40.
- [99] Shin YR, Jeon IY, Baek JB, *Carbon*, 50 (2012) 1465-76.
- [100] Datsyuk V, Kalyva M, Papagelis K, Parthenios J, Tasis D, Siokou A, et al., *Carbon*, 46 (2008) 833-40.
- [101] Rosca ID, Watari F, Uo M, Akaska T, *Carbon*, 43 (2005) 3124-31.
- [102] Cho HG, Kim SW, Lim HJ, Yun CH, Lee HS, Park CR, *Carbon*, 47 (2009) 3544-9.
- [103] Sung SJ, Kim T, Yang SJ, Oh JY, Park CR, *Carbon*, 81 (2015) 525-34.
- [104] Kumar NA, Jeon IY, Sohn GJ, Jain R, Kumar S, Baek JB, *Acs Nano*, 5 (2011) 2324-31.
- [105] Dettlaff-Weglikowska U, Skakalova V, Graupner R, Jhang SH, Kim BH, Lee HJ, et al., *J Am Chem Soc*, 127 (2005) 5125-31.
- [106] Seredych M, Bandosz TJ, *Langmuir*, 26 (2010) 5491-8.
- [107] Seredych M, Chen R, Bandosz TJ, *Carbon*, 50 (2012) 4144-54.
- [108] Petit C, Bandosz TJ, *J Phys Chem C*, 113 (2009) 3800-9.

**Part II**

**Standardization of**

**Indirect Titration Method for**

**Surface Characterization of**

**Carbon Nanomaterials**

# Chapter 2 Effects of Carbon Dioxide and Acidic Carbon Compounds on The Analysis of Indirect Titration Curves

## 2.1 Introduction

Acidic carbon compounds (ACCs) with carboxylic and phenolic groups on the periphery of polyaromatic cores are fragmented from the sidewalls of carbon nanotubes (CNTs) during acid oxidation processes [1-8]. As ACCs are easily adsorbed onto CNTs via  $\pi$ - $\pi$  interactions, they play a key role in determining the dispersion stability of CNTs in different solvents [1, 2], and they may affect the reactivity of CNTs with other reactive species [3, 8-10]. However, ACCs dissolve in the strong alkaline solution like NaOH solution due to the electrical repulsion between ionized functional groups of ACCs and CNTs, and are easily removed from the surface of CNTs [1, 2]. Therefore, it is important to characterize the surface functionalities of ACCs separately from those directly attached to CNTs.

Recently, indirect titration (so-called Boehm titration) [11] was used to measure the acidity of ACC-contaminated multi-walled CNTs (MWCNTs) [1, 2]. In this approach, nitric acid-oxidized MWCNTs both with and without the removal of ACCs were prepared and reacted with the reaction base, an aqueous NaOH solution, and then filtered. Each filtrate of the reaction base was titrated with an aqueous HCl solution. In the case of the MWCNTs without the removal of ACCs, it was reported that two end points (EPs) existed in the titration curve of the filtrate, implying the presence of two distinctive acidic

groups of ACCs, viz. carboxylic and phenolic groups, in the forms of sodium salts in NaOH solution. Although each EP would be generally attributed to the specific kind of sodium salt (sodium carboxylate or phenolate), however, this was not clearly indicated in the previous study [1].

On the other hand, it has been reported that atmospheric carbon dioxide ( $\text{CO}_2$ ) can easily be dissolved into the reaction base during sample preparation for the indirect titration and consequently influences the whole profile of the titration curve [12], because  $\text{CO}_2$ -induced sodium carbonate ( $\text{Na}_2\text{CO}_3$ ), or bicarbonate ( $\text{NaHCO}_3$ ) [12, 13] in the reaction base act as base components during the titration.

To examine the specific contributions of the carboxylic and phenolic groups of ACCs and the atmospheric  $\text{CO}_2$  on the whole profiles of and the locations of EPs in the titration curves of the filtrate of the reaction base, NaOH, I first of all developed a modified Henderson-Hasselbalch equation, and then systematically studied experimentally the influences of such chemical components on the titrations using acidic compounds containing either carboxylic (benzoic acid in this study) or phenolic groups (phenol in this study), which acted as model ACCs. These reaction bases were exposed to air for different periods in order to see the effects of atmospheric  $\text{CO}_2$  on the titrations. Further, the same effects were also examined for the filtrate of the reaction base from MWCNTs that had been nitric acid-oxidized before and after the removal of ACCs.



## 2.2 Experimental

### 2.2.1 Chemicals and materials

Benzoic acid (BA) and phenol (Ph) were purchased from Sigma-Aldrich and were used without further treatment. To prepare the nitric acid-oxidized MWCNTs, 1 g of MWCNTs (JEIO) was treated with nitric acid (70 %, 300 mL) at 110 °C for 18 hours. After the acid treatment, the dispersion was cooled to room temperature followed by filtration through 0.2 µm pore-sized PTFE filter (Adventec) and washing with deionized water. ACCs were removed by following the procedures in Ref. [12]. The sample was refluxed in 1 N NaOH solution and filtered. The filtrate appeared light brown and the remaining oxidized MWCNTs were washed until the filtrate became colorless and then neutralized with 1 N HCl solution followed by filtration and washing with deionized water until pH of the filtrate became neutral. The obtained nitric acid-oxidized MWCNTs with (NCNT) and without (NCNT<sub>ACC</sub>) removal of ACCs were vacuum-dried at 60 °C for 1 day. The other chemicals used in the titration, 0.01 N NaOH and HCl, were purchased from Daejung (Korea).

### 2.2.2 Potentiometric titration of model ACCs

Potentiometric titrations were conducted using an 888 Titrando (Metrohm), and stable pH values (stable for a maximum of 150 seconds with a drift of no more than 1 pH unit / minute) were measured using a glass electrode (Metrohm, Swiss) and were recorded according to dosed volumes of 0.01 N HCl.

For the titrations with model ACCs, different quantities (0, 0.01, 0.02, and 0.04 meq) of organic acids (BA or Ph) were dissolved in 0.01 N NaOH solution (10 mL). To quantify the effects of CO<sub>2</sub>, each solution was introduced into a polyethylene (PE) bottle and exposed to air for different periods of time (0, 1, and 2 h). Each reaction base was titrated

with 0.01 N HCl standard solution.

### **2.2.3 Indirect titration of NCNTs with and without the removal of ACCs**

For the titrations with the nitric acid-oxidized MWCNTs, NCNT (60 mg) was dispersed in PE bottle filled with the reaction base (0.01 N NaOH, 60 mL). The dispersion was sealed and shaken for 48 h, and then filtered through 0.2  $\mu\text{m}$  PTFE syringe filter. And then, 5 mL of the filtrate was titrated with 0.01 N HCl in triplicate. The same procedures were repeated with NCNT<sub>ACC</sub>. PE bottles are known to be permeable for CO<sub>2</sub>, but I confirmed that there is little permeation of CO<sub>2</sub> through the bottle-wall and hence little dissolution of CO<sub>2</sub> into NaOH solution during storage in a sealed PE bottle for up to 48 hours.

## 2.3 Results and discussion

### 2.3.1 Theoretical derivation of universal titration equation

To predict theoretically a titration curve between a reaction base and an acid (HCl) solution, I developed first of all a universal titration equation from the modification of conventional Henderson-Haselbalch (H-H) equation [14, 15]. The conventional H-H equation traditionally calculate the pH value of the weak acid aqueous solution (like buffer solution) and measure the acidity ( $pK_a$ ) of the acid. However, this typical equation neglect the effects of water self-dissociation described in **Chapter 1** (see equation (1.4)), and therefore fail to estimate the pH or titration behaviors of strong acid or base such as HCl or NaOH, respectively, which are usually involved in either direct or indirect titration experiments. Additionally, the conventional H-H equation is only appropriate to the cases where single acid or base is included in the titration environments. Meanwhile it become necessary to estimate the titration behaviors of multiple acid/base components such as ACCs, carbon dioxide (**Chapter 3**), and functional groups on carbon nanomaterials (**Chapter 4 and 5**). Therefore, universal titration equation for the estimation of the pH values and titration behaviors of multiple acid and base components (regardless they are weak or strong) is developed in the followings.

In general, the H-H equation [14, 15] describing  $n$  monoprotic base components ( $A_i^-$ , the  $i$ 'th conjugated base of  $HA_i$ ; the conventional H-H equation only describe the case where  $n = 1$ ) titrated with a strong acid assumes that all added protons ( $H^+$ ) from the dosed titrant are transferred to each base component in the titrand to form a conjugated acid ( $HA_i$ ) (Here, the titrand is the solution that is analyzed in a titration procedure, and the titrant is the solution of known concentration which is added to the titrand). Therefore, the number of unionized  $HA_i$  species ( $q_{HA_i}$ ) is equal to the number of added protons

( $Q_{H^+}$ ),

$$Q_{H^+} = \sum q_{HA_i} = \sum \frac{Q_{A_i^-}}{q_{HA_i} + q_{A_i^-}} q_{HA_i}, \quad (2.1)$$

where  $Q_{A_i^-} = q_{HA_i} + q_{A_i^-}$  is the equivalence of components  $A_i^-$  from  $HA_i$ , which does not principally change during the titration ( $Q_{A_i^-} = Q_{HA_i}$ ), and  $q_{A_i^-}$  is the number of ionized  $HA_i$ . The ratio between  $q_{A_i^-}$  and  $q_{HA_i}$  is equal to the ratio between their concentrations, as in equation (2.2), and the equilibrium equation for the base  $A_i^-$  is given in equation (2.3),

$$\frac{q_{A_i^-}}{q_{HA_i}} = \frac{q_{A_i^-} / V_{H_2O}}{q_{HA_i} / V_{H_2O}} = \frac{[A_i^-]}{[HA_i]}, \quad (2.2)$$

$$K_{b,A_i^-} = \frac{[HA_i][OH^-]}{[A_i^-]}, \quad (2.3)$$

where  $V_{H_2O}$  is the volume of solvent (water) and  $[A]$  is the concentration of the component A. Combining equations (2.1) – (2.3) yields a general relation between  $Q_{H^+}$  and  $[OH^-]$ , as in equation (2.4) [15].

$$Q_{H^+} = \sum \frac{Q_{A_i^-}}{1 + \frac{[OH^-]}{K_{b,A_i^-}}} \quad (2.4)$$

The pH, calculated from  $[OH^-]$ , diverged at the initial titration point ( $Q_{H^+} = 0$ ) and at the final ( $Q_{H^+} = \sum Q_{A_i^-}$ ) states of the titration curve (see the blue line in Fig. 2.1a) because the effects of water acting as a base in the titrand were not considered in equation (2.4). Therefore, water was assumed to form as a result of titration of the sole  $OH^-$  ions from a hypothetical water-less state to the realistic state present immediately before the start of the titration, thereby consuming a corresponding amount of hypothetical titrant ( $Q_{OH^-,titrant}$ ). When the  $OH^-$  ions acted as a base, equations (2.1) – (2.4) needed to be modified. Assuming that the  $OH^-$  ions act as a diprotic base (the conjugated acid of  $OH^-$  ion,  $H_2O$  is regarded as the base), equation (2.1) can be modified as

$$Q_{H^+} = q_{H_2O} + q_{H_3O^+} = \frac{Q_{OH^-,titrant}}{1 + \frac{q_{OH^-}}{q_{H_2O}}} + \frac{Q_{H_2O,titrant}}{1 + \frac{q_{H_2O}}{q_{H_3O^+}}} \quad (2.1.1)$$

where  $Q_{H_2O,titrant}$  is the quantity of water in the titrant which is fundamentally equivalent to  $Q_{OH^-,titrant}$ ,  $q_{OH^-}$ ,  $q_{H_2O}$ , and  $q_{H_3O^+}$  are the number of disprotonated, unprotonated, and protonated  $H_2O$ , respectively. Using the definition of molar volume ( $v_{H_2O}$ ), equation (2.2) can be modified as in equation (2.2.1) and (2.2.2),

$$\frac{q_{\text{OH}^-}}{q_{\text{H}_2\text{O}}} = \frac{q_{\text{OH}^-} / V_{\text{H}_2\text{O}}}{q_{\text{H}_2\text{O}} / V_{\text{H}_2\text{O}}} = v_{\text{H}_2\text{O}} [\text{OH}^-] , \quad (2.2.1)$$

$$\frac{q_{\text{H}_2\text{O}}}{q_{\text{H}_3\text{O}^+}} = \frac{q_{\text{H}_2\text{O}} / V_{\text{H}_2\text{O}}}{q_{\text{OH}^-} / V_{\text{H}_2\text{O}}} = \frac{1 / v_{\text{H}_2\text{O}}}{[\text{H}_3\text{O}^+]} = \frac{[\text{OH}^-]}{v_{\text{H}_2\text{O}} \cdot K_W} , \quad (2.2.2)$$

where  $K_W$  is self-ionization constant of water. Finally, equation (2.1.1) is reduced to equation (2.4.1),

$$Q_{\text{H}^+} = \frac{Q_{\text{OH}^-, \text{titrant}}}{1 + v_{\text{H}_2\text{O}} [\text{OH}^-]} + \frac{Q_{\text{H}_2\text{O}, \text{titrant}}}{1 + \frac{[\text{OH}^-]}{v_{\text{H}_2\text{O}} \cdot K_W}} , \quad (2.4.1)$$

To add the effects of titrants shown in equation (2.4.1) in equation (2.4),  $Q_{\text{OH}^-, \text{titrant}}$  must be subtracted because the effects of  $\text{OH}^-$  ions (expressed in the first term of the right-hand side of equation (2.4.1)) are hypothetical. Under these conditions, the equation that includes the effects of water from the titrand is expressed as

$$\begin{aligned}
Q_{H^+} &= \sum \frac{Q_{A_i^-}}{1 + \frac{[OH^-]}{K_{b,A_i^-}}} + \frac{Q_{H_2O,titrant}}{1 + v_{H_2O}[OH^-]} + \frac{Q_{H_2O,titrant}}{1 + \frac{[OH^-]}{v_{H_2O} \cdot K_w}} - Q_{H_2O,titrant} \\
Q_{H^+} &= \sum \frac{Q_{A_i^-}}{1 + \frac{[OH^-]}{K_{b,A_i^-}}} - \frac{Q_{H_2O,titrant} \cdot v_{H_2O} \cdot [OH^-]}{1 + v_{H_2O} \cdot [OH^-]} + \frac{Q_{H_2O,titrant} \cdot v_{H_2O}}{v_{H_2O} + \frac{[OH^-]}{K_w}} \quad (2.5) \\
Q_{H^+} &= \sum \frac{Q_{A_i^-}}{1 + \frac{[OH^-]}{K_{b,A_i^-}}} - \frac{V_{H_2O,titrant}}{v_{H_2O} + \frac{1}{[OH^-]}} + \frac{V_{H_2O,titrant}}{v_{H_2O} + \frac{[OH^-]}{K_w}}
\end{aligned}$$

where  $V_{H_2O,titrant}$  is the initial volume of the titrand. It should be noted that the concentration of the base titrand are reflected in equation (2.5).

The pH diverged when  $Q_{H^+}$  reached  $\sum Q_{A_i^-} + Q_{H_2O,titrant}$  (see the green dashed line in Fig. 2.1) because the effects of water in the titrant were not considered. The effects of additional water ( $V_{H_2O,titrant}$ ) from the titrant are reflected in equation (2.6),

$$Q_{H^+} = \sum \frac{Q_{A_i^-}}{1 + \frac{[OH^-]}{K_{b,A_i^-}}} - \frac{V_{H_2O,titrant}}{v_{H_2O} + \frac{1}{[OH^-]}} + \frac{V_{H_2O,titrant}}{v_{H_2O} + \frac{[OH^-]}{K_w}} - \frac{V_{H_2O,titrant}}{v_{H_2O} + \frac{1}{[OH^-]}} + \frac{V_{H_2O,titrant}}{v_{H_2O} + \frac{[OH^-]}{K_w}} \quad (2.6)$$

From the definition of the  $H^+$  ion concentration in the titrant,  $c_{titrant}$  is expressed according to equation (2.7),

$$\frac{Q_{H^+}}{V_{H_2O, \text{titrant}}} = c_{\text{titrant}}, \quad (2.7)$$

and equation (2.6) is rearranged by combining equations (2.6) and (2.7) to yield the modified form of the H-H equation, expressed (acid titrant form) as

$$Q_{H^+} = \frac{\sum \frac{Q_{A_i^-}}{1 + [OH^-]/K_{b, A_i^-}} - \frac{V_{H_2O, \text{titrand}}}{v_{H_2O} + 1/[OH^-]} + \frac{V_{H_2O, \text{titrand}}}{v_{H_2O} + [OH^-]/K_W}}{1 + \frac{1/c_{\text{titrant}}}{v_{H_2O} + 1/[OH^-]} - \frac{1/c_{\text{titrant}}}{v_{H_2O} + [OH^-]/K_W}}. \quad (2.8)$$

The equation for titration of acid titrand with base titrant can be obtained by similar method (base titrant form) as

$$Q_{OH^-} = \frac{\sum \frac{Q_{HA_i}}{1 + [H^+]/K_{a, HA_i}} - \frac{V_{H_2O, \text{titrand}}}{v_{H_2O} + 1/[H^+]} + \frac{V_{H_2O, \text{titrand}}}{v_{H_2O} + [H^+]/K_W}}{1 + \frac{1/c_{\text{titrant}}}{v_{H_2O} + 1/[H^+]} - \frac{1/c_{\text{titrant}}}{v_{H_2O} + [H^+]/K_W}}, \quad (2.9)$$

where  $Q_{OH^-}$  is the quantity of  $OH^-$  ion which is added from base titrant,  $K_{a, HA_i}$  is acid ionization constant of acid  $HA_i$ , and  $[H^+]$  is the concentration of  $H^+$  ion.

Equations (2.8) and (2.9) describe the relationship between the input titrant and pH. To determine pH, only  $[OH^-]$  or  $[H^+]$  were considered in the ideal case. Here after in the thesis, these modified forms of H-H equations (2.8) and (2.9) are defined universal titration equations.



Titration curves for various experimental conditions were calculated at intervals of pH 0.1, and various curves associated with the conventional titrations, of a strong acid with a strong base or of a strong acid with a weak base, were obtained without further developments. A comparison of the ideal titration curves calculated using equations (2.4), (2.6), and (2.8) is illustrated in Fig. 2.1. The titrand was 0.01 N solution (10 mL) containing an arbitrary phenolate ion with  $pK_b = 4$ , and the titrant was 0.01 N HCl solution.

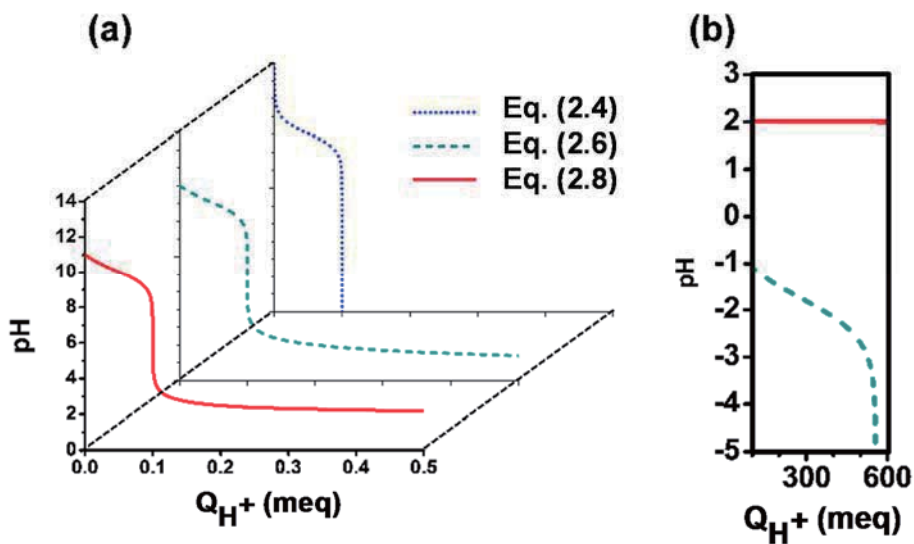


**Fig. 2.1.** (a) Titration curves of 0.01 N solution containing an arbitrary phenolate ion with  $pK_b = 4$  (10 mL), calculated according to equation (2.4) (blue dotted line), (2.6) (green dashed line), and (2.8) (red solid line). (b) pH divergence for the curve plotted according to equation (2.6), and pH convergence to 2 (pH of 0.01 N HCl solution) for the curve calculated plotted according to equation (2.8).

### 2.3.2 Adoption of model ACCs (BA, Ph) and CO<sub>2</sub> to the universal titration equation

The base components ( $A_i$ ) associated with this study were hydroxide ion ( $\text{OH}^-$ ), carbonate ion ( $\text{CO}_3^{2-}$ ), phenolate group, bicarbonate ion ( $\text{HCO}_3^-$ ), carboxylate group, and  $\text{H}_2\text{O}$ , listed in order of their base strength as listed in Table 2.1.

The  $\text{OH}^-$  ions and  $\text{H}_2\text{O}$  molecules are regarded as general base components with  $\text{p}K_b = -1.7$  and  $15.7$ , respectively.  $\text{CO}_3^{2-}$  ions are produced during the dissolution of atmospheric carbon dioxide ( $\text{CO}_2$ ) into the reaction base, NaOH solution by [13, 16]



$\text{HCO}_3^-$  ions form due to the neutralization of  $\text{CO}_3^{2-}$  ions during the titration. Phenolate and carboxylate group form as ACCs, with phenolic and carboxylic groups, are dissolved into the reaction base with an average  $\text{p}K_b = 4 - 5$  for the former and  $10 - 11$  for the latter in various aromatic organic acids and carbon materials [17-20]. In this study, phenolate ( $\text{Ph}^-$ ,  $\text{p}K_b = 4.1$ ) and benzoate ( $\text{BA}^-$ ,  $\text{p}K_b = 9.8$ ) ion are acted as model phenolate and carboxylate group of ACCs, respectively.

When the universal titration equation was applied to a multiprotic base, it was assumed that the base was divided into independent base components and proton binding sites with individual  $\text{p}K_b$  values. For example,  $\text{CO}_3^{2-}$  was assumed to be separable into the  $\text{CO}_3^{2-}$  and  $\text{HCO}_3^-$  ions individually, with  $Q_{\text{CO}_3^{2-}} = Q_{\text{HCO}_3^-}$ .

As listed in Table 2.2, three reaction bases were prepared, and each of these bases was exposed to air prior to the titration in order to see the effects of atmospheric  $\text{CO}_2$  on the titration curves. The titration curves were calculated and plotted according to the universal titration equation.

**Table 2.1.** Base components and their  $pK_b$  at 25°C.

Base component ( $A_i^-$ )	$pK_b$
Hydroxide ion ( $OH^-$ )	-1.7
Carbonate ion ( $CO_3^{2-}$ )	3.8
Phenolate group ( $-O^-$ )	3 – 6 (average)
Bicarbonate ion ( $HCO_3^-$ )	7.6
Carboxylate group ( $-COO^-$ )	8 – 11 (average)
Water ( $H_2O$ )	15.7

**Table 2.2.** The compositions of three reaction bases titrated with 0.01 N HCl, and the various neutralized (or protonated) base species (see Figs. 2.2 – 2.6).

Composition of 10 mL of the reaction base		Base components neutralized (or protonated) by HCl		
		Range I	Range II	Range III
<b>Base 1</b>	NaOH (0.1 meq)	$OH^-$ ,	$HCO_3^-$	$H_2O$
	+ $CO_2$ (variable)	$CO_3^{2-}$		
<b>Base 2</b>	NaOH (0.1 meq)	$OH^-$ ,	$HCO_3^-$	$H_2O$
	+Ph (0.02 meq) + $CO_2$ (variable)	$CO_3^{2-}$ , $Ph^-$		
<b>Base 3</b>	NaOH (0.1 meq)	$OH^-$ ,	$HCO_3^-$	$BA^-$ , $H_2O$
	+BA (0.02 meq) + $CO_2$ (variable)	$CO_3^{2-}$		

Fig. 2.2 shows the theoretical (based on the universal titration equation) and experimental titration curves of the reaction bases listed in Table 2.2. It is noteworthy in Figs. 2.2d – 2.2f that each experimentally observed titration curve is nearly perfectly coincident with the theoretically calculated one, which implies that the universal titration equation reflects well the actual titration and hence is fairly useful for deepening the understanding of the indirect titration curve.

On the other hand, it is very interesting to note that Figs. 2.2a – 2.2c show two end points (EPs; EP1 at pH 8 indicated by a white circle and EP2 at pH 5 by a white square) except for the base without dissolved CO<sub>2</sub> (indicated with the black solid lines in Figs. 2.2a–2.2c). The observation of only two EPs, despite the presence of more than two base components, indicates that some base components have similar  $pK_b$  values so as to be neutralized almost simultaneously to yield a single EP [15].

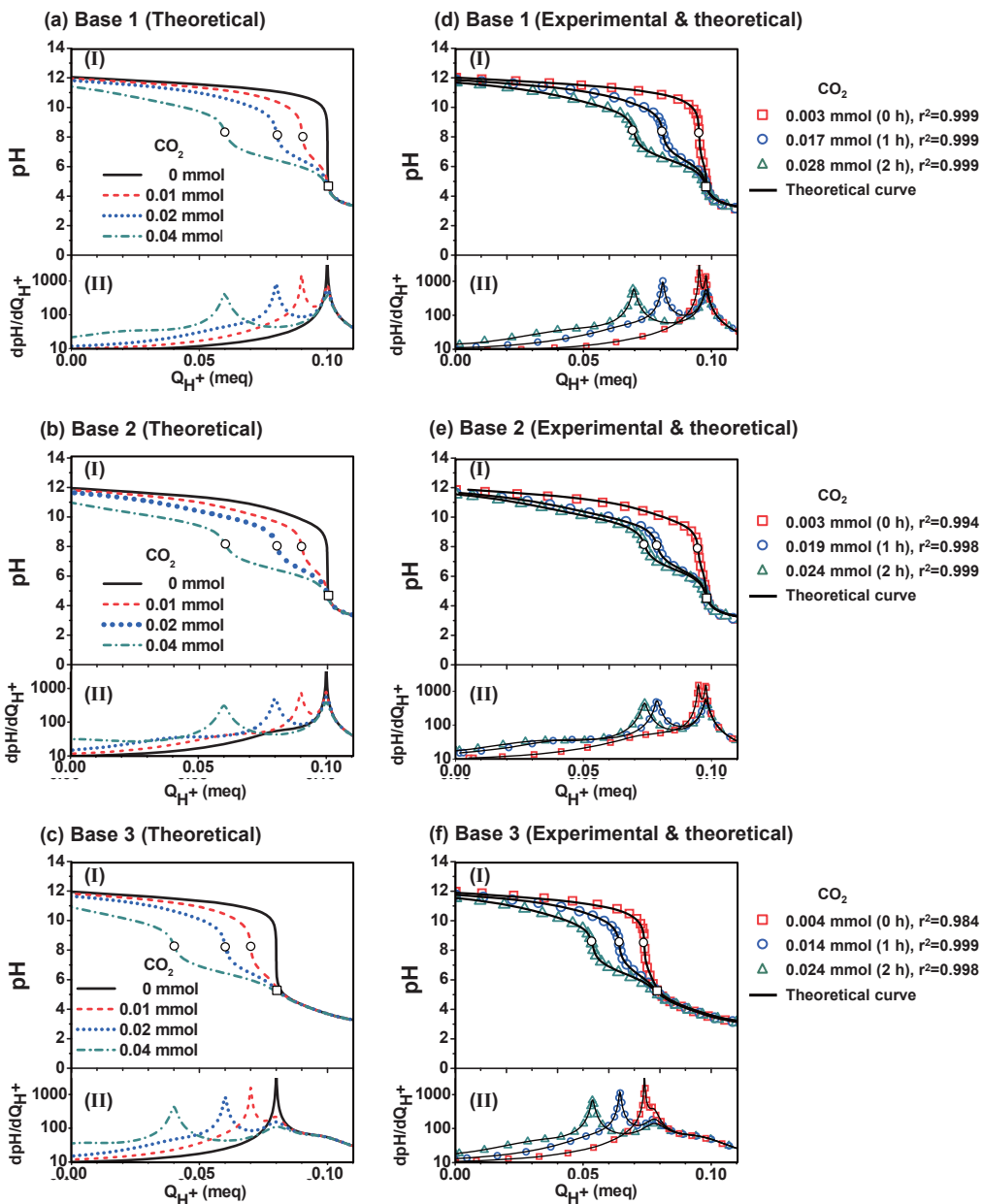


**Fig. 2.2.** (a, b, c) Theoretical only and (d, e, f) both experimental and theoretical (I) titration curves, and (II) their first order derivatives, corresponding to the titrations of the reaction bases listed in Table 2.2.

Figs. 2.3 – 2.5 illustrate the theoretically predicted titration curves for the reaction bases containing the model compounds for ACCs, viz. BA and Ph, and the quantity variation of each base component during the titration. Except the case of Fig. 2.3 where no CO<sub>2</sub> is involved, two EPs can also be clearly observed for the titration of Base 1, even though three different ions contribute to the base activity, that is, OH<sup>-</sup>, CO<sub>3</sub><sup>2-</sup> and HCO<sub>3</sub><sup>-</sup>. Considering the cases where 0.01 mmol of CO<sub>2</sub> is dissolved (Fig. 2.4), OH<sup>-</sup> and CO<sub>3</sub><sup>2-</sup> ions yield similar pK<sub>b</sub> values and are concurrently neutralized in Range I (the range of Q<sub>H</sub><sup>+</sup> between the initial point (Q<sub>H</sub><sup>+</sup> = 0 meq) to EP1) to yield EP1, as shown in Fig. 2a. HCO<sub>3</sub><sup>-</sup> ions are then neutralized in Range II (the range of Q<sub>H</sub><sup>+</sup> between EP1 and EP2), corresponding exactly to the amount of CO<sub>2</sub> dissolved, to yield EP2 (Therefore, the quantity of CO<sub>2</sub> dissolved in each reaction base can be estimated from the extent of Range II of the titration data shown in Figs. 1d-1f). The quantity of H<sub>3</sub>O<sup>+</sup> ions increases in Range III (the range of Q<sub>H</sub><sup>+</sup> from EP2) due to the protonation of H<sub>2</sub>O by HCl. Similarly, concurrent neutralization yields two EPs again in both Base 2 and Base 3. Base 2 contains not only OH<sup>-</sup>, CO<sub>3</sub><sup>2-</sup> and HCO<sub>3</sub><sup>-</sup> ions but also Ph<sup>-</sup> ions, which are neutralized in Range I (Fig. 2.4bII). The presence of Ph<sup>-</sup> ions in the reaction base clearly does not alter the Q<sub>H</sub><sup>+</sup> at the EPs. Rather, the down-shifts in the initial state of the titration along the pH axis in Range I is found from a comparison with Figs. 2.4a and 2.4b (see also Fig. 2.6). In Base 3, the additional BA<sup>-</sup> ions are neutralized in Range III along with the protonation of H<sub>2</sub>O (Fig. 2.4cII). As a result, the whole titration curve is shifted toward the lower Q<sub>H</sub><sup>+</sup> value, and no extra EP appears at the original equivalence point of the reaction base (Fig. 2.4c). The similar tendencies were observed in the other cases where more CO<sub>2</sub> was assumed to be dissolved (Fig. 2.5).

In addition, Fig. 2.6 shows the theoretical and experimental titration curves of the reaction base, NaOH in which only Ph or BA is dissolved. These curves clearly visualize

the above-mentioned effects of the phenolic (Figs. 2.6a and 2.6c) and carboxylic groups (Figs. 2.6b and 2.6d) on the titration behavior of the reaction base.

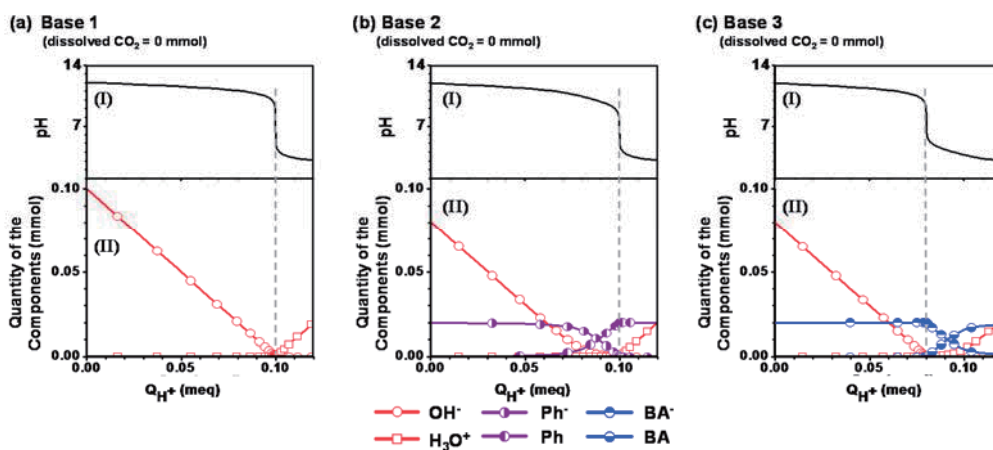


**Fig. 2.3.** (I) Theoretical titration curves of (a) Bases 1, (b) Base 2 and (c) Base 3 and (II) the quantity variation of each base component during the titration of each reaction base without any dissolved  $CO_2$ .

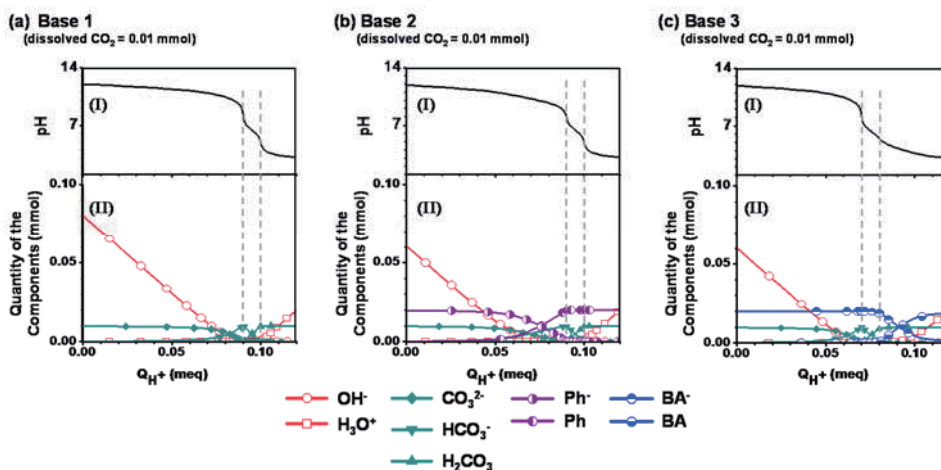


Fig. 2.4. (I) Theoretical titration curves of (a) Bases 1, (b) Base 2 and (c) Base 3 and (II) the quantity variation of each base component during the titration of each reaction base. Here, the quantity of dissolved  $\text{CO}_2$  was assumed to be 0.01 mmol

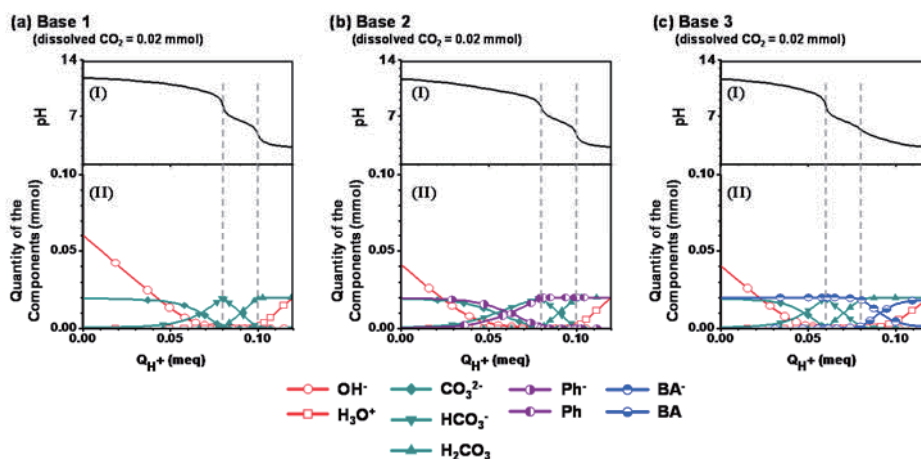
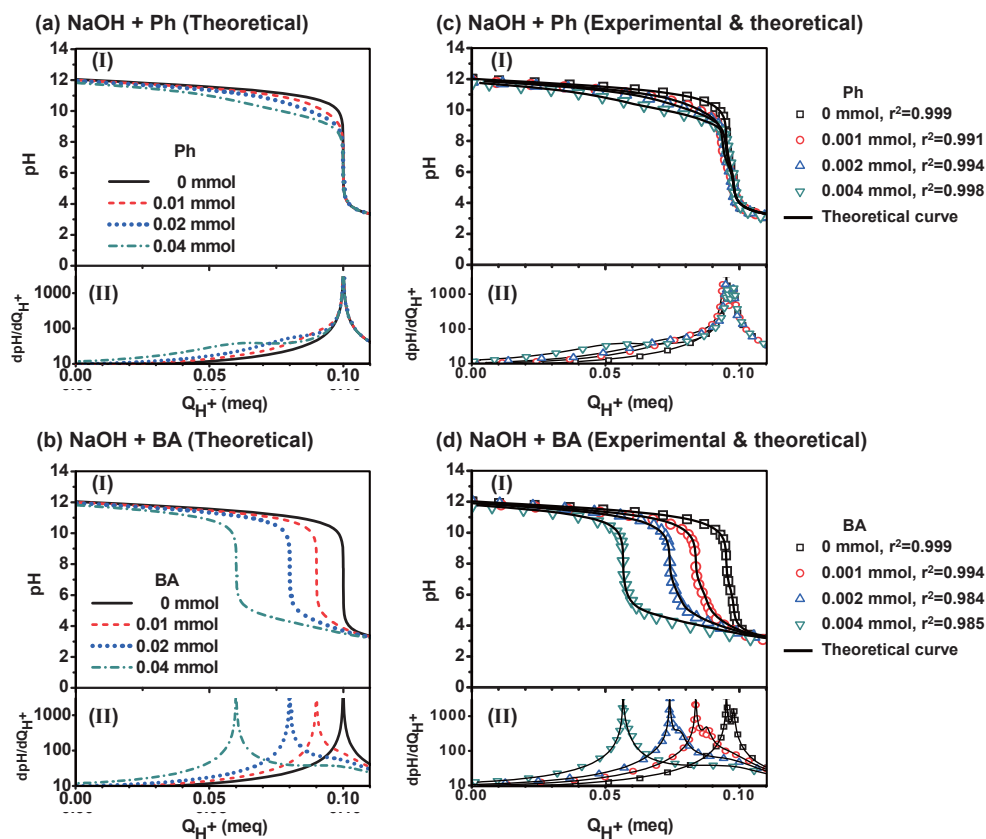


Fig. 2.5. (I) Theoretical titration curves of (a) Bases 1, (b) Base 2 and (c) Base 3 and (II) the quantity variation of each base component during the titration of each reaction base. Here, the quantity of dissolved  $\text{CO}_2$  was assumed to be 0.02 mmol.





**Fig. 2.6.** (a, b) Theoretical only and (c, d) both experimental and theoretical (I) titration curves and (II) their first-order derivatives, corresponding to the titration of the reaction base, 0.01 N NaOH (10 mL), with 0.01 N HCl. The acidic components dissolved in the reaction bases are (a, c) Ph and (b, d) BA.

### 2.3.3 Application of universal titration equation on the indirect titration of NCNTs

With the above-mentioned observation and understanding, the universal titration equation was extended to interpreting the titration curves of the filtrate of reaction base containing NCNT<sub>ACC</sub> or NCNT, and the reaction base itself shown in Fig. 2.7. As the amount of CO<sub>2</sub> dissolved in each reaction base can be determined from the difference between  $Q_{H^+}$  values of the two EPs on each titration curve, the experimental titration curve can then be reconstructed by applying the universal titration equation to exclude the effects of CO<sub>2</sub> for visualization of the own effects of ACCs on the titration curves.

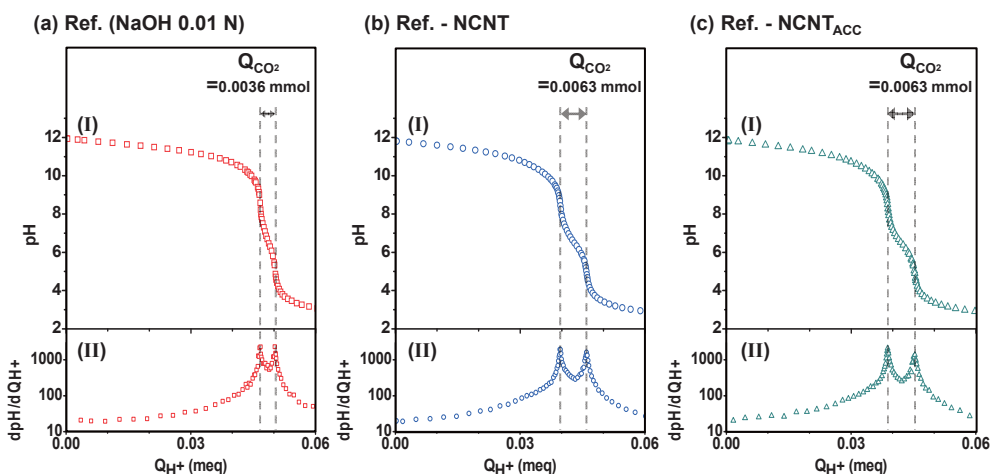


**Fig. 2.7.** (I) Titration curves of (a) the prepared reaction base, 0.01 N NaOH itself (5 mL; reference) and the filtrate from (b) NCNT and (c) NCNT<sub>ACC</sub> containing reaction base, respectively, (II) and their first-order derivatives. The amount of dissolved CO<sub>2</sub> ( $Q_{CO_2}$ ) in each reaction base was determined from the  $Q_{H^+}$  difference between the two EPs on each titration curve.

The effects of CO<sub>2</sub> were excluded from the experimental titration curves shown in Fig. 2.7 as follows. First of all, it was assumed that  $Q_{H^+}$  at a certain pH value from the experimental titration data followed universal titration equation (equation (2.8)), and then the effects of CO<sub>2</sub> can be reduced from  $Q_{H^+}$  as:

$$Q_{H^+,re} = Q_{H^+} + \frac{-\left(\frac{Q_{CO_2}}{1 + [OH^-]/K_{b,CO_3^{2-}}} + \frac{Q_{CO_2}}{1 + [OH^-]/K_{b,HCO_3^-}}\right) + \frac{2Q_{CO_2}}{1 + [OH^-]/K_{b,OH^-}}}{1 + \frac{1/c_{HCl}}{v_{H_2O} + 1/[OH^-]} - \frac{1/c_{HCl}}{v_{H_2O} + [OH^-]/K_w}}, \quad (2.11)$$

where  $Q_{H^+,re}$  is recalculated titration data ( $Q_{H^+}$ ) and  $Q_{CO_2}$  is the amount of CO<sub>2</sub> estimated from the  $Q_{H^+}$  difference between the two EPs in the titration data (see Fig. 2.7). As the equivalence of dissolved CO<sub>2</sub> (in the form of Na<sub>2</sub>CO<sub>3</sub>) is replaced by the equivalence of NaOH (of which the equivalence is the half of that of Na<sub>2</sub>CO<sub>3</sub>) when CO<sub>2</sub> is dissolved in NaOH solution [13] the effects of OH<sup>-</sup> were added to the titration data as shown in equation (2.10).

In Fig. 2.8 are illustrated the reconstructed titration curves,  $I_{ref}$ ,  $I_{NCNT}$ , and  $I_{NCNTACC}$ , of the reaction base, 0.01 N NaOH itself (5 mL; reference), the filtrate from NCNT and NCNT<sub>ACC</sub> containing reaction base, respectively. The reconstruction was made to remove the effects of CO<sub>2</sub> on the assumption that the experimental  $Q_{H^+}$  values of the titration curves in Fig. 2.7 follows the universal titration equation. So, some fluctuations in data points at around pH 7 in Fig. 2.8b indicate that there are some deviations in  $Q_{H^+}$  between experimental data and theoretical estimations. Nevertheless, it is sufficient to show that the effects of CO<sub>2</sub> on the titration curves (shown in Fig. 2.7) can be removed by this way. The theoretical titration curves that best fit with the reconstructed data, viz. CO<sub>2</sub>-effects-free experimental titration data, are also shown in the black solid lines in Fig. 2.8. The

total surface acidity of the nitric acid-oxidized MWCNTs themselves can then be estimated from the difference in the  $Q_{\text{H}^+}$  value at pH 7 between  $I_{\text{ref}}$  and  $I_{\text{NCNT}}$ , and that of ACCs between  $I_{\text{NCNT}}$  and  $I_{\text{NCNTACC}}$ , which are  $0.87 \pm 0.03$  meq/g and  $0.21 \pm 0.04$  meq/g, respectively. Since there can hardly be seen a down-shift of  $I_{\text{NCNTACC}}$  along the pH axis from the theoretical counterpart in the initial state of the titration (between  $Q_{\text{H}^+} = 0$  and 0.04 meq), it may reasonably be possible to conclude that there are little phenolic groups on ACCs, and hence the estimated surface acidity of ACCs is mostly due to the carboxylic groups. The more detailed effects of these carboxylic groups on the titration behaviors will be demonstrated in **Chapter 5**.

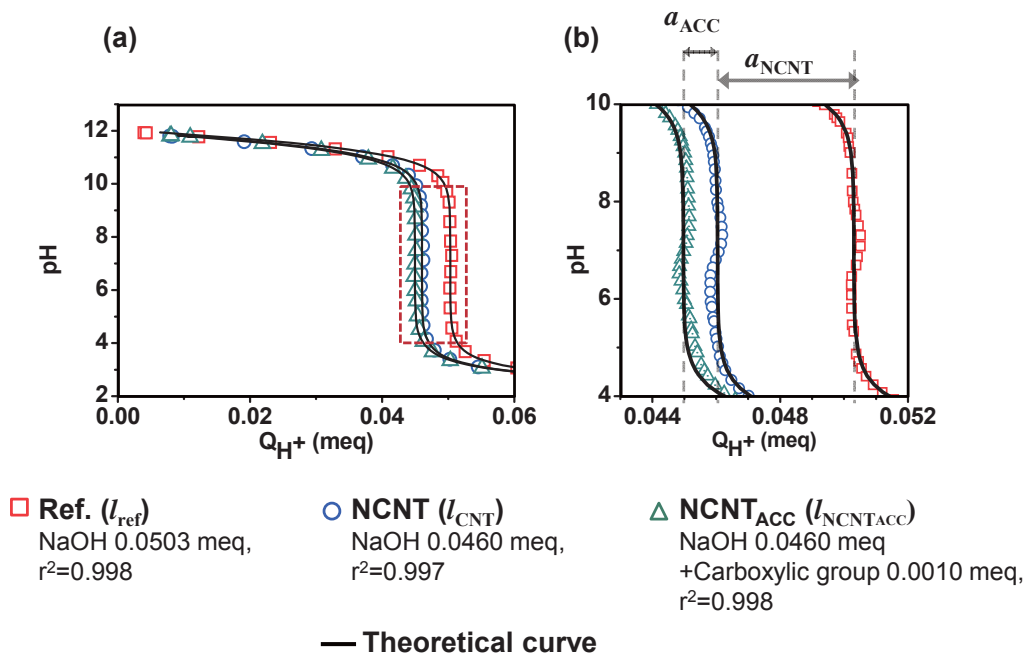


**Fig. 2.8.** (a) CO<sub>2</sub>-effects-free titration curves of the prepared reaction base, 0.01 N NaOH itself (5 mL; reference) ( $l_{ref}$ ) and the filtrate from NCNT ( $l_{NCNT}$ ) and NCNT<sub>ACC</sub> ( $l_{NCNTACC}$ ) containing reaction base, respectively, together with the theoretical titration curves. (b) Magnified view of the titration curves around the EPs (red dashed box in (a)). The difference in  $Q_{H^+}$  value at pH 7 between  $l_{ref}$  and  $l_{NCNT}$ , and that of ACCs between  $l_{NCNT}$  and  $l_{NCNTACC}$  indicate the total acidity of NCNT ( $a_{NCNT}$ ) and that of ACCs ( $a_{ACC}$ ), respectively.

## **2.4 Conclusions**

This work shows a systematic and scientific way of analyzing indirect titration curves influenced by acidic carbon compounds (ACCs) and/or atmospheric CO<sub>2</sub> by applying a newly developed universal titration equation based on the general Henderson-Hasselbalch (H-H) equation. With the suggested method it became possible to identify and quantify the effects of atmospheric CO<sub>2</sub> and carboxylic and phenolic groups of ACCs, being adsorbed on the acid-oxidized MWCNTs, on the observed indirect titration curve.

## 2.5 References

- [1] Wang ZW, Shirley MD, Meikle ST, Whitby RLD, Mikhalovsky SV, Carbon, 47 (2009) 73-9.
- [2] Rosca ID, Watari F, Uo M, Akaska T, Carbon, 43 (2005) 3124-31.
- [3] Worsley KA, Kalinina I, Bekyarova E, Haddon RC, J Am Chem Soc, 131 (2009) 18153-8.
- [4] Fogden S, Verdejo R, Cottam B, Shaffer M, Chem Phys Lett, 460 (2008) 162-7.
- [5] Worsley KA, Kondrat RW, Pal SK, Kalinina I, Haddon RC, Carbon, 49 (2011) 4982-6.
- [6] Flavin K, Kopf I, Del Canto E, Navio C, Bittencourt C, Giordani S, J Mater Chem, 21 (2011) 17881-7.
- [7] Salzmann CG, Llewellyn SA, Tobias G, Ward MAH, Huh Y, Green MLH, Adv Mater, 19 (2007) 883-7.
- [8] Del Canto E, Flavin K, Movia D, Navio C, Bittencourt C, Giordani S, Chem Mater, 23 (2011) 67-74.
- [9] Wang Z, Korobeinyk A, Whitby RLD, Meikle ST, Mikhalovsky SV, Acquah SFA, et al., Carbon, 48 (2010) 916-8.
- [10] Nasibulina LI, Anoshkin IV, Nasibulin AG, Cwirzen A, Penttala V, Kauppinen EI, J Nanomater, (2012) 169262-1-6.
- [11] Boehm HP, Carbon, 32 (1994) 759-69.
- [12] Goertzen SL, Theriault KD, Oickle AM, Tarasuk AC, Andreas HA, Carbon, 48 (2010) 1252-61.
- [13] Pohorecki R, Moniuk W, Chem Eng Sci, 43 (1988) 1677-84.
- [14] Katchalsky A, Spitnik P, J Polym Sci, 2 (1947) 432-46.
- [15] Ritchie JD, Perdue EM, Geochim Cosmochim Ac, 67 (2003) 85-96.
- [16] Plummer LN, Busenberg E, Geochim Cosmochim Ac, 46 (1982) 1011-40.
- [17] Zhang X, Bai RB, J Colloid Interf Sci, 264 (2003) 30-8.
- [18] Konkena B, Vasudevan S, J Phys Chem Lett, 3 (2012) 867-72.
- [19] Gorgulho HF, Mesquita JP, Goncalves F, Pereira MFR, Figueiredo JL, Carbon, 46 (2008)

1544-55.

[20] Petit C, Bandosz TJ, *J Phys Chem C*, 113 (2009) 3800-9.



# **Chapter 3 A Simple Method for Analysis of Indirect Titration Results Regardless of The Carbon Dioxide Effect**

## **3.1 Introduction**

The Indirect titration, or Boehm titration, has been generally adopted to characterize [1-14] and analyze the reactivity [15-18] of the surface functionality of various carbonaceous materials. In the method, three reaction bases with different basicities, such as sodium hydroxide (NaOH), sodium carbonate (Na<sub>2</sub>CO<sub>3</sub>) and sodium bicarbonate (NaHCO<sub>3</sub>), have been used to discern the kinds and amounts of surface functionalities among carboxylic, lactonic, and phenolic groups [1]. The amount of a specific surface functionality is calculated from the neutralization point usually determined as the point at pH 7 in the indirect titration curve corresponding to a specific base [7, 10, 11].

However, the neutralization point as judged at pH 7 does not always mean a precise equivalence of the given surface functionality because of the effect of atmospheric carbon dioxide (CO<sub>2</sub>) that dissolves easily into the reaction base during the filtration of the carbonaceous samples or the titration process. In fact, when atmospheric CO<sub>2</sub> dissolves into aqueous solution, it becomes carbonic acid (H<sub>2</sub>CO<sub>3</sub>), which is a weak acid [11, 19]. The presence of H<sub>2</sub>CO<sub>3</sub> in the reaction base has been known to distort the titration curve and make it difficult to get an exact neutralization point from the curve, hence, the exact amount of a specific surface functionality, which is defined as the CO<sub>2</sub> effect. To remove the CO<sub>2</sub> as completely as possible, the reaction base has to be acidified

[1, 10, 11] since CO<sub>2</sub> is driven out from the solution by acidic conditions with additional processes such as heating [1, 10, 11] or degasification with an inert gas [11]. To prevent the dissolution of CO<sub>2</sub> into the reaction base during titration, sealing, degasification of the reaction base with an inert gas [11, 13], and titration in an N<sub>2</sub> gas filled glove box [14] have been adopted. However, the introduction of these CO<sub>2</sub> removal processes makes the indirect titration complicated and inaccessible, although the indirect titration method is a practical method for the determination of the surface functionality of carbonaceous materials comparing to the direct titration method [20-26].

Having considered this situation, in this study, I tried to find a much easier method for determining the neutralization point in the indirect titration, which does not need any additional processes to remove the CO<sub>2</sub> effect from the titration process. To achieve this goal, the dissolution behavior of CO<sub>2</sub> into each reaction base, and hence its influence on the titration curve, was systemically and quantitatively analyzed using universal titration equation. The results obtained from the proposed method, which allows the dissolution of CO<sub>2</sub> throughout the whole titration process (denoted in-CO<sub>2</sub>-titration), were comparatively discussed with those of the earlier typical method in which the reaction base is acidified to remove the CO<sub>2</sub> effect (denoted ex-CO<sub>2</sub>-titration).

## 3.2 Experimental

### 3.2.1 Chemicals and materials

Chemicals for the titration such as NaOH, NaHCO<sub>3</sub>, Na<sub>2</sub>CO<sub>3</sub>, and HCl solutions (0.01 M) were purchased from Daejung (Korea). To prepare the samples of oxidized carbon nanotubes (CNTs) in which the functionality was to be analyzed, 1.00 g of multi-walled CNTs (MWCNTs; JEIO) was treated with 300 mL of mixed acid (mixture of 70 % HNO<sub>3</sub>, 75 mL and concentrated H<sub>2</sub>SO<sub>4</sub>, 225 mL) in 60 °C silicon oil for 3 hours. After the treatment, the sample was refluxed in 1 N NaOH for 1 h to eliminate the acidic carbon compounds, which might disturb the accuracy of the results [7]. The MWCNT dispersion in aqueous NaOH solution was filtered (0.2 μm PTFE filter, Adventec) and treated with 1 N HCl for 1h until the pH of the filtrate became neutral. The obtained MWCNTs were vacuum-dried at 105 °C for 1 day (denoted MCNT).

### 3.2.2 in-CO<sub>2</sub>-titration of pre-reaction bases

In this study, the general reaction bases, NaOH, Na<sub>2</sub>CO<sub>3</sub>, and NaHCO<sub>3</sub>, were used for the indirect titration. The concentration of each reaction base was limited to 0.01 N in this study. The amount of the reaction bases used in the titrations was 10 mL for the reaction bases NaOH and NaHCO<sub>3</sub>, and 5 mL for the reaction base Na<sub>2</sub>CO<sub>3</sub>. In the case of Na<sub>2</sub>CO<sub>3</sub>, a half volume of the other reaction bases was used to make the solution in the same equivalence of the base. To reduce the confusion, the reaction bases before and after the reaction with MCNTs were denoted pre- and post-reaction bases, respectively. Potentiometric titration behaviors of each reaction base were monitored with an 888 Titrand (Metrohm). To find out the CO<sub>2</sub> effects on the titration behaviors of the pre-reaction bases, the reaction bases were exposed to air for different periods of time (0, 1, 3, 6, and 12 hours) and then titrated using 0.01 N HCl standard solution (20 mL) as the

titrant (here, the titrant is a solution of known concentration that was added to the solution and analyzed in the titration procedure). The titration system allows the dissolution of CO<sub>2</sub> throughout the whole titration process. To determine the neutralization point (NP) to obtain the equivalence of the reaction base (denoted base equivalence), the inflection points in each titration curve were detected with the installed program, Tiamo (Metrohm), which is defined as the inflection measurement.

### **3.2.3 ex-CO<sub>2</sub>-titration of the pre-reaction bases**

The same amount of pre-reaction bases acidified with 20 mL of 0.01 N HCl as prepared in Section 2.2 were stirred for 4 hours to expel the dissolved CO<sub>2</sub> from the solutions. The acidified reaction base was titrated with 0.01 N NaOH standard solution as the titrant to determine the equivalence of the remaining H<sup>+</sup> ions (denoted acid equivalence) [11], and kept purged with N<sub>2</sub> gas to minimize the dissolution of CO<sub>2</sub> during the titration. Each titration was done in triplicate. In addition to the inflection measurement, the pH-7-measurement was done to determine the NP and the acid equivalence, where the titration of the acid is considered complete at pH 7. The NP determined by the pH-7-measurement is denoted as NP<sub>7</sub>. The differences between the in- and ex-CO<sub>2</sub>-titration systems are summarized in Table 3.1.

### **3.2.4 in- and ex-CO<sub>2</sub>-titration of MCNTs**

To examine the CO<sub>2</sub> effect on an actual titration of carbonaceous samples, the in-CO<sub>2</sub>-titration was first applied to the MCNTs in which ca. 60 mg of MCNTs dispersed for 48 hours with stirring in a specified aqueous reaction base solution (0.01 N NaOH, 60 mL; 0.005 N Na<sub>2</sub>CO<sub>3</sub>, 30 mL; and 0.01 N NaHCO<sub>3</sub>, 60 mL) was filtered through a 0.2 μm PTFE syringe filter (Adventec), and then, 10 mL of the filtrates (5 mL in the case of

Na<sub>2</sub>CO<sub>3</sub>) was titrated with 0.01 N HCl standard solution (20 mL). As described in Section 3.2.2, the filtrate of the reaction base after the reaction is denoted as the post-reaction base. Each titration was repeated three times in order to show the reproducibility of the result.

In the ex-CO<sub>2</sub>-titration [11] of the MCNTs, which was a comparative titration with the in-CO<sub>2</sub>-titration, the same amount of post-reaction base acidified with 20 mL of 0.01 N HCl was titrated with 0.01 N NaOH following the same procedures described in section 2.2.3, **Chapter 2**.

**Table 3.1.** Summary of in- and ex-CO<sub>2</sub>-titration systems

Titration system	in-CO <sub>2</sub> -titration	ex-CO <sub>2</sub> -titration
CO <sub>2</sub> exclusion process before the titration	None	Acidification
CO <sub>2</sub> prevention process during the titration	None	Purging with N <sub>2</sub> gas
Kind of the titrant	0.01 N HCl	0.01 N NaOH
Determination of NP	Inflection point	Inflection point, The point at pH 7

### 3.2.5 Determination of the surface functionality of the MCNTs

The amount of surface functional groups on the MCNTs was determined by the uptake of the reaction base calculated from the difference between the base equivalence of the pre- ( $eq_{B,pre}$ ) and post- ( $eq_{B,post}$ ) reaction base B (B specifies NaOH, Na<sub>2</sub>CO<sub>3</sub>, and NaHCO<sub>3</sub>). In the case of the in-CO<sub>2</sub>-titration of each reaction base, the amount of functional groups,  $n_{FG,B}$ , is calculated as follows:

$$\begin{aligned} n_{FG,B} &= \frac{c_{HCl}(V_{HCl,B,pre} - V_{HCl,B,post})}{m_{MCNT,B}} \\ &= \frac{eq_{B,pre} - eq_{B,post}}{m_{MCNT,B}} \end{aligned} \quad (3.1)$$

, where  $c_{HCl}$  is the concentration of the HCl titrant;  $V_{HCl,B,pre}$  and  $V_{HCl,B,post}$  are the volume of the HCl at the base equivalence for each of the pre- and post-reaction bases, respectively, and  $m_{MCNT,B}$  is the effective mass of the MCNTs corresponding to each post-reaction base. Therefore, the number of carboxylic groups  $n_c$ , lactonic groups  $n_l$ , and phenolic groups  $n_p$ , was calculated, respectively, as follows:

$$\begin{aligned} n_c &= n_{FG,NaHCO_3} \\ &= \frac{eq_{NaHCO_3,pre} - eq_{NaHCO_3,post}}{m_{MCNT,NaHCO_3}} \end{aligned} \quad (3.2.1)$$

$$\begin{aligned}
n_1 &= n_{\text{FG,Na}_2\text{CO}_3} - n_{\text{FG,NaHCO}_3} \\
&= \frac{eq_{\text{Na}_2\text{CO}_3,\text{pre}} - eq_{\text{Na}_2\text{CO}_3,\text{post}}}{m_{\text{MCNT,Na}_2\text{CO}_3}} - \frac{eq_{\text{NaHCO}_3,\text{pre}} - eq_{\text{NaHCO}_3,\text{post}}}{m_{\text{MCNT,NaHCO}_3}} \quad , \quad (3.2.2)
\end{aligned}$$

$$\begin{aligned}
n_p &= n_{\text{FG,NaOH}} - n_{\text{FG,Na}_2\text{CO}_3} \\
&= \frac{eq_{\text{NaOH,pre}} - eq_{\text{NaOH,post}}}{m_{\text{MCNT,NaOH}}} - \frac{eq_{\text{Na}_2\text{CO}_3,\text{pre}} - eq_{\text{Na}_2\text{CO}_3,\text{post}}}{m_{\text{MCNT,Na}_2\text{CO}_3}} \quad . \quad (3.2.3)
\end{aligned}$$

The reproducibility of the results was determined by the standard deviation in the number of each functional group as follows:

$$S_{n_c} = \left[ \frac{S_{eq_{\text{NaHCO}_3,\text{pre}}}^2 + S_{eq_{\text{NaHCO}_3,\text{post}}}^2}{m_{\text{MCNT,NaHCO}_3}^2} \right]^{1/2} \quad , \quad (3.3.1)$$

$$S_{n_1} = \left[ \frac{S_{eq_{\text{Na}_2\text{CO}_3,\text{pre}}}^2 + S_{eq_{\text{Na}_2\text{CO}_3,\text{post}}}^2}{m_{\text{MCNT,Na}_2\text{CO}_3}^2} + \frac{S_{eq_{\text{NaHCO}_3,\text{pre}}}^2 + S_{eq_{\text{NaHCO}_3,\text{post}}}^2}{m_{\text{MCNT,NaHCO}_3}^2} \right]^{1/2} \quad , \quad (3.3.2)$$

$$S_{n_p} = \left[ \frac{S_{eq_{\text{NaOH,pre}}}^2 + S_{eq_{\text{NaOH,post}}}^2}{m_{\text{MCNT,NaOH}}^2} + \frac{S_{eq_{\text{Na}_2\text{CO}_3,\text{pre}}}^2 + S_{eq_{\text{Na}_2\text{CO}_3,\text{post}}}^2}{m_{\text{MCNT,Na}_2\text{CO}_3}^2} \right]^{1/2} \quad , \quad (3.3.2)$$

where  $S_a$  is the standard deviation of the factor a. The standard deviation or the error

range in the amount for each functional group largely depends on that of the measured equivalence of each reaction base.

In the case of the ex-CO<sub>2</sub>-titration system,  $eq_{B,pre}$  and  $eq_{B,post}$  should be previously calculated from the acid equivalence of the acidified reaction base ( $eq_{ex\_B,pre(post)}$ ) as follows:

$$\begin{aligned} eq_{B,pre(post)} &= c_{HCl,ex} \cdot V_{HCl,ex} - c_{NaOH} \cdot V_{NaOH\_B,pre(post)} \\ &= c_{HCl,ex} \cdot V_{HCl,ex} - eq_{ex\_B,pre(post)} \end{aligned} \quad (3.4)$$

where  $c_{HCl,ex}$  and  $V_{HCl,ex}$  are the concentration and input volume of the HCl for the acidification of the reaction base to expel the CO<sub>2</sub> ( $V_{HCl,ex} = 20$  mL in these cases), respectively, and  $c_{NaOH}$  is the concentration of the NaOH titrant;  $V_{NaOH\_B,pre}$ , and  $V_{NaOH\_B,post}$ , are the volume of the NaOH titrant at the acid equivalence for each of the pre- and post-reaction bases acidified with HCl (0.01 N, 20 mL), respectively. Therefore,  $n_{FG,B}$  can be calculated as follows:

$$\begin{aligned} n_{FG,B} &= \frac{eq_{B,pre} - eq_{B,post}}{m_{MCNT,B}} \\ &= \frac{eq_{ex\_B,post} - eq_{ex\_B,pre}}{m_{MCNT,B}} \end{aligned} \quad (3.5)$$

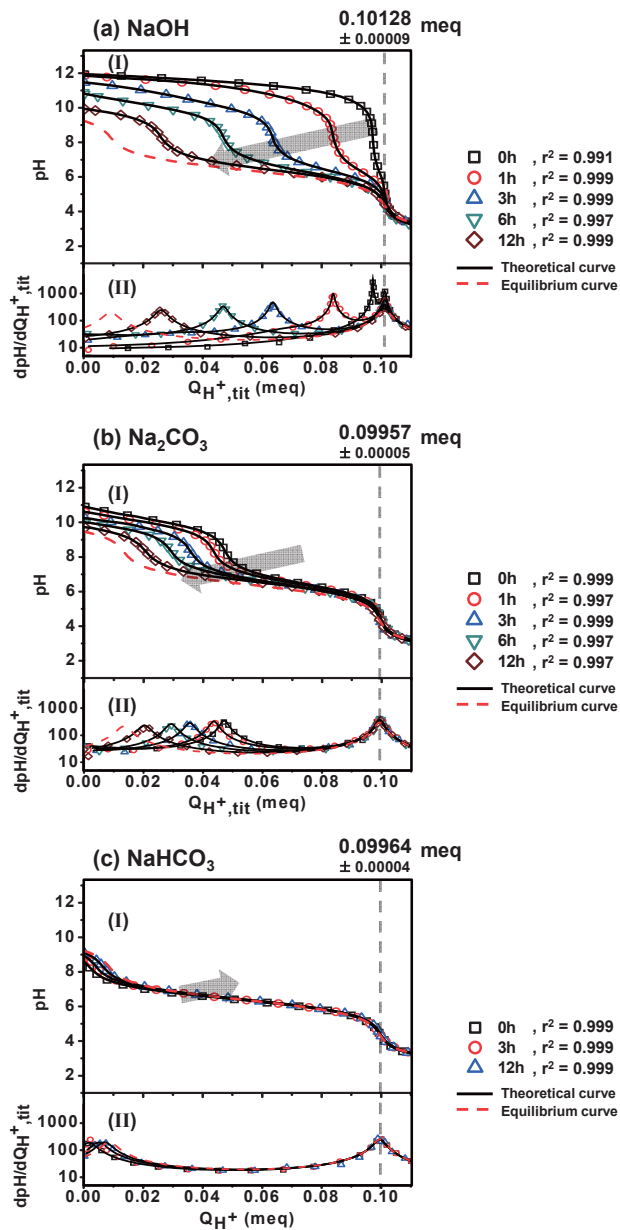
Here,  $n_c$ ,  $n_l$ , and  $n_p$ , and their standard deviations were derived similarly as described in equations (3.2.1) – (3.2.3), and (3.3.1) – (3.3.3), respectively.



### 3.3 Results and discussion

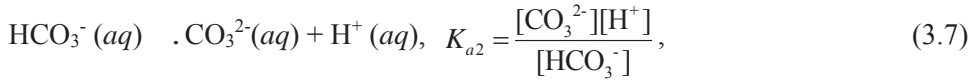
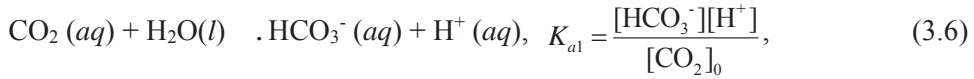
#### 3.3.1 CO<sub>2</sub> effect on the in-CO<sub>2</sub>-titration behavior of each reaction base

Fig. 3.1 shows the titration curves of the reaction bases in the in-CO<sub>2</sub>-titration system (denoted in-CO<sub>2</sub>-titration curves) with different exposure times to air before the titrations. Regardless of the exposure time, the quantity of H<sup>+</sup> from the dose of the HCl titrant ( $Q_{H^+,tit}$ ) at the second inflection point remained unchanged (straight gray dashed lines in Fig. 3.1) even though the specific shapes of the curves were distorted for all of the in-CO<sub>2</sub>-titration curves. These distortions most certainly resulted from the CO<sub>2</sub> effect since each titration curve showed two distinct inflections, which are regarded as the neutralization points (NPs) at pH 8 (NP1) and 5 (NP2). The pH value at each NP is given as the pH at neutralization of CO<sub>3</sub><sup>2-</sup> and HCO<sub>3</sub><sup>-</sup>, respectively [27], which is the product of the reaction between each reaction base and CO<sub>2</sub> [28-30].



**Fig. 3.1.** (I) Experimental and theoretical in-CO<sub>2</sub>-titration curves and (II) their first order derivatives of different pre-reaction bases (a) NaOH, (b) Na<sub>2</sub>CO<sub>3</sub>, and (c) NaHCO<sub>3</sub> with different exposure times. The gray arrows indicate an increase in the exposure time.

Theoretical titration curves for each reaction base at the equilibrium state with CO<sub>2</sub> (equilibrium curves) are shown as red dashed curves. To predict the change in the composition of the reaction base during the interaction with CO<sub>2</sub>, first, the simplest model describing the chemical equilibrium of CO<sub>2</sub> and the reaction base was utilized. In this model, it was assumed that the partial pressure of atmospheric CO<sub>2</sub> did not change (0.00035 atm) by the reaction involved in the equilibrium; therefore, the concentration of CO<sub>2</sub> is fixed as [CO<sub>2</sub>]<sub>0</sub> (1.2×10<sup>-5</sup> M) by Henry's law [19]. Thus, the acid-base equilibrium equations are the followings [19]:



and the conservation of charge for the ions in an aqueous solution is as follows:

$$[\text{H}^+] - [\text{OH}^-] - [\text{HCO}_3^-] - 2[\text{CO}_3^{2-}] + [\text{Na}^+] = 0. \quad (3.9.1)$$

Here, [Na<sup>+</sup>] is conserved as the initial concentration [Na<sup>+</sup>]<sub>i</sub> because it is a spectator ion in the reaction. Since [H<sup>+</sup>] is negligible, [Na<sup>+</sup>]<sub>i</sub> is the same as the summation of the normality of the base ions at the initial state, -[OH<sup>-</sup>]<sub>i</sub> - [HCO<sub>3</sub><sup>-</sup>]<sub>i</sub> - 2[CO<sub>3</sub><sup>2-</sup>]<sub>i</sub>. Generally, [OH<sup>-</sup>] + [HCO<sub>3</sub><sup>-</sup>] + 2[CO<sub>3</sub><sup>2-</sup>], the summation of the normality of bases, is defined as the

alkalinity ( $Alk$ ), which is a measure of the ability of an aqueous solution to neutralize acids [27]. Therefore, equation (3.9.1) can be expressed as follows:

$$\begin{aligned} [H^+] - [OH^-] - [HCO_3^-] - 2[CO_3^{2-}] &= -[Na^+]_i \\ &\approx -[OH^-]_i - [HCO_3^-]_i - 2[CO_3^{2-}]_i = -Alk_i \end{aligned} \quad (3.9.2)$$

where  $Alk_i$  is the initial alkalinity of the reaction base. Here, I consider that the initial concentration of  $[H^+]$  in the alkaline solution is negligibly small than  $Alk_i$ . Then, equations (3.6) – (3.8) and (3.9.2) can be reduced into a cubic equation as follows:

$$[H^+]^3 + Alk_i [H^+]^2 - (K_W + K_{a1} [CO_2]_0) [H^+] - 2K_{a1} K_{a2} [CO_2]_0 = 0, \quad (3.9.3)$$

where  $K_W$  is self-ionization constant of water. Since  $Alk_i$  is given for each reaction base, the concentration of each ion ( $[OH^-]$ ,  $[CO_3^{2-}]$ , and  $[HCO_3^-]$ ) and pH at the equilibrium with  $CO_2$  were calculated. If the  $Alk_i$  is the same regardless of the kind of reaction base ( $NaOH$ ,  $Na_2CO_3$ , or  $NaHCO_3$ ), the equilibrium state with atmospheric  $CO_2$  would be the same.

Fig. 3.2 shows the calculated ratio variation of the equivalence (or the normality) of  $CO_3^{2-}$  and  $HCO_3^-$  ions in the reaction base at the equilibrium state with respect to an  $Alk_i$  from 0.001 to 0.1 N, which is the usual concentration range applied in the indirect titration. At the equilibrium state, most of the base components remain in the form of  $CO_3^{2-}$  and  $HCO_3^-$  ions and the equivalence (or normality) of  $OH^-$  is almost negligible regardless of the kind of reaction base. For example, if 0.01 N  $NaOH$ ,  $Na_2CO_3$ , or  $NaHCO_3$  is exposed to air and reaches equilibrium with atmospheric  $CO_2$ , the

equilibrium normality of  $\text{CO}_3^{2-}$  and  $\text{HCO}_3^-$  would be 0.0017 and 0.0083 N, respectively, at pH 9.22. The specific mechanisms to reach the equilibrium will be discussed below.

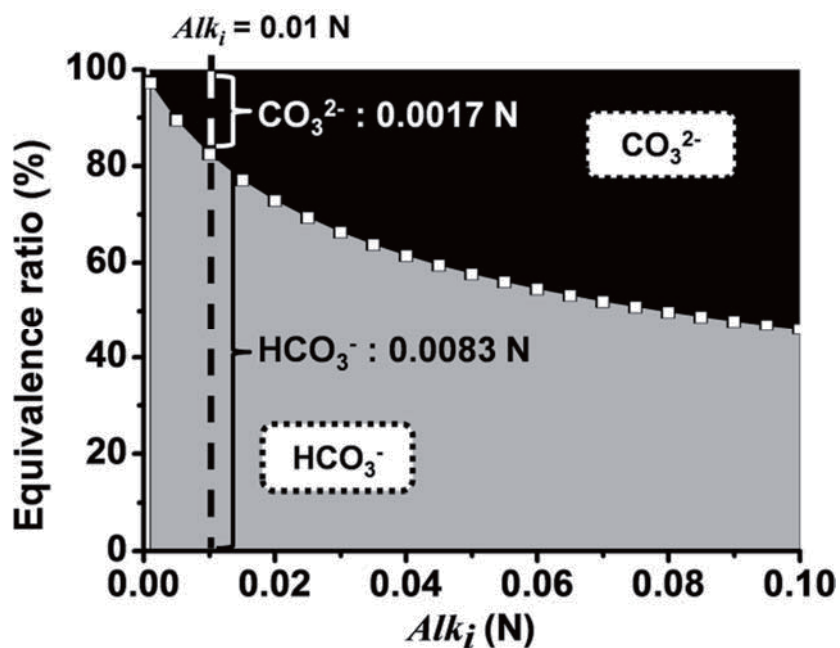


Fig. 3.2. The calculated equivalence ratio of  $\text{HCO}_3^-$  and  $\text{CO}_3^{2-}$  ions in the reaction base at the equilibrium state with  $\text{CO}_2$ .

To analyze the effects of these composition variations on the titration behaviors of the reaction bases, the theoretical titration curve of the reaction base with the influence of CO<sub>2</sub> was calculated using the universal titration equation (acid titrant form), developed in **Chapter 2** (see equation (2.8)):

$$Q_{H^+,tit} = \frac{\sum \frac{Q_{A_i^-}}{1 + [OH^-]/K_{b,A_i^-}} - \frac{V_{Base}}{v_{H_2O} + 1/[OH^-]} + \frac{V_{Base}}{v_{H_2O} + [OH^-]/K_W}}{1 + \frac{1/c_{HCl}}{v_{H_2O} + 1/[OH^-]} - \frac{1/c_{HCl}}{v_{H_2O} + [OH^-]/K_W}}, \quad (3.9.2)$$

where  $Q_{H^+,tit}$  is the amount of added HCl titrant [meq],  $Q_{A_i^-}$  is the quantity of the specific base component,  $A_i^-$  [meq] in the reaction base,  $K_{b,A_i^-}$  is the base ionization constant of a base  $A_i^-$ ,  $V_{Base}$  is the volume of the reaction base,  $v_{H_2O}$  is the molar volume of water, and  $c_{HCl}$  is the concentration of the HCl titrant. The base components ( $A_i^-$ ) associated with this study were the  $OH^-$ ,  $CO_3^{2-}$ , and  $HCO_3^-$  ions listed in order of their base strength. Different from the conventional H-H equation [31], the universal titration equation is useful to estimate a titration behavior in the whole range of the titration as described in section 2.3.1, **Chapter 2**. When the universal titration equation was applied to  $CO_3^{2-}$ , a diprotic base, it was assumed that  $CO_3^{2-}$  was divided into independent base components and proton binding sites ( $Q_{CO_3^{2-}} = Q_{HCO_3^-}$ ) with individual common  $pK_b$  values. Considering the effects of CO<sub>2</sub> on the titration curves, the first term in the numerator of equation (3.9.2) can be expressed as follow:

$$\sum \frac{Q_{A_i^-}}{1 + [\text{OH}^-]/K_{b,A_i^-}} = \frac{Q_{\text{NaOH}} - 2Q_{\text{CO}_2}}{1 + [\text{OH}^-]/K_{b,\text{OH}^-}} + \frac{Q_{\text{CO}_2}}{1 + [\text{OH}^-]/K_{b,\text{CO}_3^{2-}}} + \frac{Q_{\text{CO}_2}}{1 + [\text{OH}^-]/K_{b,\text{HCO}_3^-}}, \quad (3.10)$$

where  $Q_{\text{NaOH}}$ ,  $Q_{\text{CO}_2}$  is the initial quantity of NaOH in the titrand solution (0.1 meq in this case) and dissolved  $\text{CO}_2$  (see Step 1 in the following discussion), respectively. Applying this universal titration equation, the titration behaviors of the reaction base NaOH (0.01 N, 10 mL,  $Q_{\text{OH}^-} = 0.1$  meq) were calculated with the dissolution of different amounts of  $\text{CO}_2$  ( $Q_{\text{CO}_2} = 0, 0.025, 0.05, 0.075$  and  $0.1$  mmol), denoted Base a – Base e in order of the  $\text{CO}_2$  amount. The theoretical titration curves of Base a – Base e were drawn as  $I_a$  –  $I_e$ , respectively, in Fig. 3.3.

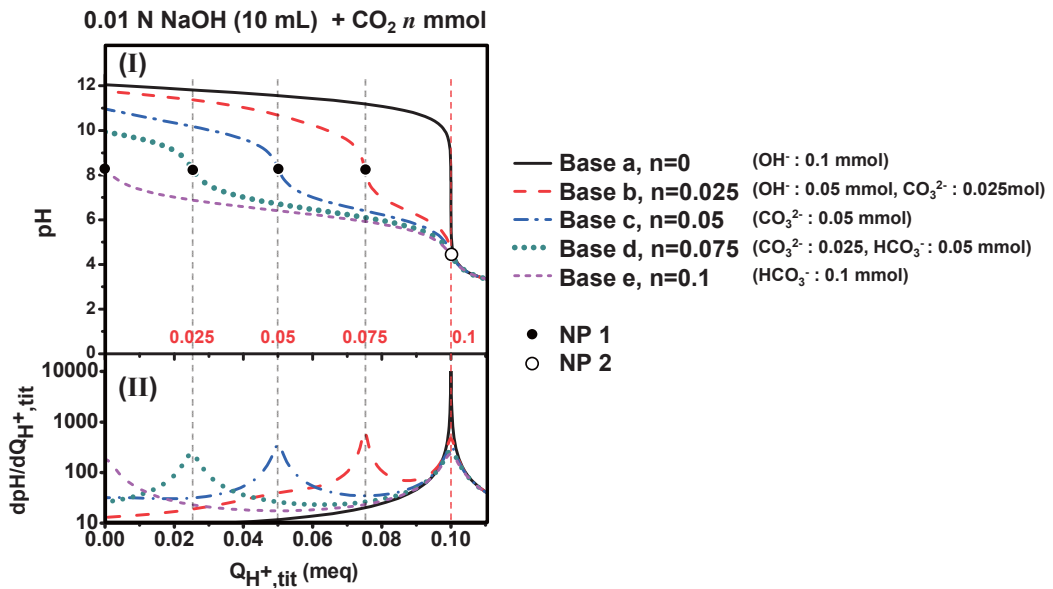
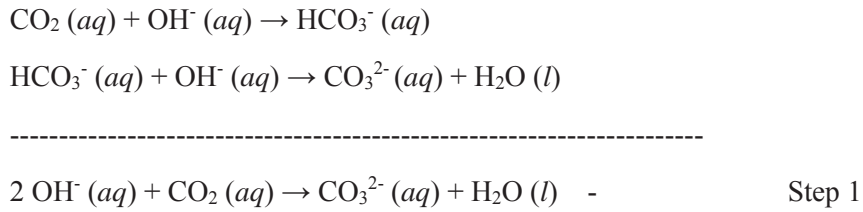


**Fig. 3.3.** (I) Theoretical titration curves and (II) their first order derivatives of 0.01 N NaOH (10 mL) reacted with different amounts of  $\text{CO}_2$ .

$l_a$  ( $Q_{\text{CO}_2} = 0$  mmol) shows the typical titration curve of an NaOH solution, and only a single NP from the  $\text{OH}^-$  ions exist at pH 7. To calculate the titration curve of Base b, in which  $Q_{\text{CO}_2}$  is 0.025 mmol, the composition of each base component should be calculated to apply the universal titration equation (equation (3.10)).  $Q_{\text{OH}^-}$  and  $Q_{\text{CO}_3^{2-}}$  in Base b can be set as 0.05 mmol and 0.025 mmol (0.05 meq), respectively, according to the well-known absorption reaction of  $\text{CO}_2$  in NaOH [28, 29] as follows:



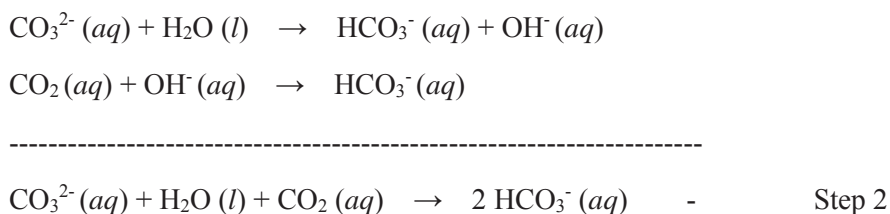
As the NaOH is reacted with  $\text{CO}_2$ , the titration curve begins to be distorted and the initial NP at pH 7 splits to make two NPs at pH 8 (NP1) and 5 (NP2), which are generally attributed to the neutralization of  $\text{CO}_3^{2-}$  and  $\text{HCO}_3^-$ , respectively [27]. These kinds of behaviors were also observed in the real titration curves as shown in Fig. 3.1a.  $Q_{\text{H}^+, \text{tit}}$  at NP1 indicates the summation of  $Q_{\text{OH}^-}$  and  $Q_{\text{CO}_3^{2-}}$ , which implies both the  $\text{CO}_3^{2-}$  and  $\text{OH}^-$  ions are neutralized at the same time since the  $\text{p}K_b$  difference between the two ions would be not large enough [26]. And then, the remaining  $\text{HCO}_3^-$  ions from the neutralization of the  $\text{CO}_3^{2-}$  ions are neutralized to make clear the NP at  $Q_{\text{H}^+, \text{tit}} = 0.1$  meq, which is the original base equivalence of the NaOH solution. It is noteworthy that the difference between the  $Q_{\text{H}^+, \text{tit}}$  values at NP1 and NP2 in  $l_b$  is exactly the same as the  $Q_{\text{CO}_2}$  and  $Q_{\text{CO}_3^{2-}}$  initially set in Base b. The in- $\text{CO}_2$ -titration curves of NaOH exposed to air for 0, 1, and 3 hours in Fig. 3.1a show the titration profiles of the reaction bases at Step 1.

In Base c ( $Q_{\text{CO}_2} = 0.05$  mmol),  $Q_{\text{OH}^-}$  is exhausted according to the reaction in Step 1, and



the base becomes exactly 0.01 N (0.005 M) Na<sub>2</sub>CO<sub>3</sub> solution. The titration curve *l<sub>c</sub>* also exhibits the titration behavior of Na<sub>2</sub>CO<sub>3</sub>.

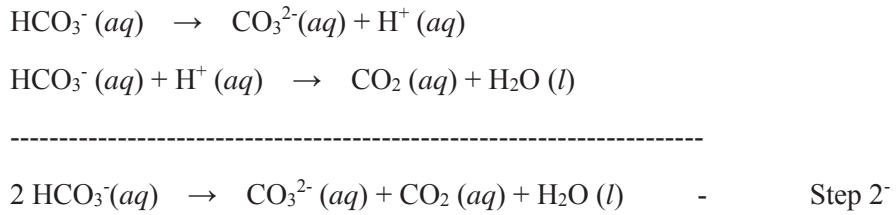
From the equilibrium diagram shown in Fig. 3.2, it is reasonable to estimate that the composition of Base c, or the Na<sub>2</sub>CO<sub>3</sub> solution, will change when it is exposed to CO<sub>2</sub>. In this case, CO<sub>3</sub><sup>2-</sup> ions are reported to mainly react with CO<sub>2</sub> instead of OH<sup>-</sup> ions and produce HCO<sub>3</sub><sup>-</sup> ions [30] as follows:



Therefore, most of the base components in the reaction base are converted into CO<sub>3</sub><sup>2-</sup> and HCO<sub>3</sub><sup>-</sup> ions, and *Q*<sub>CO<sub>3</sub><sup>2-</sup> and *Q*<sub>HCO<sub>3</sub><sup>-</sup> in Base d (*Q*<sub>CO<sub>2</sub></sub> = 0.075 mmol) were set as 0.025 mmol (0.05 meq) and 0.05 mmol, respectively, to yield the curve *l<sub>d</sub>*. In the titration of Base d, the stronger base, CO<sub>3</sub><sup>2-</sup> ions, would be neutralized prior to the HCO<sub>3</sub><sup>-</sup> ions and NP1 appears at *Q*<sub>H<sup>+</sup>,tit</sub> = 0.025 meq, of which the amount is the same as *Q*<sub>CO<sub>3</sub><sup>2-</sup></sub>. At this state, as CO<sub>3</sub><sup>2-</sup> ions are neutralized into HCO<sub>3</sub><sup>-</sup> ions, the quantity of the remaining HCO<sub>3</sub><sup>-</sup> ions is 0.075 mmol and would result in NP2 at *Q*<sub>H<sup>+</sup>,tit</sub> = 0.01 meq when they are completely neutralized. The in-CO<sub>2</sub>-titration curves of NaOH exposed to air for 6 and 12 hours in Fig. 3.1a, and all of those of Na<sub>2</sub>CO<sub>3</sub> in Fig. 3.1b show the titration profiles of each reaction base at Step 2.</sub></sub>

If *Q*<sub>CO<sub>2</sub></sub> becomes 0.01 mmol (Base e), only HCO<sub>3</sub><sup>-</sup> ions would remain to make a pure NaHCO<sub>3</sub> solution (0.01 N) and the resultant theoretical titration curve is *l<sub>e</sub>*. However, this is not a spontaneous reaction because the reaction base would reach the equilibrium

state with CO<sub>2</sub> when the normality of HCO<sub>3</sub><sup>-</sup> ions becomes 0.0083 N as described in Fig. 3.2. On the other hand, *l<sub>e</sub>* would shift toward *l<sub>d</sub>* when Base e, or 0.01 N NaHCO<sub>3</sub>, is exposed to air because more HCO<sub>3</sub><sup>-</sup> ions exist in pure NaHCO<sub>3</sub> solution than those in the solution at the equilibrium state. The change of the composition of each base component in this case is followed by CO<sub>2</sub> desorption of HCO<sub>3</sub><sup>-</sup> ion [30] as follows:



The overall reaction can be considered as the reverse reaction of the reaction in Step 2; therefore, this step is denoted Step 2<sup>-</sup>. All of the titration curves of NaHCO<sub>3</sub> in Fig. 3.1c show the titration profiles of the reaction bases at Step 2<sup>-</sup>.

Based on these considerations, the theoretical titration curve of each experimental in-CO<sub>2</sub>-titration curve was calculated and drawn as the black solid lines in Fig. 3.1 with good coincidence between each other. In addition, the theoretical titration curve of each reaction base in the equilibrium state with atmospheric CO<sub>2</sub> (denoted equilibrium curve) was calculated and drawn as the red dashed curve in Fig. 3.1. The experimental titration curves of each reaction base reached the equilibrium curve with an increase in the exposure time, which implies my theoretical approach related to the CO<sub>2</sub> interactions with the reaction bases and the estimation of the titration curves by the universal titration equation would be valid in the real case.

Further, it is shown from Step 1, 2, and 2<sup>-</sup> that the total base equivalence (the summation

of the equivalence of  $\text{OH}^-$ ,  $\text{CO}_3^{2-}$ , and  $\text{HCO}_3^-$  ions) of each reaction base remains unchanged with the interaction of  $\text{CO}_2$  since the equivalence of the base is the same in the reactants and products, respectively, in the reaction in each step. The conservation of the base equivalence ( $eq_{\text{B,pre}}$ ) is revealed in the conservation of  $Q_{\text{H}^+,\text{tit}}$  at NP2 both theoretically (Fig. 3.3) and experimentally (Fig. 3.1) regardless of the exposure of the reaction base to  $\text{CO}_2$ . From this conservation, the precise measurement of  $eq_{\text{B,pre}}$  of each reaction base is possible in the in- $\text{CO}_2$ -titration system regardless of the exposure to air as shown in Table 3.2, which implies the exclusion and prevention of  $\text{CO}_2$  would not be necessary in the indirect titration.

### 3.3.2 Comparison of the in- $\text{CO}_2$ -titration behavior with the ex- $\text{CO}_2$ -titration behavior

For comparison, the ex- $\text{CO}_2$ -titration [11] was applied to each reaction base. Fig. 3.4 shows the titration curve of the acidified reaction base  $\text{NaHCO}_3$  in the ex- $\text{CO}_2$ -titration system (denoted ex- $\text{CO}_2$ -titration curve) as a function of the amount of  $\text{OH}^-$  ions from the dosed  $\text{NaOH}$  titrant ( $Q_{\text{OH}^+,\text{tit}}$ ) (the other acidified reaction bases,  $\text{NaOH}$  and  $\text{Na}_2\text{CO}_3$ , showed similar titration behaviors).

The ex- $\text{CO}_2$ -titration curve shows almost a single inflection peak around pH 7, which implies that  $\text{CO}_2$  was almost expelled from the reaction base by the acidification. However, a magnified view shows that this peak splits into two inflection peaks at pH 5 (NP1') and pH 8 (NP2'), which would be attributed to the neutralization of  $\text{H}_2\text{CO}_3$  and  $\text{HCO}_3^-$ , respectively [27], which come from the remaining  $\text{CO}_2$  in the reaction base even though the removal and prevention of the  $\text{CO}_2$  effect were adopted.

In this case,  $Q_{\text{OH}^+,\text{tit}}$  at NP1' shows the exact acid equivalence ( $eq_{\text{ex-B,pre}}$ ) of the acidified reaction base [11]. However, as the  $Q_{\text{OH}^+,\text{tit}}$  difference between NP1' and NP2' is rather

narrow, the measurements of these NPs by the inflection measurement may not always ensure accuracy. For this reason, the pH-7-measurement has been usually utilized to determine the NP (NP<sub>7</sub>) [10, 11] in which the neutralization is assumed to be completed at pH 7. If a highly precise measurement is not necessary,  $Q_{OH^-,tit}$  at NP<sub>7</sub> is regarded as the  $eq_{ex\_B,pre}$  rather than the  $Q_{OH^-,tit}$  at NP1' [11]. After  $eq_{ex\_B,pre}$  is determined either by the inflection or pH-7-measurements, the equivalence ( $eq_{B,pre}$ ) of each pre-reaction base was calculated by equation (4) and compared to the  $eq_{B,pre}$  obtained by the inflection measurement from the in-CO<sub>2</sub>-titration system in Table 3.2.

The results imply that both inflection measurements from the in- and ex-CO<sub>2</sub>-titration provide  $eq_{B,pre}$  with high precision, which is comparable to that of a previous report [11]. However, the pH-7-measurement following the ex-CO<sub>2</sub>-titration resulted in the underestimation of  $eq_{B,pre}$  because of a slight amount of CO<sub>2</sub> remaining in the acidified reaction base. It is noteworthy that the in-CO<sub>2</sub>-titration system provides a simple but precise determination of the base equivalence.

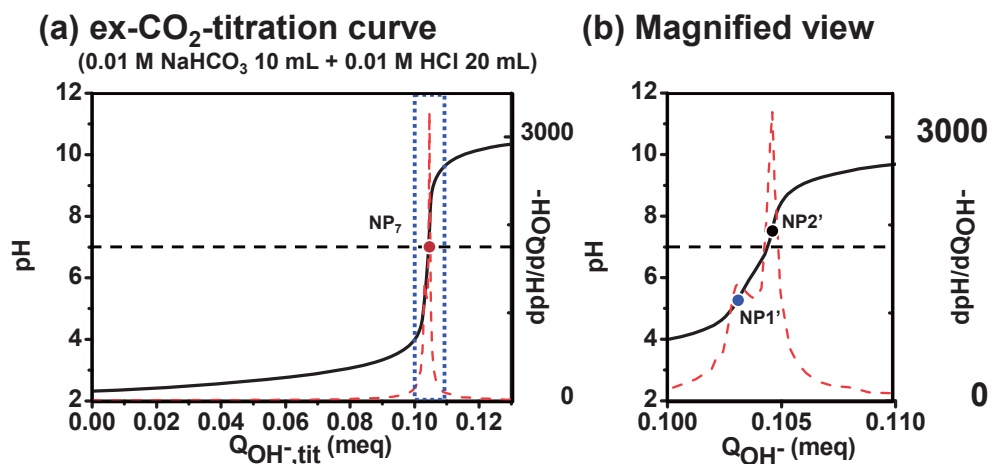


Fig. 3.4. (a) ex-CO<sub>2</sub>-titration curve and its first order derivative of the pre-reaction base NaHCO<sub>3</sub>, and (b) the magnified view around the NPs (blue dotted box in (a)).

Table 3.2. The base equivalence of each pre-reaction base ( $eq_{B,pre}$ ) determined by the different measurement methods of NP from in- and ex-CO<sub>2</sub>- titration.

Titration method	NP Measurement Method	Equivalence of the reaction base (meq)		
		NaOH	Na <sub>2</sub> CO <sub>3</sub>	NaHCO <sub>3</sub>
in-CO <sub>2</sub> -titration	Inflection point	0.10128	0.09957	0.09964
		±0.00009	±0.00005	±0.00004
ex-CO <sub>2</sub> -titration	Inflection point	0.10122	0.09970	0.09974
		±0.00006	±0.00018	±0.00002
ex-CO <sub>2</sub> -titration	The point at pH 7	0.10008	0.09887	0.09866
		±0.00030	±0.00022	±0.00013

### 3.3.3 Surface functionality of MCNTs as determined by in- and ex-CO<sub>2</sub>-titration

The amount of each functional group on MCNTs was determined by applying both the in- and ex-CO<sub>2</sub>-titrations. Fig. 3.5 shows the variations of the in- (Fig. 3.5a) and ex- (Fig. 3.5c) CO<sub>2</sub>-titration curves of the reaction base NaOH as it is reacted with MCNTs (Fig. 3.5b and 5d show the magnified view of Fig. 3.5a and 5c, respectively). NaOH uptake ( $n_{\text{FG,NaOH}}$ ), which indicates the quantity of all the functional groups of MCNTs [1], is presented in the figure with different measurements of the base or acid equivalence.

The in-CO<sub>2</sub>-titration curve shifted entirely to the left (Fig. 3.5a) as the base equivalence of the reaction base decreased after the reaction. In addition, all of the in-CO<sub>2</sub>-titration curves showed two NPs, which indicates the CO<sub>2</sub> effect [27]. In these cases,  $Q_{\text{H}^+,\text{tit}}$  at the second inflection point (NP2) should be regarded as the base equivalence of the reaction base regardless of the CO<sub>2</sub> effect. Therefore,  $n_{\text{FG,NaOH}}$  was determined from the difference between  $Q_{\text{H}^+,\text{tit}}$  at NP2 of the pre- and post-reaction base as described in equation (3.1).

In the case of the ex-CO<sub>2</sub>-titration of MCNTs, the whole curve shifted to the right. Since the amount of HCl for the acidification of the reaction base was the same, the reaction base with the lower base equivalence (pre-reaction base) had the higher acid equivalence when it was acidified, as described in equation (3.4). The difference of the acid equivalence between the pre- and post-reaction base ( $eq_{\text{ex\_NaOH,pre}}$  and  $eq_{\text{ex\_NaOH,post}}$ , respectively) indicates the  $n_{\text{FG,NaOH}}$  as described in equation (3.5). The  $n_{\text{FG,NaOH}}$  determined from the inflection measurements from the ex- and in-CO<sub>2</sub>-titrations ( $0.786 \pm 0.007$  and  $0.790 \pm 0.006$  meq/g, respectively) was almost the same. Meanwhile, it seems that the  $n_{\text{FG,NaOH}}$  was slightly overestimated by the pH-7-measurement from the ex-CO<sub>2</sub>-titration system ( $0.812 \pm 0.027$  meq/g), which is a result of the different tendency of CO<sub>2</sub> expulsion by the acidification of each reaction base. The uptake of the rest of the reaction bases Na<sub>2</sub>CO<sub>3</sub> and NaHCO<sub>3</sub> was obtained by similar methods. Additionally, the

number of each functional group on the MCNTs was calculated by equation (3.2.1), (3.2.2), and (3.2.3) and the results are listed in Table 3.3.

All of the results listed in Table 3.3 show similar tendencies. However, the results from the pH-7-measurement following the ex-CO<sub>2</sub>-titration were slightly different from those from the inflection measurements because the tendency of CO<sub>2</sub> expulsion by the acidification of each reaction base was different. On the other hand, a relatively high precision in the indirect titration results was achieved with the in-CO<sub>2</sub>-titration method compared to that in the results of the ex-CO<sub>2</sub>-titration method even though no treatments for CO<sub>2</sub> expulsion or prevention were applied before and during the titration. Therefore, additional procedures such as acidification or protection of the reaction base by an inert-gas blanket to exclude the CO<sub>2</sub> effect are not certainly necessary for the indirect titration of carbonaceous materials.

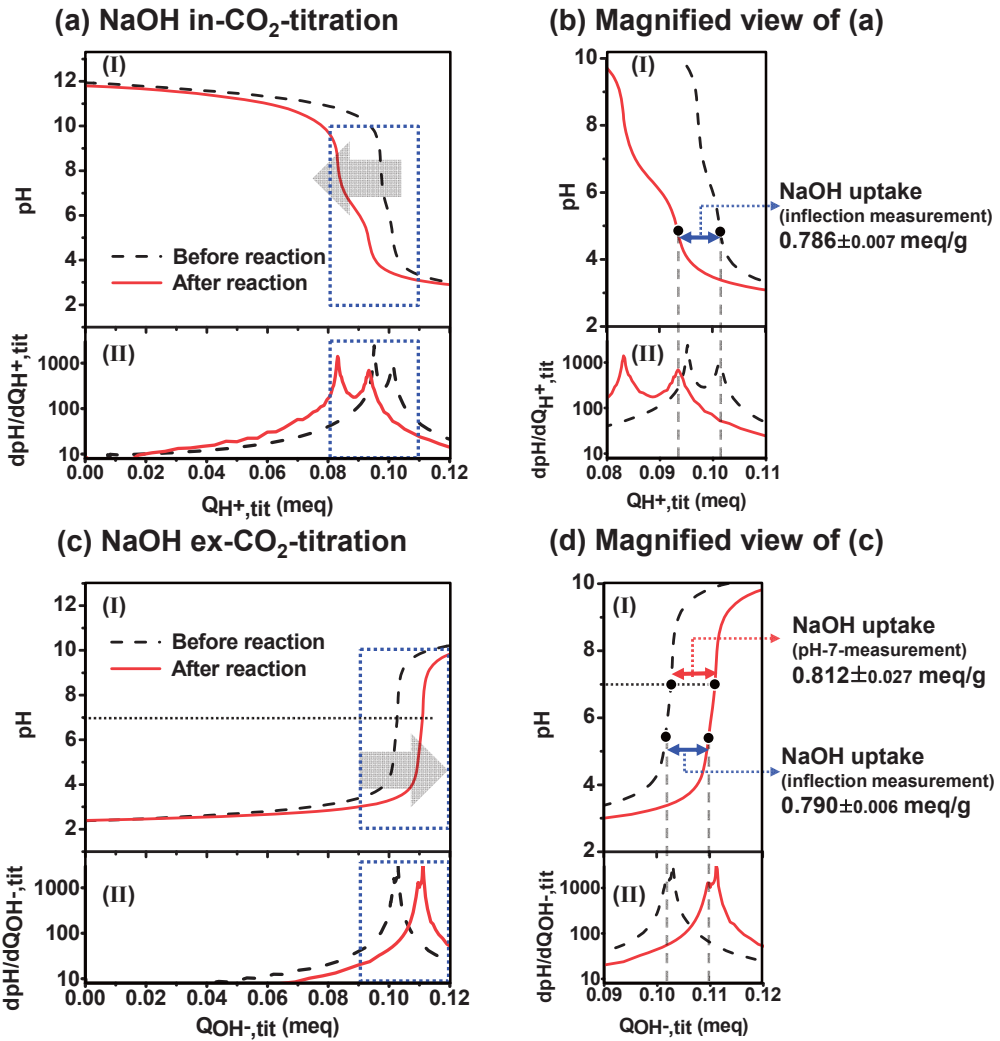


**Fig. 3.5.** (I) titration curves and (II) their first order derivatives of the reaction base NaOH from (a) the in- and (b) ex- $\text{CO}_2$ -titration systems before and after the reaction with the MCNTs. (b, d) The magnified view around the NP of the titrations (blue dotted box in (a) and (c) respectively).



**Table 3.3.** The number of each functional group on the MCNTs determined by the different measurement methods of NP from the in- and ex-CO<sub>2</sub>-titrations.

Titration method	NP	Number of functional group (meq/g)			
	Measurement Method	Carboxylic	Lactonic	Phenolic	Total
<b>in-CO<sub>2</sub>-titration</b>	Inflection point	0.498 ±0.016	0.222 ±0.018	0.066 ±0.010	<b>0.786</b> <b>±0.007</b>
	Inflection Point	0.494 ±0.006	0.239 ±0.024	0.058 ±0.024	<b>0.790</b> <b>±0.006</b>
<b>ex-CO<sub>2</sub>-titration</b>	The point at pH 7	0.508 ±0.017	0.263 ±0.027	0.041 ±0.033	<b>0.812</b> <b>±0.027</b>

### **3.4 Conclusions**

Atmospheric CO<sub>2</sub> has been considered to cause a negative effect on determining the exact neutralization point and equivalence of the reaction base in the indirect titration, and was thought to be removed or prevented using various additional procedures, which makes the indirect titration complicated and inaccessible. However, it turns out unnecessary to exclude CO<sub>2</sub> to determine the equivalence of the reaction base because the position of the second inflection point indicating the equivalence of the reaction base remains unchanged even though the reaction base interacts with CO<sub>2</sub>. In addition, the surface functionality of acid-treated MWCNTs was determined with high precision applying the titration method including the CO<sub>2</sub> effect. I believe my findings will help to establish an effective and simple indirect titration standardization.

### 3.5 References

- [1] Boehm HP, Carbon, 32 (1994) 759-69.
- [2] CarrascoMarin F, Mueden A, Centeno TA, Stoeckli F, MorenoCastilla C, J Chem Soc Faraday T, 93 (1997) 2211-5.
- [3] Hulicova-Jurcakova D, Seredych M, Jin YG, Lu GQ, Bandosz TJ, Carbon, 48 (2010) 1767-78.
- [4] Grzyb B, Hildenbrand C, Berthon-Fabry S, Begin D, Job N, Rigacci A, et al., Carbon, 48 (2010) 2297-307.
- [5] Moreno-Castilla C, Carrasco-Marin F, Mueden A, Carbon, 35 (1997) 1619-26.
- [6] Horikawa T, Kitakaze Y, Sekida T, Hayashi J, Katoh M, Bioresource Technol, 101 (2010) 3964-9.
- [7] Wang ZW, Shirley MD, Meikle ST, Whitby RLD, Mikhalovsky SV, Carbon, 47 (2009) 73-9.
- [8] Azadi P, Farnood R, Meier E, J Phys Chem A, 114 (2010) 3962-8.
- [9] Lago RM, Tsang SC, Lu KL, Chen YK, Green MLH, J Chem Soc Chem Comm, (1995) 1355-6.
- [10] Hu H, Bhowmik P, Zhao B, Hamon MA, Itkis ME, Haddon RC, Chem Phys Lett, 345 (2001) 25-8.
- [11] Goertzen SL, Theriault KD, Oickle AM, Tarasuk AC, Andreas HA, Carbon, 48 (2010) 1252-61.
- [12] Le Leuch LM, Bandosz TJ, Carbon, 45 (2007) 568-78.
- [13] Shaffer MSP, Menzel R, Lee A, Bismarck A, Langmuir, 25 (2009) 8340-8.
- [14] Rockstraw DA, Guo YP, Micropor Mesopor Mat, 100 (2007) 12-9.
- [15] Vukovic GD, Obradovic MD, Marinkovic AD, Rogan JR, Uskokovic PS, Radmilovic VR, et al., Mater Chem Phys, 130 (2011) 657-64.
- [16] Zhao CG, Ji LJ, Liu HJ, Hu GJ, Zhang SM, Yang MS, et al., J Solid State Chem, 177 (2004) 4394-8.

- [17] Wang Z, Korobeinyk A, Whitby RLD, Meikle ST, Mikhalovsky SV, Acquah SFA, et al., Carbon, 48 (2010) 916-8.
- [18] Worsley KA, Kalinina I, Bekyarova E, Haddon RC, J Am Chem Soc, 131 (2009) 18153-8.
- [19] Takemura F, Matsumoto Y, Chem Eng Sci, 55 (2000) 3907-17.
- [20] Biniak S, Szymanski G, Siedlewski J, Swiatkowski A, Carbon, 35 (1997) 1799-810.
- [21] Bandosz TJ, Jagiello J, Contescu C, Schwarz JA, Carbon, 31 (1993) 1193-202.
- [22] Contescu A, Contescu C, Putyera K, Schwarz JA, Carbon, 35 (1997) 83-94.
- [23] Gorgulho HF, Mesquita JP, Goncalves F, Pereira MFR, Figueiredo JL, Carbon, 46 (2008) 1544-55.
- [24] Seredych M, Tamashausky AV, Bandosz TJ, Adv Funct Mater, 20 (2010) 1670-9.
- [25] Konkena B, Vasudevan S, J Phys Chem Lett, 3 (2012) 867-72.
- [26] Seredych M, Bandosz TJ, Langmuir, 26 (2010) 5491-8.
- [27] Verma MP, Geostand Geoanal Res, 28 (2004) 391-409.
- [28] Plummer LN, Busenberg E, Geochim Cosmochim Ac, 46 (1982) 1011-40.
- [29] Pohorecki R, Moniuk W, Chem Eng Sci, 43 (1988) 1677-84.
- [30] Pohorecki R, Kucharski E, Chem Eng J Bioch Eng, 46 (1991) 1-7.
- [31] Ritchie JD, Perdue EM, Geochim Cosmochim Ac, 67 (2003) 85-96.

**Part III**

**One-Pot Titration Methodology for**

**Surface Characterization of**

**Carbon Nanomaterials**

# **Chapter 4 One-pot Titration Methodology for The Surface Characterization of Oxidized Carbon Nanotubes**

## **4.1 Introduction**

Carbon nanomaterials including carbon nanotubes (CNTs) [1-6], graphene [7-13], and fullerene [14, 15] have been chemically modified by various methods. It is important to determine and control the modified surface properties for their appropriate utilization. For this purpose, various chemical investigation techniques such as Fourier-transform infrared spectroscopy, Raman spectroscopy, temperature-programed desorption and X-ray photoelectron spectroscopy have been applied for the surface characterization of functionalized carbon nanomaterials [1, 10, 16-18].

Among the various characterization techniques, the titration method has been widely adopted for simple operations given the useful information it provides. Titration methods for carbonaceous materials are largely categorized into the indirect and direct methods. The indirect titration method, also known as Boehm titration [19], is commonly used due to its simple principles for the identification of the practical information on the surface of various carbonaceous materials including activated carbons, carbon fibers, carbon nanotubes, and graphene oxides [20-27]. With this method, three major types of functional groups (carboxylic, lactonic, phenolic groups) are determined. These are responsible for the surface properties and for the numerous applications of the carbon materials. For the classification and quantification of these functional groups, Boehm

suggested three bases with different basicities ( $\text{NaOH}$ ,  $\text{Na}_2\text{CO}_3$ , and  $\text{NaHCO}_3$ ) which are selectively neutralized with functional groups. In general, it is assumed that  $\text{NaOH}$  neutralizes all three functional groups, while  $\text{Na}_2\text{CO}_3$  neutralizes the carboxylic and lactonic groups, and  $\text{NaHCO}_3$  neutralizes only the carboxylic group [19].

Though indirect titration provides practical information about the surface chemistry of carbonaceous materials for their appropriate utilization, several limitations prevent the simple adoption of the indirect titration method. For example, experimental procedures such as reaction, filtration and titration are fairly time-consuming and complicated comparing to other surface characterization methods [22, 25, 26]. Specifically, a carbon sample is mixed with a reaction base for a sufficient period, followed by filtration, after which the filtrate is titrated with an acid titrant. Additionally, the filtrates are acidified to remove dissolved carbon dioxide and are then titrated with the base solution (known as the inverse or back titration method) [22]. In **Chapter 3**, the acidification step appeared to be completely unnecessary in a systematic study of the effects of carbon dioxide ( $\text{CO}_2$ ) on the titration of Boehm's reaction bases. Nevertheless, complex experimental procedures remain and must be repeated for each reaction base, which is time-consuming and also make the indirect titration method inaccessible. Moreover, filtration steps for highly oxidized CNTs individually dispersed in a reaction base [20, 28] or GO with two-dimensional nanostructures [29, 30] are hardly feasible or even impossible. These carbon nanomaterials can act as secondary filters with nanopores and inhibit the filtration of the reaction mixture, which is an essential process in the indirect titration method. In such cases, surface characterization of carbon nanomaterials with indirect titration becomes impossible.

In contrast, when using the direct titration method [31-36], the sample is simply mixed with the titrand solution and is directly titrated for the identification of the acidic or basic

characteristics of carbon materials. This method is widely used for the characterization of carbons and polymers with acidic (or basic) properties under the assumption that the  $pK_a$  values of numerous acids (or bases) are not discrete but are instead continuously distributed in a wide  $pK_a$  range expressed as the “ $pK_a$  distribution function.” While the direct titration method can effectively determine the population of the strong or weak acidic groups, the practical functions of these groups for the efficient utilization of carbon materials are not commonly provided, in contrast to indirect titration.

Therefore in this work, I develop a one-pot titration methodology penetrating the principles of direct and indirect titration for the simple elucidation of the surface properties of carbon nanomaterials. With this methodology, the  $pK_a$  distribution function of the direct titration of carbon nanomaterials is converted into practical indirect titration results based on the universal titration equation. The validity of the developed methodology is verified with functionalized multi-walled CNTs (MWCNTs).



## 4.2 Experimental

### 4.2.1 Chemicals and materials

All of the chemicals used as the titrants or titrands for the titration process, including NaOH, Na<sub>2</sub>CO<sub>3</sub>, NaHCO<sub>3</sub>, and HCl, were provided by Daejung Chemicals, Korea, and the MWCNTs were purchased from Hanwha Chemicals (CM250). For the functionalization of the MWCNTs, MWCNTs (1 g) were stirred in 300 mL of 14.2 M nitric acid at 110 °C for 6, 12, 24 and 48 hours. After an acid treatment, the MWCNTs were repeatedly filtered using a 20µm PTFE filter (Advantec) and washed with deionized water. For the complete removal of any acidic carbon compounds (ACCs) which may be destroyed from the side-walls of the MWCNTs during the acid treatment and affect the titration results were removed by washing the obtained MWCNTs with 0.01 N NaOH solution until the filtrate become colorless [20]. The ACC-removed MWCNTs were acidified by a 0.1 N HCl solution for reattachment of the protons to the ionized MWCNTs and were then filtrated. This was followed by washing thoroughly and filtration with deionized water and then drying in a 60 °C vacuum oven overnight. The nitric acid-treated MWCNTs prepared for 6, 12, 24, and 48 hours were denoted as N<sub>6</sub>CNT, N<sub>12</sub>CNT, N<sub>24</sub>CNT, and N<sub>48</sub>CNT, respectively.

### 4.2.2 Indirect titration of oxidized CNTs

For indirect titration of the prepared oxidized MWCNTs, in-CO<sub>2</sub> titration procedures standardized on **Chapter 3** were applied. This procedure consists of three steps: reaction, filtration and titration, without the need for CO<sub>2</sub> desorption by an additional acidification process. For the reaction and filtration steps, each MWCNT sample (50 mg) was stirred in 50 mL of each 0.01 N reaction base (NaOH, Na<sub>2</sub>CO<sub>3</sub>, or NaHCO<sub>3</sub>) for 48 hours (denoted reaction mixture) in HDPE bottles and then filtrated by a PTFE syringe filter

(Advantec). The reaction bases before and after the reaction step are denoted as pre- and post-reaction bases. For the titration step, 10 mL of the pre- or post-reaction bases were then titrated with a 0.01 N HCl solution as a titrant using a potentiometric titrator (888 Titrand, Metrohm). In general, two inflection points appeared in each titration curve showing the CO<sub>2</sub> effects. However only the second inflection points, at which all base components (OH<sup>-</sup>, CO<sub>3</sub><sup>2-</sup>, or HCO<sub>3</sub><sup>-</sup>) are neutralized regardless of the CO<sub>2</sub> effects, are defined as the end point of the titration curve of each reaction base; the equivalent amount of HCl at this point is regarded as that of the reaction base. The titration process was repeated three times in order to determine the average equivalence of each reaction base.

The numbers of carboxylic ( $n_c$ ), lactonic ( $n_l$ ), and phenolic ( $n_p$ ) groups were determined by the following the procedures, with equations (3.2.1 – 3.2.3) as done in **Chapter 3**.

$$n_c = n_{\text{FG,NaHCO}_3} = \frac{eq_{\text{NaHCO}_3,\text{pre}} - eq_{\text{NaHCO}_3,\text{post}}}{m_{\text{CNT,NaHCO}_3}}, \quad (3.2.1)$$

$$n_l = n_{\text{FG,Na}_2\text{CO}_3} - n_{\text{FG,NaHCO}_3} = \frac{eq_{\text{Na}_2\text{CO}_3,\text{pre}} - eq_{\text{Na}_2\text{CO}_3,\text{post}}}{m_{\text{CNT,Na}_2\text{CO}_3}} - \frac{eq_{\text{NaHCO}_3,\text{pre}} - eq_{\text{NaHCO}_3,\text{post}}}{m_{\text{CNT,NaHCO}_3}}, \quad (3.2.2)$$

$$n_p = n_{\text{FG,NaOH}} - n_{\text{FG,Na}_2\text{CO}_3} = \frac{eq_{\text{NaOH,pre}} - eq_{\text{NaOH,post}}}{m_{\text{CNT,NaOH}}} - \frac{eq_{\text{Na}_2\text{CO}_3,\text{pre}} - eq_{\text{Na}_2\text{CO}_3,\text{post}}}{m_{\text{CNT,Na}_2\text{CO}_3}}, \quad (3.2.3)$$

where  $n_{\text{FG,B}}$  is represents the concentrations of the functional groups [meq/g] determined from the uptake of reaction base B (B specifies NaOH, Na<sub>2</sub>CO<sub>3</sub>, and NaHCO<sub>3</sub>),  $eq_{\text{B,pre(post)}}$  is the equivalence of the pre(post)-reaction base of B, and  $m_{\text{CNT,B}}$  is the effective mass of the CNTs (N<sub>6</sub>, N<sub>12</sub>, N<sub>24</sub>, or N<sub>48</sub>CNTs) in the each post reaction base B during the titration step.

#### **4.2.3 One-pot titration of oxidized CNTs**

Each CNT sample was agitated in a 0.01 N HCl solution (2 mg/mL) and agitated by sonication in a bath for 30 minutes. Next, 15 mL of the mixture was injected into an incubation titration vessel and titrated with a 0.01 N NaOH solution as a titrant at 25 °C with continuous N<sub>2</sub> purging. To achieve full equilibrium between the acid functionalities of the CNTs and the titrant during the titration process, the titrant solution was dosed only when the pH variation was lower than 0.002 pH units/minute with a maximum waiting time of 20 minutes. The detailed procedures for the titration data processing will be discussed in the following section.

## 4.3 Results and discussion

### 4.3.1 Calculation of proton binding curve and $pK_a$ distribution function

The methodology for calculating the indirect titration results from the direct titration curves includes three steps. In the first step, the direct titration curves of oxidized CNTs are converted into the proton binding isotherm,  $\theta(\text{pH})$ , which exhibits the number of protonated functional groups as a function of the pH [32]. In the second step, the  $pK_a$  distribution function  $f(pK_a)$  is calculated from  $\theta(\text{pH})$ , which is discussed in detail in the following of this section. Finally, the indirect titration results are computed as a function of the concentrations of the reaction bases and the quantities of the carbon samples dissolved into the reaction bases.

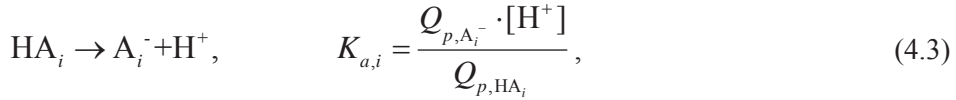
The  $pK_a$  value of a multiprotic acid such as polymeric acid or acidified carbons is generally assumed to be distributed and is described as the  $pK_a$  distribution function  $F(pK_a)$  [meq]. The number of functional groups in a certain  $pK_a$  range is calculated by integrating  $F(pK_a)$  in the  $pK_a$  range. If  $F(pK_a)$  is known, the proton-binding isotherm at a certain pH value,  $\Theta(\text{pH})$  [meq] is calculated as follows [32] :

$$\Theta(\text{pH}) = \Theta_0 + \int_{pK_{a,0}}^{pK_{a,f}} \frac{K_a}{[\text{H}^+] + K_a} F(pK_a) dpK_a, \quad (4.1)$$

where  $pK_{a,0}$  and  $pK_{a,f}$  are the initial and final  $pK_a$  values of  $F(pK_a)$ , and  $\Theta_0$  is the number of dissociated functional groups with  $pK_a$  values outside the integration limits. This equation can be easily derived, as follows. First, I convert  $F(pK_a)$  to the discrete series  $Q_{\text{HA}i}$  by defining the number of  $i$ 'th acid components  $Q_{\text{HA},i}$  with the acid constant  $K_{a,i}$  among  $n$  acid components (multiprotic acid), as follows:

$$Q_{\text{HA}_i} = \int_{pK_{a,i}}^{pK_{a,i+1}} F(pK_a) dpK_a \quad (1 \leq i \leq n-1). \quad (4.2)$$

At a certain pH point during the titration process,  $\text{HA}_i$  will be protonated to form the conjugated base  $\text{A}_i^-$ , as follows,



where  $Q_{p,\text{A}_i^-}$  and  $Q_{p,\text{HA}_i}$  are the partial quantities of the ionized and unionized acid components, respectively. The summation of  $Q_{p,\text{A}_i^-}$  and  $Q_{p,\text{HA}_i}$  should be identical to the total number (equivalence) of functional groups,  $Q_{\text{HA}_i}$  [meq], as

$$Q_{p,\text{HA}_i} + Q_{p,\text{A}_i^-} = Q_{\text{HA}_i}, \quad (4.4)$$

or

$$\frac{Q_{p,\text{A}_i^-} \cdot [\text{H}^+]}{K_{a,i}} + Q_{p,\text{A}_i^-} = Q_{p,\text{A}_i^-} \left( \frac{[\text{H}^+] + K_{a,i}}{K_{a,i}} \right) = Q_{\text{HA}_i}, \quad (4.5)$$

by combining equations (4.3) and (4.4). Therefore, the proton-binding isotherm can be obtained by the summation of all disprotonated components, as follows:

$$\sum Q_{p, A_i^-} = \sum \frac{K_{a,i}}{[H^+] + K_{a,i}} Q_{HA_i} \quad (\text{Series form}). \quad (4.6)$$

The integral from of equation (4.6) is derived by combining equations (4.2) and (4.6) as

$$\begin{aligned} \sum \frac{K_{a,i}}{[H^+] + K_{a,i}} Q_{HA_i} &= \sum \frac{K_{a,i}}{[H^+] + K_{a,i}} \int_{pK_{a,i}}^{pK_{a,i+1}} f(pK_a) dpK_a \\ &= \int_{pK_{a,j}}^{pK_{a,f}} \frac{K_a}{[H^+] + K_a} f(pK_a) dpK_a = \Theta(\text{pH}) \end{aligned} \quad (4.1.1)$$

(Here,  $\Theta_0$  can be added for derivation for equation (4.1)). The analytic solution of this integral equation (4.1) is established as follow [32, 37]:

$$\begin{aligned} F(pK_a) &= \left[ \sum_{i=0}^n (-1)^i \frac{\pi^{2i}}{(2i+1)!(\ln 10)^{2i}} \frac{\partial^{2i+1} \Theta(\text{pH})}{\partial (\text{pH})^{2i+1}} \right]_{\text{pH}=pK_a} \\ &= \left[ \frac{\partial \Theta(\text{pH})}{\partial \text{pH}} - \frac{\pi^2}{3!(\ln 10)^2} \frac{\partial^3 \Theta(\text{pH})}{\partial (\text{pH})^3} + \frac{\pi^4}{5!(\ln 10)^4} \frac{\partial^5 \Theta(\text{pH})}{\partial (\text{pH})^5} - \dots \right]_{\text{pH}=pK_a} \end{aligned} \quad (4.7)$$

In this work  $\Theta(\text{pH})$  of  $\text{N}_{12}\text{CNT}$  is induced from the direct titration curve (Fig. 1) adopting the universal titration equation developed in **Chapter 2** as shown in equation (2.8). Because the direct titration procedure was conducted with NaOH and HCl as the titrant and titrand, I will use universal titration equation (2.9) (base titrant form), which is rearranged as shown below.

$$Q_{OH^-}(\text{pH}) = \frac{\Theta(\text{pH}) + f_{\text{HCl titrand}}(\text{pH}) + f_{\text{HCl solvent}}(\text{pH})}{f_{\text{NaOH solvent}}(\text{pH})}, \quad (4.8)$$

where

$$\Theta(\text{pH}) = \sum \frac{Q_{\text{HA}_i}}{1 + [\text{H}^+] / K_{a,i}}, \quad (4.8.1)$$

$$f_{\text{HCl titrand}}(\text{pH}) = \frac{V_{\text{HCl}} \cdot c_{\text{HCl}}}{1 + [\text{H}^+] / K_{a,\text{HCl}}}, \quad (4.8.2)$$

$$f_{\text{HCl solvent}}(\text{pH}) = -\frac{V_{\text{HCl}}}{v_{\text{H}_2\text{O}} + 1 / [\text{H}^+]} + \frac{V_{\text{HCl}}}{v_{\text{H}_2\text{O}} + [\text{H}^+] / K_w}, \quad (4.8.3)$$

$$f_{\text{NaOH solvent}}(\text{pH}) = 1 + \frac{1 / c_{\text{NaOH}}}{v_{\text{H}_2\text{O}} + 1 / [\text{H}^+]} - \frac{1 / c_{\text{NaOH}}}{v_{\text{H}_2\text{O}} + [\text{H}^+] / K_w}. \quad (4.8.4)$$

The above functions show the effects of acidic functional groups of carbon sample ( $\Theta$ ), HCl titrand ( $f_{\text{HCl titrand}}$ ), solvent of HCl titrand ( $f_{\text{HCl solvent}}$ ), and solvent of NaOH titrant ( $f_{\text{NaOH solvent}}$ ) on the titration curve as a function of pH value, respectively. Here,  $Q_{OH^-}$  is the quantity of  $OH^-$  ion which is added from base titrant,  $K_{a,i}$  is acid ionization constant of acid  $HA_i$ ,  $[H^+]$  is the concentration of  $H^+$  ion,  $V_{\text{HCl}}$  is volume of the HCl titrand,  $c_{\text{HCl}}$  is the concentration of HCl titrant,  $v_{\text{H}_2\text{O}}$  is molar volume of water,  $K_w$  is self-ionization constant of water, and  $c_{\text{NaOH}}$  is the concentration of NaOH titrant.

Notably,  $\Theta(\text{pH})$  in equation (4.8.1) is a series expansion of the proton binding isotherm expressed in equation (4.1) as shown by equation (4.1.1). Therefore  $\Theta(\text{pH})$  can be obtained from direct titration curve of N<sub>12</sub>CNT (Fig. 4.1a) as follow:

$$\Theta(\text{pH}) = Q_{\text{OH}^-}(\text{pH}) \cdot f_{\text{NaOH solvent}}(\text{pH}) - f_{\text{HCl titrant}}(\text{pH}) - f_{\text{HCl solvent}}(\text{pH}). \quad (4.9)$$

Subsequently, the  $\text{p}K_a$  distribution function,  $F(\text{p}K_a)$ , of N<sub>12</sub>CNT can be obtained by adopting a series equation (4.7). Analytically, infinite expansion of the progression of equation (4.7) leads to the theoretical  $\text{p}K_a$  distribution. However, a complex smoothing process of the direct titration data is necessary for the high-order expansion of this series equation ( $i \geq 2$ ), as the actual titration curves inevitably contain experimental errors, which are geometrically accumulated as  $\Theta(\text{pH})$  becomes more differentiated at a high degree [32]. Therefore, in this work, only the first expansion of equation (4.7) was used for the  $F(\text{p}K_a)$  calculation from  $\Theta(\text{pH})$ , as follows:

$$F(\text{p}K_a) \cong \left[ \frac{\partial \Theta(\text{pH})}{\partial \text{pH}} \right]_{\text{pH}=\text{p}K_a}. \quad (4.7.1)$$

This type of first-order approximation is widely adopted for the calculation of the  $\text{p}K_a$  distribution of various carbon materials owing to its simplicity [35], and it was also practically valid for the one-pot titration methodology for surface characterization of carbon nanomaterials which will be further discussed in section 4.3.2.  $F(\text{p}K_a)$  was then normalized by the mass of carbon in the titrant to obtain normalized  $\text{p}K_a$  distribution



function,  $f(pK_a)$  [meq/g], as

$$f(pK_a) = \frac{F(pK_a)}{m_C} = \frac{F(pK_a)}{c_C \cdot V_{HCl}}, \quad (4.7.2)$$

where  $m_C$  and  $c_C$  denote the mass and concentration of the carbon samples in the HCl titrant, respectively. Similarly, the mass-normalized proton-binding isotherm,  $\theta(pH)$  [meq/g], can be defined as follows:

$$\theta(pH) = \frac{\Theta(pH)}{m_C} = \frac{\Theta(pH)}{c_C \cdot V_{HCl}}. \quad (4.9.1)$$

The obtained  $\theta(pH)$  was then substituted into equation (4.8) for the calculation of the theoretical titration curve to check the validity of the procedures. The experimental (open black squares and red circles) and recalculated titration curves (black solid lines) shown in Fig. 4.1a was identical with high precision, implying the obtained  $\theta(pH)$  and  $f(pK_a)$  is practically applicable.

The calculated  $f(pK_a)$  exhibited in Fig. 4.1c showed two distinct peaks around  $pK_a \approx 5$  and 10 and a small hump between them at  $pK_a \approx 8$  which may have originated from the carboxylic, phenolic, and lactonic groups, respectively, as generally demonstrated in previous reports[33, 35, 38].

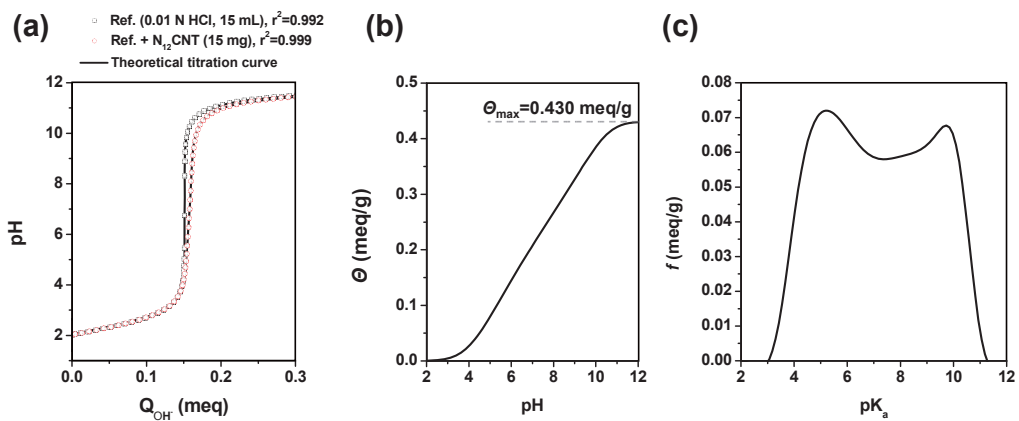


**Fig. 4.1.** (a) Direct titration curve of HCl titrant solutions with (red circle) and without (Ref.; black square) the agitation of the  $N_{12}CNT$  and their theoretical counterparts (black solid lines), where  $Q_{OH^-}$  is the quantity of NaOH titrant solution, (b) proton binding isotherm ( $\theta$ ), and (c)  $pK_a$  distribution function ( $f(pK_a)$ ) of  $N_{12}CNT$ .

### 4.3.2 Theoretical derivation of one-pot titration methodology

The basic concept of the calculation of the uptake quantities of the reaction bases (NaOH, Na<sub>2</sub>CO<sub>3</sub>, and NaHCO<sub>3</sub>) from this  $f(pK_a)$  value involves a simulation of a condition in which the acidic groups of the carbon materials are disprotonated. Herein, I assumed that the uptake amount of each reaction base is identical to the number of disprotonated sites of the functional groups of carbon samples in the reaction base. In addition, further protonation or disprotonation never occurs during the filtration step. The number of disprotonated sites is simply estimated by adopting the pH value of the mixture in an equilibrium state of the reaction base and the carbon materials (denoted  $pH_e$ ) into a proton binding isotherm (Fig. 1b in the case of N<sub>12</sub>CNT). This relationship is expressed as follows:

$$\text{Uptake} = \theta(pH_e). \quad (4.10)$$

In earlier work, this pH values were experimentally measured and utilized with the proton binding isotherms of the activated carbons for the calculation of the indirect titration results. In this approach, acidified activated carbons were reacted with the reaction bases for 24 hours and the  $pH_e$  of each reaction base mixture was then measured before the indirect titration filtration step. The proton binding isotherm at each pH value as determined with the direct titration method is in good agreement with the indirect titration result [31]. However, this process still requires a reaction step for each reaction base in each indirect titration condition, and the disprotonation behaviors of the acidic functional groups on the carbon surface with the reaction base have not been fully demonstrated.

In this work,  $\text{pH}_e$  values with different indirect titration conditions are systematically calculated from the  $f(\text{p}K_a)$  value (Fig. 1a for  $\text{N}_{12}\text{CNT}$ ) via the application of universal titration equation without any necessity of the additional experimental procedures. This computation process includes 1) a simulation of the titration curve of the mixture of the reaction base and carbon sample adopting the universal titration equation (Fig. 4.2a-4.2c), 2) a numerical calculation of the  $\text{pH}_e$  value of the simulated titration curve, and 3) substitution of  $\text{pH}_e$  into the pH axis of the proton binding isotherm of the carbon sample (Fig. 4.1c for  $\text{N}_{12}\text{CNT}$ ). The detailed derivation of the process is discussed below.

For the simulation of the titration curve of the mixture of the reaction base and the functional groups with the HCl titrant, the universal titration equation (2.8) (acid titrant form) introduced in **Chapter 2** is rearranged as follow:

$$Q_{\text{H}^+}(\text{pH}) = \frac{f_{\text{C}}(\text{pH}) + f_{\text{Base titrand}}(\text{pH}) + f_{\text{Base solvent}}(\text{pH})}{f_{\text{HCl solvent}}(\text{pH})}. \quad (4.11)$$

where

$$f_{\text{C}}(\text{pH}) = \sum \frac{Q_{\text{A}_i^-}}{1 + [\text{OH}^-] / K_{b,i}}, \quad (4.11.1)$$

$$f_{\text{Base titrand}}(\text{pH}) = \sum \frac{Q_{\text{Base,titrand}}}{1 + [\text{OH}^-] / K_{b,\text{Base}}}, \quad (4.11.2)$$

$$f_{\text{Base solvent}}(\text{pH}) = -\frac{V_{\text{Base}}}{v_{\text{H}_2\text{O}} + 1 / [\text{OH}^-]} + \frac{V_{\text{Base}}}{v_{\text{H}_2\text{O}} + [\text{OH}^-] / K_{\text{W}}}, \quad (4.11.3)$$

$$f_{\text{HCl solvent}}(\text{pH}) = 1 + \frac{1/c_{\text{HCl}}}{v_{\text{H}_2\text{O}} + 1/[\text{OH}^-]} - \frac{1/c_{\text{HCl}}}{v_{\text{H}_2\text{O}} + [\text{OH}^-]/K_w}. \quad (4.11.4)$$

As discussed in section 4.3.1, the above functions show the effects of the acidic functional groups on the carbon ( $f_c$ ), the base titrand ( $f_{\text{Base, titrand}}$ ), the solvent of the base titrand ( $f_{\text{Base solvent}}$ ), and the solvent of the HCl titrant ( $f_{\text{HCl solvent}}$ ) on the titration curve as a function of the pH value. Here,  $Q_{\text{H}^+}$  is the quantity of  $\text{H}^+$  ion which is added by acid titrant,  $K_{b,i}$  is base ionization constant of conjugated base  $\text{A}_i^-$ ,  $[\text{OH}^-]$  is the concentration of  $\text{OH}^-$  ion,  $V_{\text{Base}}$  is volume of the base titrand (reaction base in this case), and  $c_{\text{HCl}}$  is the concentration of HCl titrant. The practical applications of equation (4.11) to the titration curves of mixture of  $\text{N}_{12}\text{CNT}$  and the reaction bases are shown in Figs. 4.2a – 4.2c. The effect of the acidic sites,  $\text{HA}_i$ , on the titration curves on equation (4.11.1) can be readily calculated from the  $\text{p}K_a$  distribution function (Fig. 4.1c). Since the value of  $Q_{\text{A}_i^-}$  is fundamentally identical to that of  $Q_{\text{HA}_i}$  (equivalence of  $\text{HA}_i$ ), equation (4.11.1) can be formulated as shown below.

$$f_c(\text{pH}) = \sum \frac{Q_{\text{A}_i^-}}{1 + [\text{OH}^-]/K_{b,i}} = \sum \frac{Q_{\text{HA}_i}}{1 + K_{a,i}/[\text{H}^+]}. \quad (4.12)$$

Subsequently,  $Q_{\text{HA}_i}$  was obtained from  $\text{p}K_a$  distribution function,  $F(\text{p}K_{a,i})$  (see equation (4.7.1)) as

$$\begin{aligned}
Q_{\text{HA}_i} &= F(\text{p}K_{a,i}) \cdot (\text{p}K_{a,i+1} - \text{p}K_{a,i}) \\
&= m_C \cdot f(\text{p}K_{a,i}) \cdot (\text{p}K_{a,i+1} - \text{p}K_{a,i}) \\
&= c_C \cdot f(\text{p}K_{a,i}) \cdot (\text{p}K_{a,i+1} - \text{p}K_{a,i}) \cdot V_{\text{Base}}
\end{aligned} \tag{4.13}$$

For  $f_{\text{Base titrand}}(\text{pH})$  as described in equation (4.11.2), I apply the description discussed in section 3.3.1, **Chapter 3** showing the effects of  $\text{CO}_2$  on the titration of the Boehm's reaction bases. In the previous chapter,  $\text{Na}_2\text{CO}_3$  and  $\text{NaHCO}_3$  were considered as  $\text{CO}_2$ -contaminated  $\text{NaOH}$  solutions to estimate the titration behavior of each reaction base. The theoretical equation used to obtain the corresponding titration curves is as follows:

$$f_{\text{Base titrand}}(\text{pH}) = \frac{Q_{\text{OH}^-}}{1 + [\text{OH}^-]/K_{b,\text{OH}^-}} + \frac{Q_{\text{CO}_3^{2-}}}{1 + [\text{OH}^-]/K_{b,\text{CO}_3^{2-}}} + \frac{Q_{\text{HCO}_3^-}}{1 + [\text{OH}^-]/K_{b,\text{HCO}_3^-}}. \tag{4.14}$$

In this equation,  $\text{CO}_3^{2-}$  is assumed to be divided into an independent base component and proton binding sites, resulting in  $Q_{\text{CO}_3^{2-}} = Q_{\text{HCO}_3^-}$ . In section 3.3.1, it is assumed that  $\text{CO}_3^{2-}$  results from the dissolution of  $\text{CO}_2$  into the pure  $\text{NaOH}$  or  $\text{Na}_2\text{CO}_3$  solution by the following reactions [36, 37],



Therefore,  $Q_{\text{CO}_3^{2-}}$  is assumed to be identical to the quantity of hypothetically dissolved  $\text{CO}_2$  as

$$Q_{\text{CO}_3^{2-}} = Q_{\text{HCO}_3^-} = Q_{\text{CO}_2} \quad (4.16)$$

Additionally, NaOH can be further neutralized by  $\text{HA}_i$  from the carbon sample through the following equation:



The neutralization reactions (4.15) and (4.17) conserve the normality summation of the base components, which is defined as the alkalinity ( $Alk$ ), which can be expressed by the following equations,

$$Alk = [\text{OH}^-] + [\text{CO}_3^{2-}] + [\text{HCO}_3^-] + \sum [\text{A}_i^-]. \quad (4.18.1)$$

or

$$\begin{aligned} Q_{Alk} &= Q_{\text{OH}^-} + Q_{\text{CO}_3^{2-}} + Q_{\text{HCO}_3^-} + Q_{\text{A}^-} \\ &= Q_{\text{OH}^-} + 2Q_{\text{CO}_2} + Q_{\text{HA}} \end{aligned} \quad (4.18.2)$$

where  $Q_{Alk}$  is the total quantity (equivalence) of the base components ( $Q_{Alk} = Alk \cdot V_{\text{Base}}$ ) and  $Q_{\text{HA}} (= Q_{\text{A}^-})$  denotes the equivalence of the acidic groups on a carbon sample, which is the area of  $m_c \cdot f(pK_a)$ . Then equation (4.13) can be reconstructed as

$$f_{\text{Base titrand}}(\text{pH}) = \frac{Q_{\text{Alk}} - 2Q_{\text{CO}_2} - Q_{\text{HA}}}{1 + [\text{OH}^-]/K_{b,\text{OH}^-}} + \frac{Q_{\text{CO}_2}}{1 + [\text{OH}^-]/K_{b,\text{CO}_3^{2-}}} + \frac{Q_{\text{CO}_2}}{1 + [\text{OH}^-]/K_{b,\text{HCO}_3^-}}, \quad (4.14.1)$$

Subsequently, the CO<sub>2</sub> ratio,  $r_{\text{CO}_2}$ , is defined as

$$r_{\text{CO}_2} = \frac{Q_{\text{CO}_2}}{Q_{\text{Alk}}}. \quad (4.19)$$

$r_{\text{CO}_2}$  defined in equation (4.19) is theoretically identical to  $1 - \frac{Q_{\text{NP1}}}{Q_{\text{NP2}}}$ , where  $Q_{\text{NP1}}$  and

$Q_{\text{NP2}}$  are  $Q_{\text{H}^+}$  at the first and second neutralization points (NPs) shown on the titration curve of the reaction base with the HCl titrant. Notably, this relation was confirmed both theoretically and experimentally in titration of CO<sub>2</sub>-contaminated NaOH, Na<sub>2</sub>CO<sub>3</sub>, and NaHCO<sub>3</sub> in section 3.3.1, **Chapter 3** (see Fig. 3.1, and 3.3). Specifically, the ideal reaction bases can be demonstrated by NaOH solutions with different  $r_{\text{CO}_2}$  values; i.e.,  $r_{\text{CO}_2}$  is equal to 0, 0.5, and 1 for NaOH, Na<sub>2</sub>CO<sub>3</sub> and NaHCO<sub>3</sub>, respectively. However, at atmospheric atmosphere, these ratios are never preserved, as CO<sub>2</sub> in the air interacts with the reaction bases. For a precise comparison of the indirect titration and one-pot titration results,  $r_{\text{CO}_2}$  was measured from every pre-reaction base.

Following equation (4.19), equation (4.14.1) can be further reconstructed as



$$f_{\text{Base titrand}}(\text{pH}) = \left( \frac{\text{Alk} \cdot (1 - 2r_{\text{CO}_2}) - q_{\text{HA}} \cdot c_{\text{C}}}{1 + [\text{OH}^-] / K_{b,\text{OH}^-}} + \left( \frac{r_{\text{CO}_2}}{1 + [\text{OH}^-] / K_{b,\text{CO}_3^{2-}}} + \frac{r_{\text{CO}_2}}{1 + [\text{OH}^-] / K_{b,\text{HCO}_3^-}} \right) \text{Alk} \right) V_{\text{Base}}, \quad (4.14.2)$$

where  $q_{\text{HA}}$  is mass-normalized  $Q_{\text{HA}}$  ( $q_{\text{HA}} = \frac{Q_{\text{HA}}}{m_{\text{C}}} = \frac{Q_{\text{HA}}}{c_{\text{C}} \cdot V_{\text{Base}}}$ ) [meq/g], which is identical to the area of  $f(\text{p}K_a)$ . And then  $\text{pH}_e$  was numerically obtained by solving  $Q_{\text{H}^+}(\text{pH}_e) = 0$  on equation (4.11). This equation is identical to

$$\begin{aligned} & \sum \frac{c_{\text{C}} \cdot f(\text{p}K_{a,i}) \cdot (\text{p}K_{a,i+1} - \text{p}K_{a,i})}{1 + 10^{\text{pH}_e} \cdot K_{a,i}} \\ & + \left( \frac{\text{Alk} \cdot (1 - 2r_{\text{CO}_2}) - q_{\text{HA}} \cdot c_{\text{C}}}{1 + 10^{\text{pH}_e} \cdot K_{\text{W}} / K_{b,\text{OH}^-}} + \left( \frac{r_{\text{CO}_2}}{1 + 10^{\text{pH}_e} \cdot K_{\text{W}} / K_{b,\text{CO}_3^{2-}}} + \frac{r_{\text{CO}_2}}{1 + 10^{\text{pH}_e} \cdot K_{\text{W}} / K_{b,\text{HCO}_3^-}} \right) \text{Alk} \right) \\ & - \frac{1}{v_{\text{H}_2\text{O}} + 1 / (10^{\text{pH}_e} \cdot K_{\text{W}})} + \frac{1}{v_{\text{H}_2\text{O}} + 10^{\text{pH}_e}} = 0 \end{aligned} \quad (4.20)$$

by combining equations (4.11), (4.11.3), (4.11.4), (4.12), (4.13), and (4.14.2). Once  $f(\text{p}K_a)$  is determined for a carbon sample,  $\text{pH}_e$  should be a function of  $r_{\text{CO}_2}$ ,  $\text{Alk}$ , and  $c_{\text{C}}$ , as described in equation (4.21).

$$\text{pH}_e = f(r_{\text{CO}_2}, \text{Alk}, c_{\text{C}}). \quad (4.21)$$

Here,  $\text{pH}_e$  can be numerically calculated by equation (4.21) or from the simulated titration curves of the mixture of the carbon sample and the reaction base. It is then substituted to the pH axis of  $\theta(\text{pH})$  for the calculation of the uptake quantity of the reaction base by the functional groups. The derived one-pot titration methodology was applied to MWCNTs treated with nitric acid and the results were compared to typical indirect titration results (Table 4.1 and 4.2).

### 4.3.3 Practical application of one-pot titration methodology

For the easy understanding of the one-pot titration methodology, the essential procedures were preferentially adopted with the reaction mixture of 0.01 N reaction base and  $\text{N}_{12}\text{CNT}$  (1 mg/mL). Under this condition, the normality of the functional group ( $\theta_{\text{max}}(0.430 \text{ meq/g}) \cdot c_{\text{C}}(1 \text{ mg/mL}) = 0.430 \text{ mN}$ ) is much lower (4.3 %) than  $\text{Alk}$  (0.01 N) of the reaction bases. For the calculation of the  $\text{pH}_e$  of each reaction base, the corresponding titration curve (Figs. 4.2a – 4.2c) was calculated applying equation (4.10). As shown in the insets of Figs. 4.2a – 4.2c, the initial pH values at  $Q_{\text{OH}^-} = 0$  ( $\text{pH}_e$ ) decreased from 12.00, 10.93, and 8.31 to 11.98, 10.81, and 7.88 for  $\text{NaOH}$  ( $r_{\text{CO}_2} = 0$ ),  $\text{Na}_2\text{CO}_3$  ( $r_{\text{CO}_2} = 0.5$ ), and  $\text{NaHCO}_3$  ( $r_{\text{CO}_2} = 1$ ), respectively. Notably, the  $\text{pH}_e$  with different values of  $r_{\text{CO}_2}$  ranging from 0 to 1 possibly observable under a laboratory condition can easily be estimated by applying the one-pot titration process, as shown by the black dashed line in Fig. 4.2d.

The suggested methodology also provides a deeper understanding of the interaction between the reaction base and the functional groups expressed by  $f(\text{p}K_a)$ . This interaction can be demonstrated by showing how many functional groups are dissociated at a specific value of  $\text{p}K_a$  when the carbon sample is agitated in the reaction base. For this

purpose, the distribution function of the proton-dissociated sites of the functional groups at  $\text{pH}_e$ , which is the defined proton-dissociated  $f(\text{p}K_a)$  when  $\text{p}K_a = \text{p}K_{a,i}$ , was numerically calculated by applying equations (4.6) and (4.13) in [31, 32]

$$\text{proton dissociated } f(\text{p}K_{a,i}) = \left[ \frac{\frac{K_{a,i}}{[\text{H}^+] + K_{a,i}} Q_{\text{HA}_i}}{c_C \cdot (\text{p}K_{a,i+1} - \text{p}K_{a,i}) \cdot V_{\text{Base}}} \right]_{\text{pH}=\text{pH}_e}, \quad (4.22)$$

or

$$\text{proton dissociated } f(\text{p}K_{a,i}) = \left[ \frac{K_{a,i}}{[\text{H}^+] + K_{a,i}} f(\text{p}K_{a,i}) \right]_{\text{pH}=\text{pH}_e}. \quad (4.23)$$

Fig. 4.2e shows the proton-dissociated  $f(\text{p}K_a)$  value of  $\text{N}_{12}\text{CNT}$  (1 mg/mL) which is assumed to be mixed into the 0.01 N NaOH (red dashed line),  $\text{Na}_2\text{CO}_3$  (blue dotted line), and  $\text{NaHCO}_3$  (green dash-dotted line). The original  $f(\text{p}K_a)$  shown in Fig. 4.1c is shown as a black solid line for comparison. It is easily observed from the plot that all functional groups are dissociated when  $\text{N}_{12}\text{CNT}$  is mixed into NaOH. As  $r_{\text{CO}_2}$  of the reaction increased, the fraction of dissociated sites clearly decreased. For  $\text{Na}_2\text{CO}_3$ , for which  $r_{\text{CO}_2} = 0.5$ , all functional groups were dissociated in the range of  $3 < \text{p}K_a < 9$  and were partially dissociated when  $\text{p}K_a$  was greater than 9. Meanwhile, the  $\text{p}K_a$  limitation for the 100 % dissociation decreased to  $\text{p}K_a \approx 5.5$  while the dissociation fraction gradually decreased with  $\text{p}K_a$  in the case of  $\text{NaHCO}_3$  ( $r_{\text{CO}_2} = 0$ ). To the best of my knowledge, this

type of systematic demonstration, showing the dissociation behaviors of the functional groups in the presence of the reaction base, has rarely been reported in earlier works on  $pK_a$  distribution functions, i.e.,  $f(pK_a)$ , of various carbon materials. Typically, the fraction of functional groups with strong ( $pK_a < 7$ ) or weak ( $pK_a > 7$ ) acidic strength levels are determined by the simple division of  $f(pK_a)$  [33, 36].

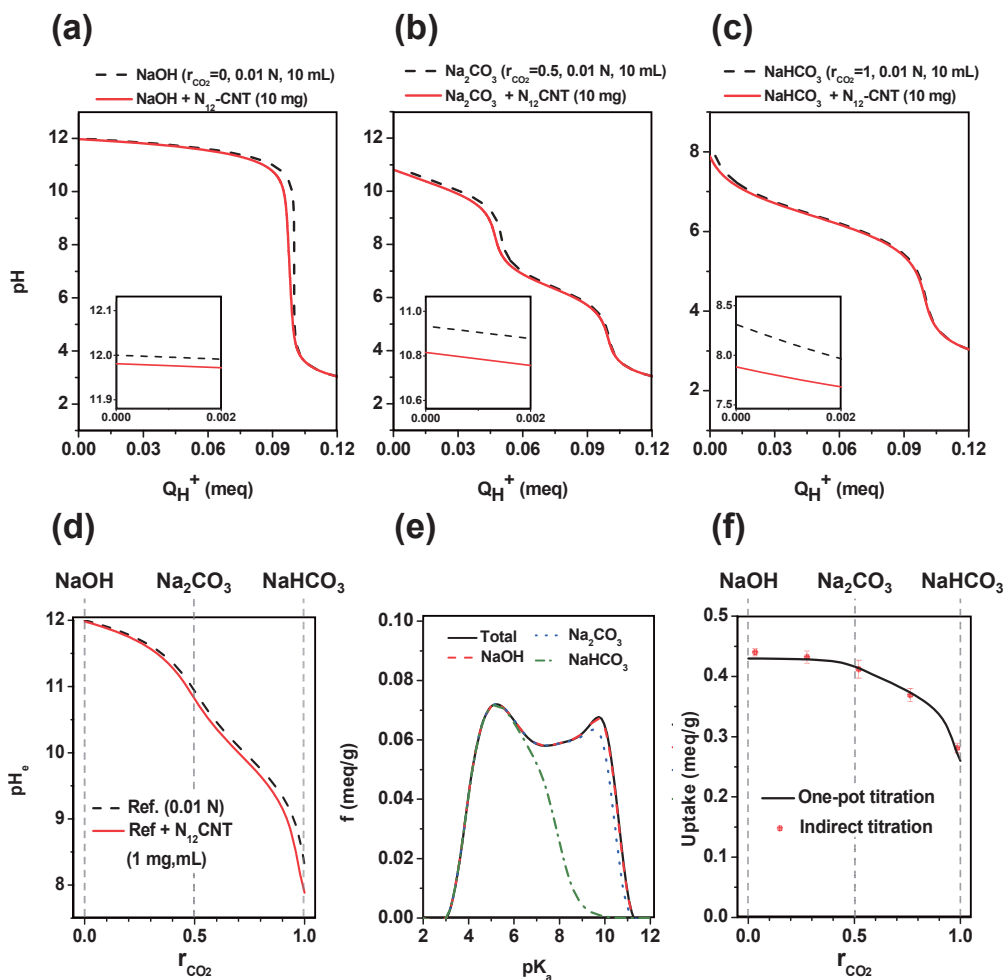


**Fig. 4.2.** Calculated titration curve of 10 mL of the 0.01 N reaction bases: (a) NaOH, (b) Na<sub>2</sub>CO<sub>3</sub>, and (c) NaHCO<sub>3</sub> (black dashed lines refer to the reference reaction bases and red solid lines denote the mixture with 10 mg of N<sub>12</sub>CNT). (d) pH<sub>e</sub> of the 0.01 N reaction base as a function of  $r_{CO_2}$ , (e) proton-dissociated  $f(pK_a)$  of N<sub>12</sub>CNT ( $c_C = 1$  mg/mL,  $Alk = 0.1$  N), and (f) reaction base uptake quantity of N<sub>12</sub>CNT as a function of  $r_{CO_2}$  from the one-pot titration (black solid line) method and the indirect titration (red dots) method.

My approach also makes it possible to estimate the indirect titration results without the need for an indirect titration process [22, 27] or even the experimental measurement of the  $\text{pH}_e$  of the reaction mixture [31]. The uptake amount of each reaction base from the indirect titration was obtained from the proton-dissociated  $f(\text{p}K_a)$  area (Fig. 4.2e) of the corresponding reaction base, or simply from the substitution of  $\text{pH}_e$  into pH axis of  $\theta(\text{pH})$ , as shown in Fig. 1b. In addition to ordinary reaction bases, the uptake of the reaction base with different  $r_{\text{CO}_2}$  values can be computed as shown in Fig. 4.2f. This calculation with a varying value of  $r_{\text{CO}_2}$  is practically significant, as a pure reaction base with an ideal  $r_{\text{CO}_2}$  can never exist under an actual real condition due to the absorption or desorption of  $\text{CO}_2$  into or from the reaction bases, respectively, as discussed in **Chapter 3**. Even in an inert condition (glove box),  $\text{Na}_2\text{CO}_3$  or  $\text{NaHCO}_3$  will desorb  $\text{CO}_2$ , which will lower their  $r_{\text{CO}_2}$  values [22, 39]. Nevertheless, the  $r_{\text{CO}_2}$  values of the reaction bases used in the indirect titration experiments were maintained as the ideal values to the greatest extent possible by minimizing their exposure to the atmosphere ( $r_{\text{CO}_2} = 0.04$ , 0.52, and 0.99 for  $\text{NaOH}$ ,  $\text{Na}_2\text{CO}_3$ , and  $\text{NaHCO}_3$ , respectively). Additionally, reaction bases with different  $r_{\text{CO}_2}$  values (0.28, 0.76) were prepared for a more detailed comparison of the one-pot and the indirect titration results (the black solid line and the red dots in Fig. 4.2f, respectively).

As shown in Fig. 4.2f, the uptake computed from the one-pot titration (black solid line) method decreased gradually from 0.430 to 0.416 meq/g as  $r_{\text{CO}_2}$  increased from 0 ( $\text{NaOH}$ ) to 0.5 ( $\text{Na}_2\text{CO}_3$ ), followed by drastic decrease to 0.260 meq/g at  $r_{\text{CO}_2} = 1$  ( $\text{NaHCO}_3$ ). This is also shown in Fig. 4.2f from the observation of the populations of proton dissociated sites in each reaction base. Notably, the typical indirect titration

results (red dots) also showed a similar tendency compared to the one-pot titration results (red dots on Fig. 2f) with a determination coefficient ( $r^2$ ) of 0.986. This similarity implies that the one-pot titration methodology is practically useful and has the potential to be an efficient alternative to the typical indirect titration procedures.

The analogy can be extensively applied to reaction mixtures while varying  $Alk$  or  $c_C$ , as described in equation (4.20) or (4.21). Figs. 4.3c and 4.4c show the uptake of the reaction base as a function of  $r_{CO_2}$  with various  $Alk$  and  $c_C$  values, respectively; these have been typically adopted in previous indirect titration experiments on various carbon materials [22-29].

As shown in Figs. 4.3 and 4.4, the one-pot titration methodology estimated that these experimental variables significantly affect the proton dissociation behaviors of the functional groups and thereby change the uptake of the reaction base. The entire proton dissociation fraction was diminished as  $c_C$  increased and as  $Alk$  decreased due to the limitation of the proton dissociating capacity of the reaction base. These tendencies were reconstructed for the representative reaction bases ( $NaOH$ ,  $Na_2CO_3$ , and  $NaHCO_3$ ) to clarify the effects of  $c_C$  and  $Alk$  on the uptake of each reaction base and the resultant estimations of the concentrations of the functional groups shown in Fig. 4.5. As shown in Figs. 4.5a and 4.5b, the uptake amount of  $NaOH$  was mostly preserved while varying the experimental variables. Meanwhile, those of  $Na_2CO_3$  and  $NaHCO_3$  are sensitive to both  $c_C$  and  $Alk$ . As a result, the concentrations of the functional groups estimated from the difference in the uptakes between the reaction bases (applying equations (3.2.1) – (3.2.3)) also changed despite the fact that the nature of the acidity did not change (Figs 4.5c and 4.5d).

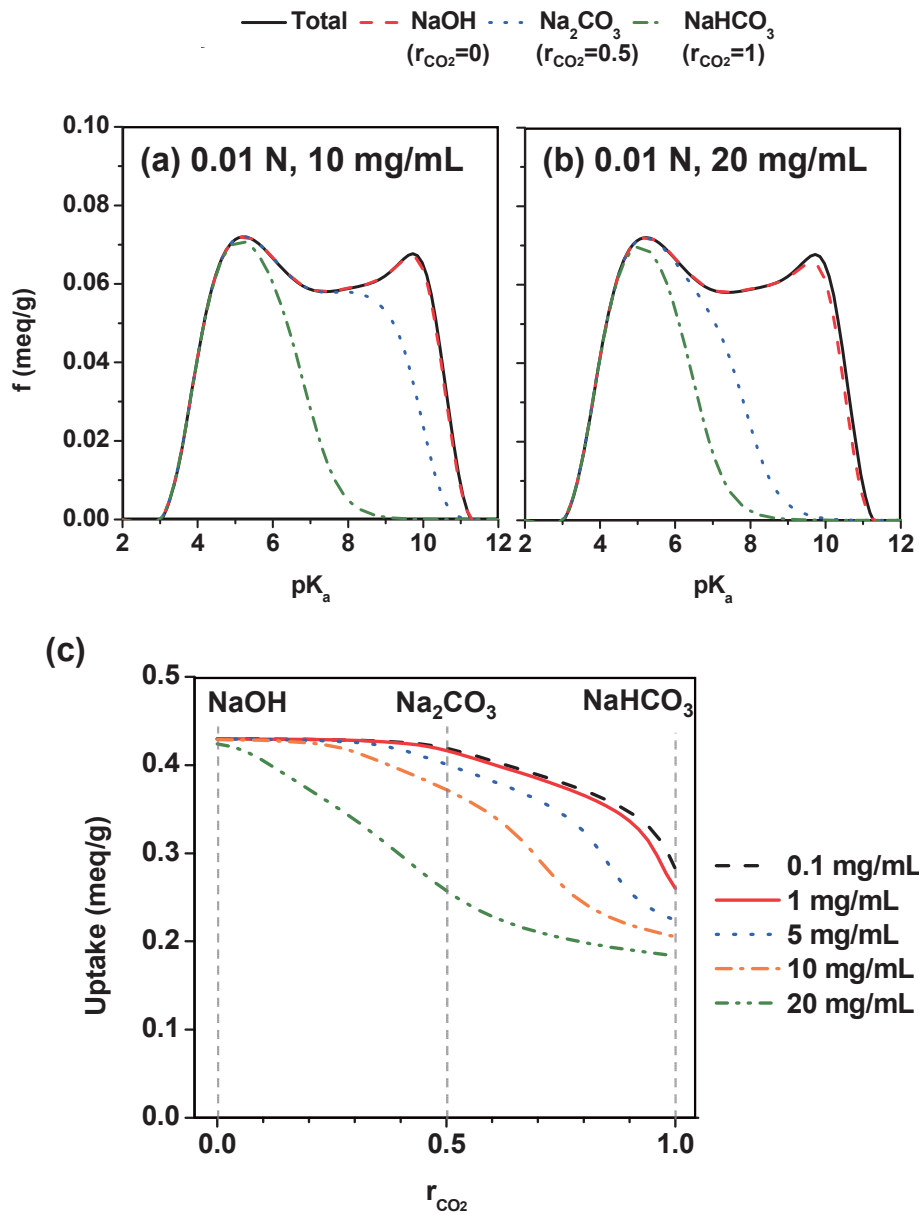


**Fig 4.3.** Proton-dissociation  $f(pK_a)$  of (a) 10 and (b) 20 mg/mL  $N_{12}CNT$  in the 0.01 N reaction base. (c) Reaction base uptake quantity of  $N_{12}CNT$  as a function of  $r_{CO_2}$  with the variation of  $c_C$  of the reaction base.



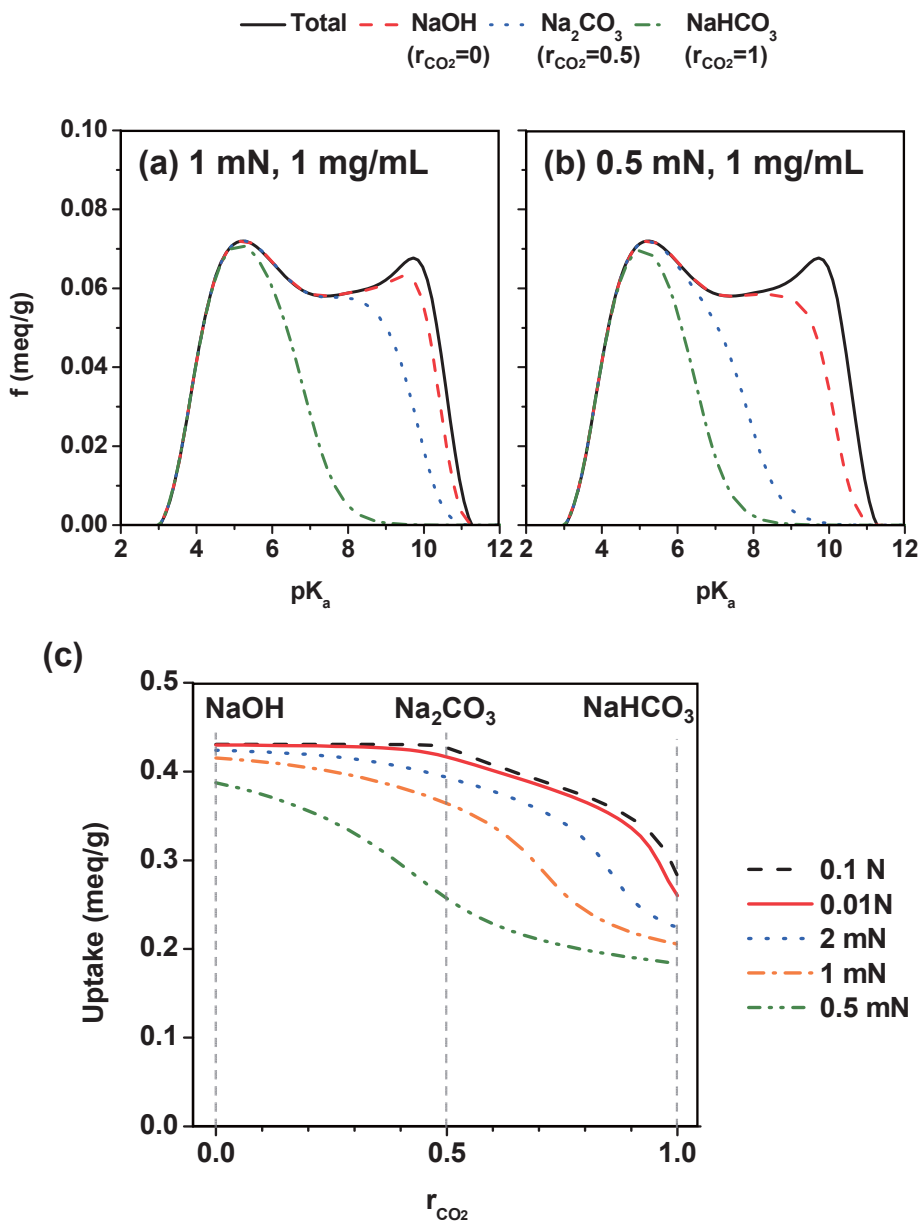


**Fig. 4.4.** Proton dissociation  $f(pK_a)$  of 1 mg/mL  $N_{12}CNT$  in the reaction base with (a)  $Alk = 1$  mN and (b) 0.5 mN. (c) Reaction base uptake quantity of  $N_{12}CNT$  as a function of  $r_{CO_2}$  with the variation of  $Alk$  of the reaction base.

Indeed, the indirect titration results in Table 4.1 shows the uptake amounts of all reaction bases were lowered as the normality of  $N_{12}CNT$  reached 0.43 of that of the reaction base ( $[c_C, Alk] = [1 \text{ mg/mL}, 1 \text{ mN}]$ , and  $[10 \text{ mg/mL}, 0.1 \text{ N}]$ ) from 0.043. In cases with a high normality ratio (0.43), the uptake quantities measured by means of indirect titration were 10 – 20 % lower than those estimated with the one-pot titration methodology, possibly due to the reattachment of some protons to the functional groups during the filtration procedures with the local increase in  $c_C$  in the reaction mixture. In these extreme cases, the major assumption that the reaction base uptake is identical to the number of proton-dissociated sites in the reaction mixture may be partially invalid. Nevertheless, the one-pot titration approach successfully forecasted the uptake variations by the carbon concentration or via normality differences in the reaction base by monitoring the interactions between the functional groups and the reaction base molecules.

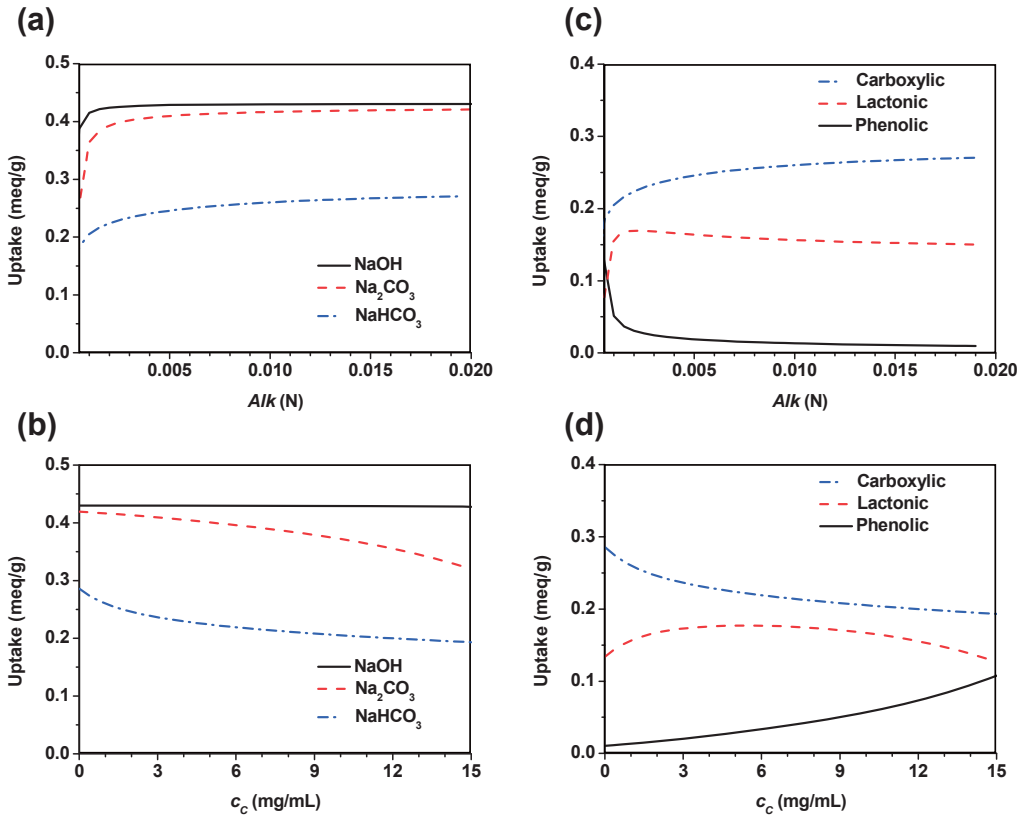


**Fig. 4.5.** Reaction base uptake quantity of  $N_{12}CNT$  as a function of (a)  $Alk$  and (b)  $c_c$  and (c, d) the corresponding resultant concentrations of the functional groups, respectively.

**Table 4.1.** Comparison between one-pot and indirect titration results for the low ( $\theta_{\max} \cdot c_C / Alk = 0.043$ ) and high ( $\theta_{\max} \cdot c_C / Alk = 0.43$ ) normality ratio of N<sub>12</sub>CNT to the reaction bases

Condition	Titration method	Uptake (meq/g)		
		NaOH	Na <sub>2</sub> CO <sub>3</sub>	NaHCO <sub>3</sub>
$c_C = 1 \text{ mg/mL}$ $Alk = 0.01\text{N}$ $(\theta_{\max} \cdot c_C / Alk = 0.043)$	One-pot	0.430	0.413	0.271
	Indirect	0.440 ±0.006	0.412 ±0.015	0.281 ±0.008
$c_C = 10 \text{ mg/mL}$ $Alk = 0.01\text{N}$ $(\theta_{\max} \cdot c_C / Alk = 0.43)$	One-pot	0.429	0.372	0.205
	Indirect	0.413 ±0.003	0.322 ±0.005	0.160 ±0.011
$c_C = 1 \text{ mg/mL}$ $Alk = 1 \text{ mN}$ $(\theta_{\max} \cdot c_C / Alk = 0.43)$	One-pot	0.404	0.360	0.208
	Indirect	0.363 ±0.008	0.325 ±0.004	0.189 ±0.003

The effects of  $Alk$  and  $c_C$  on the titration results were visualized more clearly by the construction of the three-dimensional graphics showing the uptake quantities of the reaction bases (Fig. 4.6a) and the resultant concentrations of the functional groups (Fig. 4.6b) with various combinations of  $Alk$  and  $c_C$ , which is defined ‘One-pot titration diagram’. The experimental conditions under which indirect titration should be conducted can be determined from this diagram. As shown in Fig. 4.6b, the titration results changed remarkably with the variations of  $c_C$  and  $Alk$  at the boundary, where  $\theta_{\max} \cdot c_C / Alk$  is greater than 10 %. At the lower boundary, the uptake of each reaction base nearly reached its maximum value; therefore, the variations in the results were relatively small. This observation implies that the experimental conditions during indirect titration should be carefully determined considering the nature of the acidity of the carbon materials to obtain reliable and reproducible results. Therefore, when conducting indirect titration,  $\theta_{\max}$  should be roughly measured first from the uptake of NaOH at arbitrary  $c_C$  and  $Alk$  values as a preliminary test for the determination of a valid experimental condition ( $\theta_{\max} \cdot c_C / Alk < 10\%$ ) followed by the main procedures with the reaction bases. On the other hand, the one-pot titration methodology provides all of the titration results obtainable from both conventional indirect titration without the necessity of a series of procedures during the indirect titration process.

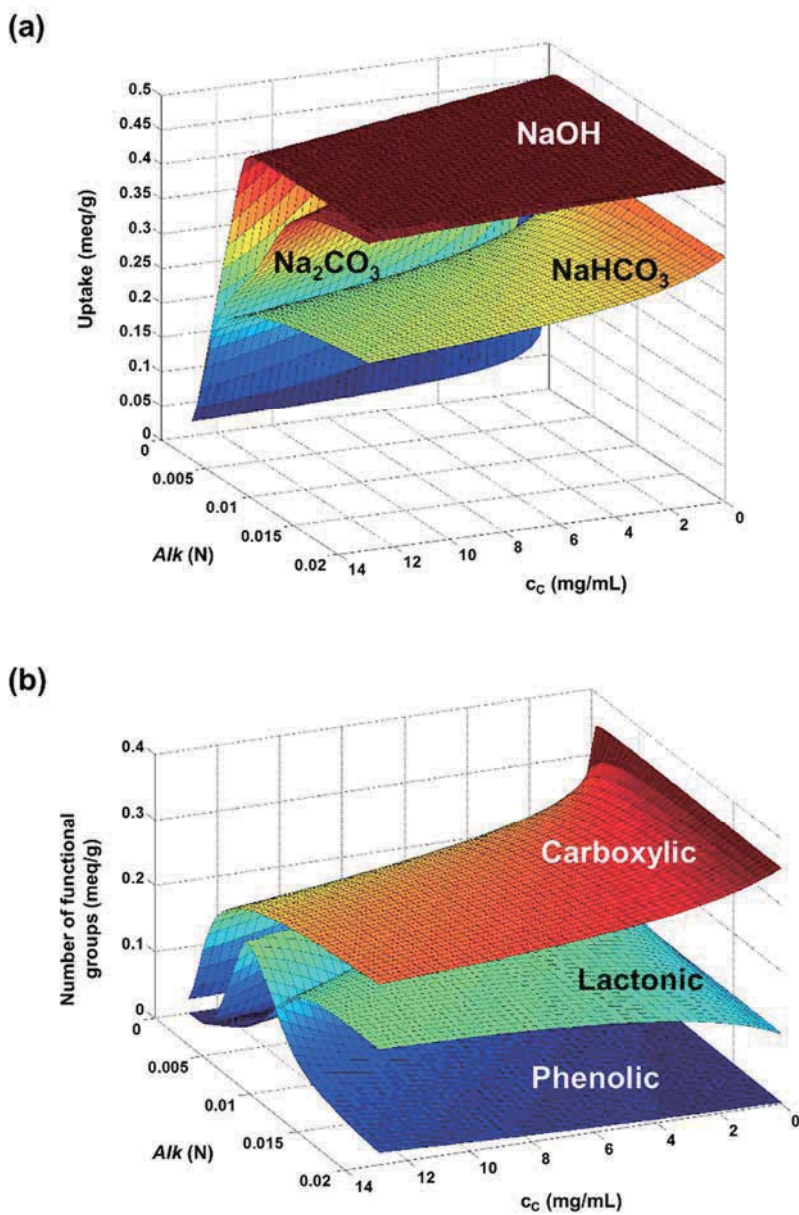


**Fig. 4.6.** One-pot titration diagram of  $\text{N}_{12}\text{CNT}$  exhibiting (a) the uptake quantity of the reaction bases and (b) the concentrations of functional groups as a function of  $Alk$  and  $c_c$ .

#### 4.3.4 Comparison between one-pot and indirect titration results of oxidized CNTs

The one-pot titration methodology developed in this work was also applied during the surface characterization of the nitric acid-oxidized MWCNTs with various oxidation periods ( $N_6$ CNT,  $N_{12}$ CNT, and  $N_{24}$ CNT). Following the same calculation procedures described in the previous section, the  $f(pK_a)$  (the black solid line in Figs. 4.8a – 4.8c) of these samples were computed from the  $\theta(\text{pH})$  derived from the corresponding titration curves (Fig. 4.7). The proton-binding isotherms showed that the total number of functional group ( $\theta_{\text{max}}$ ) increased from 0.364 to 0.754 meq/g with longer oxidation periods (see Fig. 4.7). The shape of  $f(pK_a)$  became more complex, and one or two additional peaks appeared in the low  $pK_a$  regions, possibly due to the formation of more acidic carboxylic groups as the oxidation process continued [33]. Nevertheless, the concentrations of functional groups which practically serve as carboxylic, lactonic, and phenolic groups can be readily obtained from the one-pot titration methodology. Notably, as shown in Fig. 4.8d, the uptake quantities of the reaction bases from the one-pot titration and indirect titration methods were identical to each other for all CNT samples. Additionally, the effects of  $Alk$  and  $c_C$  on the titration results of these samples are visualized in the one-pot titration diagrams shown in Figs. 4.9 – 4.11.

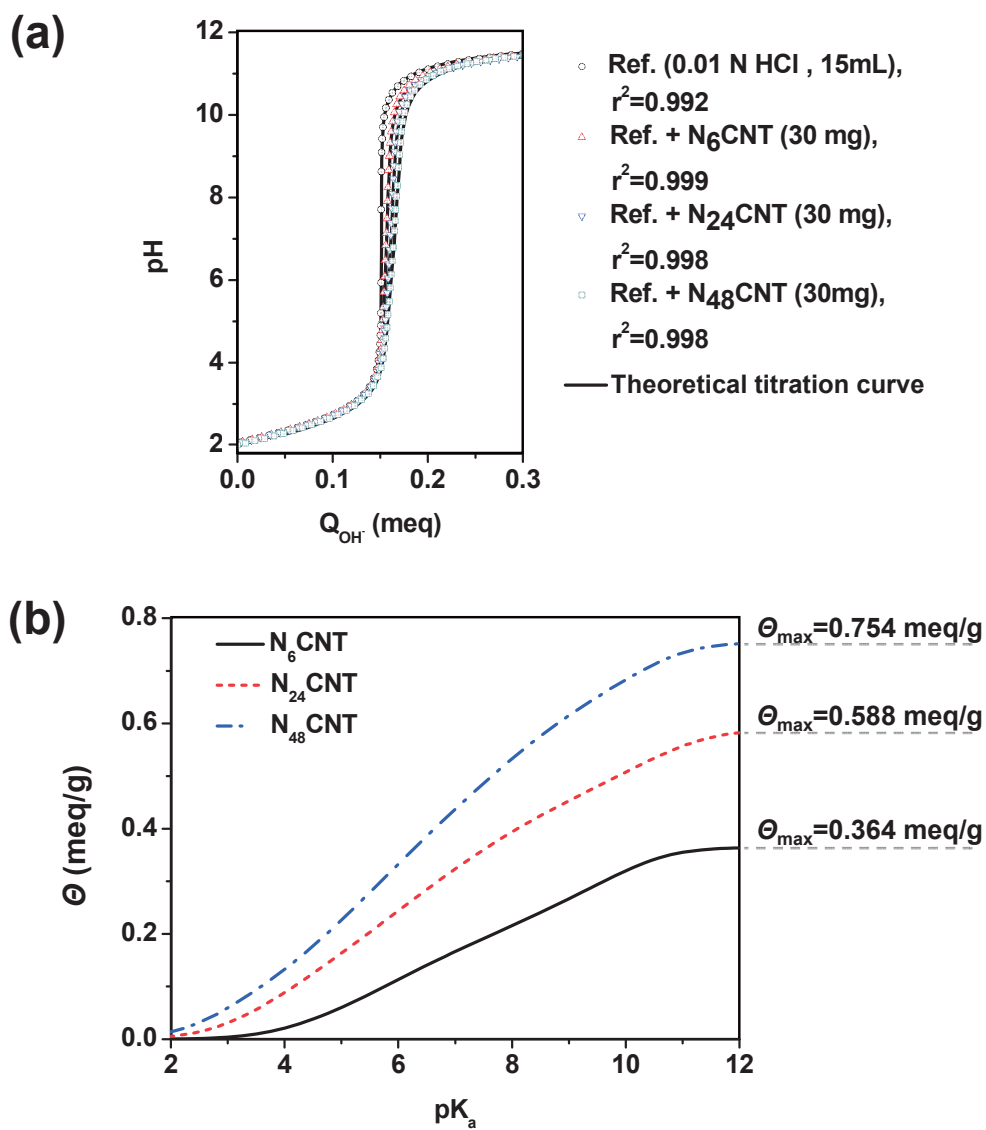
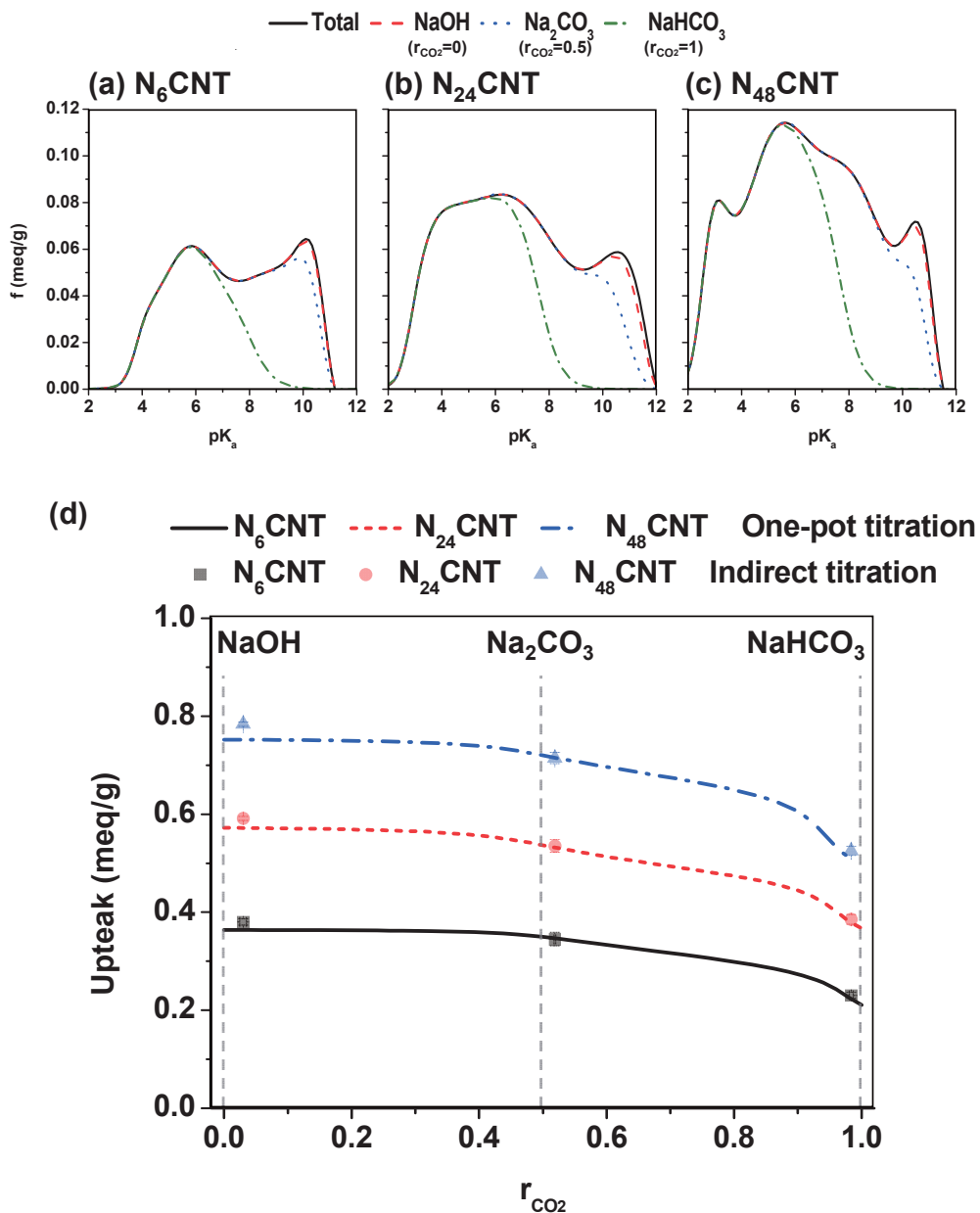
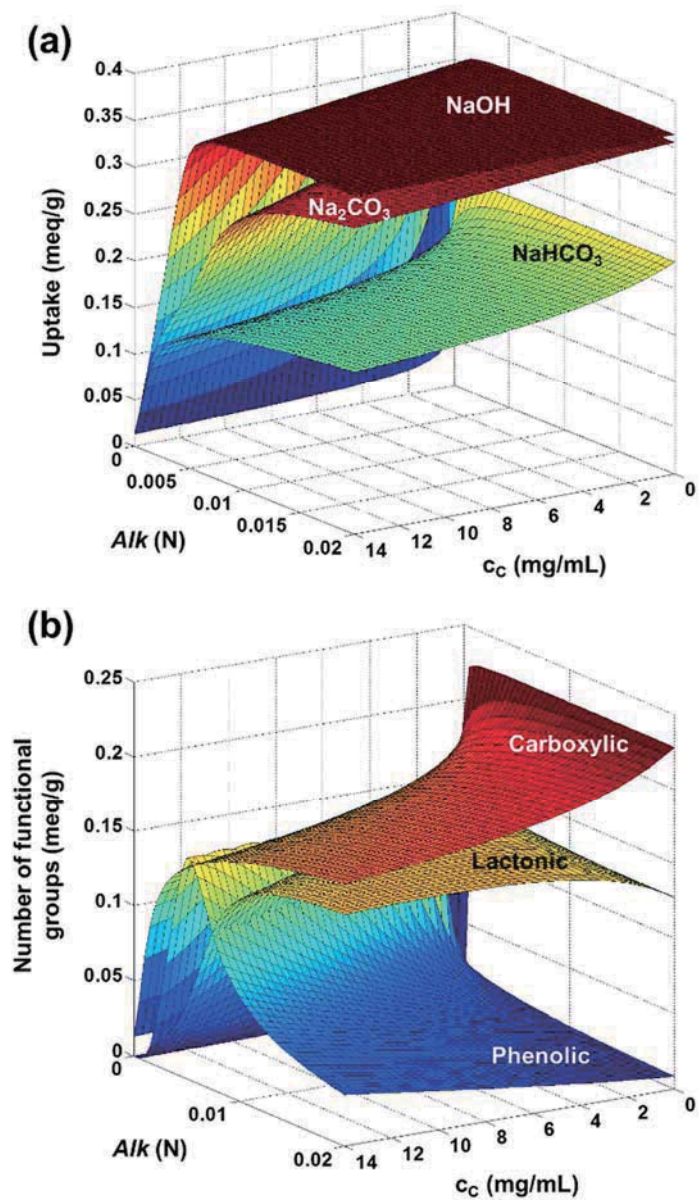


Fig. 4.7. (a) Experimental and theoretical titration curves of the mixture of 0.01 N HCl and (b) the proton-binding isotherms of N<sub>6</sub>CNT, N<sub>24</sub>CNT, and N<sub>48</sub>CNT.





**Fig 4.8.** Proton-dissociated  $f(pK_a)$  of 1 mg/mL (a)  $N_6$ CNT, (b)  $N_{24}$ CNT, and (c)  $N_{48}$ CNT in 0.01 N reaction bases. (d) Reaction base uptake quantities of  $N_6$ CNT,  $N_{24}$ CNT, and  $N_{48}$ CNT as a function of  $r_{CO_2}$  from the one-pot titration and indirect titration methods.



**Fig. 4.9.** One-pot titration diagram of N<sub>6</sub>CNT exhibiting (a) the uptake quantity of the reaction bases and (b) the concentrations of functional groups as a function of *Alk* and *c<sub>c</sub>*.

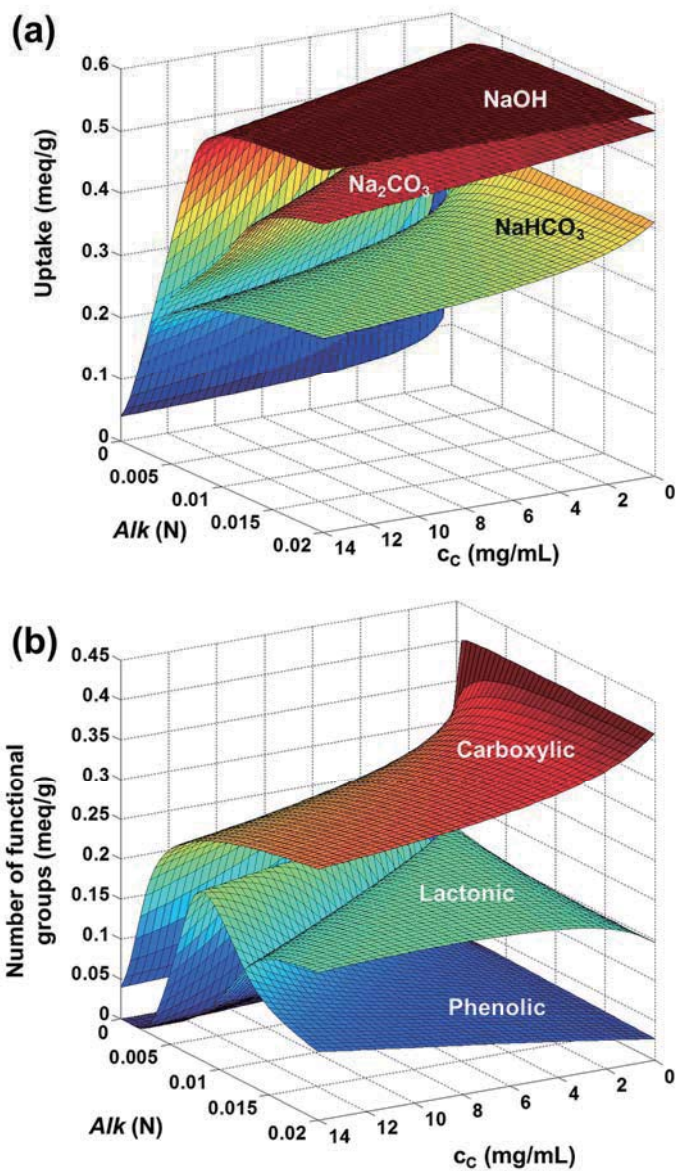


**Fig. 4.10.** One-pot titration diagram of N<sub>24</sub>CNT exhibiting (a) the uptake quantity of the reaction bases and (b) the concentrations of functional groups as a function of *Alk* and *c<sub>C</sub>*.

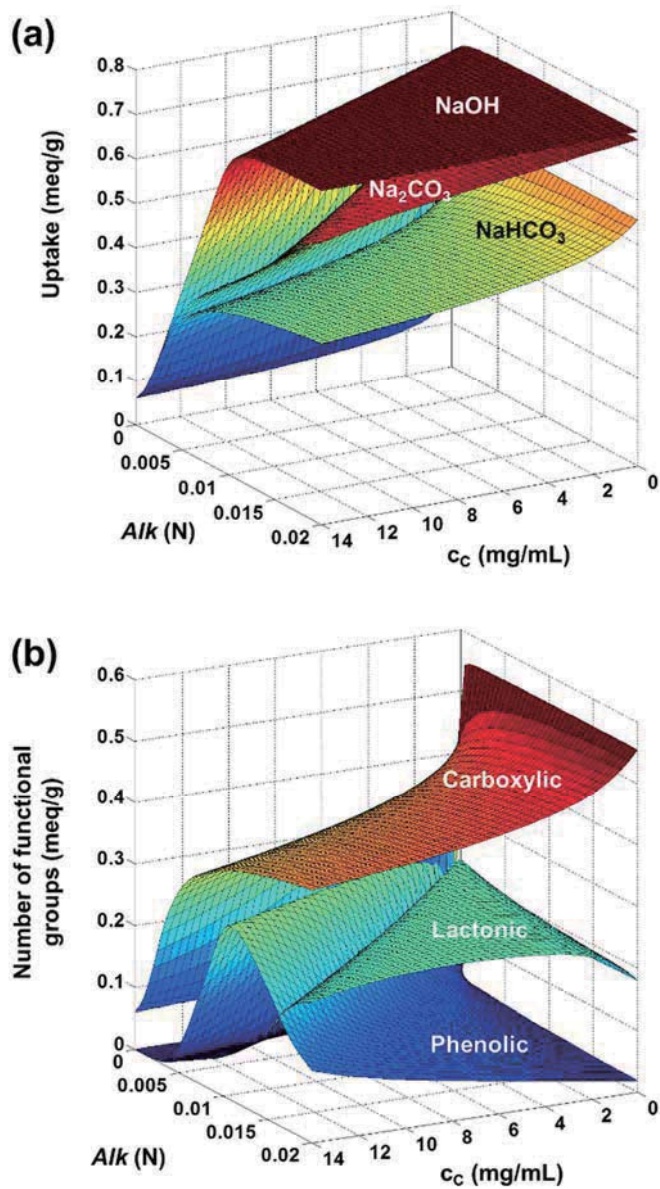


**Fig. 4.11.** One-pot titration diagram of N<sub>48</sub>CNT exhibiting (a) the uptake quantity of the reaction bases and (b) the concentrations of functional groups as a function of *Alk* and *c<sub>C</sub>*.

These results were compared to the indirect titration results in the specific experimental conditions. Herein,  $c_C$  and  $Alk$  of the reaction bases were determined to be 1 mg/mL and 0.01 N, respectively; therefore, the  $\theta_{\max} \cdot c_C / Alk$  values are lower than 10 % for all samples. For a fair comparison, 2% of the uncertainties in the experimental procedures during the preparation of the samples and the reaction bases arose in the one-pot titration calculation. Specifically,  $c_C$  and  $Alk$  were assumed to be between 0.98 and 1.02 mg/mL and 0.0098 and 0.0102 N, respectively. Considering the absorption and desorption behaviors of the reaction bases discussed in section 3.3.1, **Chapter 3**,  $r_{CO_2}$  was assumed to be in the ranges of 0 – 0.04, 0.5 – 0.54, and, 0.96 – 0.1 for NaOH, Na<sub>2</sub>CO<sub>3</sub>, and NaHCO<sub>3</sub>, respectively.

Table 4.2 and 4.3 compare the one-pot and conventional indirect titration results of the prepared CNTs. Significantly, the results were fairly identical within acceptable error ranges. These correspondences imply that the suggested computation methodology of one-pot titration is practically valid for estimations of indirect titration results from direct titration procedures. More importantly, the repetition of complex procedures with each reaction base during the typical indirect titration process is clearly unnecessary when utilizing the one-pot titration methodology, remarkably reducing the efforts and periods required in the determination of practical functional groups.

This methodology can be especially useful for highly oxidized CNTs [20, 28] or graphene oxides [29, 30] for which filtration is difficult or impossible when using the indirect titration method. Additionally, the logic used in the one-pot titration methodology has the potential to be applied to estimate the interaction between carbon nanomaterials with a variety of acid or base environments, thus breaking the

aforementioned limitation and enhancing the possible applications of the titration methodology, which will be shown in **Chapter 5** and **6**.

**Table 4.2.** Comparison between the uptake quantities of the reaction bases from one-pot and indirect titration.

Sample	Titration method	Uptake (meq/g)		
		NaOH	Na <sub>2</sub> CO <sub>3</sub>	NaHCO <sub>3</sub>
N <sub>6</sub> CNT	One-pot	0.364 ±0.001	0.347 ±0.002	0.226 ±0.013
	Indirect	0.376 ±0.006	0.342 ±0.014	0.231 ±0.006
N <sub>12</sub> CNT	One-pot	0.430 ±0.001	0.414 ±0.002	0.278 ±0.016
	Indirect	0.440 ±0.006	0.412 ±0.015	0.281 ±0.015
N <sub>24</sub> CNT	One-pot	0.581 ±0.001	0.539 ±0.004	0.390 ±0.015
	Indirect	0.587 ±0.004	0.531 ±0.011	0.381 ±0.010
N <sub>48</sub> CNT	One-pot	0.752 ±0.001	0.716 ±0.004	0.513 ±0.016
	Indirect	0.780 ±0.004	0.711 ±0.012	0.521 ±0.008

**Table 4.3.** Comparison of the concentrations of functional groups from the one-pot and indirect titration methods (calculations based on Figs. 4.2f and 4.8d)

Sample	Titration method	Concentrations of functional groups (meq/g)			
		Carboxylic	Lactonic	Phenolic	Total
<b>N<sub>6</sub>CNT</b>	One-pot	0.226 ±0.013	0.120 ±0.013	0.017 ±0.002	<b>0.364</b> <b>±0.001</b>
	Indirect	0.231 ±0.006	0.110 ±0.015	0.035 ±0.014	<b>0.376</b> <b>±0.006</b>
<b>N<sub>12</sub>CNT</b>	One-pot	0.278 ±0.016	0.136 ±0.016	0.016 ±0.002	<b>0.430</b> <b>±0.001</b>
	Indirect	0.281 ±0.015	0.130 ±0.016	0.028 ±0.015	<b>0.440</b> <b>±0.006</b>
<b>N<sub>24</sub>CNT</b>	One-pot	0.390 ±0.015	0.149 ±0.015	0.042 ±0.003	<b>0.581</b> <b>±0.001</b>
	Indirect	0.381 ±0.010	0.145 ±0.015	0.062 ±0.013	<b>0.587</b> <b>±0.004</b>
<b>N<sub>48</sub>CNT</b>	One-pot	0.513 ±0.016	0.203 ±0.017	0.037 ±0.004	<b>0.752</b> <b>±0.001</b>
	Indirect	0.521 ±0.008	0.189 ±0.014	0.069 ±0.012	<b>0.780</b> <b>±0.004</b>

## 4.4 Conclusions

I develop a convenient and fundamental one-pot titration methodology for the conversion of the  $pK_a$  distribution function from direct titration results to practical indirect titration results for the surface characterization of carbon nanomaterials. The developed one-pot titration methodology may ultimately break the boundary between the indirect and direct titration methods for the characterization of practical functional groups and further investigations of their roles in applications of carbon nanomaterials.



## 4.5 References

- [1] Kim SW, Kim T, Kim YS, Choi HS, Lim HJ, Yang SJ, et al., *Carbon*, 50 (2012) 3-33.
- [2] Cho HG, Kim SW, Lim HJ, Yun CH, Lee HS, Park CR, *Carbon*, 47 (2009) 3544-9.
- [3] Wang YB, Iqbal Z, Mitra S, *J Am Chem Soc*, 128 (2006) 95-9.
- [4] Datsyuk V, Kalyva M, Papagelis K, Parthenios J, Tasis D, Siokou A, et al., *Carbon*, 46 (2008) 833-40.
- [5] Zhang XF, Sreekumar TV, Liu T, Kumar S, *J Phys Chem B*, 108 (2004) 16435-40.
- [6] Sung SJ, Kim T, Yang SJ, Oh JY, Park CR, *Carbon*, 81 (2015) 525-34.
- [7] Park S, Ruoff RS, *Nat Nanotechnol*, 4 (2009) 217-24.
- [8] Kim D, Yang SJ, Kim YS, Jung H, Park CR, *Carbon*, 50 (2012) 3229-32.
- [9] Pei SF, Cheng HM, *Carbon*, 50 (2012) 3210-28.
- [10] Yang SJ, Kim T, Jung H, Park CR, *Carbon*, 53 (2013) 73-80.
- [11] Yang SJ, Kang JH, Jung H, Kim T, Park CR, *J Mater Chem A*, 1 (2013) 9427-32.
- [12] Jung H, Yang SJ, Kim T, Kang JH, Park CR, *Carbon*, 63 (2013) 165-74.
- [13] Kim T, Kang JH, Yang SJ, Sung SJ, Kim YS, Park CR, *Energ Environ Sci*, 7 (2014) 3403-11.
- [14] Nebhani L, Barner-Kowollik C, *Macromol Rapid Comm*, 31 (2010) 1298-305.
- [15] Iehl J, de Freitas RP, Delavaux-Nicot B, Nierengarten JF, *Chem Commun*, (2008) 2450-2.
- [16] Park S, Ruoff RS, *Nat Nanotechnol*, 4 (2009) 217-24.
- [17] Okpalugo TIT, Papakonstantinou P, Murphy H, McLaughlin J, Brown NMD, *Carbon*, 43 (2005) 153-61.
- [18] Frank O, Tsoukleri G, Riaz I, Papagelis K, Parthenios J, Ferrari AC, et al., *Nat Commun*, 2 (2011) 255-1-7.
- [19] Boehm HP, *Carbon*, 32 (1994) 759-69.
- [20] Worsley KA, Kalinina I, Bekyarova E, Haddon RC, *J Am Chem Soc*, 131 (2009) 18153-8.
- [21] Puri BR, Bansal RC, *Carbon*, 1 (1964) 457-64.
- [22] Goertzen SL, Theriault KD, Oickle AM, Tarasuk AC, Andreas HA, *Carbon*, 48 (2010)

1252-61.

- [23] Whitby RLD, Korobeinyk A, Glevatska KV, Carbon, 49 (2011) 722-5.
- [24] Hulicova-Jurcakova D, Seredych M, Jin YG, Lu GQ, Bandosz TJ, Carbon, 48 (2010) 1767-78.
- [25] Oickle AM, Goertzen SL, Hopper KR, Abdalla YO, Andreas HA, Carbon, 48 (2010) 3313-22.
- [26] Hanelt S, Orts-Gil G, Friedrich JF, Meyer-Plath A, Carbon, 49 (2011) 2978-88.
- [27] Garcia-Gallastegui A, Iruretagoyena D, Gouvea V, Mokhtar M, Asiri AM, Basahel SN, et al., Chem Mater, 24 (2012) 4531-9.
- [28] Contescu A, Contescu C, Putyera K, Schwarz JA, Carbon, 35 (1997) 83-94.
- [29] Bandosz TJ, Jagiello J, Contescu C, Schwarz JA, Carbon, 31 (1993) 1193-202.
- [30] Gorgulho HF, Mesquita JP, Goncalves F, Pereira MFR, Figueiredo JL, Carbon, 46 (2008) 1544-55.
- [31] Seredych M, Tamashausky AV, Bandosz TJ, Adv Funct Mater, 20 (2010) 1670-9.
- [32] Konkana B, Vasudevan S, J Phys Chem Lett, 3 (2012) 867-72.
- [33] Seredych M, Bandosz TJ, Langmuir, 26 (2010) 5491-8.
- [34] Jagiello J, Bandosz TJ, Putyera K, Schwarz JA, J Colloid Interf Sci, 172 (1995) 341-6.
- [35] Petit C, Bandosz TJ, J Phys Chem C, 113 (2009) 3800-9.
- [36] Plummer LN, Busenberg E, Geochim Cosmochim Acta, 46 (1982) 1011-40.
- [37] Pohorecki R, Moniuk W, Chem Eng Sci, 43 (1988) 1677-84.
- [38] Rockstraw DA, Guo YP, Micropor Mesopor Mat, 100 (2007) 12-9.
- [39] Pohorecki R, Kucharski E, Chem Eng J Bioch Eng, 46 (1991) 1-7.
- [40] Haddon RC, Sippel J, Rinzler AG, Papadimitrakopoulos F, Mrs Bull, 29 (2004) 252-9.
- [41] Bunch JS, Verbridge SS, Alden JS, van der Zande AM, Parpia JM, Craighead HG, et al., Nano Lett, 8 (2008) 2458-62.

## **Part IV**

# **One-Pot Titration Methodology for Applications of Carbon Nanomaterials**

# **Chapter 5 High-Quality Aqueous Dispersions of Carbon Nanotubes for Preparation of High-Performance Buckypapers**

## **5.1 Introduction**

Carbon nanotubes (CNTs) are widely recognized as the potential candidates for the structural materials due to their extraordinary stiffness and strength with perfect electricity [1, 2]. To realize these excellent mechanical properties in nanoscale to the bulk state, CNTs have been assembled into various forms from one-dimensional fibers [3, 4] to three-dimensional blocks [5, 6]. Buckypaper is one of the CNT-assembled structures fabricated into two-dimension which can be applied into strong actuators, sensors, filter membranes and the electrical devices [7-17]. The general procedures to fabricate these freestanding buckypapres include the dispersion of CNTs into the appropriate aqueous or organic solvents followed by the vacuum filtration of the dispersions [7, 14]. While fabrication of buckypaper adopting vacuum filtration system is quite simple, the mechanical properties are still limited comparing to the other kinds of assemblies such as CNT fibers [3, 4]. To maximize the potential applications of buckypaper as a structural material, it would be significant to fabricate highly dense network of CNTs in the mats.

The formation of densely packed network might be highly dependent of the dispersion quality of the precursor CNT solutions [18, 19]. The CNTs in the dispersion should be individually distributed without any aggregates which might disturb the close packing

of CNTs and potentially role as the crack sources limiting the performances of the fabricated buckypapers. Indeed, achievement in the preparation of highly distributed CNT dispersions is recognized as the essential step on engineering of CNTs for the assemblies and polymer composites [18, 20, 21]. For this purpose, numerous methods have been developed to disperse CNTs in the various solvents with high qualities and long-term stabilities [22-26].

Functionalization by acid treatment for the direct modification of the CNTs' surface into hydrophilic makes CNTs dispersed well in the polar or hydrophilic solvents [7, 23, 27-31]; hence has a potential to fabricate densely packed buckypaper. Especially, Acidic carbon compounds (ACCs) detached from the sidewalls of CNTs during the acid treatment are reported to play an important role in stabilizing CNTs dispersion due to their aromatic structure covered by the numerous acidic functional groups [23, 32-36]. However, the fundamental principles describing the concrete role of ACCs on the dispersion behaviors of CNTs were rarely discussed in the previous reports. The lack of understanding of these roles of ACCs on the CNT dispersions may limit the potential of ACCs engineering for CNT applications.

It was reported ACCs are readily removable when dissolved in the basic solution followed by the filtration [23, 32-34]. However in this work, I found that the ACCs with the strong carboxylic groups are inevitably lost even by the conventional purification of oxidized CNTs with neutral water. It appeared in this work that these carboxylated ACCs plays a key role for the dispersion of CNTs in aqueous systems. As a result, the mechanical performances of the CNT buckypapers were doubled with these aid of these ACCs.

For the effective fabrication of CNT dispersions and buckypapers, this work mainly concentrates on 1) the development of the process for the maximal preservation of the

ACCs on the surface of the CNTs after the oxidation, and 2) the systematic analysis of the chemical properties and the ionization behaviors of these ACCs in the aqueous dispersions of CNTs.

## 5.2 Experimental

### 5.2.1 Preparation of oxidized CNTs

All of the chemicals including nitric acid (70%, HNO<sub>3</sub>), sulfuric acid (99%, H<sub>2</sub>SO<sub>4</sub>), hydrochloric acid (HCl), and sodium hydroxide (NaOH) were purchased from Daejung, Korea. For preparation of oxidized MWCNTs, 1 g of MWCNTs (CM250, Hanhwa Chemicals) were dispersed in the mixture of HNO<sub>3</sub> (75 mL) and H<sub>2</sub>SO<sub>4</sub> (225mL) at 60 °C for 3 hours. After the acid treatment the dispersion was cooled into room temperature until the oxidized MWCNTs precipitated. The typical purification process includes the repetition of filtering and washing of the CNTs until the filtrate becomes colorless and neutral. However this purification process with neutral water potentially remove the ACCs which might conduct crucial roles on the properties of the resultant MWCNTs. Additionally this washing and filtration is time-consuming process since the oxidized CNTs become dispersible in the neutral condition to decrease the filtration rate [23, 37]. Therefore in this work, the supernatant of the reaction mixtures was carefully poured out and 0.1 N HCl solution was supplemented to the sediment. The MWCNTs readily settled down again in the acidic media and this process was repeated until the supernatant become colorless. The supernatant was filtrated thorough 0.2 μm PTFE membrane filter (Adventec) and the black filter cakes were mixed again with 0.1 N HCl solution. The filtration and washing process was repeated for 3 times and the remained filter cakes were dried on the heating stage at 60 °C for evaporation of HCl and water. After the preliminary drying, MWCNTs were put into 60 °C vacuum oven overnight for complete removal of HCl and water. This procedure purifying the mixed acid-oxidized CNTs with HCl solution was defined as the acid washing process and the resultant MWCNTs were denoted MCNT<sub>AW</sub>.

To examine the solubility of the ACCs attached on CNTs from MCNT<sub>AW</sub> sample in the various pH conditions, MCNT<sub>AW</sub> was dispersed in the HCl or NaOH solutions in which pH ranged from 1 to 14 by stirring for 24 hours followed by the filtrations. Each filtrate was brown implying the dissolution of ACCs [23, 33], except in the case of pH 1 solution (Fig. 5.1a). 1mL of the filtrates were diluted in 9 mL water and absorbance of visible light of each diluted filtrate was measured by UV-Vis.-NIR absorption spectrometer (Cray 5000, Varian) [23].

For the comparison of the acid washing to the conventional neutral washing, MCNT<sub>AW</sub> was dispersed in neutral water in 1 mg/mL. The filtration and washing process was repeated until the filtrate became colorless (denoted neutral wash). For the complete elimination of ACCs from CNTs, MCNT<sub>AW</sub> was washed with basic solution following the same procedure of neutral wash (denoted base wash). For this purpose, 0.01 N NaOH was used as a basic solution ACCs tended to dissolved maximally in this concentration (Fig.5.1b). After the base washing, the CNTs were dispersed in 0.01 N HCl solution for the acidification of the deprotonated functional groups followed by filtration and washing with deionized water until pH of the filtrate was neutral. The CNTs prepared by neutral and base wash were denoted MCNT<sub>NW</sub> and MCNT<sub>BW</sub>, respectively.

### **5.2.2 Preparation of CNT dispersions and buckypapers**

20 mg of each CNT sample was dispersed in 20 mL of deionized water by horn sonication instrument (Sonoplus, Bandelin electronic) for 20 minute. 40 mL of CNT dispersions were prepared by the sonication and carefully decanted to the vacuum filtration system with 0.2  $\mu\text{m}$  anodized aluminum oxide disc filter (Whatman). The filtration was finished within an hour but prepared buckypaper was remained in the filtration system for the complete removal of water for 5 hours. The dried buckypaper



was easily detached from the filter and additionally dried at vacuum oven at 60 °C overnight.

### 5.2.3 Characterization

For the characterization of the functional groups on the CNT samples, X-ray photoelectron spectroscopy (XPS) was conducted by AXIS-His (Kratos analytical). To examine thermal degradation behaviors of CNT samples, each sample was heated to 900 °C in 10 °C/minute after the isothermal process at 60 °C for 1 hour to desorb the physically attached water molecules on the surface of CNTs using thermogravimetric analysis (TGA) instrument (SDT Q600, TA instruments) . The acidity distribution of CNT samples were analyzed by one-pot titration methodology developed in **Chapter 4**. For this purpose, 20 mg of CNT samples were agitated in 20 mL of 0.01 N HCl solution, and 15 mL of the mixture was titrated by 0.01 N NaOH solution as a titrant at 25 °C using Titrand 888 (Metrohm). The titration system was completely sealed and N<sub>2</sub> gas was continually purged to exclude carbon dioxide. To guarantee the equilibrium between functional groups on CNTs and NaOH, additional titrant was dosed only when the pH change rate was lower than 0.02 pH unit/minute. The titration curves were then converted to the proton binding isotherms  $\theta(\text{pH})$  indicating the concentration [meq/g] of proton dissociated sites of the functional groups [38] following equations (4.9) and (4.9.1) described in Chapter 4. The  $\text{p}K_a$  distribution ( $f(\text{p}K_a)$ ), the indication of the population of the acidic groups on the specific  $\text{p}K_a$  range [38], was then obtained applying first-order approximation [39] from the proton binding isotherms as

$$f(\text{p}K_a) \cong \left[ \frac{\partial \theta(\text{pH})}{\partial \text{pH}} \right]_{\text{pH}=\text{p}K_a} \quad (5.1)$$

For the determination of the dispersion state of CNTs in water, zeta potential of the 1/10 time diluted CNT dispersions were measured by zeta potentiometer (ELSZ-1000, Otsuka electronics) to define the effective charges and dispersion states of CNTs. Additionally, absorbance of visible light ( $\lambda = 550$  nm) of the CNT dispersions was measured after centrifugation (Heraeus megafuge 16, Thermo scientific) of the dispersions at 3,000 rpm for 20 minutes followed by 1/20 times dilution of the supernatants with water [40].

Surface morphology of the bucky papers were observed by scanning electron microscopy (SEM; JSM-6700F, JEOL). For the measurement of the mechanical properties of the buckypapers, each buckypaper was cut into the rectangular strips in a 2.5 mm width and 30 mm length. The mechanical tensile test was performed with universal tensile machine (Inston-5543, Instron). At least 10 samples were tested with a 10 mm length and a 10 %/minute strain rate. The electrical properties of the buckypapers were determined from the resistance measurements of the strips utilized by Keithley 2643B (Keithley instruments) before the tensile tests [17].

## 5.3 Results and discussion

### 5.3.1 Preservation and removal of ACCs from CNTs after oxidation

The base solution washing has been generally recognized as the essential procedures for the removal of ACCs attached on oxidized CNTs [23, 33]. However, the possibility of the dissolution of ACCs in the neutral or even acidic condition was never considered because of the lack in investigation of the ionization behaviors of ACCs on CNTs. Typically, the acid treated CNTs were purified by washing and filtration of the CNTs with deionized water which may remove the ACCs dissolved in the neutral condition [7, 29]. To avoid the potential removal of these ACCs, the purification of CNTs was conducted by 0.1 N HCl solution instead of neutral water followed by evaporation of the residual HCl at elevated temperature. The resultant MCNT<sub>AW</sub> was then mixed in pH-controlled aqueous solutions by NaOH or HCl followed by filtration of the mixtures. Indeed, the brown color appeared, implying the dissolution of ACCs [23, 33], in the filtrates not only from the basic (pH 10 – 14) but also in the neutral (pH 7) or acidic (pH 2 – 4) environments (Fig. 5.1a). Fig. 5.2b shows the absorbance of visible light ( $\lambda = 550$  nm) of the diluted filtrates indicating the relative concentrations of ACCs in the filtrates. The concentration of ACC gradually increased with pH raising until pH 7 followed by drastic increase in basic region (pH 7 – 12). However as pH became higher than 12, the ACCs tended to reattach on the surface of CNTs because the ionic strength of the solution was high enough to make the attraction force dominant between CNTs and ACCs [41]. Therefore, the relative concentration of ACC in the filtrated decreased when pH was higher than 12. The dissolution behaviors ACCs will be correlated to the ionization behaviors of ACCs after the detailed investigation of  $pK_a$  distribution of ACCs shown in Fig. 5.3.

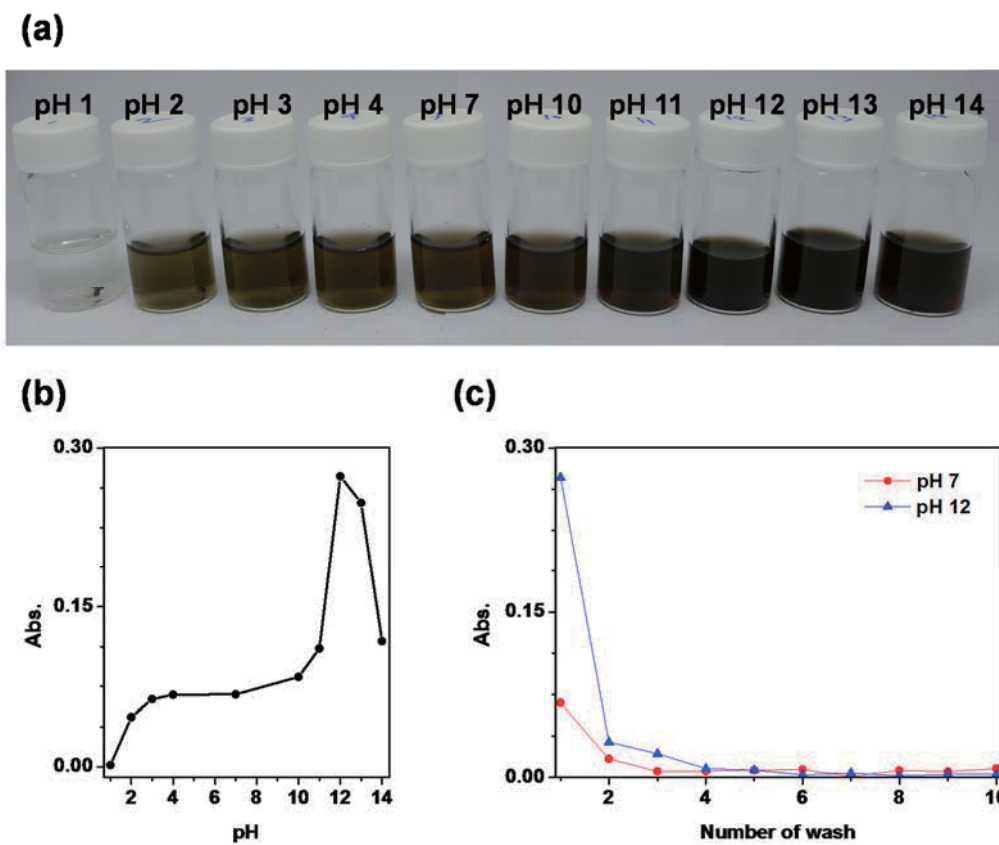


**Fig. 5.1.** (a) The filtrates of MCNT<sub>AW</sub> dissolved in the pH controlled water with HCl or NaOH and (b) absorbance at  $\lambda = 550$  nm of the diluted filtrates. (c) Absorbance at  $\lambda = 550$  nm of the diluted filtrates of MCNT<sub>AW</sub> and neutral deionized water (pH 7) and NaOH aqueous solution (pH 12) as a function of number of wash.

The ACCs on MCNT<sub>AW</sub> were then thoroughly washed in neutral (pH 7; MCNT<sub>NW</sub>) or basic (pH 12; MCNT<sub>BW</sub>) condition to investigate the effects of ACCs on chemical and physical properties and the solution behaviors of the oxidized CNTs. Washing and filtration was repeated at least 10 times until each filtrate became colorless to remove ACCs as many as possible [23]. Note that MCNT<sub>NW</sub> represents the oxidized CNTs obtained from typical purification process by deionized water after the acid treatment [7, 29].

### 5.3.2 Surface properties of ACC-removed and unremoved CNTs

This pH-controlled step-by-step removal of ACCs was confirmed by chemical investigation of CNT samples with XPS, TGA, and one-pot titration. Fig. 5.2 presents the XPS C1s spectra of MCNT<sub>AW</sub>, MCNT<sub>NW</sub>, and MCNT<sub>BW</sub> showing the atomic composition of carbon atom in the oxidized state. All of the samples showed the typical peaks shown in functionalized carbon materials originated from carbon single (C-C, Peak 1) and double bonds (C=C, Peak 2), the oxygen containing functional groups such as epoxy/hydroxyl (C-OH/C-O-C, Peak 3), ketone (C=O, Peak 4), and carboxylic (COO, Peak 6) groups, and  $\pi$ - $\pi$  interaction ( $\pi$ - $\pi$ , Peak 6) [31, 42, 43]. The quantitative analysis (Table 5.1) shows that the number of oxidized carbon decreased from 30.7 (MCNT<sub>AW</sub>) to 28.5 (MCNT<sub>NW</sub>) and 22.9 (MCNT<sub>BW</sub>) atomic % as the ACCs were removed from CNTs by washing with neutral water or NaOH solution, respectively (Table 5.1). The results showed that all of the functional groups decreased as ACCs were removed by base wash of MCNT<sub>AW</sub> to make MCNT<sub>BW</sub>. Meanwhile, comparison between the quantitative analysis of MCNT<sub>AW</sub> and MCNT<sub>NW</sub> indicates that neutral water selectively eliminated the ACCs with carboxylic groups in majority. These removed carboxylic groups positively enhanced the dispersibility due to their strong acidic property and hence the

mechanical properties of buckypapers assemblies of CNTs which will be discussed later in detail.

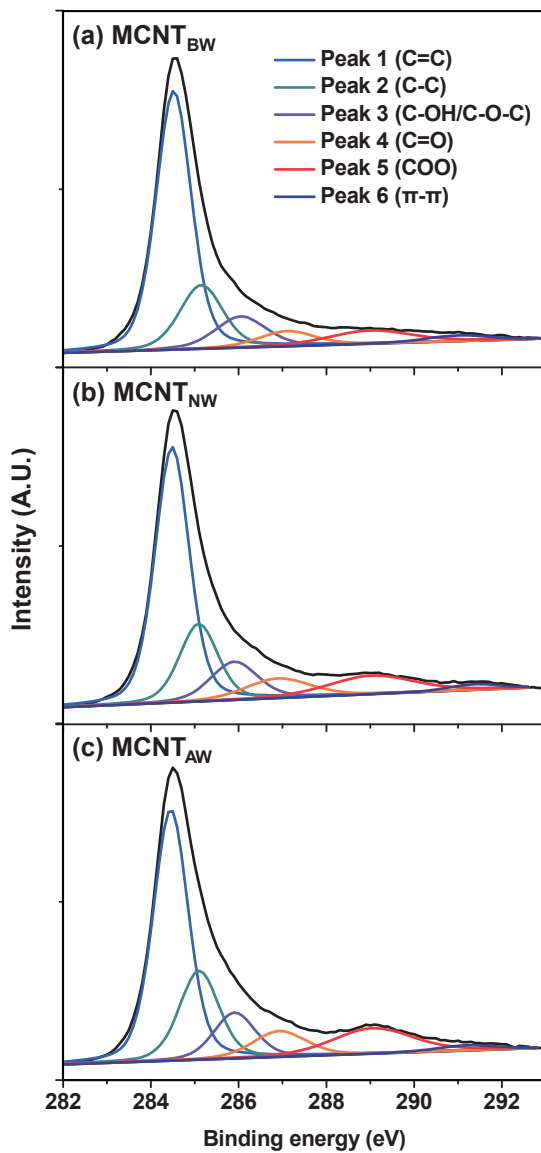


**Fig. 5.2.** XPS C1s spectra of (a) MCNT<sub>BW</sub>, (b) MCNT<sub>NW</sub>, and (c) MCNT<sub>AW</sub>.

**Table 5.1.** Quantitative analysis of XPS C1s spectra of MCNT<sub>BW</sub>, MCNT<sub>NW</sub>, and MCNT<sub>AW</sub> in Fig. 5.2.

<b>Sample</b>	<b>sp<sup>2</sup></b> <b>[atomic%]</b>	<b>sp<sup>3</sup></b> <b>[atomic%]</b>	<b>C-O/C-O-C</b> <b>[atomic%]</b>	<b>C=O</b> <b>[atomic%]</b>	<b>O-C=O</b> <b>[atomic%]</b>
<b>MCNT<sub>BW</sub></b>	59.2	17.9	10.2	5.5	7.2
<b>MCNT<sub>NW</sub></b>	53.7	17.8	11.0	7.8	9.7
<b>MCNT<sub>AW</sub></b>	50.3	19.0	11.1	8.0	11.5

The evidence of the removal of ACCs from CNTs were also demonstrated in TGA results. Fig. 5.3 presents the thermal degradation behaviors of CNT samples and isolated ACCs. Comparing to the CNTs, ACCs were thermally less stable due to the lower molecular weights and more amount of oxygen-containing groups. The gradual weight loss of ACCs during the temperature ramp process is due to thermal degradation of the functional groups dominated by carboxylic or phenolic groups, which is also shown in the case of ACC-removed CNT by base washing (MCNT<sub>BW</sub>) [44-46]. Meanwhile, the distinct weight drop at 450 °C was possibly attributed to the boiling of the low-molecular-weight components or breakdown of the aromatics structures on the ACCs [46, 47]. Because of the lower thermal stability of ACCs, the thermal degradation rates became faster as more amount of ACCs were attached on the surface of the CNTs (MCNT<sub>AW</sub>, MWCNT<sub>NW</sub>). Since the ACCs might be uniformly distributed on the sidewall of CNTs, the peak of ACCs around 450 °C was partially or completely disappeared in MCNT<sub>AW</sub> and MCNT<sub>NW</sub>, respectively, and these components of ACCs attached on CNTs would be gradually vaporized during the thermal treatments.

The TGA results were additionally applied for the estimation of the weight fraction ( $wf$ ) of ACCs on MCNT<sub>AW</sub> or MCNT<sub>NW</sub>, assuming the remained weight ( $W$ ) of ACC-attached CNTs are the linear summation of those of CNTs and ACCs as shown in equation (5.2) in the case of MCNT<sub>AW</sub> [48].

$$\begin{aligned}
 W_{\text{MCNT}_{\text{AW}}} &= W_{\text{CNT}} \cdot wf_{\text{CNT}} + W_{\text{ACC}} \cdot wf_{\text{ACC}} \\
 &= W_{\text{MCNT}_{\text{BW}}} \cdot wf_{\text{CNT}} + W_{\text{ACC}} \cdot (1 - wf_{\text{CNT}})
 \end{aligned}
 \tag{5.2}$$



Here,  $W_A$  and  $wf_A$  is the weight loss percentage and weight percent of component A, respectively.  $W_{CNT}$  is supposed to be identical to  $W_{MCNT_{BW}}$  on the assumption that ACCs were completely removed by repeated washing of oxidized CNTs with 0.01 N NaOH solution. Therefore the weight fraction of CNT ( $W_{CNT}$ ) can be readily obtained as follow:

$$wf_{CNT} = \frac{W_{MCNT_{AW}} - W_{ACC}}{W_{MCNT_{BW}} - W_{ACC}}, \quad (5.3.1)$$

or,

$$wf_{CNT} = \frac{W_{MCNT_{NW}} - W_{ACC}}{W_{MCNT_{BW}} - W_{ACC}}. \quad (5.3.2)$$

in the case of  $MCNT_{NW}$ . The  $W$  at 800 °C, at which the thermal degradation rate became stable for the whole samples, was chosen for  $wf_{CNT}$  calculation from equations (5.3.1) and (5.3.2). The estimation of the weigh fraction of CNT and ACC in each sample is summarized in Table 5.2. The table shows the weight fraction of ACC became half as  $MCNT_{AW}$  is washed and purified by neutral water ( $MCNT_{NW}$ ). Along with XPS investigations, the TGA results also verified that the typical purification process inevitably remove the ACCs from the surface of CNTs which can be potentially useful in CNT applications. In the next description, the effects of ACCs on the acidic properties of CNTs will be demonstrated in detail.

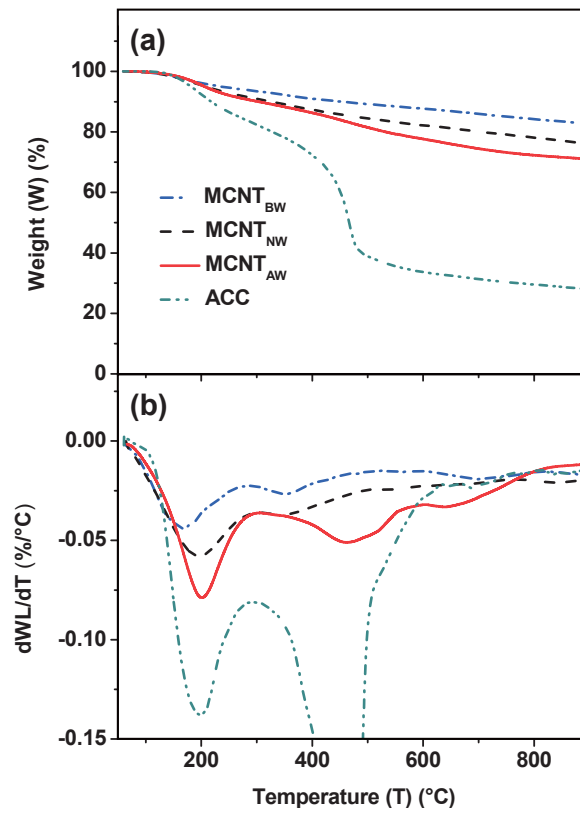


**Fig. 5.3.** (a) TGA and (b) differential thermogravimetry (DTG) profiles of MCNT<sub>BW</sub>, MCNT<sub>NW</sub>, MCNT<sub>AW</sub>, and ACC.

**Table 5.2.** Weight percent (*W*) at 800 °C and the resultant estimation of weight fraction (*w<sub>f</sub>*) of CNT and ACC of CNT samples and ACC.

	<i>W</i> at 800 °C (%)	<i>w<sub>f</sub></i> <sub>CNT</sub>	<i>w<sub>f</sub></i> <sub>ACC</sub>
MCNT <sub>BW</sub>	84.2	1	0
MCNT <sub>NW</sub>	78.1	0.89	0.11
MCNT <sub>AW</sub>	72.3	0.78	0.22
ACC	29.5	0	1

It is widely established that the surface nature and dispersion properties of CNTs are strictly affected by the acidic surface functional groups including carboxylic, lactonic, and phenolic groups [32]. The ACCs which is enriched by these variety of acidic groups make CNT more dispersible in the numerous aqueous or organic solvents, and thereby widening the possible application of CNTs [23, 33]. In terms of titration methods, the previous reports only showed the difference between the numbers of functional groups on the oxidized CNTs before and after the removal of ACCs to show the effects of ACCs on the various properties of CNTs [33]. However, the details on the mechanism how the ACCs promote the dispersion of CNTs are hardly established because of the lack on the concrete investigation on ACCs themselves. Therefore, the engineering of the ACCs on the surface of CNTs to promote the application of CNTs was hardly available. Here, I investigated and compared the acidic properties of both CNTs and ACCs, one of the keys of the dispersion of carbon nanomaterials, by analysis of one-pot titration results of MCNT<sub>BW</sub>, MCNT<sub>NW</sub>, and MCNT<sub>AW</sub>.

Fig. 5.4a presents the proton binding isotherms ( $\theta(\text{pH})$ ) of the CNT samples showing the number of dissociated protons from the acidic groups at the specific pH points during the titrations. And then  $\text{p}K_a$  distribution functions ( $f(\text{p}K_a)$ ) (Fig 5.4b) of CNTs were obtained by first-order differentiation of proton binding isotherms at  $\text{pH} = \text{p}K_a$  [39]. Due to the presence of ACCs on CNTs, the number and  $\text{p}K_a$  range of the acidic groups of MCNT<sub>AW</sub> (3.21 meq/g) are much bigger and wider than those of MCNT<sub>NW</sub> (1.91 meq/g) and MCNT<sub>BW</sub> (1.06 meq/g). The peaks on  $\text{p}K_a$  around 5 – 6 and 9 – 9.5 displayed in all CNTs implied the existence of carboxylic and phenolic groups which were majorly formed during the mixed acid treatment of CNTs [39, 49, 50]. The additional peak on  $\text{p}K_a = 2.9$  in the distribution function of MCNT<sub>AW</sub> indicated the more acidic carboxylic groups attached only on ACCs [49].

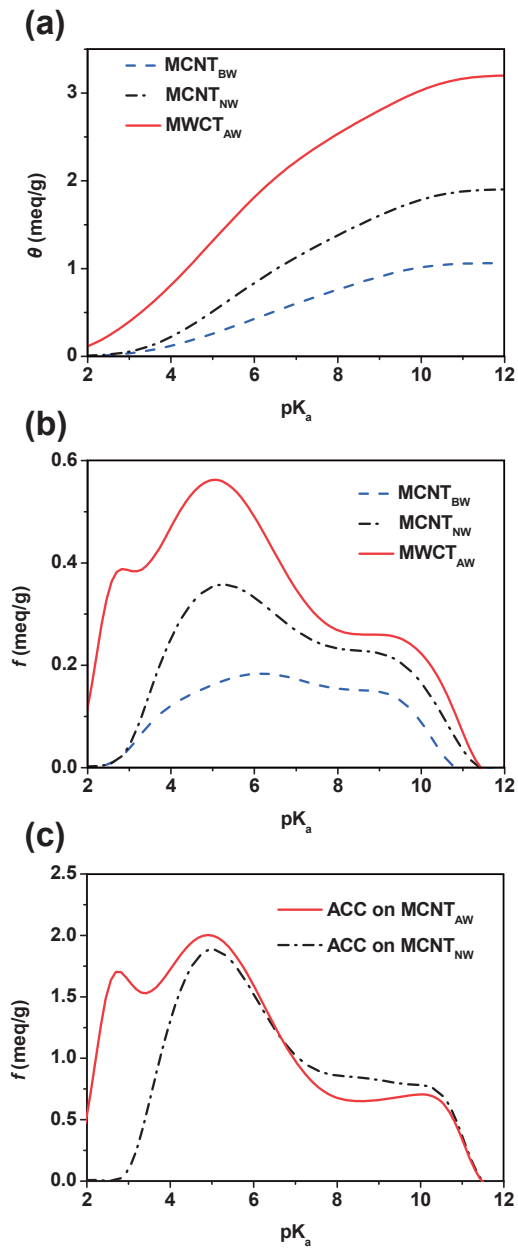


**Fig. 5.4.** (a) Proton binding isotherms ( $\theta$ ), (b)  $pK_a$  distribution functions ( $f$ ) of MCNT<sub>BW</sub>, MCNT<sub>NW</sub>, and MCNT<sub>AW</sub>. (c)  $pK_a$  distribution functions ( $f$ ) of ACCs on MCNT<sub>AW</sub> and MCNT<sub>NW</sub>.

For the calculation of  $pK_a$  distribution function of ACC ( $f_{ACC}$ ) dissociated from that of CNT ( $f_{CNT}$ ), I assume that the  $pK_a$  distribution function of ACC-attached CNT (MCNT<sub>AW</sub> or MCNT<sub>NW</sub>) is the linear summation of that of CNT ( $f_{CNT}$ ) and ACC, and no ACC is additionally attached on MCNT<sub>BW</sub>. Equation (5.4) shows the calculation process of  $f_{ACC}$ .

$$\begin{aligned}
 f_{MCNT_{AW}} &= f_{CNT} \cdot wf_{CNT} + f_{ACC} \cdot wf_{ACC} \\
 &= f_{MCNT_{BW}} \cdot wf_{CNT} + f_{ACC} \cdot (1 - wf_{CNT}), \quad (5.4) \\
 \therefore f_{ACC} &= \frac{f_{MCNT_{AW}} - f_{MCNT_{BW}} \cdot wf_{CNT}}{1 - wf_{CNT}}
 \end{aligned}$$

where  $f_A$  is the  $pK_a$  distribution function of component A, and  $wf_{CNT}$ ,  $wf_{ACC}$  are the weight fractions of CNT and ACC in MCNT<sub>AW</sub> estimated from TGA results shown in Table. 5.2. The same logic was adopted for the calculation of  $f_{ACC}$  on MCNT<sub>NW</sub> by substitution of  $f_{MCNT_{AW}}$  into  $f_{MCNT_{NW}}$  in equation (5.4). Fig. 5.4c presents the  $pK_a$  distribution function of ACC of MCNT<sub>AW</sub> (red solid line) and MCNT<sub>NW</sub> (blue dash-dotted line), respectively. These two curves resembled each other in the displayed  $pK_a$  range except the peak on  $pK_a = 2.9$  shown in  $f_{ACC}$  of MCNT<sub>AC</sub>. This difference implied that the typical washing process of CNTs by neutral water after acid oxidation completely remove the ACCs with strong carboxylic groups which may play a crucial role on the function of CNTs in the various applications. Note that the elimination of these carboxylic groups were also confirmed in the XPS analysis (see Fig. 5.2 and Table 5.1).

The ionization behaviors of ACCs on MCNT<sub>AC</sub> were then analyzed applying the universal titration equation previously developed in **Chapter 2** and applied further in **Chapter 3** and **4**. In this work, MCNT<sub>AC</sub> (1 mg/mL) was dispersed in the NaOH or HCl solution of which pH ranged from 1 to 14 to remove ACCs (Fig. 5.1). The concentration

of ACC in the filtrates of this removal process would be seriously related to the number of the ionized functional groups on ACCs which will be estimated by the following procedures. This procedures are analogy of those for the calculation of proton dissociated sites of nitric-acid-oxidized MWCNTs in the presence of the Boehm's reaction bases discussed in section 4.3.2, **Chapter 4**.

First, pH of the MCNT<sub>AW</sub>-dissolved NaOH solution at the equilibrium state (pH<sub>e</sub>) was numerically calculated following the equation (4.20) described in **Chapter 4** as

$$\sum \frac{c_C \cdot f(\text{p}K_{a,i}) \cdot (\text{p}K_{a,i+1} - \text{p}K_{a,i})}{1 + 10^{\text{pH}_e} \cdot K_{a,i}} + \frac{c_{\text{NaOH}} - q_C \cdot c_C}{1 + 10^{\text{pH}_e} \cdot K_W / K_{b,\text{NaOH}}} - \frac{1}{v_{\text{H}_2\text{O}} + 1 / (10^{\text{pH}_e} \cdot K_W)} + \frac{1}{v_{\text{H}_2\text{O}} + 10^{\text{pH}_e}} = 0 \quad (5.5)$$

Here,  $c_C$ ,  $c_{\text{NaOH}}$  is the concentration of CNT and NaOH in the solution,  $\text{p}K_{a,i}$  is the  $i$ 'th component of the distributed  $\text{p}K_a$  values in  $f(\text{p}K_a)$  of CNTs,  $q_C$  is the concentration [meq/g] of acidic groups on CNTs (identical to the area of  $f(\text{p}K_a)$ ),  $K_W$  is self-ionization constant of water,  $K_{b,\text{NaOH}}$  is base ionization constant of NaOH, and  $v_{\text{H}_2\text{O}}$  is molar volume of water. In the case of HCl solution with concentration  $c_{\text{HCl}}$ , the equation (5.5) can be converted into the following form,

$$\sum \frac{c_C \cdot f(\text{p}K_{a,i}) \cdot (\text{p}K_{a,i+1} - \text{p}K_{a,i})}{1 + 10^{-\text{pH}_e} / K_{a,i}} + \frac{c_{\text{HCl}}}{1 + 10^{-\text{pH}_e} / K_{a,\text{HCl}}} - \frac{1}{v_{\text{H}_2\text{O}} + 10^{\text{pH}_e}} + \frac{1}{v_{\text{H}_2\text{O}} + 10^{-\text{pH}_e} / K_W} = 0 \quad (5.6)$$

And then, the population of proton dissociated functional groups, or proton dissociated  $f(pK_a)$  [38, 51], of ACC was obtained as follow (see derivation of equation (4.23), **Chapter 4**).

$$\text{proton dissociated } f(pK_{a,i}) = \left[ \frac{K_{a,i}}{[H^+] + K_{a,i}} f(pK_{a,i}) \right]_{\text{pH}=\text{pH}_e}, \quad (5.7)$$

where  $f(pK_a)$  applied in this equation is that of ACCs on MCNT<sub>AC</sub> drawn as red solid line in Fig. 5.4c. Subsequently, the number of the ionized functional groups on ACCs can be obtained from the area of the proton dissociated  $f(pK_a)$  is. Fig. 5.5a shows proton dissociated  $f(pK_a)$  of ACCs in the mixture of MCNT<sub>AC</sub> and aqueous solution with pH 2, 3, 7, 11, and 12. Indeed, the ACCs tended to ionize even in the acidic condition (pH 2 and 3) in a certain extent (4.6 and 13.4 % of degree of ionization, respectively) resulting in the dissociation of ACCs from the surface of CNTs by filtration as shown in Fig. 5.1a. The ionization degree was raised to 19.1 % and the majority of stronger carboxylic groups around  $pK_a = 2.9$  was ionized as pH increased to 7, the neutral condition. Indeed, these groups were absent in  $f(pK_a)$  of ACCs on CNTs purified by neutral water (MCNT<sub>NW</sub>) as shown in Fig. 5.4c (blue dash-dotted line) and also verified in the XPS analysis on Table 5.1. As pH increased to 12 (basic condition), the acidic groups in the whole  $pK_a$  window are deprotonated, which resulted in the complete removal of the ACCs from the surface of CNTs after the filtration process. It was also confirmed in the XPS results that the population of all kinds of oxygen-containing functional groups diminished after washing with NaOH solution (Table 5.1).

The area of the proton dissociated  $f(pK_a)$  indicating the number of functionalized groups on ACCs was plotted as a function of the initial pH ( $pH_i$ ) of the solution as presented in Fig. 5.5b. The degree of ionization gradually increased until pH increased from 1 to 4 followed by the plateau region on pH 4 – 10. After this region, the ionization degree drastically increased until the degree reach 100 % on pH 12. It is noteworthy that the shape of this plot is similar to that of Fig. 5.1b exhibiting the relative concentration of ACC in the filtrates at the ACC-removal process. It was noted that a concentration drop after pH 12 shown in Fig. 5.1b was due to the enhanced attraction between CNTs and ACCs as the ionic strength of the solution become stronger [41]. This similarity implies that my approach on the investigation of acidity of ACCs from one-pot titration methodology are practically useful. Therefore, this method was applied further for the investigation of the dispersion properties and the resultant assembly of CNTs in the following section.



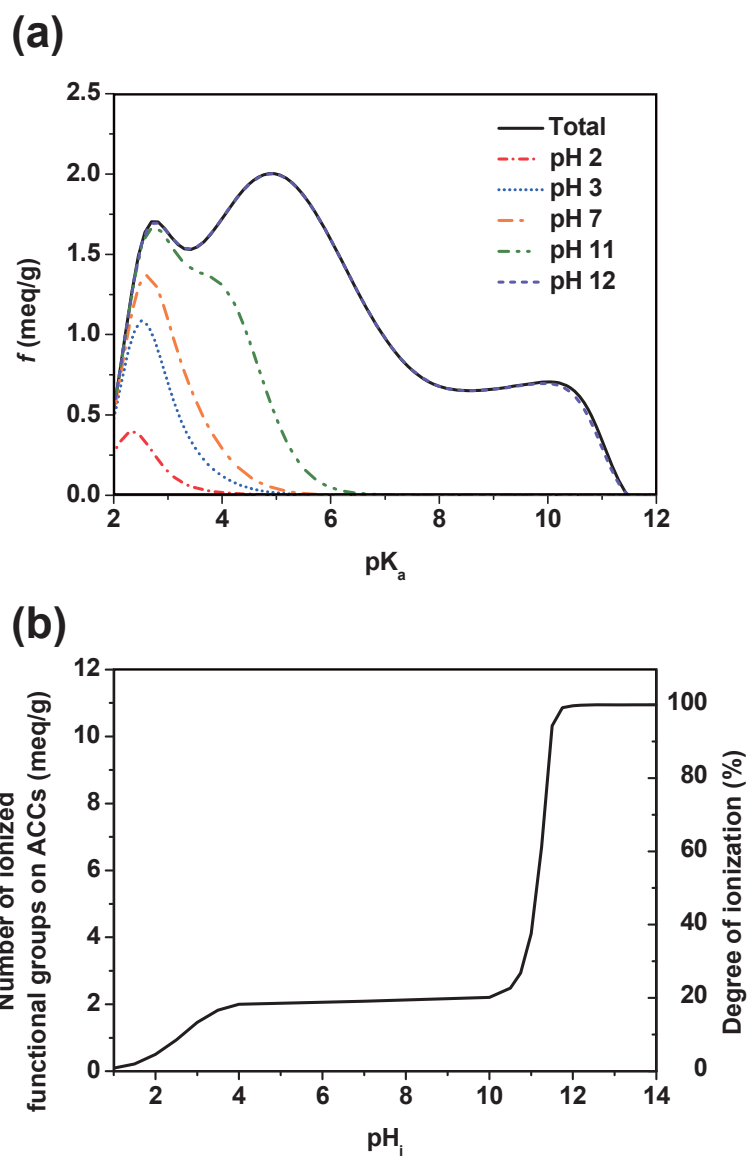


**Fig. 5.5.** (a) Proton dissociated  $f(pK_a)$  of ACCs on MCNT<sub>AW</sub> (1 mg/mL) in the pH-controlled aqueous solutions, and (b) the number and the percent degree of ionized functional groups on the ACCs as a function of the initial pH ( $pH_i$ ) of the aqueous solutions.

### 5.3.3 Dispersion properties of CNTs in aqueous solution

As discussed in the above section, the dispersion properties of CNTs are crucially affected by the ionization behaviors of the acidic functional groups either attached directly on their surfaces or indirectly on ACCs [19, 33]. Based on the titration results analyzed in Fig. 5.4, the ionization tendencies of both CNTs and ACCs when supposed to be dissolved in the neutral water were estimated and displayed in Fig. 5.6. The figures show the proton dissociated  $f(pK_a)$  of MCNT<sub>BW</sub> (CNTs without ACC) and ACCs of MCNT<sub>NW</sub> and MCNT<sub>AW</sub> when the CNT samples are dissolved in deionized neutral water (pH 7), respectively, following equations (5.5) – (5.7). To proceed the discussions on the basis of CNTs,  $f(pK_a)$  of ACCs in Fig. 5.3c were normalized by the weight fraction of CNT ( $WL_{CNT}$ ) estimated in Table 5.2.

Fig. 5.6a shows that 10.2 % (0.109 meq/g) of the acidic groups on CNTs were ionized when only MCNT<sub>BW</sub> were dispersed in water. In this case, none of the acidic groups on ACCs was supposed to be ionized since ACCs were completely removed by NaOH wash. However the ionization degree of CNT decreased to 8.3 (0.091 meq/g) and 5.5 % (0.050 meq/g) as ACCs were attached onto the surface of CNTs in the cases of MCNT<sub>NW</sub> and MCNT<sub>AW</sub>, respectively. In the dispersion of MCNT<sub>NW</sub> (Fig. 5.6b), addition of ACCs provided proton to the functional groups on CNTs by the Le Chatelier's principle inducing a slight decrease in the ionization of CNT's functional groups. On the other hands, only the half of these functional groups were deprotonated in the case of MCNT<sub>AW</sub> because of the presence of the stronger acidic groups in  $pK_a$  region lower than 3 possibly originated from the strong carboxylic groups [49]. In this case the acidified CNT relatively acted as weak base significantly lowering the degree of ionization of CNTs.

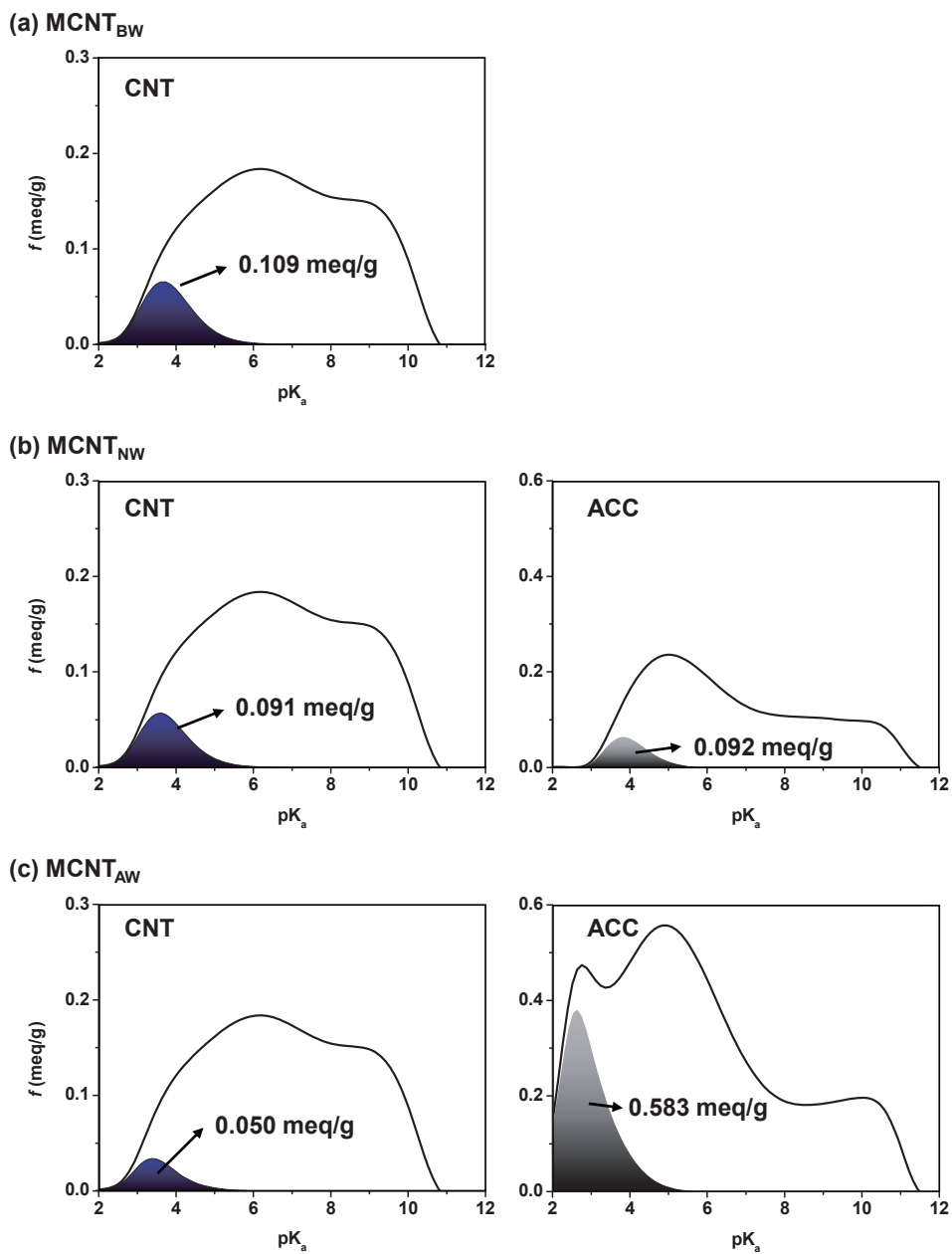


**Fig. 5.6.** Proton dissociated  $f(pK_a)$  of CNT and ACC normalized by weight of CNT showing the ionization behavior of (a)  $MCNT_{BW}$ , (b)  $MCNT_{NW}$  and (c)  $MCNT_{AW}$  dispersed in neutral water (1 mg/mL).

Though, the less functional groups were ionized from CNTs with the addition of ACCs, much more acidities were activated from the ACCs. Almost the same (0.092 meq/g) or even 11 times higher (0.583 meq/g) quantity of acidic groups were ionized from ACCs of MCNT<sub>NW</sub> and MCNT<sub>AW</sub>, respectively. These ionized ACCs (defined active ACCs) can function as surfactants by attaching themselves on the surface of CNTs by  $\pi$ - $\pi$  interaction when dispersed in water or other organic solvents, and thereby making CNTs more dispersible [33]. The deprotonation of CNTs due to the strong acidity of ACCs would decrease the repulsion between CNTs and ACCs, and increase the effective negative charge on CNTs in the dispersion.

Indeed, the amplitude of zeta potential ( $|\xi|$ ), indicating the effective charge on the colloidal particles [39], increased as more ACCs became active (see black circles in Fig. 5.7). The zeta potential of MCNT<sub>BW</sub> dispersion (-40.2 mV) where no ACC was included would be originated from the negatively charged functional groups on CNTs indicated in Fig. 5.5a.  $|\xi|$  of the MCNT<sub>NW</sub> and MCNT<sub>AW</sub> dispersion became 1.3 (51.4 mV) and 1.5 (59.9 mV) times higher, respectively, in spite of the decrease in the charges on CNTs themselves (Fig 5.6b and 5.6c). This paradoxical increase in  $|\xi|$  certainly implied the ionized ACCs were efficiently attached on the CNT's surface. Additionally, this  $|\xi|$  increase also implied that the dispersion state and stability of CNTs in water became much better and ACCs were effectively role as the dispersion agents of CNTs [39, 52]. Additionally, the quality and the stability of dispersions of CNT samples were estimated by measuring the absorbance of the visible light ( $\lambda = 550$  nm) showing the relative concentration of stable CNT after centrifugation at 3,000 rpm [23, 40]. The red circles in Fig. 5.7 shows the absorbance data of the CNT dispersions normalized by their concentrations (as done in the previous report [23]) to show the relative solubility of the CNT samples in water. As expected from ionization behaviors (Fig. 5.6) and zeta

potential results, the solubility of CNT from acid wash process ( $MCNT_{AW}$ ) much more increased as ACCs generated additional negative charges on the surface of CNTs to make them more stable in the aqueous dispersion even in the high gravity-environment comparing to CNTs washed by neutral water ( $MCNT_{NW}$ ) or base ( $MWCNT_{BW}$ ). These observations implies that the newly suggested purification method of oxidized CNTs with HCl solution certainly remained the strongly carboxylated ACCs on CNTs which conducted the significant role on the dispersion of CNTs.

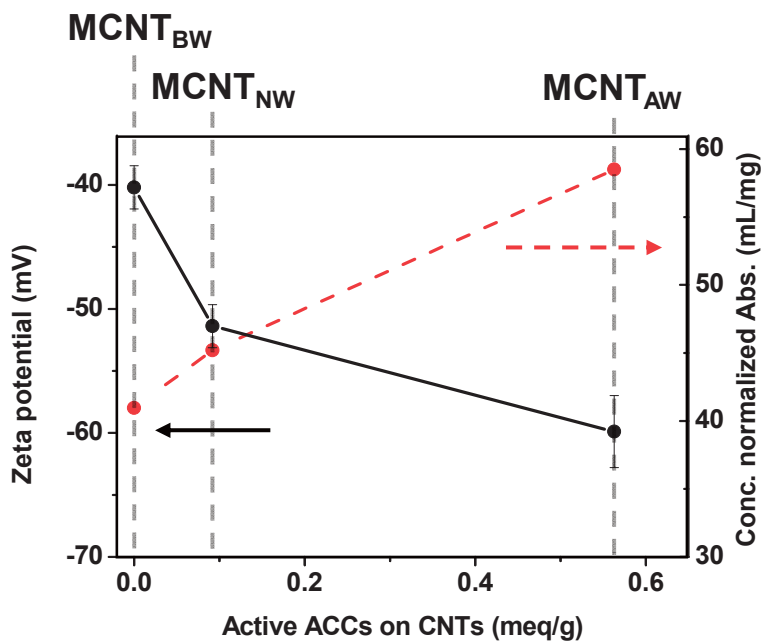


**Fig. 5.7.** Concentration-normalized absorbance of visible light ( $\lambda = 550$  nm) after the centrifugation (red dashed line) and zeta potential (black solid line) of CNT aqueous dispersions as a function of the number of active ACCs on CNTs.

### 5.3.4 Morphologies and properties of CNT buckypapers

The enhanced dispersibility of CNTs in water with the addition of ACCs especially for MCNT<sub>AW</sub> shown by zeta potential and solubility measurement (Fig. 5.7) gives the potential to enlarge the application fields of CNTs with environment-friendly processes. In this work, the assembly of these CNTs into the high-density buckypaper was applied as an example. For the preparation of this free standing two-dimensional assembly of CNTs, each aqueous dispersions of CNT samples were filtrated and dried following the conventional process reported previously [8-10, 13].

Fig. 5.8 shows the shape and microstructures of the resultant buckypapers made from MCNT<sub>BW</sub>, MCNT<sub>NW</sub>, and MCNT<sub>AW</sub>. As shown in the SEM images, the CNTs were randomly oriented and entangled in MCNT<sub>BW</sub> and MCNT<sub>NW</sub> buckypapers (Fig. 5.8e, 5.8f, respectively), which has been conventionally observed in the previously reported buckypapers [10, 13]. Meanwhile, domains with uniform orientation and compact packing of CNTs were easily seen when MCNT<sub>AW</sub> was assembled into the buckypaper (5.8f). The pore structure formed in the buckypaper of MCNT<sub>BW</sub> and MCNT<sub>NW</sub> was hardly found in that of MCNT<sub>AW</sub>. Accordingly, the apparent CNT density of MCNT<sub>AW</sub> buckypaper (1.19 g/cm<sup>3</sup>) became much higher than MCNT<sub>BW</sub> (1.00 g/cm<sup>3</sup>) and MCNT<sub>NW</sub> (0.74 g/cm<sup>3</sup>) buckypapers (Table 5.3).

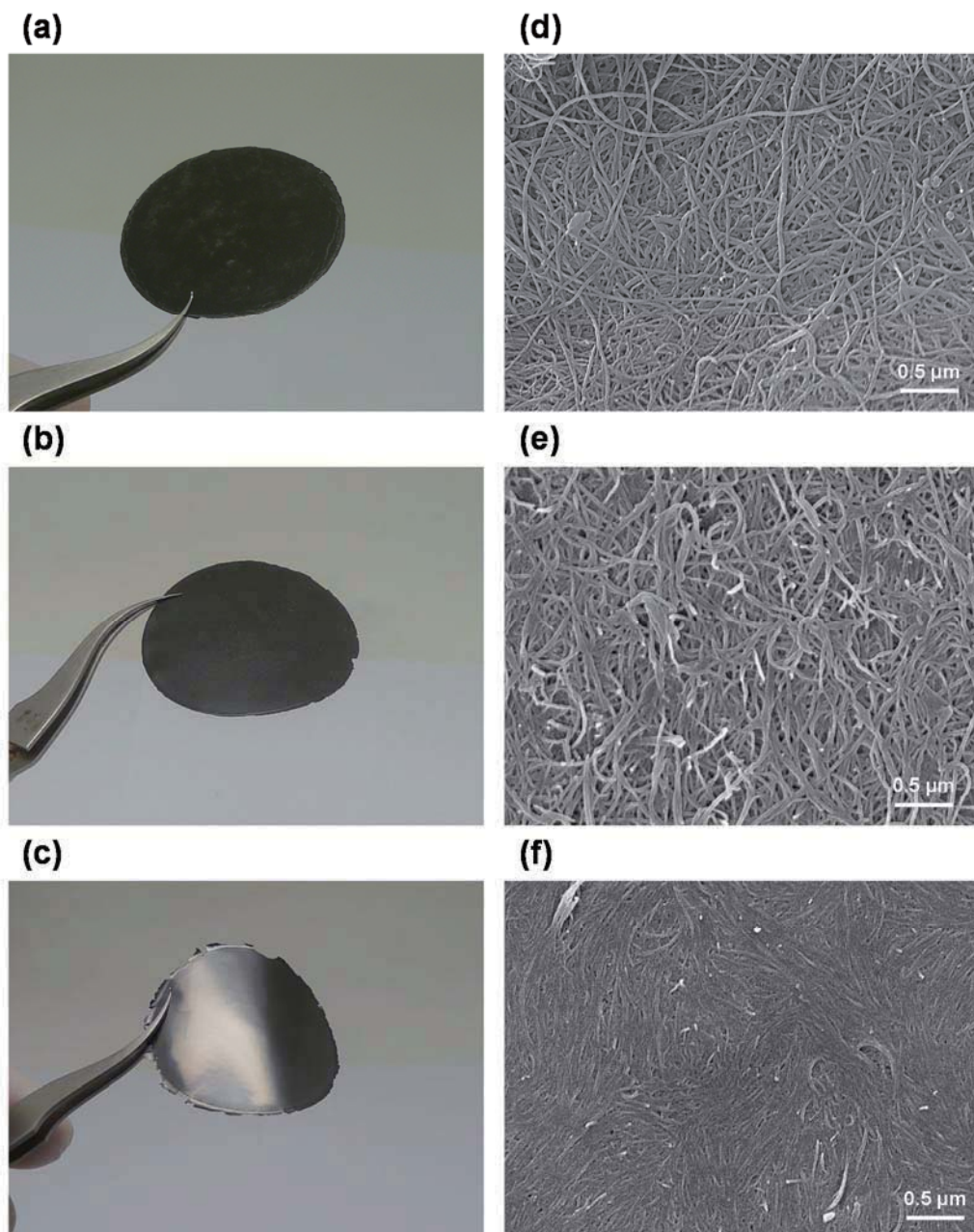


**Fig. 5.8.** (a, b, c) Digital photos and (d, e, f) SEM images of the buckypapers fabricated from (a, d) MCNT<sub>BW</sub>, (b, e) MCNT<sub>NW</sub>, and (c, f) MCNT<sub>AW</sub>.

The detailed mechanism of the formation of the condensed alignment of CNTs are uncertain in the current state. However, it is quite reasonable to conclude that this highly compact structure of MCNT<sub>AW</sub> buckypaper would be at least attributed to the highly dispersed state of the CNTs assisted by the strongly carboxylated ACCs. These CNTs in the highly dispersed states might have more chance for themselves to arrange each other side-by-side by strong  $\pi$ - $\pi$  interactions as the concentration became higher during the filtration [29]. Indeed, the condensing of CNTs in the dispersion induce the reattachment of the protons back to the functional groups of CNTs or ACCs. The decrease in the disprotonation of ACCs with increase in the concentration of MCNT<sub>AW</sub> ( $c_C$ ) is recognizable from the principle of Le Chatelier. These proton dissociation behaviors were quantitatively estimated by increasing  $c_C$  in equation (5.6) for the recalculation of the number of proton dissociated sites on the functional groups of ACCs, or active ACCs. Fig. 5.9 shows that the active ACCs would be continuously decreased with increase in  $c_C$  during the filtration, and thereby reducing the repulsion forces between CNTs. Therefore, the individually separated CNTs at the initial state might gradually attract each other by the van der Waals interactions and assemble into the compact structures shown in Fig. 5.8f [29]. Meanwhile, CNTs of MCNT<sub>NW</sub> and MCNT<sub>BW</sub> with much smaller number of active ACCs might be partially aggregated even at the initial dispersion state since the repulsions between them were even lower than those in MCNT<sub>AW</sub> dispersion.



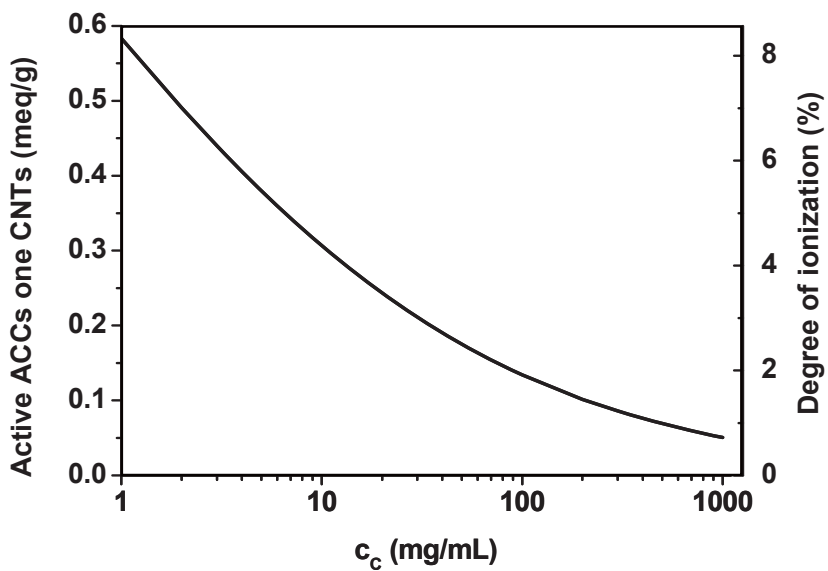


**Fig. 5.9.** The active number and degree of ionization of ACCs of MCNT<sub>AW</sub> as a function of concentration of CNT in water.

The condensed structures of MCNT<sub>AW</sub> buckypaper resulted in the superior mechanical properties comparing to the previously reported ones prepared by the similar filtration procedures [7, 10, 12-15] (Table 5.3). Notably, both tensile strength and Young's modulus of MCNT<sub>AW</sub> buckypaper were much higher than those from ACC-removed MCNT<sub>NW</sub> and MCNT<sub>BW</sub> exhibiting the similar results to the previous works (Fig. 5.10). The increments in the mechanical properties were certainly attributed to the densely packed structure which potentially maximized the contact area between CNTs to enhance the  $\pi$ - $\pi$  interactions and hydrogen bonding of functional groups. Additionally the electrical conductivity of MCNT<sub>AW</sub> buckypaper was also improved comparing to the ACCs-removed CNT (MCNT<sub>NW</sub>, MCNT<sub>BW</sub>) buckypapers possibly owing to this densely packed structure despite the presence of the electrical insulating ACCs [17].

It is noticeable that though the oxidation condition for CNT's surface functionalization is the same, the physical and mechanical properties of the resultant materials significantly depended on the presence of ACCs formed during the acid treatment. Moreover, these mechanical properties are exceeding or comparable to the previous records possibly due to the preparation of highly water-dispersible CNTs in the presence of the ACCs with the strong carboxylic groups. My findings imply the suggested acid wash method followed by the oxidations for the maintenance of the ACCs is the practically useful technique for the CNTs applications by improving their dispersion states with the possible additional post-processes such as heterogeneous hybridization [53, 54], ACCs-carbonization [55], and cross-linking of CNTs [56].

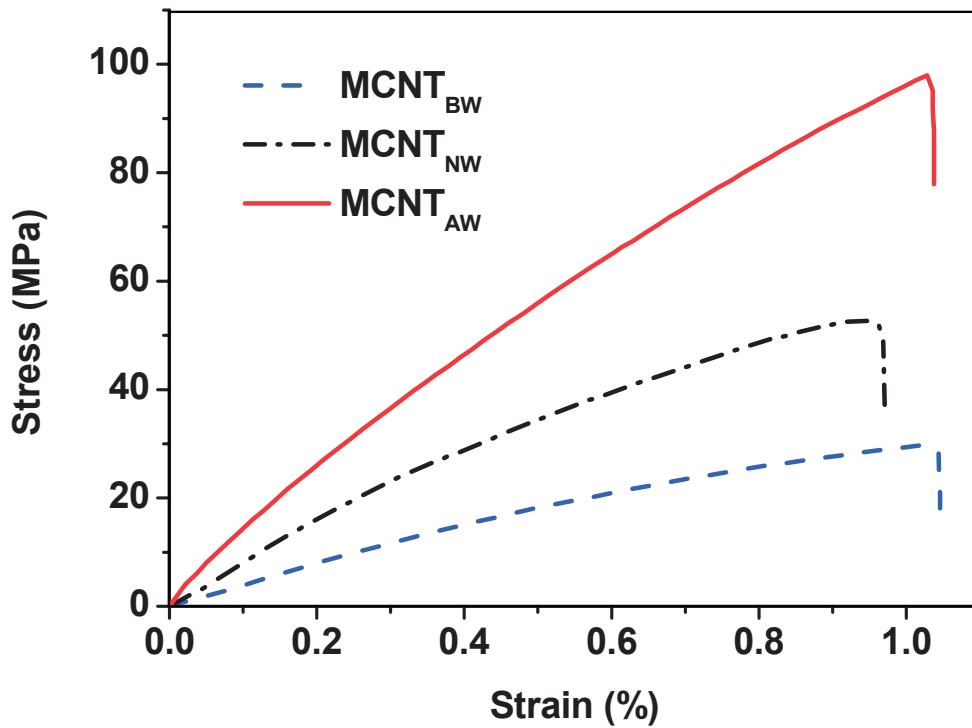


**Fig. 5.10.** Representative stress–strain curves collected from the buckypapers of MCNT<sub>BW</sub>, MCNT<sub>NW</sub>, and MCNT<sub>AW</sub>.

**Table 5. 3.** Comparison between the properties of freestanding CNT buckypapers in this work and those reported previously.

CNT functionalization	Solvent	Apparent Density of CNT (g/cm <sup>3</sup> )	Young's modulus (GPa)	Tensile strength (MPa)	Electrical conductivity (S/cm)	Ref.
HNO <sub>3</sub> /H <sub>2</sub> SO <sub>4</sub> (Acid wash, MCNT <sub>AW</sub> )	Water	1.19 ± 0.05	12.0 ± 0.74	91.1 ± 10.9	57 ± 2	This work
HNO <sub>3</sub> /H <sub>2</sub> SO <sub>4</sub> (Neutral wash, MCNT <sub>NW</sub> )	Water	1.00 ± 0.06	8.70 ± 0.83	48.5 ± 6.3	38 ± 1	This work
HNO <sub>3</sub> /H <sub>2</sub> SO <sub>4</sub> (Base wash, MCNT <sub>BW</sub> )	Water	0.74 ± 0.04	4.06 ± 0.20	27.3 ± 2.6	37 ± 1	This work
HNO <sub>3</sub>	Water	-	5.0 ± 0.2	74 ± 2	120	[7]
SOCl <sub>2</sub>	SOCl <sub>2</sub>	-	0.95	37	3500	[13]
4-Ethoxybenzoic acid	Water	-	12 – 13	35 – 80	294	[15]
Aniline	NMP	0.98 ± 0.09	1.54 ± 0.39	7.80 ± 2.06	-	[10]
None	Triton X-100 /water	-	4	35	-	[14]
None	SDS/water	0.64	2.5	18	-	[12]

## 5.4 Conclusions

Numerous studies have focused on the improvement of the dispersion state of CNTs to synthesize well-organized buckypapers. The side-walls of CNTs were directly functionalized with acidic media ( $\text{HNO}_3$ ,  $\text{SOCl}_2$ ) or organic reagents (esters, amines). Non-covalent functionalization utilizing the surfactants (Triton X-100, sodium dodecyl sulfate [SDS]) was also adopted. My approach for the preparation of highly dispersible CNTs in water and ultra-condensed buckypaper takes the advantages of both functionalization principles. In addition to the covalently attached acidic groups on the CNTs surfaces, ACCs detached from the sidewalls of the CNTs during the oxidation process played a significant role on the dispersion of CNTs and buckypaper formation. For this purpose ACCs were maximally preserved on the CNTs by washing the oxidized CNTs with HCl solution. Additionally the ionization behaviors of ACCs in the CNT dispersions were systematically analyzed applying one-pot titration methodology for the first time. The results showed that the strongly carboxylated ACCs readily removable by conventional neutral wash of the oxidized CNTs was the key for the dispersion of CNTs in water, and hence formation of the highly packed buckypapers.

## 5.5 References

- [1] De Volder MFL, Tawfick SH, Baughman RH, Hart AJ, *Science*, 339 (2013) 535-9.
- [2] Demczyk BG, Wang YM, Cumings J, Hetman M, Han W, Zettl A, et al., *Mat Sci Eng a-Struct*, 334 (2002) 173-8.
- [3] Zhu HW, Xu CL, Wu DH, Wei BQ, Vajtai R, Ajayan PM, *Science*, 296 (2002) 884-6.
- [4] Boncel S, Sundaram RM, Windle AH, Koziol KKK, *Acs Nano*, 5 (2011) 9339-44.
- [5] Sato Y, Ootsubo M, Yamamoto G, Van Lier G, Terrones M, Hashiguchi S, et al., *Acs Nano*, 2 (2008) 348-56.
- [6] Khanderi J, Hoffmann RC, Schneider JJ, *Nanoscale*, 2 (2010) 613-22.
- [7] Zhang XF, Sreekumar TV, Liu T, Kumar S, *J Phys Chem B*, 108 (2004) 16435-40.
- [8] Steiner S, Busato S, Ermanni P, *Carbon*, 50 (2012) 1713-9.
- [9] Blighe FM, Lyons PE, De S, Blau WJ, Coleman JN, *Carbon*, 46 (2008) 41-7.
- [10] Whitten PG, Spinks GM, Wallace GG, *Carbon*, 43 (2005) 1891-6.
- [11] Coleman JN, Blau WJ, Dalton AB, Munoz E, Collins S, Kim BG, et al., *Appl Phys Lett*, 82 (2003) 1682-4.
- [12] Suppiger D, Busato S, Ermanni P, *Carbon*, 46 (2008) 1085-90.
- [13] Dettlaff-Weglikowska U, Skakalova V, Graupner R, Jhang SH, Kim BH, Lee HJ, et al., *J Am Chem Soc*, 127 (2005) 5125-31.
- [14] Berhan L, Yi YB, Sastry AM, Munoz E, Selvidge M, Baughman R, *J Appl Phys*, 95 (2004) 4335-45.
- [15] Kumar NA, Jeon IY, Sohn GJ, Jain R, Kumar S, Baek JB, *Acs Nano*, 5 (2011) 2324-31.
- [16] Xu GH, Zhang Q, Zhou WP, Huang JQ, Wei F, *Appl Phys a-Mater*, 92 (2008) 531-9.
- [17] Park JG, Li S, Liang R, Fan X, Zhang C, Wang B, *Nanotechnology*, 19 (2008) 18710-1-7.
- [18] Kim SW, Kim T, Kim YS, Choi HS, Lim HJ, Yang SJ, et al., *Carbon*, 50 (2012) 3-33.
- [19] Chen J, Hamon MA, Hu H, Chen YS, Rao AM, Eklund PC, et al., *Science*, 282 (1998) 95-8.
- [20] Kwon Y, Yim BS, Kim JM, Kim J, *Microelectron Reliab*, 51 (2011) 812-8.

- [21] Thomassin JM, Molenberg I, Huynen I, Debuigne A, Alexandre M, Jerome C, et al., *Chem Commun*, 46 (2010) 3330-2.
- [22] Vukovic G, Marinkovic A, Obradovic M, Radmilovic V, Colic M, Aleksic R, et al., *Appl Surf Sci*, 255 (2009) 8067-75.
- [23] Worsley KA, Kalinina I, Bekyarova E, Haddon RC, *J Am Chem Soc*, 131 (2009) 18153-8.
- [24] Zhang JP, Wang AQ, *J Colloid Interf Sci*, 334 (2009) 212-6.
- [25] Paredes JI, Burghard M, *Langmuir*, 20 (2004) 5149-52.
- [26] Pantarotto D, Singh R, McCarthy D, Erhardt M, Briand JP, Prato M, et al., *Angew Chem Int Edit*, 43 (2004) 5242-6.
- [27] Shin YR, Jeon IY, Baek JB, *Carbon*, 50 (2012) 1465-76.
- [28] Datsyuk V, Kalyva M, Papagelis K, Parthenios J, Tasis D, Siokou A, et al., *Carbon*, 46 (2008) 833-40.
- [29] Rosca ID, Watari F, Uo M, Akaska T, *Carbon*, 43 (2005) 3124-31.
- [30] Cho HG, Kim SW, Lim HJ, Yun CH, Lee HS, Park CR, *Carbon*, 47 (2009) 3544-9.
- [31] Sung SJ, Kim T, Yang SJ, Oh JY, Park CR, *Carbon*, 81 (2015) 525-34.
- [32] Salzmann CG, Llewellyn SA, Tobias G, Ward MAH, Huh Y, Green MLH, *Adv Mater*, 19 (2007) 883-7.
- [33] Wang ZW, Shirley MD, Meikle ST, Whitby RLD, Mikhalovsky SV, *Carbon*, 47 (2009) 73-9.
- [34] Flavin K, Kopf I, Del Canto E, Navio C, Bittencourt C, Giordani S, *J Mater Chem*, 21 (2011) 17881-7.
- [35] Del Canto E, Flavin K, Movia D, Navio C, Bittencourt C, Giordani S, *Chem Mater*, 23 (2011) 67-74.
- [36] Worsley KA, Kondrat RW, Pal SK, Kalinina I, Haddon RC, *Carbon*, 49 (2011) 4982-6.
- [37] Haddon RC, Sippel J, Rinzler AG, Papadimitrakopoulos F, *Mrs Bull*, 29 (2004) 252-9.
- [38] Bandoz TJ, Jagiello J, Contescu C, Schwarz JA, *Carbon*, 31 (1993) 1193-202.
- [39] Konkena B, Vasudevan S, *J Phys Chem Lett*, 3 (2012) 867-72.

- [40] Lim HJ, Lee K, Cho YS, Kim YS, Kim T, Park CR, *Phys Chem Chem Phys*, 16 (2014) 17466-72.
- [41] Puri BR, Bansal RC, *Carbon*, 1 (1964) 457-64.
- [42] Kim D, Yang SJ, Kim YS, Jung H, Park CR, *Carbon*, 50 (2012) 3229-32.
- [43] Yu H, Jin YG, Peng F, Wang HJ, Yang J, *J Phys Chem C*, 112 (2008) 6758-63.
- [44] Figueiredo JL, Pereira MFR, *Catal Today*, 150 (2010) 2-7.
- [45] Yang SJ, Kim T, Jung H, Park CR, *Carbon*, 53 (2013) 73-80.
- [46] Giovanela M, Parlanti E, Soriano-Sierra EJ, Soldi MS, Sierra MMD, *Geochem J*, 38 (2004) 255-64.
- [47] Peuravuori J, Paaso N, Pihlaja K, *Thermochim Acta*, 325 (1999) 181-93.
- [48] Ashrafi B, Guan JW, Mirjalili V, Hubert P, Simard B, Johnston A, *Compos Part a-Appl S*, 41 (2010) 1184-91.
- [49] Gorgulho HF, Mesquita JP, Goncalves F, Pereira MFR, Figueiredo JL, *Carbon*, 46 (2008) 1544-55.
- [50] Petit C, Bandoz TJ, *J Phys Chem C*, 113 (2009) 3800-9.
- [51] Contescu A, Contescu C, Putyera K, Schwarz JA, *Carbon*, 35 (1997) 83-94.
- [52] Jung H, Yang SJ, Kim T, Kang JH, Park CR, *Carbon*, 63 (2013) 165-74.
- [53] Spitalsky Z, Tsoukleri G, Tasis D, Krontiras C, Georga SN, Galiotis C, *Nanotechnology*, 20 (2009) 405702-1-7.
- [54] Song L, Zhang H, Zhang Z, Xie SS, *Compos Part a-Appl S*, 38 (2007) 388-92.
- [55] Park JG, Yun NG, Park YB, Liang R, Lumata L, Brooks JS, et al., *Carbon*, 48 (2010) 4276-82.
- [56] Biso M, Ansaldo A, Futaba DN, Hata K, Ricci D, *Carbon*, 49 (2011) 2253-7.



# **Chapter 6 Ionic Cross-Linking of Graphene Oxide and Diamines for Preparation of High-Performance Graphene Oxide Fibers**

## **6.1 Introduction**

Since its discovery in 2004, graphene, a novel two-dimensional material, has been touted as a candidate for a variety of applications in the areas of structural materials, energy storage/generation, electronic devices, and sensors [1, 2]. The excellent mechanical, electrical, and thermal properties of graphene compared with other reported materials have been observed in single-layered or few-layered graphene synthesized through chemical vapor deposition or epitaxial growth methods [3, 4]; however, the ideal properties of graphene have yet to be achieved in assembled graphene layer structures, such as graphene foams or papers [5-11].

Recent research efforts have attempted to employ the superior properties of graphene by creating graphene-based fibrous materials in which graphene layers were anisotropically aligned along the fiber axis direction [12-19]. Graphene alignment could be achieved readily by spinning a liquid crystalline graphene oxide (GO) spinning dope solution into a bath containing coagulation agents (a coagulation bath). These laboratory-scale fabrication methods for spinning GO fibers are similar to established industrial techniques for preparing polymeric or carbon fibers and may, therefore, be readily extended to the industrial scale. The mechanical and electrical properties of the GO fibers may be adjusted by altering the interlayer spacings between graphene layers using

appropriate chemical or thermal treatments to fabricate optimized graphene fibers for use in a variety of fields [8-10, 20-22].

Comparing to the graphene-layer based fibers including carbon nanotube (CNT) fibers or carbon fibers, GO fibers have great advantages and potential to be applied to the next generation multifunctional textiles. Specifically, CNT fibers fabricated by chemical vapor deposition (CVD) or wet spinning of CNT dispersions exhibited superior mechanical and electrical properties [23, 24]. Unfortunately, these CNT fibers synthetic methods require harsh processing conditions including extremely elevated temperature (over 1000°C) and explosive gases ( $H_2$ ,  $CH_4$ ) with high cost for the CVD process, or usage of hazardous acid like sulfuric acid as a dispersion media for the wet spinning process. Meanwhile, GO sheets are easily dispersed in the safe aqueous or polar solvents and show the liquid crystalline behaviors. Thus, graphene layers can be easily aligned by the typical industrial solution spinning process to form one-dimensional macroscopic arrays with high cost efficiency.

Additionally, a fluent of oxygen functional groups on GO sheets are easily converted or reduced, giving these fibers the great opportunities to be the potential candidates for the multifunctional textiles including flexible sensors or electronics [25-27]. Besides, since these intrinsic or converted functionalities on GO sheets can be compatible to the various polymers, the GO fibers are perfectly applicable to the high performance fiber composites originated from the good interfacial interaction with the matrix [28].

Therefore, a variety of approaches have been tested in an effort to improve these superior performances of GO or graphene fibers. These approaches include 1) introducing coagulation agents that reduce electrical repulsion and increase hydrogen bonding and van der Waals interactions between graphene layers to preferentially and anisotropically

orient the as-spun GO gel fibers along an axis [14-17], or 2) hydrothermal reduction of the GO solution filled in the one-dimensional template such as ultrathin pipeline [18]. Currently reported coagulating agents can act by coordinatively cross-linking the GO fibers with divalent ions ( $\text{CaCl}_2$ ,  $\text{CuSO}_4$ ), partially reduce the GO fibers with hydroxide ions ( $\text{NaOH}$ ,  $\text{KOH}$ ), or reduce the surface charges on the GO fibers by introducing positively charged molecules or polymers (hexadecyltrimethyl ammonium bromide; CTAB, chitosan) onto the surfaces of the GO layers [12, 15, 17, 19]. However, these coagulating agents tested inevitably require the additional use of a post-drawing process, such as rotating the coagulation stage, to uniformly orient the GO fibers and maximize the packing density of the graphene layers in the GO fibers. Post-drawing processes unfortunately tend to be difficult to implement, and they tend to limit the applications of graphene-based fibrous materials.

To resolve these problems, one-step hydrothermal fabrication method, where coagulating agents are unnecessary, can be utilized [18]. In this method, GO solution are filled in the ultrathin pipeline and thermally reduced in the elevated temperature to fix the orientation of the GO layers in the pipeline. Though highly aligned GO fibers can be easily obtained in a single step in the laboratory-scale, scaling-up into the industrial scale might be difficult comparing to the general wet-spinning method. In addition, additional thermal or chemical treatment of as-received graphene fibers for multifunctional applications is unavailable since the oxygen containing functional groups are reduced during the fiber fabrication.

Therefore in this work, readily self-assembled graphene based fibers with perfect alignment were fabricated, where the additional post-drawing process or usage of the template are unnecessary, by applying the diamine molecules as the coagulation agents. The diamine molecules fix the orientation of the GO layers and stabilize the GO fibers

1) electrically during the spinning and 2) covalently during the drying process, respectively. The properties of the resultant fibers could be readily adjusted by varying the structures of the diamine groups. This approach provides a facile method for fabricating GO fibers that display excellent tunable mechanical properties for use as precursors in optimized graphene-based fibrous materials.

## 6.2 Experimental

### 6.2.1 Preparation of GO solution spinning dope

All materials used in these studies were purchased from Sigma-Aldrich, except for the concentrated sulfuric acid (98%) and hydrogen peroxide solution (30%), which were obtained from Daejung (Korea). The GO solution was fabricated based on a modified Hummer's method [29, 30]. In the first step, graphite flakes (2.4 g) were pre-oxidized to expand the graphite in a potassium persulfate (2 g) and phosphorous pentoxide (2 g) solution in concentrated sulfuric acid (10 mL) with heating at 80°C for 3 days. The expanded graphite was then carefully poured into deionized (DI) water, filtered through a 0.45  $\mu\text{m}$  PTFE membrane filter, and washed with DI water. After drying under vacuum at room temperature for one day, the expanded graphite was oxidized in a potassium permanganate (12 g) solution in concentrated sulfuric acid (92 mL) at 35 °C for 2.5 hours. After the oxidation step, the mixture was cooled to 0 °C, and DI water (1.0 L) was cautiously added to the oxidation mixture over 30 minutes. A hydrogen peroxide solution (10 mL) was added to terminate the oxidation reaction. The obtained bright yellowish GO was centrifuged at 10,000 rpm for 15 min, mixed with a 1 N HCl solution, and centrifuged three times to remove impurities generated during the oxidation reaction. After purification in the HCl solution, the GO was neutralized with DI water by centrifugation at 13,000 rpm for 40 minute until the pH of the supernatant exceeded 5.0. The GO solution was neutralized to yield a highly concentrated graphene oxide solution, dark brown in color, that exhibited liquid crystalline behavior, as confirmed by polarized optical microscopy (POM) measurements.

### 6.2.2 Preparation of diamine cross-linked GO fibers

The graphene oxide fibers were fabricated using the coagulation bath dissolving 0.1 M of diamines of various chain lengths (ethylenediamine, hexamethylenediamine, or 1,8-diaminooctane) in DI water. The diamines were denoted DA<sub>2</sub>, DA<sub>6</sub>, and DA<sub>8</sub>, according to the chain length, respectively. A 5 mL syringe was filled with the aqueous GO solution (10 mg/mL), and the solution was spun into the diamine coagulant bath using a spinning needle (0.413 mm ID) at a rate of 10 mL/minute. The GO solution coagulated to form a GO gel fiber immediately during spinning by the formation of the ion bridges between diamine molecules and the acidic functional groups GO layers. The as-spun GO gel fiber was washed with methanol and rolled up onto a collection spool or was vertically aligned and dried at room temperature. The dried GO fibers spun from the DA<sub>2</sub>, DA<sub>6</sub>, and DA<sub>8</sub> coagulant bath were denoted GOF\_DA<sub>2</sub>, GOF\_DA<sub>6</sub>, and GOF\_DA<sub>8</sub>, respectively.

### 6.2.3 Characterization

The as-produced GO was uniformly deposited onto an ozone-treated silicon substrate and characterized by scanning electron microscopy (SEM; JSM-6700F, JEOL) and atomic force microscopy (AFM; Nanostation II, Pucotech) to analyze the dimensions of the single GO sheet. For the characterization of liquid crystalline behavior of GO, GO solutions were loaded into the planar cells and observed with POM (BX 51, Olympus) in transmission mode.

The acidic properties of GO were characterized by one-pot titration methods developed in **Chapter 4** for the analysis of proton binding isotherm ( $\theta(\text{pH})$ ) and  $\text{p}K_a$  distributions ( $f(\text{p}K_a)$ ) analysis. 1 mg/mL GO solution was dried by freeze dryer (Bondiro, Ilshin) at 40 °C in vacuum condition. The freeze-dried GO sample (6 mg) was then mixed with 0.01 N HCl solution (20 mL) and titrated with 0.01 N NaOH solution as a titrant. The

titration vessel was continuously purged with N<sub>2</sub> flowing gas at 25 °C, and the additional dosing step of the titrant solution was conducted only when the pH of the titration system become stable (pH variance lower than 0.02 pH unit/minute). The resultant titration curve was converted to  $\theta(\text{pH})$  showing the number of ionized functional groups on GO sample as a function of pH during the titration applying the methodology developed in **Chapter 4** (using equation (4.9) and (4.9.1)). Subsequently  $f(\text{p}K_a)$ , indicating the population of the acidic groups in the specific  $\text{p}K_a$  range, was obtained from converting the proton binding isotherms by

$$f(\text{p}K_a) \cong \left[ \frac{\partial \theta(\text{pH})}{\partial \text{pH}} \right]_{\text{pH}=\text{p}K_a}, \quad (6.1)$$

applying the first-order approximation [31].

The surface and cross-sectional morphologies of each GO fiber were analyzed using SEM. The chemical states of the GO fibers were investigated by examining the fibers using Fourier transform infrared spectroscopy (FT-IR; Nicolet iS10, Thermo Scientific) and X-ray photoelectron spectroscopy (XPS; AXIS-HSi, KRATOS). The microstructure of the GO fiber was further characterized using an X-ray diffractometer (XRD; D8 advance, Bruker) equipped with a 0.154 nm Ni-filtered CuK $\alpha$  radiation source. The mechanical properties the GO fibers were characterized using a tensile test machine (Instron-5543, Instron) with a 1 cm gauge length and a 10 %/minute strain rate. The results reported are the average measured values obtained from at least 10 samples of each GO fiber.

## 6.3 Results and discussion

### 6.3.1 Physical and chemical properties of GO

Prior to spinning the GO solution for fiber fabrication, the lateral dimensions and thickness of the single GO sheets were measured to determine whether the synthesized GO could exhibit liquid crystalline behavior. SEM analysis revealed that the lateral dimensions of the GO sheets ranged from 10 to 50  $\mu\text{m}$  (Fig. 6.1a) and the AFM results exhibited an average layer thickness of 1.2 nm (Fig. 6.1b). The aspect ratio was sufficiently high to allow the as-prepared aqueous GO solution to display liquid crystalline behavior [13, 15]. As expected from the dimension observation of GO layers, GO solutions exhibited typical Schlieren textures of liquid crystals between the crossed polarizer over a range of concentrations, from 0.5 to 10 mg/mL (Figs. 6.2a – 6.2f). Generally, the size of the texture became larger as the concentrations of GO solutions increased, implying more uniform ordering of GO sheets was formed.<sup>31</sup> Based on the POM observation, 10 mg/mL GO solution especially showed the liquid crystalline behaviors with the largest area of uniform orientation, thereby being the suitable candidate for the fiber spinning.



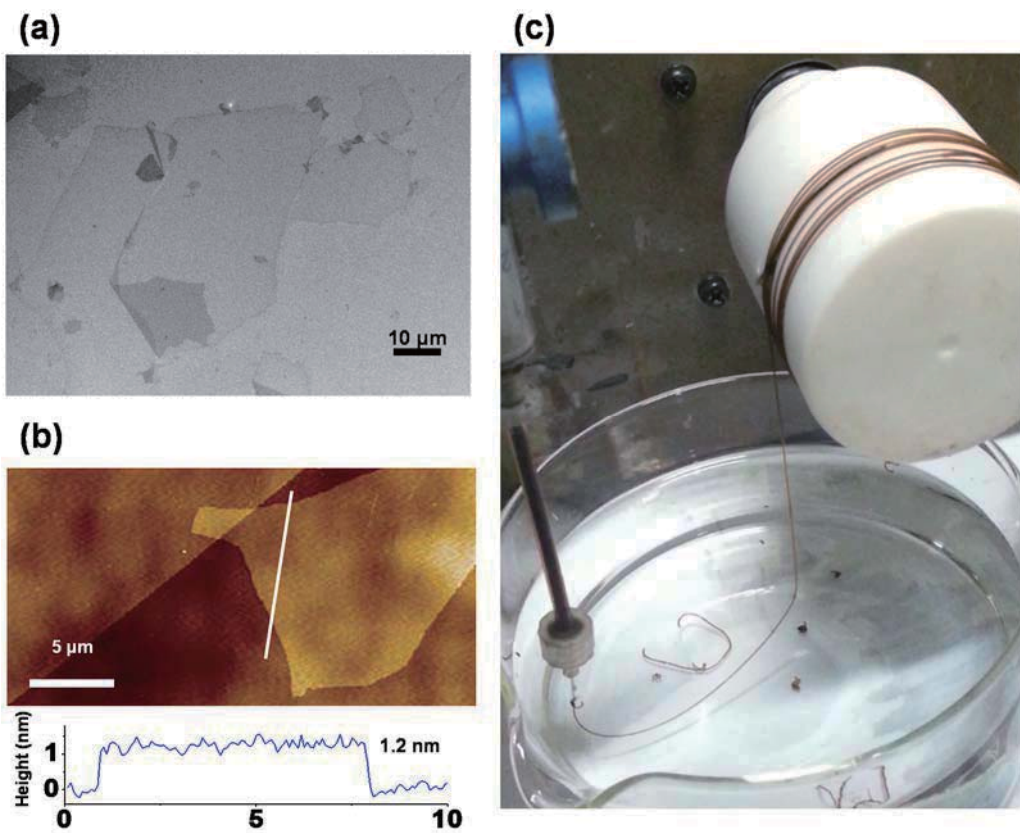


**Fig. 6.1.** (a) SEM, (b) AFM images of single layer GO sheets, and (c) photograph of the collected as-spun GO gel fibers.

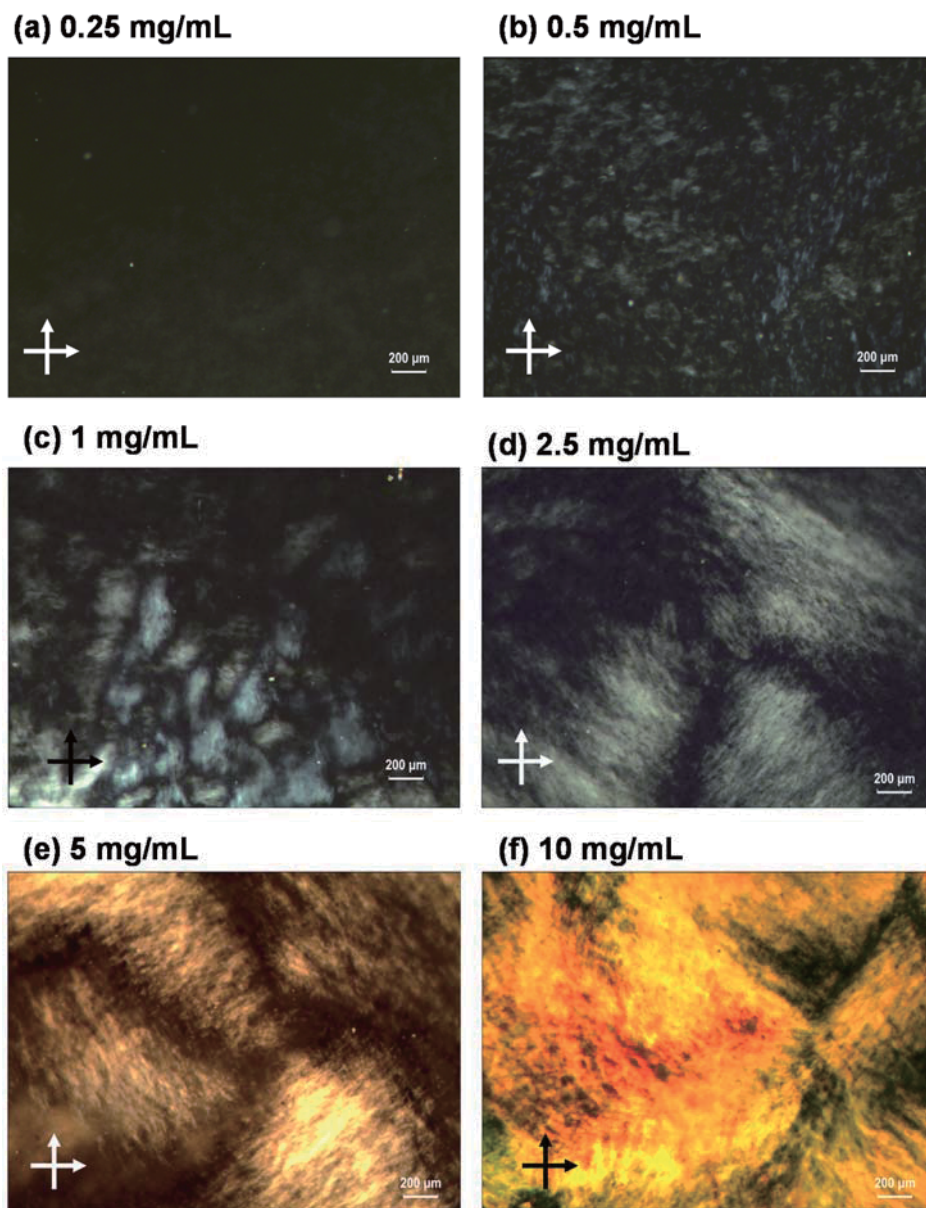


**Fig. 6.2.** POM images of (a) 0.25, (b) 0.5, (c) 1, (d) 2.5, (e) 5, and (f) 10 mg/mL aqueous GO solutions.

The acidic groups are the other contributing factors of the fiber spinning along with the liquid crystalline behaviors of GO solutions by acting as the source of the ion bridge of diamine molecules.  $\theta(\text{pH})$  presented in Fig.6.3a certainly showed that the GO contained a fluent of the acidic functional groups (3.9 meq/g) which can interact with the diamine molecules in the coagulating bath. Additionally,  $f(\text{p}K_a)$  (Fig. 6.3b) exhibit that the surface of GO sheets were covered by three major acidic acidic groups with  $\text{p}K_a = 4.4$ , 7.3, and 9.7 which might be correspond to the carboxylic, lactonic, and phenolic groups, respectively [31]. Especially the contribution of phenolic groups was the largest among the functional groups which as generally accepted and also confirmed by XPS analysis of GO film shown in Fig. 6.5a.

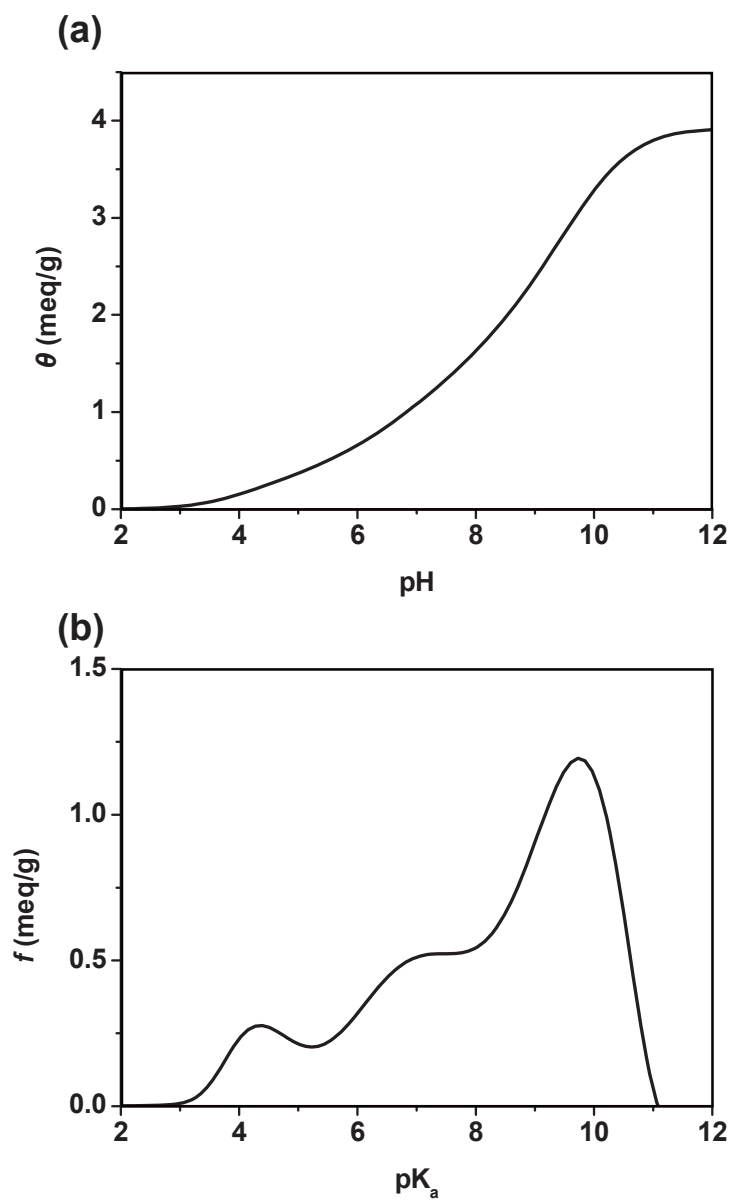


**Fig. 6.3.** (a) Proton binding isotherm ( $\theta(\text{pH})$ ) and (b)  $pK_a$  distribution function ( $f(pK_a)$ ) of GO sample.

### 6.3.2 Formation mechanism of GO fibers

The GO solution exhibited excellent liquid crystalline behavior; therefore, the graphene layer could be easily aligned under shear forces as the GO solution passed through the capillary needle during the spinning process [13]. This alignment was stabilized to form a GO gel fiber in the presence of appropriate coagulating agents, which enhanced the interactions between the graphene layers. In this work, the diamine molecules with different length ( $DA_2$ ,  $DA_6$ , and  $DA_8$ ) were applied as the coagulation agents since these molecule can stabilize the GO fiber by the formations of the ion bridges with a fluent of functional groups on GO sheets (Fig. 6.3) in the as-spun gel fibers and covalent bonds during the drying, without any necessity of additional drawing process.

By adopting diamine coagulants, coagulation occurred rapidly (within a second) to create gel fibers that were strong enough to preserve their shape during drying or additional processes, such as drawing. The diamine molecules behaved well as coagulation agents by linking the GO layers through ion bridges during the spinning process [32, 33]. The ion bridges were generated by rapid acid–base reactions between the acidic functional groups on the GO layers and the basic amine functional groups on the diamine linkers. Once the GO solution had been immersed in the fiber spinning coagulation bath, the acidic groups, such as the in-plane hydroxyl or edge-attached carboxylic groups on the GO layer, donated protons to the amine group on the linker to form a conjugated base and acid, respectively. The oppositely charged conjugated base and acid formed a strong ion bridge between the diamine linker and the GO surface as shown by the schematic illustration in Figs. 6.4a – 6.4c, thereby enabling rapid coagulation of the GO solution into gel fibers.

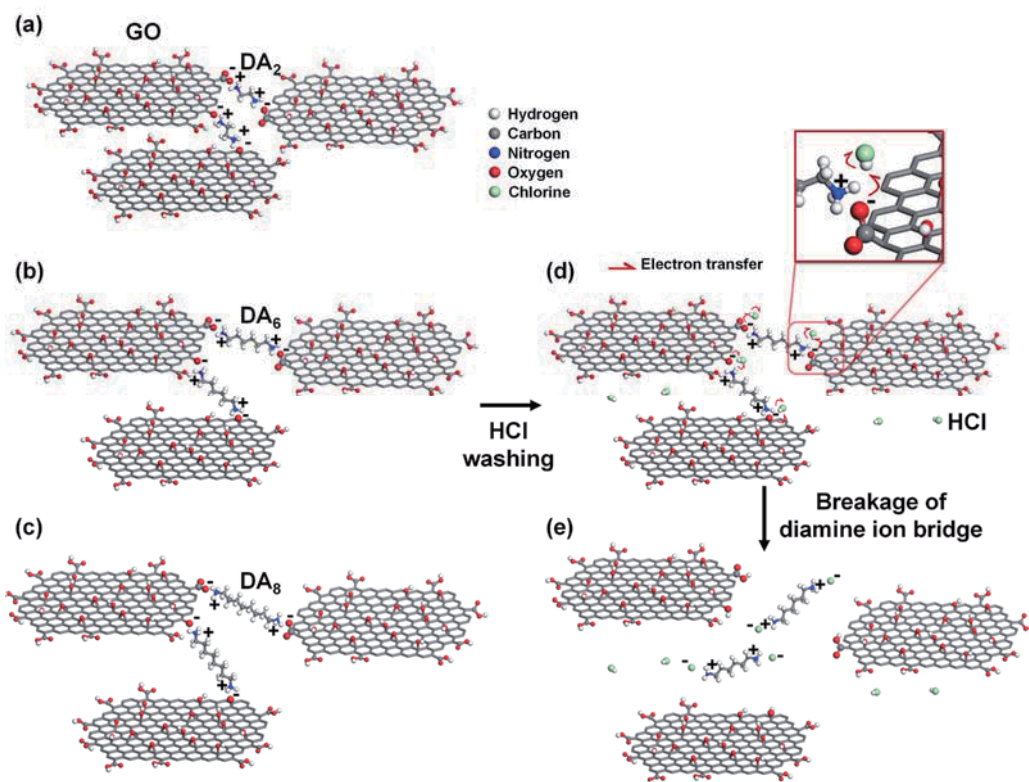


**Fig. 6.4.** Schematic illustrations of formation of ion bridges between GO layers and (a) DA<sub>2</sub>, (b) DA<sub>6</sub>, (c) DA<sub>8</sub>, and (d, e) break of ion bridge by HCl washing (DA<sub>6</sub> in this case).

For the diamines to function as the ion bridges between GO sheets during the fiber spinning, the concentrations of fully ionized diamine molecules where two amine groups were protonated should be essentially generated. The formation of these fully protonated diamine groups are monitored as a function of the concentrations of diamines in the 10 mg/mL GO solutions. For this purpose, pH at the equilibrium states ( $\text{pH}_e$ ) these mixtures were calculated by modification of equation (4.20) developed in **Chapter 4** as follow:

$$\sum \frac{c_C \cdot f(\text{p}K_{a,i}) \cdot (\text{p}K_{a,i+1} - \text{p}K_{a,i})}{1 + 10^{\text{pH}_e} \cdot K_{a,i}} + \left( \frac{c_{\text{DA}_k}}{1 + 10^{\text{pH}_e} \cdot K_W / K_{b,\text{DA}_k}} + \frac{c_{\text{DA}_k}}{1 + 10^{\text{pH}_e} \cdot K_W / K_{b,\text{DA}_k^+}} \right) - \frac{1}{v_{\text{H}_2\text{O}} + 1 / (10^{\text{pH}_e} \cdot K_W)} + \frac{1}{v_{\text{H}_2\text{O}} + 10^{\text{pH}_e}} = 0 \quad (6.2)$$

where  $c_C$  is the concentration of GO,  $\text{p}K_{a,i}$  is the  $i$ 'th component of  $\text{p}K_a$  values divided into  $n$  components,  $f(\text{p}K_{a,i})$  is the proton distribution function at  $\text{p}K_a = \text{p}K_{a,i}$ ,  $c_{\text{DA}_k}$  is the concentration of  $\text{DA}_k$  ( $k$  specifies 2, 6, and 8 in this work, respectively),  $K_{b,\text{DA}_k}$ ,  $K_{b,\text{DA}_k^+}$  is the base ionization constant of  $\text{DA}_k$  and ionized conjugated base of ( $\text{DA}_k^+$ ), respectively (summarized in Table 6.1),  $K_W$ ,  $v_{\text{H}_2\text{O}}$  is the self-ionization constant and molar volume of water, respectively. The concentrations of  $\text{DA}_k^{2+}$  ( $c_{\text{DA}_k^{2+}}$ ) in the mixtures can be subsequently calculated by

$$c_{\text{DA}_k^{2+}} = \frac{K_{b,\text{DA}_k^+}}{[\text{OH}^-]_e + K_{b,\text{DA}_k^+}} c_{\text{DA}_k^+} = \left( 1 + \frac{K_W \cdot 10^{\text{pH}_e}}{K_{b,\text{DA}_k^+}} \right) c_{\text{DA}_k^+} \quad (6.3)$$

where  $[\text{OH}^-]_e$  is the concentration of  $\text{OH}^-$  ion at  $\text{pH}_e$  ( $\text{pH}_e = -\log\left(\frac{K_w}{[\text{OH}^-]_e}\right)$ ),

respectively. Equation (6.3) is analogous of equation (4.6) in **Chapter 4** where detailed derivation is described.

Fig. 6.5 certainly shows that the fully ionized conjugated base of diamines potentially acting as the ion bridges are generated, and the suggested mechanism for GO fibers formations suggested in Fig. 6.4 is available. However, increasing  $c_{\text{DA}_k}$  may decrease the concentrations of these ion bridges because of the higher chance of protonation of the stronger first amine (Table 6.1). This observation indicates the concentrations of the coagulants should be properly adjusted for efficient formation of GO fibers.

In the real case,  $c_{\text{DA}_k}$  in GO dopes at the initial state, when spun into the diamine coagulant, should be zero and increased by the diffusions of the diamine molecules as the as-spun GO fibers are submerged in the diamine solution. Therefore, the appropriate concentrations of the diamines in the coagulant bath would be much higher than proper  $c_{\text{DA}_k}$  determined from Fig. 6.4 of which the precise values are uncertain in the current state. Nevertheless, this approach truly suggest the potential of diamine molecules to function as the ion bridges between GO sheets for fiber spinning.



**Table 6.1.**  $pK_b$  values of  $DA_k$  and  $DA_k^+$  ( $k = 2, 6,$  and  $8$  in this work).

Diamine	$pK_{b,DA_k}$	$pK_{b,DA_k^+}$
$DA_2$	4.1	7.1
$DA_6$	2.1	3.2
$DA_8$	3.0	3.9

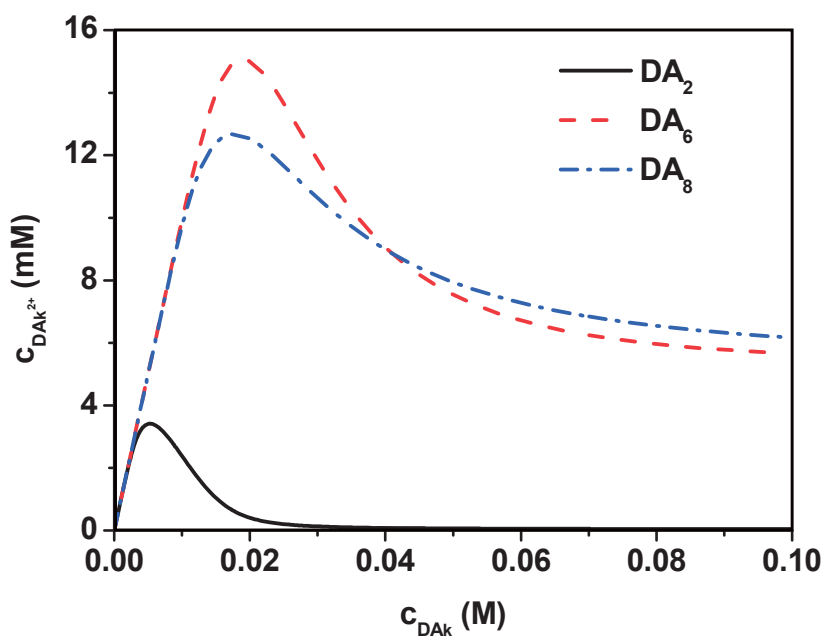


**Fig. 6.5.** Concentrations of fully ionized diamines ( $c_{DA_k^{2+}}$ ) with respect to that of diamine molecules ( $c_{DA_k}$ ) in 10 mg/mL GO solutions.

Indeed, GO gel fibers, strong enough to be rolled up to the taking-up spool (Fig. 6.1c) or put out from the coagulation bath up to or over 1 m (without any support), were able to be spun right after the spinning of aqueous GO spinning dope into the diamine coagulation bath. However, washing the gel fiber with an acidic solution, such as aqueous HCl, weakened and broke the gel fibers such that they could not be pulled from the washing bath. This severance of the gel fiber is due to the breakage of the ion bridge between the GO layers originated from proton donation of HCl to ionized acidic functional groups on GO layers (Fig. 6.4d). The protonated diamine molecules were then unavailable to function as the ion bridges between the GO layers (Fig. 6.2e), thereby easily being dissolved in HCl solution and removed from GO sheets. Different from the diamine cross-linked GO fibers, the microstructure of HCl-washed GO fibers confirmed by XRD patterns were similar to the unreacted GO films (Fig. 6.9), suggesting that the diamine molecules are eliminated by HCl washing. The details of the XRD analysis will be discussed in the XRD analysis section.

Notably, these GO fibers could be spun without the need for a pH lowering or the addition of a co-coagulant into the aqueous coagulating media. Alternative coagulating agents, such as sodium hydroxide (NaOH), which partially reduces the GO, or calcium chloride (CaCl<sub>2</sub>), which forms coordinative cross-links with the divalent ion, require the addition of organic solvents as co-coagulants, such as alcohols or alkyl acetates [14, 15, 17]. In the absence of a co-coagulant, the GO fibers could not be spun. Additionally, the strength of coagulation conveyed by these coagulants may not be sufficiently large to stabilize the anisotropic alignment of the GO layers during the drying process. Other drawing procedures involving a rotating coagulation stage or a post-drawing roller may be needed to fabricate highly aligned and close-packed GO fibers with strong mechanical properties [14, 15, 17]. Significantly, the GO spinning method described here using

diamine linkers provided GO fibers in which the GO layers were perfectly aligned and compacted, yielding excellent mechanical properties. The use of organic co-coagulants and post-drawing processes could be avoided. The morphologies and properties of the diamine cross-linked GO fibers are discussed in subsequent sections.

After washing the gel fibers with a volatile solvent, such as methanol, the fibers shrank along the radial direction perpendicular to the fiber axis by the strong electrical interaction between GO layer and diamine ion bridges. The remaining solvent easily evaporated during the drying process within a few hours.

Fig. 6.6 shows the morphology of the surface and a cross-sectional SEM images of the dried GO fibers linked through the various diamine linkers. As shown in the SEM images, the GO layers were well aligned along the longitudinal spinning direction (Figs. 6.6a – 6.6c), and the layers were closely packed in a lamellar structure (Figs. 6.6d – 6.6i) without the need for a post-drawing process. This type of lamellar structure has been reported previously in GO fibers coagulated using other coagulants, such as CTAB or  $\text{CaCl}_2$  [14, 19].

As with the diamines, these other coagulants included ammonium groups ( $-\text{NH}_3^+$ ) or  $\text{Ca}^{2+}$  ions that shielded the negatively charged oxygen-containing acidic groups on the GO surfaces to reduce electrical repulsion and facilitate the assembly of GO layers into a fibrous shape. The counter ions present with these anions ( $\text{Br}^-$  or  $\text{Cl}^-$ ) unfortunately tended to disrupt the efficient packing of the GO layers. Because strong electrical attraction between diamine ion bridges and GO layers cannot be interrupted by a counter ion, the GO layers prepared using the method described here displayed a high degree of alignment and packing among compared to the GO fibers reported previously, without the need for a drawing procedure.

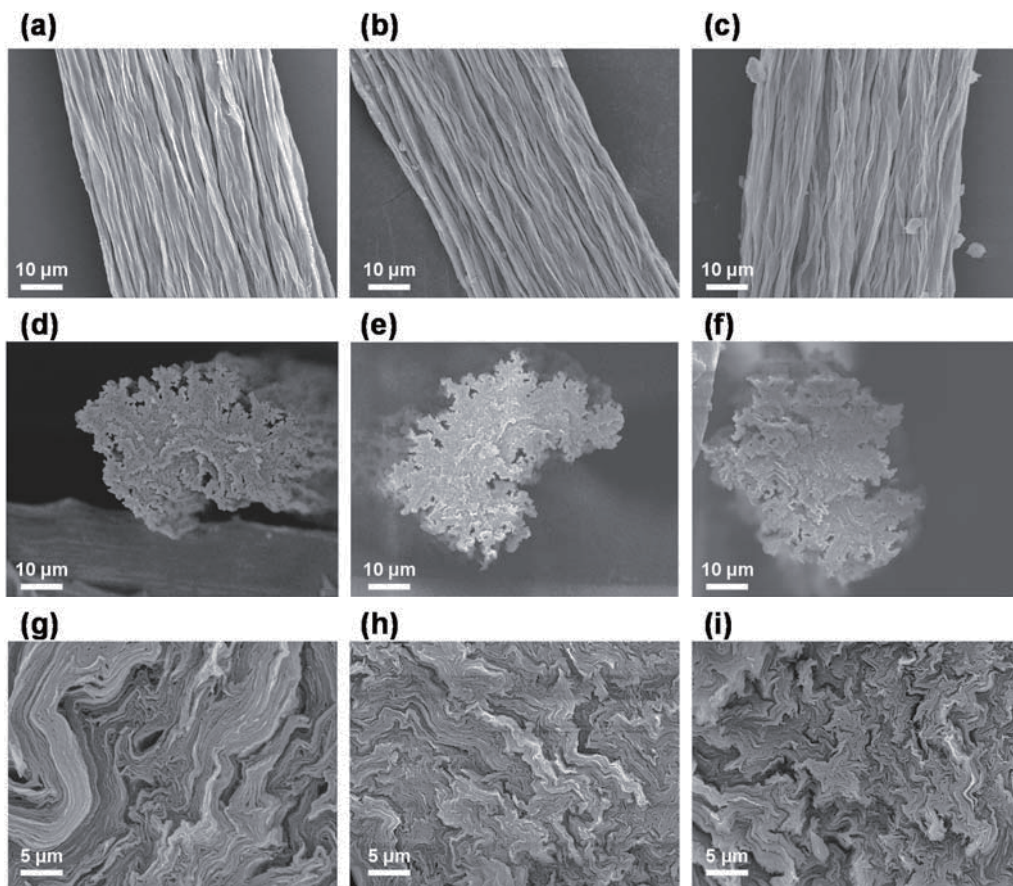


**Fig. 6.6.** SEM images showing the surfaces and cross-sectional morphologies of (a, d) GO\_DA<sub>2</sub>, (b, e) GO\_DA<sub>6</sub>, (c, f) GO\_DA<sub>8</sub>, and (g, h, i) magnified view of cross-section of each GO fiber ((d, e, f), respectively).

### 6.3.3 Properties and performances of GO fibers

The alignment and packing state of the GO fibers were further stabilized by the formation of the covalent bonds between diamine molecules and GO layers during the drying process. As the distance between GO layers decreased and the concentration of the GO increased during drying, the remaining diamine molecules reacted with the in-plane hydroxyl or epoxide groups on the GO layer surfaces, similar to previous reports of amine- or diamine-treated GO particles or densely packed GO papers [7, 9, 32, 34]. In previous studies, the GO or GO composite papers were immersed in methanol to dissolve the amine molecules over 12 hours at room temperature. The amine groups then reacted with the in-plane epoxide and hydroxyl groups on the GO layer surfaces through nucleophilic addition and condensation reactions, respectively [7, 9]. Similar reactions would be available in the present method, as the distance between GO layers is small enough to permit this reaction.

Evidence for these reactions was obtained from the FT-IR spectra (Fig. 6.7) and XPS (Fig. 6.8) analysis. Fig. 6.7 presents the FT-IR spectra of an unreacted GO film and the GOF\_DA<sub>2</sub>, GOF\_DA<sub>6</sub>, and GOF\_DA<sub>8</sub> samples. The unreacted GO film displayed a typical stretching vibration mode, as described in previous reports, including the vibrational modes of the O-H hydroxyl (3400 cm<sup>-1</sup>), C=C aromatic rings (1626 cm<sup>-1</sup>), C-O carboxylic (1416 cm<sup>-1</sup>), epoxy (1222 cm<sup>-1</sup>), and alkoxy (1049 cm<sup>-1</sup>) groups, and C=O carboxylic (1728 cm<sup>-1</sup>) groups [11, 35]. Comparing to the GO film, the C=O stretching mode of the carboxylic groups in the GOF\_DA<sub>2</sub> reduced and the peak around 1620 cm<sup>-1</sup> was broadened. This indicates the carboxylic groups ionized to form carboxylates (COO<sup>-</sup>) which was linked to diamine ion bridges in the GO fiber [36]. The reaction between the hydroxyl or epoxy groups and the diamine linker during the fiber drying process was supported by the observation of C-N (1392 cm<sup>-1</sup>) and N-H (1510 cm<sup>-1</sup>)

<sup>1</sup>) stretching and bending modes, respectively [11, 37]. In addition, symmetric and asymmetric stretching modes of methylene groups (CH<sub>2</sub>) from cross-linked diamine molecules were also appeared at 2850 and 2920 cm<sup>-1</sup>, respectively [38]. Similar vibrational modes were observed in the GOF\_DA<sub>6</sub> and GOF\_DA<sub>8</sub> samples.

The FT-IR results, which supported the formation of a C-N bond, were corroborated by the XPS C1s peak analysis (Fig. 6.8). The unreacted GO film surface included carbon single/double bonds (C-C/C=C, peak 1, 284.5 eV), and oxygen-containing functional groups dominated by hydroxyl and epoxy groups (C-OH/C-O-C, peak 2, 286.5 eV) with relatively small amounts of carbonyl (C=O, peak 3, 287.9 eV) and carboxylic (COO, peak 4, 289.2 eV) groups [20]. During fiber fabrication via diamine cross-linking of the epoxy and hydroxyl group, as shown in the XPS of GOF\_DA<sub>2</sub>, the relative proportion of hydroxyl and epoxy groups decreased and a new peak corresponding to a C-N bond appeared at 285.8 eV (peak 2') [10]. Similarly, the formation of a C-N bond was confirmed by the XPS analysis of the GOF\_DA<sub>6</sub> and GOF\_DA<sub>8</sub> samples.

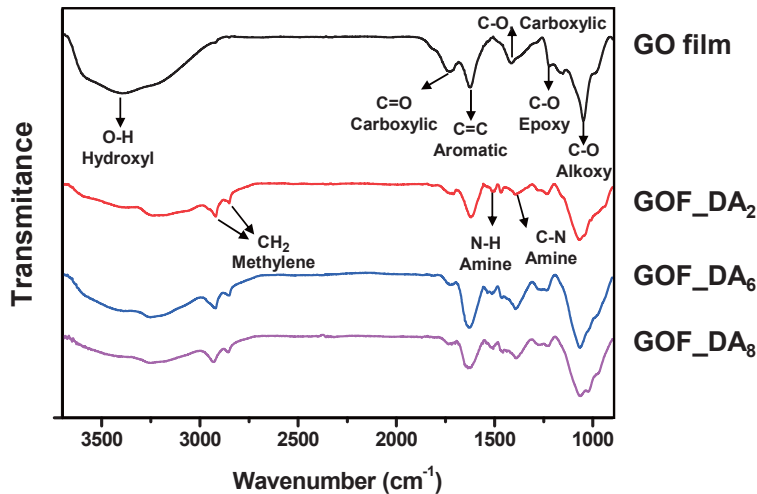


**Fig. 6.7.** FT-IR spectra of the unreacted GO film and the diamine cross-linked GO fibers.

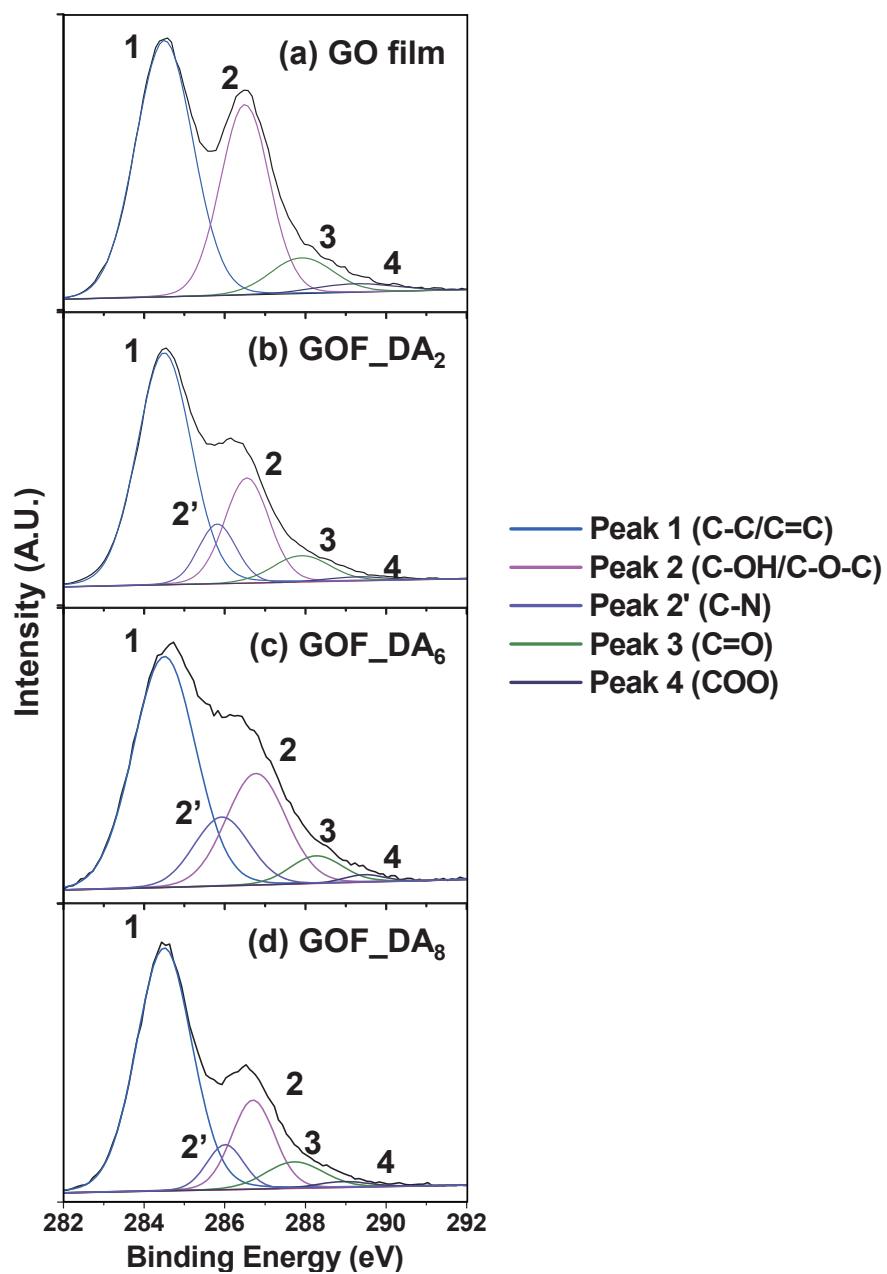


**Fig. 6.8.** XPS C1s spectra of the (a) unreacted GO film, and of the diamine cross-linked GO fibers ((b) GOF<sub>DA2</sub>, (c) GOF<sub>DA6</sub>, and (d) FOG<sub>DA8</sub>)).

The interlayer microstructures of the GO fibers were investigated by analyzing the XRD patterns of the unreacted GO film and the fibers cross-linked by diamines with different molecular structures (Fig. 6.9). As was observed among the GO papers or particles functionalized with various bi- or monofunctional molecules or polymers, the interlayer distance specified by the d-spacing distance of the (002) plane ( $d_{002}$ ) depended on the length of the cross-linked diamine molecule [9, 32]. The value of  $d_{002}$  in GO increased from 8.3 to 9.2, 10.1, and 13.8 Å as the GO was cross-linked by DA<sub>2</sub>, DA<sub>6</sub>, and DA<sub>8</sub>, respectively, to form fibers. However, the  $d_{002}$  retains for HCl-washed GO fibers since the diamine ion bridges between GO layers were broken and eliminated by methanol washing. Therefore, continuous spinning of the fibers was not available after washing the fibers with the acidic solution as demonstrated in the previous discussion.

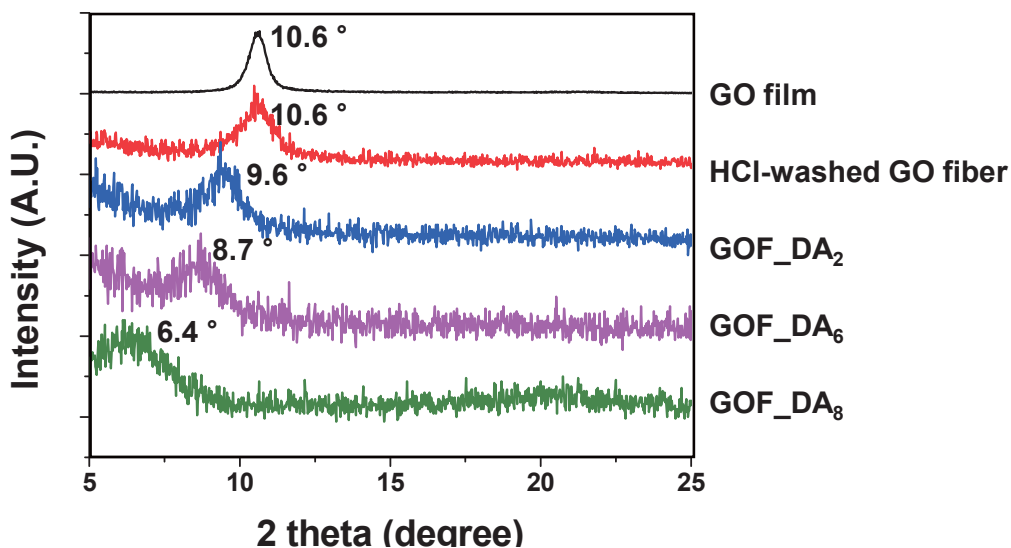
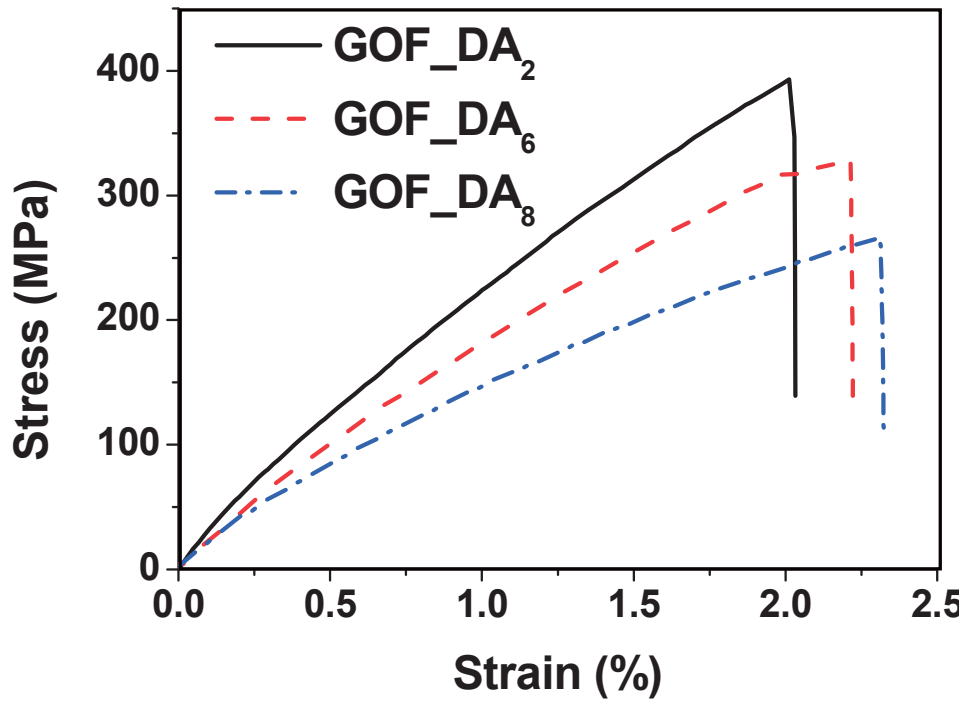


Fig. 6.9. XRD patterns collected from the unreacted GO film and from the diamine cross-linked GO fibers.



The GO layers were effectively cross-linked by both ion bridge formation and covalent bonds during the spinning and drying processes, respectively. The resultant GO fibers showed excellent mechanical properties without the need for a post-drawing process. Fig. 6.10 shows representative stress–strain curves collected from the GO fibers prepared using each of the cross-linked diamine molecules. The average Young’s moduli of the GO fibers were within the range 17.3 – 26.6 GPa, and the average tensile strengths were within the range 275.1 – 384.3 MPa, depending on the length of the cross-linked diamine molecules (Table 6.2). These results were consistent with the predictions obtained from the XRD analysis (Fig. 6.9).

As mentioned, GO fibers with excellent mechanical properties have been typically fabricated with the aid of post-drawing processes involving a rotating coagulation stage or a drawing roller. For example, Xu et al. utilized a rotating coagulation bath to fabricate GO fibers that were coordinately cross-linked by  $\text{Ca}^{2+}$  ions. They emphasized that the post-drawing process was essential for fabricating ultra-strong GO fibers. Indeed, post-drawing of the  $\text{Ca}^{2+}$ -cross-linked as-spun GO fibers increased the Young’s modulus by 65% and the tensile strength by 48% (Table 6.2) [17]. Xiang et al. reported similar results by post-drawing as-spun GO gel fibers and varying the speed of the fiber-collecting drum. They reported a 236% increase in the Young’ modulus and a 73% increase in the tensile strength under the optimized fabrication conditions (Table 6.2). Excessive drawing (a 1.45 drawing ratio) can increase the brittleness of the GO fibers and decrease the elongation at break (from 1.64 to 0.61%), thereby limiting the applicability of the fibers [14].



**Fig. 6.10.** Representative stress–strain curves collected from the GOF\_DA<sub>2</sub>, GOF\_DA<sub>6</sub>, and GOF\_DA<sub>8</sub> samples.

**Table 6.2.** Comparison of the mechanical properties of the GO fibers prepared in this work and those reported previously and coagulated using different coagulants, before and after a drawing process.

Coagulant	Before drawing process			After drawing process			Ref.
	Young's Modulus	Tensile Strength	Elongation at Break	Young's Modulus	Tensile Strength	Elongation at Break	
	(GPa)	(MPa)	(%)	(GPa)	(MPa)	(%)	
Ethylene-diamine (DA <sub>2</sub> )	26.6 ± 1.2	384.3 ± 19.1	1.87 ± 0.16	-	-	-	This work
Hexamethylene-diamine (DA <sub>6</sub> )	20.3 ± 1.5	304.4 ± 18.0	1.89 ± 0.20	-	-	-	This work
1,8 diaminooctane (DA <sub>8</sub> )	17.3 ± 1.3	275.1 ± 15.2	2.10 ± 0.17	-	-	-	This work
KOH	1.6	125	10	3.2	184.6	7.5	[17]
CuSO <sub>4</sub>	2.3	258.6	13.3	6.4	274.3	5.9	[17]
CaCl <sub>2</sub>	3.7	245.8	9.8	6.3	364.4	6.8	[17]
CaCl <sub>2</sub>	-	-	-	20.1 ± 2.1	412 ± 30	3.2	[15]
Chitosan	-	-	-	22.6 ± 1.9	442 ± 18	3.6	[15]
NaOH	-	-	-	11.0 ± 2.4	183 ± 25	2.5	[15]
Ethyl acetate	14.0 ± 1.5	124 ± 8	1.64 ± 0.12	47 ± 8	214 ± 38	0.61 ± 0.1	[14]
CTAB	4.2	145	4.0	-	-	-	[19]

\*In the case of using NaOH coagulant, the fabricated fiber is partially reduced GO fiber, as NaOH reacts as weak reductant during the fiber formation.

Notably, complex post-drawing were unnecessary for the production of GO fibers using my newly developed method. The GO fibers displayed competitive mechanical properties, with a good modulus and strength (Table 6.2). Comparing to the previously reported GO fibers without any post-drawing process, even GOF\_DA<sub>8</sub>, the weakest GO fibers in this work, records the best tensile modulus and strength to the best of my knowledge.

Numerous approaches still remain to maximize and tune the properties of GO fibers fabricated using the coagulation method described here. GO sheets with a larger lateral size may be used [14-16]. Post-treatments may be adopted, such as heterogeneous complexion to form GO composite fibers [25, 28]. The oxygen-containing groups on the GO layer surfaces may be chemically or thermally reduced to form graphene fibers [20-22]. Therefore, the diamine cross-linked GO fibers developed here provide excellent candidate precursors for use in multifunctional graphene-based fibrous materials, broadening the field of graphene applications.

## **6.4 Conclusions**

A novel method was used to fabricate GO fibers with excellent mechanical properties and without the need for post-processing steps. The GO fibers were condensed by electrical attraction between the ionized diamine molecules and the hydroxyl and carboxylic groups on the GO layers, which preserved the uniform orientations along the longitudinal axis and the compact packing structures of the GO layers along the spinning direction. The mechanical properties of the GO fibers could be tuned by varying the structure of the cross-linked diamine molecules, which altered the microstructures of the fibers. These results suggest that this novel GO fabrication method is readily applicable to the optimized fabrication of one-dimensional fibrous graphene materials.

## 6.5 References

- [1] Novoselov KS, Geim AK, Morozov SV, Jiang D, Zhang Y, Dubonos SV, et al., *Science*, 306 (2004) 666-9.
- [2] Allen MJ, Tung VC, Kaner RB, *Chem Rev*, 110 (2010) 132-45.
- [3] Craciun MF, Russo S, Yamamoto M, Oostinga JB, Morpurgo AF, Tarucha S, *Nat Nanotechnol*, 4 (2009) 383-8.
- [4] Reina A, Jia XT, Ho J, Nezich D, Son HB, Bulovic V, et al., *Nano Lett*, 9 (2009) 30-5.
- [5] Dong XC, Xu H, Wang XW, Huang YX, Chan-Park MB, Zhang H, et al., *Acs Nano*, 6 (2012) 3206-13.
- [6] Wang ZL, Xu D, Xu JJ, Zhang LL, Zhang XB, *Adv Funct Mater*, 22 (2012) 3699-705.
- [7] Wei-Song Hung CHT, Manuel De Guzman, Quan-Fu An, Ying-Ling Liu, Ya-Ming Zhang, Chien-Chieh Hu, Kueir-Rarn Lee, and Juin-Yih Lai, *Chem Mater*, (2014)
- [8] Matsuo Y, Miyabe T, Fukutsuka T, Sugie Y, *Carbon*, 45 (2007) 1005-12.
- [9] Stankovich S, Dikin DA, Compton OC, Dommett GHB, Ruoff RS, Nguyen ST, *Chem Mater*, 22 (2010) 4153-7.
- [10] Yang SJ, Kang JH, Jung H, Kim T, Park CR, *J Mater Chem A*, 1 (2013) 9427-32.
- [11] Lee JU, Lee W, Yi JW, Yoon SS, Lee SB, Jung BM, et al., *J Mater Chem A*, 1 (2013) 12893-9.
- [12] Wang RR, Sun J, Gao L, Xu CH, Zhang J, *Chem Commun*, 47 (2011) 8650-2.
- [13] Xu Z, Gao C, *Nat Commun*, 2 (2011), 8650-2.
- [14] Xiang CS, Young CC, Wang X, Yan Z, Hwang CC, Ceriotti G, et al., *Adv Mater*, 25 (2013) 4592-7.
- [15] Jalili R, Aboutalebi SH, Esrafilzadeh D, Shepherd RL, Chen J, Aminorroaya-Yamini S, et al., *Adv Funct Mater*, 23 (2013) 5345-54.
- [16] Chen L, He YL, Chai SG, Qiang H, Chen F, Fu Q, *Nanoscale*, 5 (2013) 5809-15.
- [17] Xu Z, Sun HY, Zhao XL, Gao C, *Adv Mater*, 25 (2013) 188-93.
- [18] Dong ZL, Jiang CC, Cheng HH, Zhao Y, Shi GQ, Jiang L, et al., *Adv Mater*, 24 (2012)

1856-61.

- [19] Cong HP, Ren XC, Wang P, Yu SH, *Sci Rep*, 2 (2012) 613-1-6.
- [20] Kim D, Yang SJ, Kim YS, Jung H, Park CR, *Carbon*, 50 (2012) 3229-32.
- [21] Jung H, Yang SJ, Kim T, Kang JH, Park CR, *Carbon*, 63 (2013) 165-74.
- [22] Yang SJ, Kim T, Jung H, Park CR, *Carbon*, 53 (2013) 73-80.
- [23] Li YL, Kinloch IA, Windle AH, *Science*, 304 (2004) 276-8.
- [24] Ericson LM, Fan H, Peng HQ, Davis VA, Zhou W, Sulpizio J, et al., *Science*, 305 (2004) 1447-50.
- [25] Huang TQ, Zheng BN, Kou L, Gopalsamy K, Xu Z, Gao C, et al., *Rsc Adv*, 3 (2013) 23957-62.
- [26] Yunzhen Chang GH, Dongying Fu, Feifei Liu, Miaoyu Li, Yanping Li, *Journal of Power Sources*, 252 (2014) 113-21.
- [27] Cheng HH, Liu J, Zhao Y, Hu CG, Zhang ZP, Chen N, et al., *Angew Chem Int Edit*, 52 (2013) 10482-6.
- [28] Jiang ZX, Li Q, Chen ML, Li JB, Li J, Huang YD, et al., *Nanoscale*, 5 (2013) 6265-9.
- [29] Hummers WS, Offeman RE, *J Am Chem Soc*, 80 (1958) 1339.
- [30] Park S, Ruoff RS, *Nat Nanotechnol*, 4 (2009) 217-24.
- [31] Konkena B, Vasudevan S, *J Phys Chem Lett*, 3 (2012) 867-72.
- [32] Matsuo Y, Niwa T, Sugie Y, *Carbon*, 37 (1999) 897-901.
- [33] Shen JD, Huang WS, Wu LP, Hu YZ, Ye MX, *Mat Sci Eng a-Struct*, 464 (2007) 151-6.
- [34] Liu ZH, Zhou HH, Huang ZY, Wang WY, Zeng FY, Kuang YF, *J Mater Chem A*, 1 (2013) 3454-62.
- [35] Niyogi S, Bekyarova E, Itkis ME, McWilliams JL, Hamon MA, Haddon RC, *J Am Chem Soc*, 128 (2006) 7720-1.
- [36] Kakade BA, Pillai VK, *Appl Surf Sci*, 254 (2008) 4936-43.
- [37] Hung WS, Tsou CH, De Guzman M, An QF, Liu YL, Zhang YM, et al., *Chem Mater*, 26 (2014) 2983-90.

[38] Worsley KA, Kalinina I, Bekyarova E, Haddon RC, *J Am Chem Soc*, 131 (2009) 18153-8.



## Chapter 7 Concluding Remarks

The surface characterization of carbon nanomaterials is one of the most important procedures pertaining to their proper utilization for various applications. Numerous empirical techniques have been adopted for the qualification and quantification of the surface functional groups on carbon nanomaterials. Among these techniques, titration is an efficient method for the surface acidic or basic functional groups of carbon nanomaterials, which mostly affect the surface properties, to show 1) their exact concentrations, and 2) practical functions related to their applications. However, conventional titration techniques, as represented by indirect and direct titration methods, have several practical drawbacks with regard to their procedures and analysis methods. Hence, a new concept of a titration methodology which differs from conventional titration methods is necessary.

In this thesis, I develop a universal titration equation based on the conventional Henderson-Hasselbalch equation, which has been traditionally used for pH calculations or titration curve estimations for simple molecules or elements. The universal titration equation not only considers the titration moieties in the analysis but also the titration environment, including those of the titrants and titrands, thereby perfectly predicting 1) the titration behaviors and 2) the ionization behaviors of various acidic or basic elements ranging from monoprotic simple molecules to multiprotic carbon nanomaterials.

The titration methodology, developed based on the adoption of the universal titration equation, penetrates the experimental boundaries of indirect and direct titration. Indirect titration for carbon nanomaterials was simplified and standardized after the systematic

consideration of the effects of the acidic elements (e.g., acidic carbon compounds, carbon dioxide) dissolved in the reaction bases during the titration procedures. The  $pK_a$  distribution functions of carbon nanomaterials from direct titration measurements were successfully converted to estimate the concentrations of the practical functional groups obtainable from the indirect titration results. The titration methodology was also fundamentally used to analyze the ionization behaviors of carbon nanomaterials in various environments for their application of dispersion and second-generation functionalization.

These theoretical and experimental works discussed in this thesis suggest that the titration methodology ultimately breaks the boundary between the indirect and direct titration methods for the characterization of practical functional groups and for investigations of their roles in applications of carbon nanomaterials. Therefore, the developed titration methodology will pioneer other surface characterization techniques and engineering efforts related to carbon nanomaterials.

## 요약 (국문 초록)

이 논문은 통합 적정식을 기반으로 한 탄소나노재료의 표면 분석과 응용을 위한 적정 방법론에 대해 연구하고자 한다. 탄소나노재료는 그 뛰어난 특성으로 인하여 차세대 기능성 재료로 활용될 것이라고 기대 받고 있다. 표면에 다양한 기능기를 도입하는 탄소나노재료의 기능화는 이 재료의 실질적인 응용을 위한 필수적인 기술 중 하나이다. 이러한 기능기는 탄소나노재료의 표면 특성을 조절하여 분산성, 흡착성, 반응성 등을 향상시킴으로써 탄소나노재료의 적용 범위를 확장한다. 이러한 과정에서 표면 기능기를 효율적으로 활용하기 위한 정확한 표면 분석이 수반되어야 하고, 이러한 표면 분석법 중 적정 방법은 유용한 정보를 편리하게 파악할 수 있기 때문에 널리 활용되어 왔다.

탄소 재료를 위한 적정 방법은 크게 간접 적정 방식과 직접 적정 방식으로 구분된다. 이 중 직접 적정 방식은  $pK_a$  분포 함수라고 불리는 탄소 표면의 산도 분포를 제공하는 반면, 간접 적정 방식은 실제로 탄소 재료에 곧바로 적용할 수 있는 실질적인 기능기의 양을 쉽게 정량한다. 따라서 간접 적정 방식은 다양한 탄소 재료의 표면 분석에 활용되어 왔다. 그러나 이러한 간접 적정을 탄소나노재료에 쉽게 적용하기 위해서는 몇 가지 문제점이 개선되어야 한다. 하나는 직접 적정 방식에 비해 실험 과정이 복잡하다는 점이고, 또 다른 하나는 탄소나노재료의 특성과 관련된 문제점이다. 따라서 직접 적정의 단순함 실험 과정을 포함하고 간접 적정의 실질적인 정보를 얻을 수 있는 통합적인 적정 방법론을 개발할 필요성이 대두된다. 이에 본

연구는 탄소나노재료의 표면 분석과 응용을 위하여 직접 적정과 간접 적정 방식을 통합적으로 아우르는 적정 방법론을 개발하는 것을 목표로 한다.

1 부에서는 탄소나노재료의 산도에 관한 기본적인 개념과 정의를 설명하고, 이를 분석하기 위한 기본적인 적정 방법을 소개한다. 이어 기존 적정 방법의 문제점과 이를 해결하기 위한 기존 연구에 대한 이론적 고찰을 통하여 본 연구에 대한 필요성과 당위성을 역설한다.

2 부에서는 적정 방법론을 위한 통합 적정식을 이론적으로 유도하고 실험적으로 그 효용성을 입증한다. 유도된 적정 방정식을 탄소나노재료의 기능화에서 유도되는 산성 탄소 화합물이나 대기 중의 이산화탄소와 같은 간단한 산성 분자가 포함된 간접 적정 환경에 적용함으로써, 간접 적정 방식을 간단하게 표준화한다. 이 과정에서 산성 탄소 화합물과 이산화탄소의 영향이 명확하게 밝힌다. 또한 간접 적정에 관한 심층적인 고찰을 통하여 일반적으로 간접 적정에서 필수적인 요소로 알려져 왔던 이산화탄소의 제거 과정이 불필요하다는 것을 규명하여 간접 적정 방식을 보다 쉽고 정확하게 수행할 수 있는 방법을 마련한다.

3 부에서는 기존의 간접 적정과 직접 적정 방식을 대체할 수 있는 통합 적정 방법론을 개발한다. 이를 통하여 직접 적정을 통해 유도한 질산 산화

탄소나노튜브의  $pM_d \# " 8 \# : \& t \# , \ll \# , , fl + " 5^\circ \# + "$   
'~.b, , # ? °+ # ^ #J # \# : 9 ~ 1 # 6 O : # , , fl # ^! / \alpha +  
, , fl #J . # , \ll \# , , fl # J \* # , 2 : + #! , + (   
, , fl # ^! / \alpha , # ' ~. b, + # 6 O + C' \# \& t \# , " ~ . # + # : ,  
7 # " \* j \% ¶ . # , , fl # ^! / \alpha + # + ° + C9 \* # : : \%J #12

분산 거동을 규명한다. 강한 카복실기로 구성된 산성 탄소 화합물이 탄소나노튜브에 부착되었을 때, 이 산성 탄소 화합물이 탄소나노튜브 수용액의 분산도와 안정도에 막대한 영향을 끼침을 밝힌다. 또한, 적정 방법론을 활용하여 디아민 이온 다리를 활용한 그래핀 옥사이드의 가교 메커니즘을 규명하고, 이를 통하여 효율적으로 그래핀 옥사이드 섬유를 제조하는 방법을 제공한다. 이러한 연구를 통하여 본 논문에서 개발한 적정 방법론이 탄소나노재료의 실질적인 응용에 효과적으로 적용 가능성을 확인한다.

주요어: 탄소나노재료, 표면 기능화, 표면 기능기, 표면 특성 분석, 통합 적정 방정식, 적정 방법론

학번: 2010-20584